Post-Combustion CO_2 Capture: Energetic Evaluation of Chemical Absorption Processes in Coal-Fired Steam Power Plants

Vom Promotionsausschuss der
Technischen Universität Hamburg-Harburg
zur Erlangung des akademischen Grades

Doktor Ingenieur (Dr.-Ing.)

genehmigte Dissertation

von
Jochen Oexmann

aus
Bremen

2011

Gutachter: 1. Prof. Dr.-Ing. Alfons Kather
2. Prof. Dr.-Ing. Irina Smirnova

Datum der mündlichen Prüfung: 14. Januar 2011

urn:nbn:de:gbv:830-tubdok-10829

ACKNOWLEDGEMENTS

Diese Arbeit entstand während meiner Tätigkeit als wissenschaftlicher Mitarbeiter am Institut für Energietechnik der Technischen Universität Hamburg-Harburg. Für die Hilfe und Unterstützung, die ich in dieser Zeit von verschiedenen Personen erfahren habe, möchte ich mich im Folgenden bedanken.

Herrn Prof. Alfons Kather danke ich für seinen Rat in inhaltlichen Fragen und für seine außerordentliche Unterstützung, die ich mir nicht besser hätte wünschen können. Seine Herangehensweise an Probleme und seine Gelassenheit in stressigen Zeiten haben mich sehr geprägt und werden mir helfen, zukünftige berufliche Herausforderungen zu meistern.

Meinen Kolleginnen und Kollegen des Instituts für Energietechnik danke ich für vier großartige Jahre. Ihnen ist es zu verdanken, dass ich nicht an einem einzigen Tag ungern die Elbe überquert habe. Besonderen Dank schulde ich Christoph Hasenbein, ohne den die Realisierung des Modells in seiner jetzigen Form nicht möglich gewesen wäre, und Sebastian Linnenberg für die vielen Diskussionen, für die Einführung in die technischen und taktischen Tiefen des Kickerns und für seine Fähigkeit, mit den Unwägbarkeiten eines Bürokollegens entspannt umzugehen.

Prof. Gary Rochelle von der University of Texas in Austin (USA) danke ich für seine unverwechselbare Art, die auch mich auf den richtigen Weg gebracht hat (*High heat of absorption is good!*). Ebenso danke ich seinen Mitarbeiterinnen und Mitarbeitern Stephanie Freeman, Peter Frailie, Fred Closman, Jorge Plaza, David van Wagener und Xi Chen für Erklärungen und Informationen, die so in keiner Veröffentlichung zu finden sind.

Jacob Knudsen und Willy von Well von DONG Energy möchte ich für die zusätzlichen Informationen zur Pilotanlage in Esbjerg (Dänemark) danken.

Jan Hendrik Wülbern und Arne Ewald danke ich zunächst für die vielfältigen Kommentare zur ersten Fassung der Arbeit. Zudem danke ich Ihnen und allen meinen Freunden für all das, was gerade nicht mit dieser Arbeit zu tun hat.

Meiner Familie und insbesondere meine Mutter Renate gebührt Dank für das Vertrauen in mich und meine Entscheidungen und dafür, dass ich immer alles

so in die Tat umsetzten konnte, wie ich mir das vorgestellt habe. Auch meinem Vater Dirk, der diese Arbeit sicher gern gelesen hätte, danke ich dafür, die Hürden seines Lebens überwunden zu haben, um mir ein Aufwachsen zu ermöglichen, wie er es selber nie erleben durfte.

Zum Schluss danke ich Momo, die mir immer wieder zeigt, was wirklich wichtig ist.

SUMMARY

The performance of state-of-the-art steam power plants and the impact of optimisation measures can be evaluated with a high degree of accuracy by using modern simulation tools which have been developed for this particular purpose. CO_2 capture units can be modelled with the help of equally powerful simulation tools developed for chemical and process engineering purposes and by making use of complex rigorous thermodynamic models. The quality of such models varies significantly in particular for novel solvents which impedes a fair energetic evaluation and comparison. Furthermore, since the simulation of the capture process as well as of the power plant process is computationally intensive and thus time-consuming, a direct link between the two models to establish an integrated representation of the overall process is intricate. Such a connection is oftentimes infeasible or does not yield the envisaged purpose.

The power plant simulation tool EBSILON®*Professional* provides detailed models of all standard components of thermal power plants such as heat exchangers, pumps, and compressors. It is therefore possible to represent the majority of the components in a chemical absorption process for CO_2 capture with this simulation tool. Absorption and desorption columns, however, cannot be represented since the necessary models for a description of the chemical coherences of CO_2 mass transfer from a gas phase into a chemical solvent or vice versa are not available in the simulation tool.

In this work a simplified semi-empirical model for the representation of the absorption and desorption columns of the CO_2 capture unit is implemented in EBSILON®*Professional* to allow for the direct simulation of the overall process. CO_2 solubility, heat capacity, and density of the solvent are represented by empirical correlations. Trilinos – an open source library providing algorithms for the solution of linear and non-linear systems of equations – is used to solve the MESH (mass, equilibrium, summation, enthalpy) equations representing the columns to determine the interface quantities that connect the columns to the CO_2 compressor, the power plant, and the other components of the CO_2 capture unit. To employ the semi-empirical column model in the simulation tool, the equation solver together with routines for the set-up of the equation system and its corresponding Jacobi matrix, for the control of

input and output data, and for the initialisation of the variables are implemented in a Direct Link Library (DLL). The overall model of the CO_2 capture unit is validated with measurement data from a pilot plant.

The outlined approach allows evaluating any aqueous solvent for which a minimum of fundamental measurement data is available with respect to the energy requirement of the CO_2 capture unit (heat, power, cooling). The connection of the model of the CO_2 capture unit to detailed models of a power plant as well as of a CO_2 compressor facilitates the optimisation of process parameters – such as, for example, the solution flow rate – with respect to a maximal net power output of the power plant. Since the impact of the individual solvent properties in combination with the chosen process parameters on the overall power plant process is taken into consideration, the methodology allows for a fair comparison of the energetic performance of chemical solvents for CO_2 capture. Furthermore, the impact of the integration strategy and the power plant configuration can be analysed. Six solvents are selected to represent certain solvent groups. The choice of solvents enables to draw general conclusions for the optimal integration of CO_2 capture processes by chemical absorption in coal-fired steam power plants.

An overall process evaluation reveals that under the specific boundary conditions of this work, a 7 m MDEA / 2 m PZ solvent blend is best suited for a retrofit integration in the considered hard-coal-fired steam power plant. With this solvent a net efficiency penalty of 8.47 %-pts. compared to 10.15 %-pts. with 7 m MEA is achieved for a CO_2 capture rate of 90 % and subsequent CO_2 compression to 110 bar. For a new power plant that is specifically designed for operation with CO_2 capture (greenfield integration), the net efficiency penalty can be reduced to 8.11 %-pts. (7 m MEA: 9.57 %-pts.).

Keywords: Semi-empirical column model, EBSILON; Chemical solvents; Overall power plant process;

ZUSAMMENFASSUNG

Die Leistungscharakteristik moderner kohlebefeuerter Dampfkraftwerke sowie der Einfluss von Optimierungsmaßnahmen auf solche Prozesse können heute mithilfe speziell für diesen Zweck entwickelter Simulationstools evaluiert werden. CO_2-Rauchgaswäschen können mit ebenso leistungsfähigen, für die Chemie- und Verfahrenstechnik entwickelten Simulationstools untersucht werden. Die Qualität der dafür notwendigen thermodynamischen Modelle ist jedoch insbesondere für neuartige Lösungsmittel stark schwankend. Daher ist deren Verwendung in einem Modell einer CO_2-Rauchgaswäsche für einen objektiven Vergleich verschiedener Lösungsmittel nicht zielführend. Weiterhin ist die Zusammenführung der Teilprozesse Kraftwerk und CO_2-Rauchgaswäsche zu einem Gesamtmodell durch die Komplexität der Einzelmodelle nicht praktikabel oder erfüllt durch die damit verbundene hohe Rechenintensität nicht den gewünschten Zweck einer schnellen energetischen Bewertung und der Durchführbarkeit von umfassenden Sensitivitätsanalysen.

Das Simulationstool EBSILON®*Professional* enthält detaillierte Modelle aller Standardkomponenten eines Wärmekraftwerks (Wärmeübertrager, Pumpen, Verdichter). Daher ist es möglich, mit diesem Simulationstool den Großteil der Komponenten einer CO_2-Rauchgaswäsche darzustellen. Die Absorptions- und Desorptionskolonnen eines CO_2-Abtrennungsprozesses können jedoch nicht abgebildet werden, da die Modelle zur Darstellung der maßgeblichen Vorgänge des Stoffübergangs von CO_2 in ein chemisches Lösungsmittel in wässriger Lösung (chemische Reaktion, Wärme- und Stoffübertragung) nicht vorhanden sind.

In der vorliegenden Arbeit wird daher ein semi-empirisches Modell für die Darstellung der Absorptions- und Desorptionskolonnen einer CO_2-Rauchgaswäsche in EBSILON®*Professional* implementiert, um den Gesamtprozess mithilfe eines einzigen Simulationstools beschreiben zu können. Die CO_2-Löslichkeit, die Wärmekapazität und die Dichte des Lösungsmittels werden durch empirische Korrelationen abgebildet. Trilinos – eine frei verfügbare Bibliothek bestehend aus Algorithmen zur Lösung von linearen und nichtlinearen Gleichungssystemen – wird verwendet, um die MESH Gleichungen (*mass, equilibrium, summation, enthalpy*), welche die beiden Kolonnen darstellen, zu lösen und um die Schnittstellgrößen zu ermitteln, welche die Kolonnen mit dem CO_2-Verdichter, dem Kraftwerk sowie den anderen Kompo-

nenten des CO_2-Abtrennungsprozesses verbinden. Für die Verwendung des Kolonnenmodells in dem Simulationstool werden der Gleichungslöser sowie Routinen zur Steuerung der Ein- und Ausgabeschnittstellen, zur Initialisierung der Variablen und zur Aufstellung des Gleichungssystems in einer *Direct Link Library* (DLL) implementiert. Das Gesamtmodell der CO_2-Rauchgaswäsche wird anhand von Messdaten einer Pilotanlage validiert.

Durch das beschriebene Vorgehen kann jedes Lösungsmittel, für welches ein Minimum an fundamentalen Messdaten vorliegt, im Hinblick auf den Energiebedarf der CO_2-Rauchgaswäsche (Wärme, elektrischer Eigenbedarf, Kühlbedarf) im integrierten Gesamtkraftwerksprozess untersucht werden. Durch eine direkte Verbindung zu einem detaillierten Modell eines steinkohlebefeuerten Dampfkraftwerks sowie zu einem Modell eines CO_2-Verdichters können Prozessparameter der CO_2-Rauchgaswäsche – wie z. B. die Lösungsmittelumlaufrate – hinsichtlich einer maximalen Nettoleistung des Kraftwerks optimiert werden. Da die Auswirkungen der individuellen Lösungsmitteleigenschaften im Zusammenspiel mit den gewählten Prozessparametern auf den Gesamtprozess berücksichtigt werden, erlaubt das Vorgehen die Durchführung eines objektiven, energetischen Vergleichs verschiedener Lösungsmittel. Weiterhin kann der Einfluss verschiedener Integrationsstrategien und der Kraftwerkskonfiguration untersucht werden. Durch die Auswahl von sechs Lösungsmitteln, die repräsentativ für bestimmte Lösungsmittelgruppen sind, können außerdem generelle Schlussfolgerungen für die optimale Integration von CO_2-Rauchgaswäschen in kohlebefeuerten Dampfkraftwerken abgeleitet werden.

Die Untersuchungen zeigen, dass eine 7 m MDEA / 2 m PZ Lösungsmittelmischung unter den spezifischen Randbedingungen am geeignetsten für eine Retrofitintegration in das betrachtete steinkohlebefeuerte Dampfkraftwerk ist. Bei der Verwendung dieses Lösungsmittels beträgt der Wirkungsgradverlust bei einer CO_2-Abtrennungsrate von 90 % und bei einer anschließenden Verdichtung des CO_2-Stroms auf 110 bar 8,47 %-Pkt. gegenüber 10,15 %-Pkt. bei der Verwendung von 7 m MEA. In einem Neubaukraftwerk, welches für den Betrieb mit CO_2-Abtrennung ausgelegt ist (Greenfieldintegration), kann der Wirkungsgradverlust auf 8,11 %-Pkt. gesenkt werden (7 m MEA: 9,57 %-Pkt.).

Schlagworte: Semi-empirisches Kolonnenmodell; EBSILON; Chemische Lösungsmittel; Gesamtkraftwerksprozess;

CONTENTS

LIST OF FIGURES

LIST OF TABLES

ABBREVIATIONS AND SYMBOLS

Abbreviations

APH	air preheater
CCS	carbon dioxide capture and storage
CCU	CO_2 capture unit
DIPPR	Design Institute for Physical Property Data
DLL	direct link library
ESP	electrostatic precipitator
EU	European Union
FGC	flue gas cooler
FGD	flue gas desulphurisation unit
FWP	feed water pump
FWT	feed water tank
GHG	greenhouse gas
GUI	graphical user interface
HETS	height equivalent to a theoretical stage
HPP	high pressure preheater
HP	high pressure
ID	induced draft
IGCC	integrated gasification combined cycle
IL	ionic liquid
IP	intermediate pressure
LHV	lower heating value
LMTD	logarithmic mean temperature difference
LPP	low pressure preheater
LP	low pressure
MESH	material, equilibrium, summation, and enthalpy
NGCC	natural-gas-fired combined cycle
OHC	overhead condenser
PCC	post-combustion CO_2 capture
PMV	pressure maintaining valve

RLHX	rich-lean heat exchanger
SCR	selective catalytic reduction
SG	steam generator
VLE	vapour-liquid-equilibrium
WS	washing section

Chemical symbols

AMP	aminomethylpropanol
CO_2	carbon dioxide
COS	carbonyl sulphide
DEA	diethanolamine
H_2O	water
H_2S	hydrogen sulphide
K	potassium
K_2CO_3	potassium carbonate
MDEA	methyldiethanolamine
MEA	monoethanolamine
NaOH	sodium hydroxide
NH_3	ammonia
NO_x	nitrogen oxides
PZ	piperazine
SO_x	sulphur oxides

Latin symbols

a	activity	-
C_p	mass-specific heat capacity	J / (kg K)
C_p^m	molar heat capacity	J / (mol K)
f	fugacity	Pa
h	enthalpy	J / mol
k'_g	liquid film mass transfer coefficient	mol / (s Pa m^2)
K_g	overall mass transfer coefficient	mol / (s Pa m^2)
K_r	equilibrium constant	-
$\overline{m}_i$	molality of species i	mol i / kg H_2O

$\dot{m}$	mass flow	kg / s
M_i	molar weight of species i	kg / kmol
$\dot{n}$	mole flow	mol / s
n	number of data points	-
ns	number of stages	-
N	mole flux	mol / (s m^2)
p_i	partial pressure of species i	Pa
p_{tot}	total pressure	Pa
P	power	W_{el}
q	specific heat	GJ_{th} / t CO_2
$\dot{Q}$	heat stream	W_{th}
R	universal gas constant	8.31451 J / (mol K)
t	temperature	°C
T	temperature	K
w_i	mass fraction of species i in liquid phase	-
x_i	mole fraction of species i in liquid phase	-
y_i	mole fraction of species i in gas phase	-

Greek symbols

α	CO_2 loading	mol CO_2 / mol alkali
γ	activity coefficient	-
ε	CO_2 capture rate	-
η	efficiency	-
κ	CO_2 capacity	mol CO_2 / (kg H_2O + kg alkali)
ρ	density	kg / m^3
σ	mean relative error	-
φ	fugacity coefficient	-

Indices

*	equilibrium
abs	absorption
alk	alkali fraction
comp	CO_2 compressor

cw	cooling water
des	desorber
el	electrical
fg	flue gas
g	gas phase
G	gas stream
hot	hot (upper) terminal side of RLHX
int	gas-liquid interface
l	liquid phase
L	liquid stream
m	Murphree
reb	reboiler
ref	reference
s	saturation
sens	sensible
sol	total solution
S	side stream
vap	vaporisation

1 INTRODUCTION

Growing awareness of the ongoing climate change has led to increasing research activity in the field of CO_2 mitigating technologies. According to the current status of knowledge the emissions of carbon dioxide and other greenhouse gases (GHG) need to be reduced significantly in order to limit global warming. There is a broad political consensus that the global temperature rise should be limited to two degrees Celsius, compared with preindustrial temperatures. However, up to today there is no binding successor to the Kyoto Protocol under which 37 industrialised countries committed themselves to a reduction of GHG emissions by 5.2 % from the 1990 level until the end of 2012.

If the global temperature increase is to be limited to below 2 °C – a goal that has recently been affirmed by the United Nations Climate Change Conference in Copenhagen in December 2009 – global GHG emissions need to be reduced significantly [1]. As 41 % of global GHG emissions result from the combustion of fossil fuels for electricity generation, power plants play a critical role in the struggle against global warming [2].

Three fundamental paths exist to achieve a reduction in the emissions of GHG emanating from electricity generation:

1. change to less carbon-intensive energy sources such as natural gas, nuclear power, and in particular renewables;
2. increase in energy efficiency both in electricity production and consumption;
3. capture and storage of the produced carbon dioxide from fossil-fired power plants.

It is predicted that renewables and nuclear energy will only provide part of the world's energy needs in the next decades and that fossil fuels will remain a key energy source. Of all fossil fuels, coal has the largest resources and shows a wide global distribution of reserves. The continuing use of coal ensures a diversification of the energy supply and thus safeguards security of supply, especially in countries lacking their own natural gas and oil resources. 7,756 TWh_{el} or 41 % of global electricity generation in 2006 originated from coal where the share is predicted to increase to 44 % by 2030. In the EU

1,021 TWh_{el} (31 %) originated from coal-fired power plants in 2006. In China electricity generation from coal has more than doubled between 2000 and 2006 to a total of 2,328 TWh_{el} (80 %) [2].

GHG emissions from coal-fired power plants can be reduced by increasing the energy conversion efficiency of these plants or by separating the emanating CO_2, commonly referred to as carbon (dioxide) capture and storage (CCS).

CO_2 emission reduction by efficiency increase offers the benefit of reduced fuel consumption while keeping the net power generation constant. Yet, the resulting reduction in emissions is limited. Current efficiencies of coal-fired power plants have reached a plateau at which further efficiency increases demand a major effort in material development in case of conventional steam power plants or the commercial introduction and optimisation of the integrated gasification combined cycle (IGCC) [3].

CCS would permit the continuing use of coal and other fossil fuels while significantly reducing GHG emissions. CCS has been discussed since the 1980s, but the lack of economic incentives as well as political and legal uncertainties have only allowed for the realisation of a few pilot plants worldwide and recently for the planning of some demonstration plants [4]. Besides the technical and economic aspects, safety and regulatory issues with respect to transport and storage of CO_2 remain unclear. Until today the concept of CCS for coal-fired power plants has not been realised on a large scale.

To inject CO_2 into adequate storage sites such as saline aquifers or depleted oil and gas fields, it needs to be separated from other gas components. Three technology routes exist to perform this separation. Figure 1.1 shows a schematic of each of the three technology routes that are commonly referred to as post-combustion, pre-combustion, and oxyfuel[1].

Even though pre-combustion and oxyfuel processes are considered to suffer a less significant decrease in efficiency when applied to power plants, post-combustion CO_2 capture (PCC) is technologically more mature. Commercial experience from gas treating applications is available at large scale in industry and existing power plants can be retrofitted more easily [5, 6].

[1] For a detailed explanation of all three CCS technology routes refer to [3].

There is a large number of separation technologies for PCC in coal-fired steam power plants, but it is agreed that the implementation of an absorption-desorption-process using a chemical solvent is the most developed and adequate process for deployment in the near- to middle-term [7].

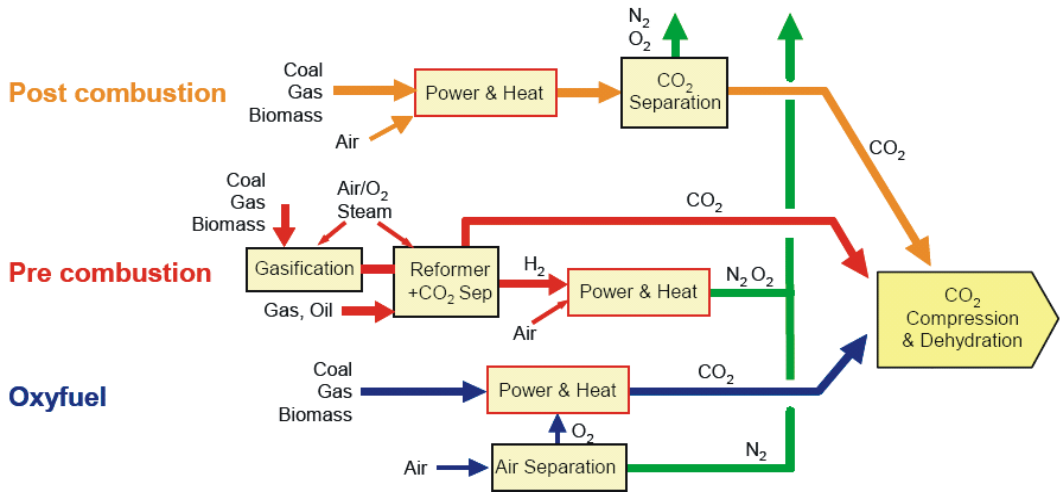

Figure 1.1: Technology routes for CO_2 capture [5]

1.1 Background

The application of a PCC process in a coal-fired steam power plant is associated to a significant loss in power output and a related net efficiency penalty of 8–12 %-pts. Besides considerable capital expenditures for engineering, procurement, and construction of a PCC process, the loss in power output leads to significant additional costs for the operation of a coal-fired steam power plant with CO_2 capture. Thus, an optimisation of the overall process and a reduction of the efficiency penalty is required for the commercial deployment of this technology and the application at industrial scale. An integrated model of the overall process would allow evaluating the impact of the choice of chemical solvent, process configuration, and operational parameters on the performance, thus on the net output, of the power plant.

The performance of state-of-the-art steam power plants and the impact of optimisation measures can be evaluated with a high degree of accuracy by using modern simulation tools that have been developed for this particular purpose. PCC by chemical absorption can be modelled with the help of equally powerful simulation tools developed for chemical and process engineering purposes. Accurate models of steam power plants as well as of CO_2

capture processes are, however, of high complexity. Consequently, simulations are computationally intensive and a direct link between the two models is intricate. Such connection is hence either infeasible or does not allow to consider all key process parameters in the optimisation of the overall process with reasonable effort and within a reasonable timeframe.

1.2 Aim and scope

Due to the increasing interest in CO_2 capture technologies in the power industry, research concerning the energetic evaluation of chemical solvents for CO_2 capture from flue gas has grown considerably in the past years. The majority of research is found on the fundamental physicochemical properties of novel chemical solvents such as CO_2 solubility, viscosity, density, or heat capacity. Industrial and academic research activities make use of the results of the fundamental research to develop models for the representation of absorber [8, 9, 10, 11, 12] and desorber (stripper) [13, 14, 15] columns.

In a smaller number of scientific publications the complete CO_2 capture process is evaluated with a focus on the minimisation of its energy requirement [16, 17, 18, 19, 20, 21]. NOTZ *et al*. developed a short-cut method for the energetic assessment of solvents for PCC within the CO_2 capture island [22]. The method uses a modified Kremser equation which requires a linearised relation for the representation of CO_2 solubility as a function of temperature and CO_2 concentration in the liquid. Additionally, the simplified assumption of a constant gas flow rate over the whole column is required for the application of the Kremser equation. In some studies the interaction of the capture process with the power plant is estimated by employing simplified correlations which relate the required energy to the corresponding loss in power output of the power plant [23, 24].

There exists a variety of studies that focus on the optimal integration of PCC processes in power plants. The integration in gas-fired combined cycles is, for example, discussed in [25, 26, 27]. Due to the significant differences in the boundary conditions of such power plants (e.g., different steam power process configuration, lower CO_2 partial pressure in flue gas) the transfer of the results of these studies onto coal-fired steam power plants is limited. The integration of CO_2 absorption processes in coal-fired steam power plants is also covered in literature [28, 29, 30, 31]. Many studies, however, use simula-

tion tools which are not specifically designed to represent the complex interrelations in power plant processes and suffer from a high degree of simplification.

A chemical absorption process for CO_2 capture based on an aqueous solution of monoethanolamine (MEA) is often considered as the benchmark since commercial processes with MEA that are designed for the application with coal-derived flue gas already exist (cf. e.g., [32, 33]). Consequently, the majority of mentioned publications focus on MEA. There are other well known solvents such as diethanolamine (DEA), methyldiethanolamine (MDEA), and aminomethylpropanol (AMP) for which also a considerable amount of scientific literature is available. Information on novel solvents that have been identified as promising candidates for CO_2 capture from flue gas, however, is scarce and focuses on more fundamental research aspects rather than on the energetic performance of the capture unit or the overall process.

The aim of this work is the energetic evaluation and comparison of chemical solvents for post-combustion CO_2 capture in a typical absorption-desorption process integrated into a coal-fired steam power plant. The performance of the overall process depends on the individual solvent properties in combination with the choice of process parameters of the CO_2 capture unit. A fair comparison on the basis of constant boundary conditions and assumptions therefore requires the optimisation of these parameters for each solvent with respect to a minimal impact on the power plant.

To accomplish this aim, the overall process – including the power plant, the CO_2 capture unit, and the CO_2 compressor – must be represented in adequate detail. The model should be capable of representing any novel chemical solvent for which a minimal amount of information and measurement data is available. To account for the intricate interaction of the CCU with the steam power process and to allow for comprehensive sensitivity analyses of key process parameters, the overall process model needs to be developed in a single simulation environment. To ensure the practicability and relevance of the overall process model, the use of a simulation tool that has proven its applicability in the power generation industry is favourable.

1.3 Methodology

The simulation tool EBSILON®*Professional* complies with the above list of requirements [34]. It is widely used for planning, construction, optimisation, and control of thermal power plants. Additionally, its solution algorithm has proven to be fast and to show favourable convergence properties to solve the mass- and energy balances of power plant processes.

EBSILON®*Professional* comprises detailed models of standard components such as heat exchangers, pumps, and compressors. Provided that solvent properties such as density and heat capacity are made available in adequate form, the simulation tool is therefore capable of representing most of the components in a CO_2 capture process. Absorption and desorption columns, however, cannot be modelled with EBSILON®*Professional*, as it is not capable of describing the thermodynamic coherences which determine the transition of a gaseous species into a chemical solvent or vice versa.

The description of mass transfer between multicomponent gas and liquid phases in countercurrent flow columns always includes the consideration of phase equilibrium. The equilibrium of a gas mixture and a chemical solvent in aqueous solution as a function of pressure and temperature is commonly represented by complex rigorous thermodynamic models that consist of a large number of non-linear equations. To realise an overall process model in one single simulation tool, the system of equations would have to be solved in parallel to the equally complex equation system that represents mass and energy balances of the power plant process. This task is impeded by the considerable computational effort related to the solution of these coupled systems and the lack of rigorous thermodynamic models for novel solvents. Therefore, a simplified representation of solvent properties with regard to the development of an accurate column model is necessary.

Correlations for estimating the CO_2 solubility in aqueous alkanolamine solutions exist that describe the partial pressure of CO_2 as a function of total pressure, temperature, and CO_2 concentration in the solution. Examples are the works by DESHMUKH AND MATHER (MEA, DEA, AMP, and blends), POSEY *et al.* (MDEA), GABRIELSEN *et al.* (MEA, DEA, MDEA), and ARCIS *et al.* (AMP, based on the model by POSEY) [35, 36, 37, 38]. In all of these works it is attempted to find simplified correlations that are based on fundamental chemical and thermodynamic relationships of the species on a molecular level. In contrast

to more sophisticated approaches, these models typically account for the equilibrium speciation by a series of simplifying assumptions.

In the column model that is developed in this work, CO_2 solubility and other solvent properties are represented by employing empirical correlations that describe the relations between the measured parameters in a suitable mathematical manner. Although physical dependencies of these parameters are not taken into account, the approach allows a continuous representation of the CO_2-H_2O-solvent system in the range of temperatures and CO_2 partial pressures that are relevant for CO_2 capture processes in coal-fired steam power plants. The developed column model can be used with any chemical solvent for which a minimum of information and measurement data is available.

To facilitate the selection and evaluation of new solvents for post-combustion CO_2 capture in coal-fired steam power plants, this work aims at elucidating fundamental integration principles with regard to the overall process. Due to the large diversity of steam power plant types, chemical solvents, and possible capture process configurations, the aim is pursued by employing the example of a state-of-the-art hard-coal-fired steam power plant in combination with a simple, yet typical, absorption-desorption-type CO_2 capture process using six different chemical solvents.

Chapter 2 gives an overview of the functional principles of a CO_2 capture process and of candidate solvents that are generally qualified to be used in such processes. Six promising solvents representing different solvent groups are selected for energetic evaluation in this work.

Chapter 3 outlines the semi-empirical column model that makes use of correlations to represent solvent properties such as CO_2 solubility, heat capacity, and density over a certain range of CO_2 partial pressures and temperatures. The column model is validated with measurement data from a CO_2 capture pilot plant.

Chapter 4 explains how the semi-empirical column model is implemented in the chosen simulation tool and how it is coupled to the models of the power plant and the CO_2 compressor. The integrated overall process model is capable of describing the dependence of energy requirements and process parameters of the CO_2 capture process in interaction with the CO_2 compressor and the steam power plant.

Chapter 5 first discusses some fundamental solvent characteristics and interrelations of power plant, CO_2 capture unit, and CO_2 compressor, which are important in the discussion and for the understanding of the results of the energetic evaluation. For each of the six selected solvents, key process parameters of the CO_2 capture unit are optimised with respect to an optimal net output of the power plant. Finally, the results of the overall process optimisation for each of the selected solvents are discussed with regard to different power plant configurations and integration strategies.

2 POST-COMBUSTION CO_2 CAPTURE

In post-combustion CO_2 capture (PCC) carbon dioxide is separated from the flue gas of a conventional power plant. The major disadvantage of this technology path is the net efficiency penalty related to it, which is generally higher than that of pre-combustion and oxyfuel CO_2 capture processes. An advantage of PCC processes is the low level of necessary integration with the conventional steam power plant. Therefore, the retrofit of existing power plants is afflicted with less interferences of the capture process with other components. Furthermore, one can draw on the considerable experience with similar CO_2 removal processes in gas purification applications at large scale. However, the boundary conditions of PCC processes in power plants differ significantly from those of existing applications. Above all, the PCC process needs to handle significantly larger flue gas volume flows at low pressure and with low CO_2 content. Additionally, the process needs to be adapted to cope with sour gas fractions (SO_x and NO_x) and considerable amounts of oxygen in the flue gas [5, 6].

A general schematic of a power plant layout with PCC is given in Figure 2.1. The CO_2 capture unit (CCU) is located downstream of the existing equipment for flue gas cleaning. The flue gas from the boiler passes a selective catalytic reduction reactor (SCR) to reduce the NO_x concentration, an electrostatic precipitator (ESP) for dust removal, and a flue gas desulphurisation unit (FGD) before entering the CCU. In the CCU the CO_2 is separated from the flue gas stream and the remaining treated flue gas is released to the atmosphere. The separated CO_2 can then be compressed and transported to an adequate storage site.

The CO_2 content in the flue gas of typical coal-fired power plants lies in the range of 12–15 vol.-% (wet) where the gas is present at atmospheric pressure. Therefore, the partial pressure of CO_2 in the flue gas is low compared to existing gas purification applications or processes of the other two CCS technology routes (pre-combustion and oxyfuel). Consequently, PCC technologies which require high CO_2 partial pressure differences, such as adsorption or membrane processes, suffer from an inherent disadvantage [7]. For the same reason the possible CO_2 loading (e.g., mole CO_2 per mole of solvent) of physical solvents is limited, resulting in large solution flow rates and ultimately in

large amounts of heat required for the regeneration of the solvent. In the relevant range of low CO_2 partial pressures in the flue gas, only chemical solvents show an absorption capacity large enough to be applicable for CO_2 capture. It is commonly agreed that the implementation of a process applying the concept of CO_2 absorption by a chemical solvent is best suited for the first generation of PCC process in coal-fired power plants [3].

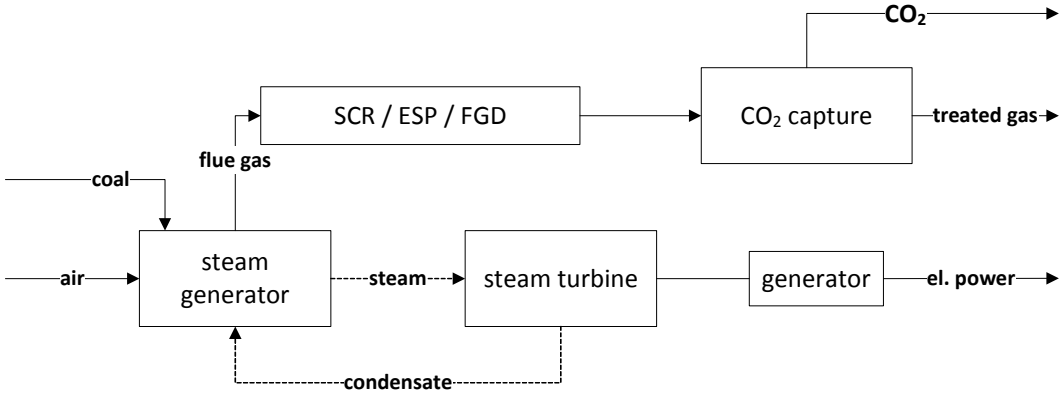

Figure 2.1: Schematic of a coal-fired steam power plant with post-combustion CO_2 capture

2.1 Process

A schematic of a typical plant for post-combustion CO_2 capture by chemical absorption is shown in Figure 2.2. To improve the absorption process, the flue gas is cooled before entering the absorber column at the bottom. As the flue gas rises in the column, the CO_2 is absorbed by a chemical solvent in aqueous solution in counter-current flow. The column is filled with random or structured packing to increase the interfacial area between gas and liquid phase. A washing section at the top of the absorber reduces the slip of solvent to the environment by contacting the gas with cold water. An induced draft (ID) fan is required to overcome the additional pressure losses in the flue gas path. The treated CO_2-lean flue gas at the top of the absorber is released to the atmosphere. The absorbed CO_2 is stripped from the rich solution in a separate desorber column. At the bottom of the absorber the CO_2-rich solution is gathered and pumped to the desorber, passing a rich-lean heat exchanger (RLHX) where it is preheated to a temperature close to desorber level.

In the desorber the CO_2-rich solution flows downwards. The rich solution releases the captured CO_2, which rises to the top of the column. The necessary driving force (partial pressure difference) and heat for the separation of CO_2 from the solvent is delivered by a counter-current flow of vapour (stripping steam), consisting mainly of steam and CO_2. The vapour is generated in the reboiler which functions as a combined condenser-evaporator: Low-pressure steam from the water-steam-cycle of the power plant is condensed at one side, transferring its latent heat to the solution on the other side.

At the head of the desorber the gas is led to a condenser where the CO_2-rich gas stream is cooled and part of the water vapour is condensed. The remaining gas stream can be compressed and is then ready for transportation to a storage site. The CO_2-lean solution is gathered at the bottom of the reboiler and is returned to the absorber, passing the RLHX and another heat exchanger (solution cooler) in which the temperature is lowered to the desired absorber temperature. The lean solution is dispersed at the top of the absorber column, closing the process cycle.

Alternative process configurations such as split flow, absorber intercooling, multi-flash, multi-pressure, or matrix stripping can reduce the reboiler heat duty compared to the standard absorber-desorber design that is shown in Figure 2.2 [23]. As the optimal process configuration depends on the individual solvent, in this work all solvents are compared on the basis of the simple absorber-desorber configuration.

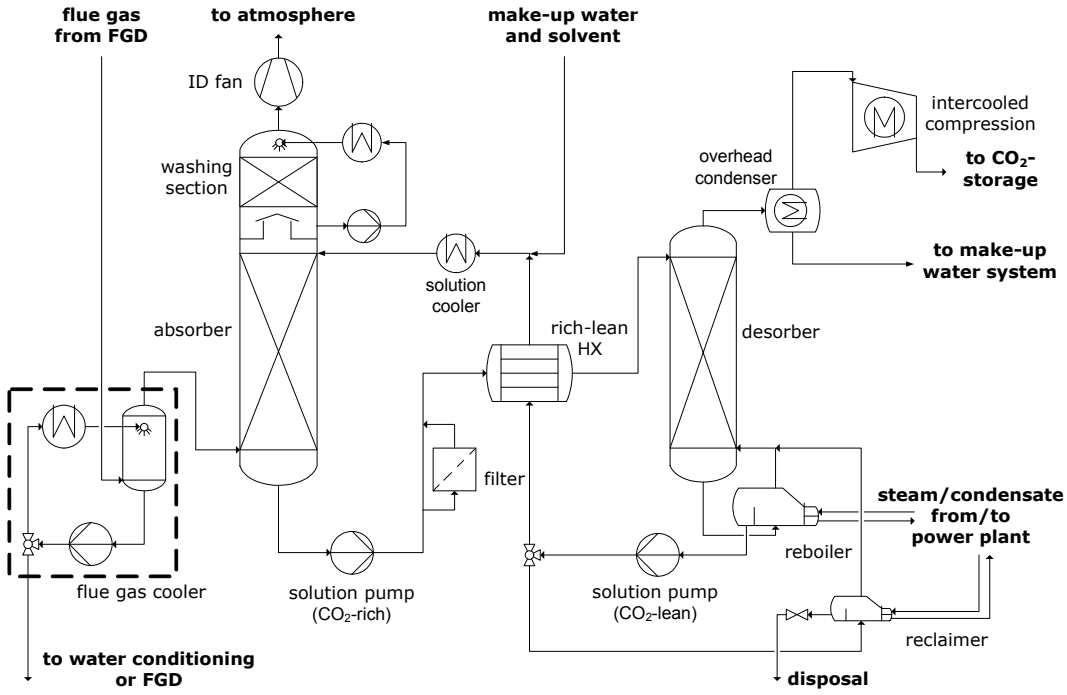

Figure 2.2: Schematic of a chemical absorption process for CO_2 capture

2.2 Solvents

Generally, an ideal solvent for CO_2 capture by chemical absorption has to fulfil the following requirements:

- high inherent CO_2 capacity per weight of solvent;
- high absorption rate;
- low cost;
- non-corrosive behaviour;
- no degradation under the operating conditions of the absorber and desorber;
- low vapour pressure;
- low viscosity;
- non-toxic and non-hazardous.

The inherent CO_2 capacity of the solvent determines the maximal amount of CO_2 that can theoretically be absorbed by the solution under equilibrium conditions. The absorption rate determines how close the practical CO_2 uptake in a real column can approach the maximal value. The more CO_2 is absorbed, the less solution needs to be circulated in the process which is beneficial for the heat requirement in the reboiler and the auxiliary power demand of the solution pumps.

In the following sections, various solvent types are introduced and advantages and disadvantages of the individual solvent type considering the above list of optimal solvent properties are discussed. All chemical solvents are used in aqueous solution with concentrations between approximately 10 and 50 wt.-%. The choice of solvent concentration involves a trade-off between a high desired CO_2 capacity and an undesired high viscosity of the aqueous solutions as well as an increased risk of corrosion.

The characteristics of some solvent groups with respect to the key factors which are relevant for CO_2 capture are listed in Table 2.1. The table is based on the analysis of solvent properties from various sources given in the following paragraphs and Section 3.1. As available information and measurement data for solutions of amino acid salts and ionic liquids are scarce, these two solvent groups are not included in the table.

Table 2.1 allows a first evaluation of possible solvents for CO_2 capture from flue gas. Primary amines feature high reaction and therefore high CO_2 absorption rates but suffer from a mediocre inherent CO_2 capacity. Therefore, large solution circulation is required with a corresponding negative effect on the required energy for regeneration. Secondary and tertiary amines have a higher inherent CO_2 capacity but absorption rates are too low to use these solvents without an additional activator (i.e., rate promoter). Aqueous solutions of alkali salts (e.g., potassium carbonate) suffer the same fate and also require an activator. Sterically hindered amines and ammonia have an increased inherent CO_2 capacity while showing reasonable absorption rates. Polyamines have multiple functional amino groups and therefore offer large inherent CO_2 capacities with generally high reaction rates. The individual solvent groups are discussed in more detail in the following sections.

Table 2.1: Solvent properties

	heat of absorption*	absorption rate	CO_2 capacity	degradation tendency
primary amines	●	●	◑	●
secondary amines	●	◑	◑	◑
tertiary amines	◑	○	●	○
sterically hindered amines	●	◑	●	○
polyamines	●	●	◑	○
alkali salts	○	○	●	○
ammonia	◑	◑	●	○

● = high; ◑ = medium; ○ = low;

* Note that the heat of absorption represents only a fraction of the total energy requirement for the regeneration of the solution (cf. Section 5.1.2).

2.2.1 Amines

Amines are organic compounds with a functional group that contains nitrogen as the key atom. Structurally, amines resemble ammonia (NH_3) where one or more hydrogen atoms are replaced by an organic substituent. Primary amines arise when one of the three hydrogen atoms in ammonia is replaced by an organic substituent, secondary amines have two hydrogen atoms replaced, and tertiary amines have all three hydrogen atoms substituted. Table 2.2 shows a selection of amines that come into consideration for CO_2 capture from flue gas.

Table 2.2: Candidate amines for CO_2 capture from flue gas

name	abbreviation	type*	structure [39]
monoethanolamine	MEA	1	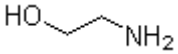
diglycolamine	DGA®	1	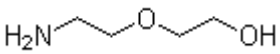
diethanolamine	DEA	2	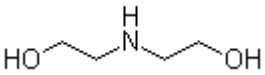
diisopropanolamine	DIPA	2	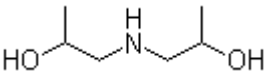
triethanolamine	TEA	3	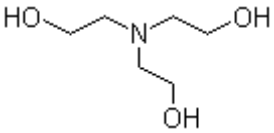
methyldiethanolamine	MDEA	3	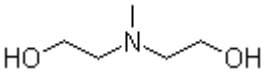
aminomethylpropanol	AMP	1-h	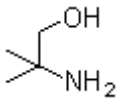
2-piperidineethanol	2-PE	2-ch	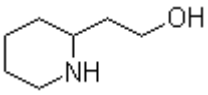
ethylenediamine	EDA	1/1	
piperazine	PZ	2/2-c	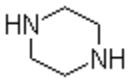
hydroxyethylpiperazine	HEP	2/3-c	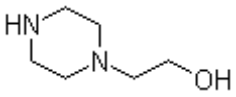
aminoethylethanolamine	AEEA	1/2	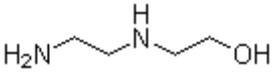
aminoethylpiperazine	AEP	1/2/3-c	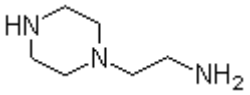

* 1 = primary amine; 2 = secondary amine; 3 = tertiary amine; h = sterically hindered; c = cyclic; poly-amines can have amine groups of different order, e.g., 2/3 is a diamine with one secondary and one tertiary amino group;

Amines are used as chemical solvents for acid gas removal in aqueous solution. The amine reacts with CO_2 in the liquid phase to form carbamate ($RNHCOO^-$) and/or bicarbonate (HCO_3^-) via the following reactions [40]:

$$CO_2 + 2RNH_2 \rightleftarrows RNH_3^+ + RNHCOO^- \quad , \tag{2.1}$$

$$CO_2 + RNH_2 + H_2O \rightleftarrows RNH_3^+ + HCO_3^- \quad . \tag{2.2}$$

Carbamate production occurs when the CO_2 replaces a hydrogen atom of the amine. This reaction allows the capture of 0.5 mole CO_2 per mole of amine due to the reaction between the free hydrogen atom and another amine molecule (protonation). The formation of bicarbonate is beneficial to a higher CO_2 loading of the absorbent, since 1 mole of CO_2 per mole of amine can be chemically absorbed.

In general, there is a tendency for secondary amines to be weaker bases and have less stable carbamate forms than primary amines; therefore, the formation of bicarbonate becomes more relevant. The same is true for amines with substituent groups on the carbon atoms bonded to the amine functional group. This group of solvents is referred to as sterically hindered amines (cf. Section 2.2.1.3). Tertiary amines do not form carbamate species, thus the CO_2 is exclusively absorbed via reaction (2.2) and their reactivity is determined entirely by their base strength [41].

Amines offer high possible CO_2 loadings at low CO_2 partial pressures. However, they suffer from some practical problems such as high volatility, leading to vaporisation losses, as well as degradation due to increased temperatures and due to reactions with other flue gas components such as oxygen and sour gas fractions. Oxygen can rapidly degrade amines and inhibitors need to be added in order to reduce solvent loss. SO_x and NO_x can also degrade solvents in chemical absorption systems since the amine reacts with these acidic contaminants in the flue gas to form heat-stable salts that cannot be broken down in the desorber. Despite a degree of amine recovery with sodium hydroxide (NaOH) in the reclaimer, there is still a net loss of amine through the entry of these gases into the absorber.

Chemical absorption with amines has been applied for H_2S, COS, and CO_2 separation in several applications, such as natural gas sweetening, for many years. The boundary conditions of these applications, however, are very different compared to CO_2 capture from power plant flue gas: Natural gas is usually present at high pressures and only a small quantity of CO_2 needs to be

separated from the gas stream [42]. Furthermore, the reducing conditions of natural gas prevent oxidative degradation of the amine solvent. A comprehensive description of sour gas removal technologies is given by KOHL AND NIELSEN [43].

Besides numerous pilot plants (with a capacity of up to 5 t CO_2 / h), there exist examples for amine-based CO_2 capture from coal-derived flue gas at large scale such as the power plants Shady Point (320 MW_{el}) and Warrior Run (180 MW_{el}) in the USA [6]. However, in these plants only a split stream of the flue gas is treated to produce small amounts of no more than 200 tonnes CO_2 of high purity per day for the food industry. So far, amine-based CO_2 absorption has not been fully adapted to the specific conditions for complete flue gas treatment in a large coal-fired power plant. A state-of-the-art hard-coal-fired power plant with a net power output of 1,000 MW_{el} generates around 750 tonnes of CO_2 per hour. Due to the net efficiency penalty related to the application of the CO_2 capture process, a power plant with an equivalent net power output and a CO_2 capture rate of 90 % would require the capture of approximately 900 tonnes of CO_2 per hour.

2.2.1.1 Primary amines & monoethanolamine

Monoethanolamine (MEA) is currently considered the baseline solvent for post-combustion CO_2 capture by chemical absorption and therefore represents the most studied solvent for PCC in power plants. This is due to industrial experience with this primary amine in acid gas treatment, where several commercialised processes utilise aqueous solutions of 15–30 wt.-% MEA [44, 32].

MEA shows a relatively high reaction rate with CO_2 compared with other amines, an important property to achieve a high CO_2 absorption rate and practical CO_2 loadings close to the theoretical maximum. But MEA also has a number of undesired characteristics – above all, the large amount of regeneration heat of about 3.5 GJ_{th} per tonne of captured CO_2 [45]. It is, however, claimed that through process and solvent optimisation the heat duty can be reduced to values as low as 3.0 GJ_{th} / t CO_2 [46]. Additionally, the tendency of MEA to degrade demands a thorough removal of SO_x and NO_x to reduce solvent make-up. Processes with MEA require SO_x and NO_x levels below 10 ppmv and 20 ppmv, respectively [47]. These levels are lower than currently re-

quired by legislation for coal-fired power plants. They are attainable with existing technology but are associated with a cost increase [48].

The degradation products of amines in general and MEA in particular show highly corrosive behaviour. Corrosion inhibitors need to be added in order to allow the use of regular carbon steels in the capture unit [49]. Since the risk of corrosion increases with higher amine concentrations, solutions with no more than 15–30 wt.-% MEA have been realised in commercialised plants. Higher amine concentrations, however, would be beneficial to reduce the heat requirement for the regeneration of the solution [50].

2.2.1.2 Secondary and tertiary amines

As mentioned above, secondary and tertiary amines such as DEA and MDEA show some beneficial characteristics in comparison to primary amines, for example a higher inherent CO_2 capacity and a lower degradation tendency. Yet, the reaction rate of these amines is in general significantly lower than of primary amines so that the use of aqueous solutions consisting exclusively of secondary or tertiary amines is not feasible under the conditions of coal-fired steam power plants.

The blending of secondary or tertiary amines with other solvents (promotion/activation), however, appears promising, since it can lead to a combination of favourable characteristics. A blend can combine the high reaction rate of one solvent with the low regeneration heat duty as well as reduced corrosion and degradation tendency of another. Yet, blending can also amplify existing drawbacks of the combined solvents or generate new shortcomings. For example, a blend of MEA and PZ shows a significant rate of degradation at low temperatures, although the thermal degradation rate of concentrated PZ solutions is comparatively low for temperatures of up to 150 °C [51]. A MEA/PZ blend is also more corrosive than aqueous solutions of just MEA [52]. The blending of solvents therefore always implies a trade-off of favourable and unfavourable characteristics.

2.2.1.3 Sterically hindered amines

The main characteristic of so-called sterically hindered amines is a bulky organic substitute to the nitrogen atom of the amine. The bulky substituent lowers carbamate stability [38]. As a result, carbamate is reversed to bicarbonate ion and free amine, increasing the inherent CO_2 capacity of the solvent

to one mole of CO_2 per mole of amine [53]. A disadvantage is the reaction kinetics which is generally lower than that of primary amines such as MEA.

2-amino-2-methyl-1-propanol (AMP) is the hindered form of MEA [53]. 2-piperidineethanol (2-PE), a secondary hindered amine, forms even less carbamate than AMP as a result of the lower carbamate stability [54].

A proprietary sterically hindered amine is KS-1. This solvent was developed further and followed by KS-2 and KS-3 [55]. YAGI *et al.* report reaction kinetics and effective CO_2 loading of these solvents as being superior to that of MEA [56]. Regeneration occurs at temperatures around 110 °C, the regeneration heat duty is reported to be around 10–15 % less than for MEA and solvent losses due to degradation in the presence of oxygen are significantly lower. A number of industrial CO_2 recovery plants operating with KS-1 exist in Asia, with plant sizes of up to 450 tonnes CO_2 captured per day [57, 56]. However, these plants do not capture CO_2 from flue gas, but rather from industrial sources such as urea production plants. Two small pilot plants working with coal-derived flue gas are in operation.

2.2.1.4 Polyamines

Polyamines feature more than one functional amino-group and therefore offer an enhanced inherent CO_2 capacity. Piperazine (PZ) as a diamine represents the most discussed solvent of this type [58, 59, 24]. Its cyclic structure exposes the nitrogen groups resulting in favourable reaction rates with CO_2 [60]. Previously PZ has been considered as an activator at low concentration in blends with other amines to increase overall mass transfer rates (MDEA/PZ [61], MEA/PZ [60], AMP/PZ [62], K_2CO_3/PZ [59]). Recently, pure PZ is considered in concentrated aqueous solutions, which can offer up to twice the CO_2 capacity and CO_2 absorption rate of comparable MEA solutions [63]. Additionally, concentrated PZ shows a low degradation tendency [64]. Drawbacks of polyamines include higher solvent costs, high viscosity, which limits the solvent concentration in aqueous solution, and a comparatively high vapour pressure related to larger solvent loss.

Another prominent polyamine is (2-aminoethyl)ethanolamine (AEEA) which also offers a high absorption rate combined with high inherent CO_2 capacity [65, 66]. A proprietary diamine is also considered for CO_2 capture from power plant flue gas in a process that is currently being commercialised [67].

2.2.2 Solutions of alkali salts

In contrast to earth-alkali salts (i.e., magnesium, calcium) which are mostly considered as solid sorbents in so-called carbonate looping processes[2], the solubility of alkali salts such as potassium (K) and sodium (Na) in water is large enough to apply them in aqueous solution as chemical solvents for CO_2 capture from flue gas. Many commercial processes for the removal of carbon dioxide from high-pressure gas use aqueous potassium carbonate (K_2CO_3, potash) solutions. They have gained widespread acceptance for the removal of CO_2 from natural gas and in the production of hydrogen for ammonia synthesis as they are cheap, non-volatile, and non-toxic.

Aqueous alkali salt solutions have a potentially low regeneration heat duty. In addition, the size of the rich-lean heat exchanger can be reduced significantly, if not completely discarded altogether, since absorber and desorber can be operated at similar temperatures [68]. Also the degradation propensity and the price of alkali-based solvents are lower compared to amines. However, CO_2 absorption rates of non-activated aqueous alkali salt solutions are low. For this reason, the pressure of the process gas which is to be treated needs to be increased to about 7 bar [69]. Due to the large flue gas volume flow in coal-fired power plants the compression of the entire gas stream to such pressures is neither technically nor economically feasible. Non-activated alkali salt solutions are therefore not applicable for post-combustion CO_2 capture in power plants.

The activation of potassium carbonate with PZ has proven to be an effective option for decreasing the regeneration duty for CO_2 capture from coal-derived flue gas [70, 71]. Degradation of the activated solvent remains lower than for MEA and the blend exhibits 1.5–3 times higher rates of CO_2 absorption compared with equivalent solutions of MEA [72, 73].

Yet, the use of K/PZ solvent blends may be impaired by potassium sulphate precipitation. The solubility of potassium sulphate in aqueous K/PZ solutions is low. Therefore, the undesired absorption and oxidation of SO_2 to sulphate

[2] For an explanation of such processes refer, for example, to [178].

in the bottom of the absorber may require operation with a slurry of potassium sulphate solids [74].

Other amines can also possibly be used as activators, but primary and secondary amines increase the regeneration heat duty while tertiary and sterically hindered amines only allow for a moderate increase in absorption rate [58].

The proposed concentration of aqueous potassium carbonate is 20–30 wt.-%, because higher concentrations yield the risk of solid precipitation of the absorption product potassium bicarbonate ($KHCO_3$). During the absorption process the CO_2 becomes chemically bound to the potassium carbonate according to the following reaction:

$$K_2CO_3 + H_2O + CO_2 \rightleftarrows 2KHCO_3 \quad . \tag{2.3}$$

Apart from potassium carbonate, sodium carbonate can be used as a potential CO_2 absorbent. There are certain aspects that may make sodium carbonate based systems feasible for CO_2 capture. Sodium carbonate solutions are non-hazardous, non-volatile, and the corrosion rate is low. They are also non-fouling and do not degrade easily [75]. The regeneration heat duty is low, compared with MEA, but the absorption rate of sodium carbonate solutions is rather low. It has been proposed that there is a potential for low regeneration heat duty of sodium-based CO_2 capture if the process allows the presence of solids [76].

2.2.3 Ammonia

A process in which ammonia (NH_3) is used as a solvent is similar to CO_2 capture with organic amines. Both require liquid solutions that chemically react with CO_2 to enhance both CO_2 capacity and mass transfer rate. The schematic of an ammonia-based process is similar to the configuration for CO_2 capture with other solvents (cf. Figure 2.2). The main differences are the possible precipitation of solid salts at temperatures below approximately 80 °C and the relatively high vapour pressure of ammonia which requires regeneration of the solvent at high pressure to minimise solvent slip. The high volatility of ammonia also requires a large washing section at the top of both absorber and desorber. To recover NH_3 from the washing water, additional heat needs to be supplied.

The CO_2 contained in the flue gas is absorbed by the solution mainly by reacting with ammonium carbonate ($(NH_4)_2CO_3$) to form ammonium bicarbonate (NH_4HCO_3) according to:

$$(NH_4)_2CO_3 + CO_2 + H_2O \rightleftarrows 2NH_4HCO_3 \quad . \tag{2.4}$$

If the solubility product of ammonium bicarbonate is exceeded, a fraction of it precipitates in the absorber as a crystalline product [77]. By precipitation of the product, the absorption process is promoted and the CO_2 capacity is increased. However, precipitation of ammonium bicarbonate in the rich solution can lead to plugging of equipment in the lower part of the absorber and in the rich-lean heat exchanger.

The CO_2-rich slurry, consisting mainly of ammonium bicarbonate, is pumped through a heat exchanger to the high-pressure desorber. By pumping the slurry to higher pressure, the power demand for CO_2 compression is reduced. The high viscosity of the CO_2-rich slurry results in a high specific energy consumption of the pumps. At temperatures above approximately 80 °C the ammonium bicarbonate dissolves completely in the solution.

The absorption of CO_2 can either take place under atmospheric conditions (aqueous ammonia) or at low temperature of 0–10 °C (chilled ammonia).

2.2.3.1 Aqueous ammonia

Processes using aqueous ammonia show some promising features for CO_2 capture from flue gas. Some studies claim that the regeneration energy can be reduced significantly in comparison to MEA-based processes [78, 79]. The optimisation potential lies mainly in the high inherent CO_2 capacity of aqueous ammonia solutions. However, the specific loading capacity decreases with increasing solvent concentration [80]. The high possible CO_2 loading of ammonia allows a low solution circulation rate which reduces the regeneration heat duty.

Ammonia is a relatively cheap solvent. YEH AND BAI report a price level for industrial-grade ammonia at one sixth of the price for MEA [77]. Degradation of the solvent due to sulphur dioxide and oxygen present in the flue gas is not expected when aqueous ammonia is used [81]. This leads to benefits in terms of operational costs, since solvent make-up is reduced in comparison to amine-based capture systems. Furthermore, ammonia solutions do not show the corrosive behaviour of partly degraded amine solutions and therefore

allow the use of carbon steels in the capture unit. It is therefore assumed that maintenance costs can be reduced [79].

The low vapour pressure of ammonia and thus its high volatility constitute a challenge for its implementation in CO_2 capture processes. Ammonia slip must be prevented due to its hazardous nature and to keep solvent make-up low. The necessary large water wash sections at the top of the absorber and desorber column result in additional investment costs.

A commercial process based on aqueous ammonia is currently being developed [82].

2.2.3.2 Chilled ammonia

A variation of the aqueous ammonia process is the so-called chilled ammonia process, in which the absorber is kept at a significantly lower temperature. Therefore, the cooler in the flue gas path upstream of the absorber needs to be equipped with an additional chiller to reach the desired temperatures of 0–10 °C. The low temperature and the elimination of most of the water in the flue gas leads to a substantial reduction in volume and mass flow. This is beneficial to the size and energy consumption of the downstream equipment, especially of the ID fan, and also reduces the NH_3 slip to the environment. However, cooling the flue gas is not free of cost. A temperature reduction to 2 °C can consume of up to 2 % of the net output of the power plant [83]. Additionally, lowering the temperature also decreases reaction rates. This effect might require the enlargement of gas-liquid contacting surfaces with a respective adverse impact on absorber size and cost. As a result of the low absorber operating temperature, a reheater may also be required to assure sufficient buoyancy of the vented flue gas [77].

In literature varying statements on the potential of this process can be found. MATHIAS *et al.* claim that the energy requirement of chilled ammonia processes is at best comparable to that of MEA-based processes [84]. DARDE *et al.* claim that chilled ammonia processes allow for a significant reduction of the energy consumption in the desorber [21]. They, however, neglected the additional energy requirement for flue gas cooling and ammonia recovery. BLACK also states that the heat requirement for the regeneration of the CO_2-loaded ammonia solution can be reduced significantly in comparison to an MEA absorption process. Additionally, although a flue gas chiller is needed, the auxil-

iary power of a chilled ammonia plant is expected to be lower than that of a comparable MEA plant due to the smaller ID fan and CO_2 compressor [83, 85].

The chilled ammonia process is currently developed with the aim of commercialisation by 2015 [86]. The potential benefits of both aqueous and chilled ammonia processes remain to be shown in pilot and demonstration plants.

2.2.4 Solutions of amino acid salts

Amino acids contain the same functional groups as amines. Therefore, they can be expected to behave similarly towards carbon dioxide but do not deteriorate in the presence of oxygen [87]. Their reactivity and CO_2 absorption capacity are comparable to aqueous amines of related classes [88, 89, 90]. Although amino acids are more expensive than amines, they have certain unique advantages due to their physical and chemical properties. Aqueous solutions of amino acid salts are found to have better resistance to degradation, especially in the removal of acid gases from oxygen-rich gas streams such as flue gas. Due to the ionic nature of the solutions they also show negligible volatility and higher surface tension [91]. The latter might enable the use of commercially available and cheap polypropylene membranes as an alternative to conventional packing type column internals [92].

A commercial process which proposes a proprietary amino acid salt for CO_2 capture in fossil-fired power plants has been announced recently [93]. Besides the inherent advantages due to the physiochemical properties of amino acid salt solutions, a potential for a significant reduction in regeneration heat duty as well as total energy requirement compared to amine-based processes is mentioned by the manufacturer.

2.2.5 Ionic liquids

Ionic liquids (IL) are organic salts consisting of cations and anions, which are usually liquid at room temperature. Generally, they are non-volatile, thermally stable, and non-flammable. Due to their non-volatility, solvent slip is basically eliminated and IL can be regarded as environmentally benign [94]. IL can be used in pure form and thus do not need to be dissolved in water [95].

Generally IL show relatively good solubility of CO_2, compared with other flue gas components such as nitrogen, oxygen, or carbon monoxide [96, 97]. The

aim is to develop new IL adapted to CO_2 capture by tailoring their specific properties with regard to solubility of CO_2, density, and viscosity. It is possible to design IL with suitable properties by combining appropriate anions and cations and by varying their chain lengths [98]. Regeneration by flashing and stripping with low-temperature steam appears feasible. However, research on IL is at present concentrating on the fundamental understanding of the solubility of different flue gas species.

2.3 Solvent selection

One of the aims of this work is to draw general conclusions for an optimal integration of CO_2 capture processes in steam power plants depending on individual solvent characteristics. As certain solvent groups show similar characteristics, at least one representative solvent of each of the promising solvent groups discussed above is selected for energetic analysis and comparison.

The selection process of a solvent for an industrial CO_2 capture unit is usually done under the consideration of a prerequisite list such as the one shown at the beginning of Section 2.2. For a pre-screening and general energetic comparison as done in this work, there is another criterion to be fulfilled: Measurement data of adequate quality and sufficient quantity must be available. Proprietary solvents such as KS-1 lack this prerequisite and are therefore excluded from the evaluation in this work. Amino acid salts and ionic liquids can also not be considered in this work, as publicly available measurement data for these types of solvents is still scarce.

Once a promising solvent candidate is found, the question of solvent concentration in aqueous solution arises. This quantity is generally limited by the solvent solubility in water, the degradation as well as corrosion tendency, and by the viscosity of the resulting solution. Generally, the larger the solvent concentration in solution, the larger is the inherent CO_2 capacity. Thus, less solution needs to be circulated in an absorption-desorption process when using higher concentrated solutions. However, both degradation tendency and viscosity increase with increasing solvent concentration.

Primary amines: MEA is often regarded as the first chemical solvent to be used in the early large-scale applications of post-combustion CO_2 capture in coal-fired power plants and can therefore be considered as a baseline for all

other solvents. The MEA concentration is limited by the degradation and corrosion tendency. **7 m (30 wt.-%) MEA** is selected for evaluation in this work. Note that MEA at this concentration already requires extensive solvent management such as the addition of inhibitors and low temperature reclaiming.

Polyamines: The available data for polyamines is in general quite limited. Only piperazine (PZ) has been evaluated in more detail. Modelling work indicates that the heat requirement of concentrated PZ solutions is lower than of comparable MEA-based systems [24]. PZ generally shows less corrosive behaviour in comparison to MEA. However, aqueous PZ solutions become highly viscous for concentrations above **8 m (41 wt.-%) PZ,** which is therefore chosen for energetic evaluation in this work.

Sterically hindered amines: A promising hindered amine is 2-piperidineethanol (2-PE). There exists, however, no published data for the CO_2-solubility of 2-PE. So far, this solvent has exclusively been considered in solvent blends with, for example, sulfolane (TMS) [99]. Therefore, the hindered form of MEA, 2-amino-2-methyl-1-propanol (AMP) with a concentration of **4.8 m (30 wt.-%) AMP** is considered in this work.

Alkali salts: Results from pilot plants have shown that the CO_2 absorption rate of an aqueous PZ activated potassium carbonate solution with **5 m (14 wt.-%) K+ / 2.5 m (15 wt.-%) PZ** is 1–1.5 times higher than that of 7 m MEA [100]. Consequently, the application of such solution has the potential for a lower regeneration heat duty than MEA [70, 71].

Amine blends: The use of PZ activated aqueous MDEA solutions was patented as early as 1982 as it proved to be successful when applied in the bulk removal of CO_2 in ammonia plants [101]. The reason for the use of such a blend is related to the high rate of reaction of CO_2 with the activator combined with the advantages of MDEA concerning its inherent CO_2 capacity. The combination leads to higher rates of absorption in the absorber column while maintaining a low heat of regeneration in the desorber column. The concentration of aqueous MDEA/PZ blends is also limited by viscosity issues. In this work a concentration of **7 m (42 wt.-%) MDEA / 2 m (8.6 wt.-%) PZ** is therefore chosen which yields a similar viscosity as 8 m PZ solutions. Recently, the use of AMP with PZ for CO_2 capture has been suggested. Due to the limited availability of CO_2 solubility data for this solvent blend, a concentra-

tion of **5 m (27 wt.-%) AMP / 2.5 m (13 wt.-%) PZ** is selected for evaluation in this work.

For the sake of readability, in the following the selected solvents with the concentrations as stated above are referred to as MEA, PZ, AMP, K/PZ, MDEA/PZ, and AMP/PZ without further notation of the corresponding molality. The six solvents are to be energetically evaluated with respect to the overall power plant process. A model capable of adequately describing the coherences in the absorber and desorber column of the CCU which influence the interface quantities between CCU, power plant, and CO_2 compressor is required. The development of such column model is discussed in the following chapter.

3 SEMI-EMPIRICAL COLUMN MODEL

For the energetic evaluation of chemical solvents in post-combustion CO_2 capture processes, a model is needed which is capable of describing the relevant coherences in the absorber and desorber column. Such column model needs to take into consideration only those effects that influence the overall energy demand of the process.

The core of any column model is a thermodynamic representation of gas and liquid phase of the considered CO_2-H_2O-solvent system depending on pressure and temperature. The vapour-liquid-equilibrium (VLE) of the gas and liquid phase of such systems is important for equilibrium models, such as the one proposed in this work, as well as for more complex rate-based models.

In rigorous models the chemical equilibrium of the liquid phase is commonly represented by a reaction scheme, such as shown in Figure 3.1 for MEA, in combination with the activity-based and temperature dependant equilibrium constants

$$K_r(T) = \prod_i a_i^{\nu_{i,r}} \quad , \tag{3.1}$$

where $\nu_{i,r}$ describes the stoichiometry of species i in reaction r, and where

$$a_i = x_i \, \gamma_i \tag{3.2}$$

is the activity, γ_i is the activity coefficient, and x_i is the mole fraction of species i in the liquid phase.

There exist various approaches to model the activity coefficients. Such models, for example the *electrolyte non-randomness two-liquid model* (ENRTL), consider the ionic interaction forces of the individual species. The model parameters are regressed by fitting the results to extensive measurement data of, for example, CO_2 solubility, speciation, and heat capacity. The regression is a complex task and only a few rigorous models for the most common solvents exist that reproduce measurement data over a wide range of temperature, CO_2 loading, and solvent concentration with a reasonable degree of accuracy.

The composition of the vapour phase can be determined via

$$x_i \, \gamma_i \, f_i^0 = y_i \, \varphi_i^{\vee} \, p_{\text{tot}} \quad , \tag{3.3}$$

where f_i^0 is the standard fugacity[3], which is usually chosen to be the fugacity of the pure liquid for non-supercritical species or the Henry constant for supercritical components such as CO_2, y_i is the mole fraction of species i in the gas phase, and p_{tot} is the total pressure. Non-ideality of the gas phase is represented by the vapour phase fugacity coefficient $\varphi_i^{\vee}$, which can be determined via an equation of state for real gases. Under ideal conditions, $\varphi_i^{\vee}$ as well as the activity coefficient γ_i of species i in the liquid phase become unity while f_i^0 is equal to the vapour pressure of the pure liquid p_i^{s}. In that case, Eq. (3.3) simplifies to Raoult's law

$$x_i \, p_i^{\text{s}} = y_i \, p_{\text{tot}} = p_i \quad , \tag{3.4}$$

where p_i is the partial pressure of species i.

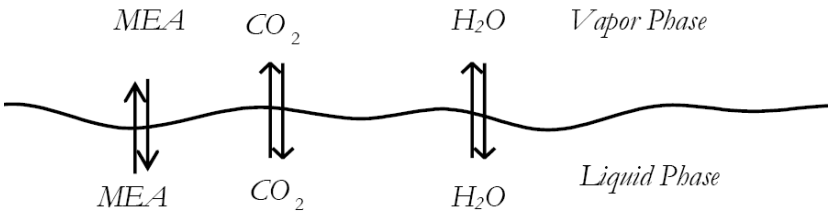

$$H_2O \leftrightarrow H^+ + OH^-$$

$$CO_2 + H_2O \leftrightarrow H^+ + HCO_3^{-1}$$

$$HCO_3^{-1} \leftrightarrow H^+ + CO_3^{-2}$$

$$MEAH^{+1} \leftrightarrow MEA + H^+$$

$$MEACOO^{-1} + H_2O \leftrightarrow MEA + HCO_3^{-1}$$

Figure 3.1: Chemical reaction scheme for CO_2-H_2O-MEA system [7]

[3] The fugacity $f_i \equiv p_{\text{tot}} \, y_i \, \varphi_i = p_i \, \varphi_i$ represents the corrected or effective partial pressure. The fugacity coefficient φ_i can be considered as how closely the substance follows the behavior of an ideal gas.

Due to the novelty of some of the selected solvents, no consistent rigorous thermodynamic model exists that predicts the thermodynamic characteristics of all six CO_2-H_2O-solvent systems with similar accuracy. Therefore, in this work a simplified semi-empirical column model is developed for the specific purpose of an energetic evaluation of chemical solvents for CO_2 capture in power plants. The model is capable of representing each of the six selected solvents based on a consistent set of assumptions and simplifications. The term "semi-empirical" refers to the representation of CO_2 solubility, heat capacity, and density by empirical correlations in which the thermodynamic dependencies of the involved parameters are neglected (cf. Section 3.1).

In the following an equilibrium stage model for the representation of countercurrent flow columns, in which the mass transfer of CO_2 in combination with chemical solvents occurs, is developed. In equilibrium models the column is represented by a series of theoretical stages (cf. Figure 3.2), where the gas and liquid phase leaving the stage (e.g., G(0) and L(2) for stage 0) are assumed to be in phase and temperature equilibrium. Deviations from equilibrium that are observed in real columns can be taken into account by introducing an efficiency factor (e.g., Murphree efficiency).

The semi-empirical column model as well as the standard components such as pumps and heat exchangers in the simulation tool EBSILON®*Professional* require information on certain properties of the CO_2-loaded solution (CO_2 solubility, heat of absorption, heat capacity, density) to determine the quantities which are relevant in the calculation of the overall energy requirement of the CCU. The availability and representation of measurement data of these properties with respect to the selected solvents is discussed in Section 3.1. The implementation of the mass, equilibrium, summation, and enthalpy (MESH) equations that are set up for each stage of the column is discussed in Section 3.2. Finally, the validation of the semi-empirical column model considering measurement data from a multitude of test runs of a CO_2 capture pilot plant is discussed in Section 3.3.

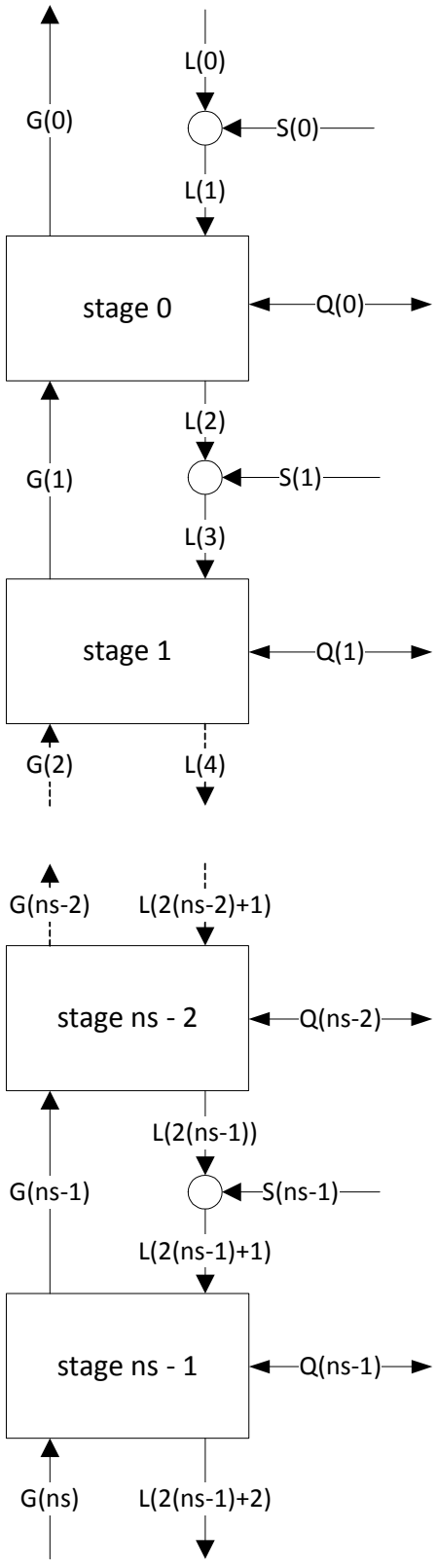

Figure 3.2: Countercurrent flow column model as a series of equilibrium stages

3.1 Solvent properties

The MESH equations of the semi-empirical column model require a variety of quantities that characterise the solvent. These are the CO_2 solubility (expressed as the equilibrium partial pressure p^*_{CO2} as a function of CO_2 loading α and temperature T), the heat of absorption $\Delta h_{abs,CO2}$, the specific heat capacity $C_{p,L}$, and the density ρ. Table 3.1 and Table 3.2 show the available data and correlations of these quantities for the solvents selected in this work.

In rigorous models, the four solvent properties are determined from fundamental thermodynamic relationships. To determine the CO_2 solubility, for example, one must consider the chemical equilibrium which can be represented by an equilibrium reaction scheme in combination with temperature dependant equilibrium constants, an activity coefficient model, and an adequate equation of state.

There exist rigorous thermodynamic models in commercial process simulation tools which claim to adequately predict the thermodynamic characteristics of a CO_2-H_2O-solvent system. These models are of varying degree of detail and accuracy and suffer from different or unclear boundary conditions. In this work the relevant solvent properties are represented by empirical correlations which equate the solvent properties with the temperature, the CO_2 loading, and the solvent concentration. The correlations are derived from measurement data, allowing a fast inclusion of all solvents for which adequate data are available. The derivation of the correlations for the selected solvents is described in the following paragraphs.

Table 3.1: Available data and correlations of CO_2 solubility and heat of absorption for selected solvents

solvent	CO_2 solubility	heat of absorption
MEA	[40, 59, 60]	[102, 103, 65, 104]
PZ	[105, 59, 60]	[104]
AMP	[106, 107, 108, 53, 109, 110, 111]	[38, 104]
K/PZ	[59]	[65, 59, 104]
MDEA/PZ	[112, 113, 61, 114, 115, 116, 117, 118]	[119]
AMP/PZ	[111, 118]	-

Table 3.2: Available data and correlations of heat capacity and density for selected solvents

solvent	heat capacity		density	
	$\alpha = 0$	$\alpha \neq 0$	$\alpha = 0$	$\alpha \neq 0$
MEA	[120, 121, 122]	[123, 59]	[120, 121, 124]	[125, 126]
PZ	[127]	[59, 128]	[58, 129]	[130, 131]
AMP	[122, 132]	-	[133, 124, 134]	[135]
K/PZ	-	[59]	-	[58]
MDEA/PZ	[136]	[137]	[138, 117]	[137]
AMP/PZ	[139]	-	[138, 140]	-

3.1.1 CO_2 solubility

The CO_2 solubility for each solvent at a certain concentration is determined by fitting a function with two variables (temperature and loading) to CO_2 solubility measurement data at a constant solvent concentration: $p^*_{CO2} = f(T, \alpha)$. Due to the nature of this approach, any extrapolation that lies beyond the range of operating parameters for which the correlation is developed is inappropriate.

The derivation of correlations that are not based on thermodynamic coherences suffers from a disadvantage. This approach requires a consistent data set containing various data points at one solvent concentration in the relevant temperature and CO_2 partial pressure range. CO_2 solubility, however, is often reported for changing solvent concentrations in aqueous solution. Such data are applicable for the derivation of a rigorous thermodynamic model, which can account for the variation in solvent concentration. In case of a purely mathematical representation of CO_2 solubility, the consideration of changing solvent concentration would require a correlation with three or (in case of mixed solvents such as e.g., MDEA/PZ) four variables. Therefore, with regard to the aim of this work, only data of solvents with constant solvent concentration can be drawn upon.

For those solvents, in which the main path of CO_2 absorption is the formation of carbamate, the CO_2 solubility, if expressed as the CO_2 partial pressure as a function of the loading and temperature, does not change with the solvent concentration [60]. In the range of CO_2 partial pressures which are relevant in

the case of CO_2 capture from flue gas, only PZ shows a VLE behaviour independent of solvent concentration. For MEA this statement is only true for loadings below 0.5 mol CO_2 / mol alk. In case of the remaining four solvents, for which the formation of carbamate is not the principle mechanism of CO_2 absorption, the solvent concentration significantly influences the VLE behaviour. Consequently, only for PZ all available CO_2 solubility data can be used for the regression of adequate mathematical correlations without the necessity to differentiate the data into blocks of constant solvent concentration. An increase in PZ concentration only increases the specific CO_2 capacity (per kg of solution) but does not influence the relationship between equilibrium CO_2 partial pressure, CO_2 loading, and temperature.

Figure A.1 to Figure A.6 in Annex A.3.1 show the measurement data and the results of the fitted correlations for the CO_2 solubility for the six selected solvents. A polynomial of fourth order with respect to loading and of first order with respect to the reciprocal temperature is applied to achieve a good fit in the relevant CO_2 partial pressure region between 10^0 and 10^5 Pa and the temperature region between 40 and 150 °C:

$$\ln p^*_{CO2} = c_{pco2,0} + c_{pco2,1}\,\frac{1}{T} + c_{pco2,2}\,\alpha + c_{pco2,3}\,\frac{\alpha}{T} + c_{pco2,4}\,\alpha^2 + c_{pco2,5}\,\frac{\alpha^2}{T} + c_{pco2,6}\,\alpha^3 + c_{pco2,7}\,\frac{\alpha^3}{T} + c_{pco2,8}\,\alpha^4\,, \tag{3.5}$$

with p^*_{CO2} in Pa, T in K, and α in mol CO_2 / mol alk (cf. Annex A.2). The coefficients c_{pco2} of Eq. (3.5) as well as the valid operating range for temperature and loading for each of the selected solvents are listed in Table A.1 in Annex A.3.1.

Even ordered polynomials have the disadvantage of a non-monotonically increasing behaviour. This might lead to numerical instabilities when applying numerical methods to solve the non-linear equation system. Such problems are avoided by providing a valid loading and temperature range and by ensuring an adequate initialisation algorithm for all variables (cf. Section 4.4).

For 7 m MEA, Eq. (3.5) is fitted to the most reliable CO_2 solubility data by JOU *et al.* [40]. Additionally, data by HILLIARD and DUGAS are considered, who have complemented the data for those CO_2 partial pressure regions in which the data by JOU are rather sparse [59, 60].

Unlike the CO_2 partial pressure measurements in the MEA system, the PZ system does not show a dependence of amine concentration at higher loadings. This is because the CO_2 loading is not high enough to observe significant quantities of bicarbonate. Since only carbamate is formed, none of the data show an effect of amine concentration when plotted against CO_2 loading [60]. Most of the published data is for lower concentrated PZ solutions (e.g., 2–4 m [114]). Therefore, the correlation is regressed using the data sets by ERMACHTKOV *et al.*, HILLIARD, and DUGAS who measured the CO_2 solubility in solutions with PZ molalities between 0.9 and 12 m [105, 59, 60].

ROBERTS AND MATHER, TENG *et al.*, TONTLWACHWUTHLKUL *et al.,* and YANG *et al.* report on solutions with low concentrations of AMP (2.4–4.1 m) [106, 108, 107, 111]. Higher concentrated solutions with a larger CO_2 capacity are beneficial for CO_2 capture from flue gas. SILKENBÄUMER *et al.* reported on the CO_2 solubility for aqueous solutions with six different concentrations between 2.4 and 6.5 m AMP [109]. The data sets are, however, limited to one temperature per concentration and are therefore not applicable for a consistent correlation regression. Only LI AND CHANG and PARK *et al.* report on more concentrated AMP solutions (30 wt.-% = 4.8 m) that still show a reasonable viscosity and that are therefore applicable for chemical absorption purposes [53, 110]. Note that data points with a CO_2 loading of above 0.55 mol CO_2 / mol AMP by LI AND CHANG are neglected due to the large deviations to the newer measurement data by PARK *et al*.

The most recent data on PZ activated potassium carbonate solutions (K/PZ) are by HILLIARD [59]. In his work HILLIARD noted an inconsistency of the CO_2 solubility data for PZ and K/PZ solvents reported by CULLINANE [58]. The latter are therefore excluded from consideration in this work. A concentration of 5 m K^+ / 2.5 m PZ is chosen as it was suggested that the application of this specific solvent blend leads to a low regeneration heat duty [71, 141, 142].

PZ can also be used as an activator for aqueous MDEA solutions. Plenty of data for this solvent are publicly available. The large amount of available solubility data for this solvent blend is due to the fact that it was patented for sour gas treatment by BASF as early as 1982, referred to as “activated MDEA” or aMDEA® [101]. However, for this solvent most data sets lack consistent measurement series at constant concentrations for a wide range of temperatures and relevant CO_2 partial pressures. Throughout the available data sets, MDEA concentrations vary between 2.0 m and 8.5 m with PZ addition from

zero to as high as 3.5 m PZ (cf. Table 3.1). Therefore, in this work a detour is taken in the regression of adequate coefficients for the representation of CO_2 solubility in 7 m MDEA / 2 m PZ solutions. By applying the symbolic regression tool Eureqa (Version 0.81 [143]) on the newest CO_2 solubility data for MDEA-PZ-H_2O-CO_2 systems by SPEYER *et al.* and VAHIDI *et al.* [116, 117], in which the MDEA molality varies between 1.6 and 10.9 mol MDEA / kg H_2O and the PZ molality varies between 0.2 and 4.1 mol PZ / kg H_2O, the following expression is found, which is capable of representing all 333 data points with a mean relative error of 22.8 %:

$$\begin{aligned}\ln p^*_{CO2} = 2.57051 \\ \cdot \Bigg(& 5.25113\, \bar{m}_{PZ}\, \alpha^{1.74975} + 0.153159\, T \\ & + 14.5209\, \alpha - \bar{m}_{PZ} \\ & - \frac{105994}{7059.57 + 17599\, \bar{m}_{MDEA}\, \alpha} \\ & - 34.0172 \Bigg)^{0.55601} - 2.52615 \end{aligned} \quad . \tag{3.6}$$

with p^*_{CO2} in Pa, T in K, $\bar{m}_i$ in mol i / kg H_2O, and α in mol CO_2 / mol alk (cf. Annex A.2). Eq. (3.6), however, is highly complex and therefore impractical to be used in the equation system as an alternative to the generic polynomial in Eq. (3.5). The complexity of the equation system would be further augmented if the heat of absorption was derived from Eq. (3.6) via the Gibbs-Helmholtz relationship (cf. Section 3.1.2). Therefore, the coefficients of Eq. (3.5) are fitted to the results of Eq. (3.6), substituting solvent concentrations that have been identified to be applicable for CO_2 capture from flue gas ($\bar{m}_{MDEA} = 7$; $\bar{m}_{PZ} = 2$). Figure A.5 in Annex A.3.1 shows the results of the correlation for 7 m MDEA / 2 m PZ and selected measurement data by SPEYER *et al.,* where the MDEA and PZ concentration varies within a narrow range (40 °C: 8.1–8.5 m MDEA / 2.1 m PZ; 80 and 120 °C: 7.6–7.9 m MDEA / 1.9–2.1 m PZ).

Another promising solvent blend is PZ activated AMP. There is, however, only limited publicly available solubility data for this solvent blend. YANG *et al.* report on the solubility of CO_2 in aqueous solutions with an AMP/PZ concentration between 2.6 m / 0.6 m and 5 m / 2.5 m [111]. There seems to be a potential for process improvement in increasing the PZ fraction of the solvent. However, CHEN measured the CO_2 solubility of 4 m AMP / 6 m PZ and experienced precipitation of solid salts at high CO_2 partial pressures and low tem-

peratures [118]. Therefore, the data for 5 m AMP / 2.5 m PZ by YANG *et al.* is selected for evaluation in this work.

3.1.2 Heat of absorption

The published experimental heat of absorption data of chemical solvents in aqueous solutions, which are applicable for CO_2 capture from flue gas is scarce. MATHONAT *et al*. and CARSON *et al.* determined the heat of absorption of CO_2 in aqueous MEA solutions [102, 103]. SCHÄFER *et al.* measured the heat of absorption for CO_2 in mixed solvents including aqueous solutions of 2.2/4.2 m MDEA with 1.6/1.9 m PZ [119]. KIM *et al.* report heat of absorption data for MEA and 2-(aminoethyl)ethanolamine (AEEA) solutions [65]. ARCIS *et al.* measured the enthalpies of absorption of CO_2 in aqueous solutions of AMP [38]. HILLIARD reports measured heat of absorption data for PZ and K/PZ solutions [59]. KIM AND SVENDSEN recently published a comprehensive study on the heats of absorption of a variety of solvents [104].

Of the solvents selected for energetic evaluation in this work, detailed and reliable heat of absorption data at the considered solvent concentration is reported for MEA and K/PZ only. For the other selected solvents the information is yet to be measured in equal quality. To provide for a consistent evaluation and a fair comparison of the six solvents selected in this work and as detailed and reliable data are missing for the majority of the selected solvent systems, in this work the heat of absorption is derived from the CO_2 solubility correlation via the Gibbs-Helmholtz equation:

$$\frac{d(\ln p^*_{CO2})}{d(1/T)} = -\frac{\Delta h_{abs,CO2}}{R} \quad . \tag{3.7}$$

Note that the determination of the heat of absorption via CO_2 solubility data and Eq. (3.7) increases the uncertainty related to the measurement of p^*_{CO2} [65]. The use of CO_2 partial pressure in Eq. (3.7) instead of CO_2 fugacity further increases the uncertainty in the estimated heats of absorption. Nevertheless, taking into consideration the aim of this work to provide for a fair basis of comparison and as long as direct measurement data for the heat of absorption for some of the selected solvents is missing, the use of Eq. (3.7) is the most reasonable option in the estimation of the overall energy requirement for the regeneration of the solution in the desorber.

The correlation for the representation of the equilibrium CO_2 partial pressure p^*_{CO2} in this work is a first order polynomial of the reciprocal temperature (cf. Eq. (3.5)). Therefore, the heat of absorption calculated in this work changes with CO_2 loading and is independent of temperature (cf. Figure A.7 in Annex A.3.2):

$$\Delta h_{\mathrm{abs,CO2}} = -\mathrm{R}\left(\mathrm{c}_{\mathrm{pco2,1}} + \mathrm{c}_{\mathrm{pco2,3}}\,\alpha + \mathrm{c}_{\mathrm{pco2,5}}\,\alpha^2 + \mathrm{c}_{\mathrm{pco2,7}}\,\alpha^3\right) \quad , \tag{3.8}$$

with $\Delta h_{\mathrm{abs,CO2}}$ in J / mol CO_2 and α in mol CO_2 / mol alk (cf. Annex A.2).

3.1.3 Heat capacity

The regularly stated assumption that the specific heat capacity does not vary significantly among various solvents in aqueous solution is not true as shown in Figure A.8 and Figure A.9 in Annex A.3.3. For an accurate estimation of the regeneration energy requirement, the solution heat capacity must be considered in detail since it strongly depends on the solvent type, composition, temperature, and CO_2 loading.

Heat capacity data and correlations are available for all of the selected solvents (cf. Table 3.2), where the focus of most of the studies is unloaded solutions. The heat capacity, however, strongly depends on the CO_2 loading and solvent concentration. Generally, the heat capacity is a decreasing function of CO_2 loading and a higher alkaline concentration leads to greater sensitivity to the CO_2 content [123].

The heat capacity of CO_2-loaded solutions in this work is described by a modified equation based on an expression by HILLARD [59]:

$$\begin{aligned} C_{\mathrm{p,L}} = {} & \mathrm{c}_{\mathrm{Cp,0}} + \mathrm{c}_{\mathrm{Cp,1}}\,t + \mathrm{c}_{\mathrm{Cp,2}}\,t^2 + \mathrm{c}_{\mathrm{Cp,3}}\,\alpha + \mathrm{c}_{\mathrm{Cp,4}}\,\alpha^2 + \mathrm{c}_{\mathrm{Cp,5}}\,\bar{m}_{\mathrm{alk}} \\ & + \mathrm{c}_{\mathrm{Cp.6}}\,\bar{m}^2_{\mathrm{alk}} + \mathrm{c}_{\mathrm{Cp,7}}\,t\,\alpha + \mathrm{c}_{\mathrm{Cp,8}}\,t\,\bar{m}_{\mathrm{alk}} \\ & + \mathrm{c}_{\mathrm{Cp,9}}\,\alpha\,\bar{m}_{\mathrm{alk}} + \mathrm{c}_{\mathrm{Cp,10}}\,t\,\alpha\,\bar{m}_{\mathrm{alk}} \quad , \end{aligned} \tag{3.9}$$

with $C_{\mathrm{p,L}}$ in J / (kg K), α in mol CO_2 / mol alk, $\bar{m}_{\mathrm{alk}}$ in mol alk / kg H_2O, and where the liquid temperature t is given in Celsius rather than in Kelvin:

$$t = \frac{T}{\mathrm{K}} - 273.15 \quad . \tag{3.10}$$

The coefficients c_{Cp} of Eq. (3.9) for the selected solvents are shown in Table A.2 in Annex A.3.3.

For CO_2-loaded MEA and PZ solutions, heat capacity data with a wide range of concentrations (3.5–7 m MEA [59]; 3.6–11 m PZ [59, 128]), temperatures (40–120 °C) and CO_2 loadings are available. For K/PZ and MDEA/PZ the correlation for the representation of $C_{p,L}$ is regressed to represent the blend compositions that are considered in this work [59, 137]. There is a lack of $C_{p,L}$ data for CO_2-loaded 4.8 m AMP and 5 m AMP / 2.5 m PZ solutions. Since AMP represents the hindered form of MEA, the correlations for MEA and MEA/PZ are used for the AMP and AMP/PZ solvents, respectively, adapting $c_{Cp,0}$ so that the heat capacity at zero loading is equivalent to the corresponding data by CHEN *et al.* [132, 139].

3.1.4 Density

Although physical properties of the CO_2-H_2O-solvent system such as the density, viscosity, or surface tension are not part of the equilibrium calculations for the gas and liquid phase, information on the density is needed to calculate the power demand of the solution pumps.

Density is represented by an equation similar to Eq. (3.9) for the calculation of the specific heat capacity of the solution. However, eight coefficients are sufficient to represent the available measurement data in satisfactory accuracy:

$$\rho = c_{dens,0} + c_{dens,1}\, t + c_{dens,2}\, t^2 + c_{dens,3}\, \alpha + c_{dens,4}\, \alpha^2 + c_{dens,5}\, \bar{m}_{alk} + c_{dens.6}\, \bar{m}_{alk}^2 + c_{dens,7}\, \alpha\, \bar{m}_{alk} \quad . \tag{3.11}$$

with ρ in kg / m³, α in mol CO_2 / mol alk, and $\bar{m}_{alk}$ in mol alk / kg H_2O. The coefficients c_{dens} of Eq. (3.11) for the selected solvents are shown in Table A.3 in Annex A.3.4.

The coefficients of Eq. (3.11) for MEA and PZ are fitted to available measurement data for CO_2-loaded solutions. For the other four selected solvents, little measurement data are available and an individual approach to represent the density of these solvents in aqueous solutions must be taken. To model the density of AMP solutions, $c_{dens,0}$ is adapted to fit the four data points of 4.5 m AMP solutions at 20 °C with a loading between zero and 0.4 mol CO_2 / mol AMP by GABRIELSEN [135]. The correlation is then used with $\bar{m}_{alk} = 4.8$. The coefficients for 5 m K^+ / 2.5 m PZ are regressed to reproduce the results of the density correlation given by CULLINANE in the given tempera-

ture and loading range [58]. The coefficients for MDEA/PZ are regressed to reproduce the results of the density correlation given by FRAILIE [137]. For an estimation of the influence of the CO_2 loading on AMP/PZ solutions, the first three coefficients of the correlation for MEA with $\bar{m}_{alk} = \bar{m}_{alk,AMP} + \bar{m}_{alk,PZ} =$ 6.9 mole CO_2 per mole alkali[4] are adapted to fit the measurement data of PAUL AND MANDAL for unloaded 2.88 m AMP / 1.99 m PZ solutions [138]. The correlation is then used with $\bar{m}_{alk} = 10$ to represent 5 m AMP / 2.5 m PZ.

3.2 Implementation

The semi-empirical column model in this work is based on a desorber model by OYENEKAN [144] but is modified and extended in the following points:

- To ensure an adequate representation of the absorber, nitrogen is considered as third species in the gas phase.
- The representation of the partial pressure of water takes into account the mole fraction of water in solution.
- The heat capacity of the selected solvents is represented as a function of temperature and CO_2 loading.
- The heat of vaporisation of water is considered as a function of temperature.
- Correlations for the representation of the vapour-liquid-equilibrium of the system CO_2-H_2O-solvent are modified and extended to the solvents selected for evaluation in this work.

Each stage in the equilibrium stage series (cf. Figure 3.2) has a numerous number of input and output variables as shown in Figure 3.3. These variables are used to set up the MESH equations for the overall column model.

For the representation of the equation system, three index variables are defined. The index variable j represents the ns stages in the series:

$$j = \{0 \,..\, (ns - 1)\} \quad .$$

[4] One mole of PZ contains two mole of alkali components (cf. Annex A.2).

The index variable k is used for the representation of equations which describe coherences that are valid for the $2ns + 1$ liquid streams:

$$k = \{0 \,..\, 2ns\} \quad .$$

Finally, equations that are set up for each of the $ns + 1$ gas streams use the index variable l:

$$l = \{0 \,..\, ns\} \quad .$$

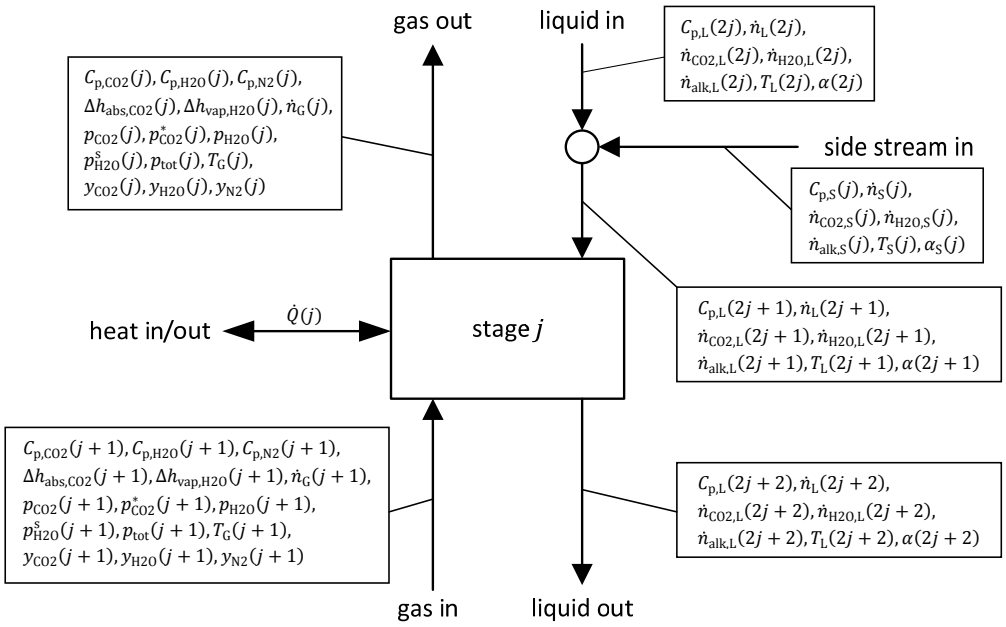

Figure 3.3: Input and output variables of equilibrium stage

3.2.1 Mass balance, equilibrium, and summation equations

Each liquid and each side stream is assumed to consist of CO_2, H_2O, and alkali fraction only. The physical solution of additional gas components such as nitrogen, oxygen, or argon is neglected as it plays a minor role for the overall energetic evaluation. The solution of flue gas pollutants such as NO_x and SO_x, which might chemically react with the solvent, is also neglected due to the complex nature of heat stable salt formation. This simplification is reasonable, if it is assumed that NO_x and SO_x concentrations are reduced to (solvent

dependant) acceptable levels by adequate measures (improved FGD and SCR, polisher unit with NaOH). Solvent vaporisation is neglected as it can be assumed that for the selected solvents, which show comparably low vapour pressures, only small amounts migrate into the gas phase. Solvent slip to the environment might pose a challenge in terms of operational costs for solvent make-up as well as with regard to legal and environmental issues, but it has a negligible impact on the overall energetic evaluation.

The composition of liquid and side streams is defined by a summation equation and the definition of loading α that describes the molar ratio of CO_2 to the alkali component in the solution:

$$\dot{n}_{\mathrm{L}}(k) = \dot{n}_{\mathrm{CO2,L}}(k) + \dot{n}_{\mathrm{H2O,L}}(k) + \dot{n}_{\mathrm{alk,L}}(k) \quad , \tag{3.12}$$

$$\dot{n}_{\mathrm{S}}(j) = \dot{n}_{\mathrm{CO2,S}}(j) + \dot{n}_{\mathrm{H2O,S}}(j) + \dot{n}_{\mathrm{alk,S}}(j) \quad , \tag{3.13}$$

$$\alpha(k) = \frac{\dot{n}_{\mathrm{CO2,L}}(k)}{\dot{n}_{\mathrm{alk,L}}(k)} \quad , \tag{3.14}$$

$$\alpha_{\mathrm{S}}(j) = \frac{\dot{n}_{\mathrm{CO2,S}}(j)}{\dot{n}_{\mathrm{alk,S}}(j)} \quad . \tag{3.15}$$

The mixing of side and liquid streams is considered by

$$\dot{n}_{\mathrm{CO2,L}}(2j+1) = \dot{n}_{\mathrm{CO2,L}}(2j) + \dot{n}_{\mathrm{CO2,S}}(j) \quad , \tag{3.16}$$

$$\dot{n}_{\mathrm{H2O,L}}(2j+1) = \dot{n}_{\mathrm{H2O,L}}(2j) + \dot{n}_{\mathrm{H2O,S}}(j) \quad , \tag{3.17}$$

$$\dot{n}_{\mathrm{alk,L}}(2j+1) = \dot{n}_{\mathrm{alk,L}}(2j) + \dot{n}_{\mathrm{alk,S}}(j) \quad . \tag{3.18}$$

Since solvent vaporisation is neglected, the mole flow of alkali fraction in the liquid phase is constant and the total pressure of gas stream is simply the sum of the partial pressures of CO_2 and H_2O:

$$\dot{n}_{\mathrm{alk,L}}(2j+2) = \dot{n}_{\mathrm{alk,L}}(2j+1) \quad , \tag{3.19}$$

$$p_{\mathrm{tot}}(l) = p_{\mathrm{CO2}}(l) + p_{\mathrm{H2O}}(l) \quad . \tag{3.20}$$

Since an ideal gas phase is assumed, the partial pressures of CO_2 and H_2O are the product of the corresponding mole fraction and the total pressure:

$$p_{\mathrm{CO2}}(l) = y_{\mathrm{CO2}}(l)\, p_{\mathrm{tot}}(l) \quad , \tag{3.21}$$

$$p_{\mathrm{H2O}}(l) = y_{\mathrm{H2O}}(l)\, p_{\mathrm{tot}}(l) \quad . \tag{3.22}$$

In addition, an ideal liquid phase is assumed. Therefore, the partial pressure of water in the gas phase is the product of H_2O mole fraction in the liquid

phase x_{H2O} and the saturation vapour pressure $p^{\mathrm{s}}_{\mathrm{H2O}}$ (q.v. Eqs. (3.3) and (3.4)):

$$p_{\mathrm{H2O}}(j) = x_{\mathrm{H2O}}(2j+2)\, p^{\mathrm{s}}_{\mathrm{H2O}}(j) = \frac{\dot{n}_{\mathrm{H2O,L}}(2j+2)}{\dot{n}_{\mathrm{L}}(2j+2)}\, p^{\mathrm{s}}_{\mathrm{H2O}}(j)\,. \tag{3.23}$$

The saturation vapour pressure of water is calculated by applying a correlation from the DIPPR database [144]:

$$\begin{aligned}\ln(p^{\mathrm{s}}_{\mathrm{H2O}}(j)/\mathrm{Pa}) &\\ = 73.649 &- \frac{7258.2}{T_{\mathrm{G}}(j)/\mathrm{K}} - 7.3037\ln(T_{\mathrm{G}}(j)/\mathrm{K}) + 4.1653 \\ &\cdot 10^{-6}\,(T_{\mathrm{G}}(j)/\mathrm{K})^2 \quad .\end{aligned} \tag{3.24}$$

The equilibrium CO_2 partial pressure is determined by an empirical correlation, which links this quantity to the temperature T and the CO_2 loading α of the liquid stream leaving the stage (q.v. Section 3.1.1 and Eq. (3.5)):

$$\begin{aligned}\ln p^{*}_{\mathrm{CO2}}(j) = {} & \mathrm{c}_{\mathrm{pco2,0}} + \mathrm{c}_{\mathrm{pco2,1}}\,\frac{1}{T_{\mathrm{L}}(2j+2)} + \mathrm{c}_{\mathrm{pco2,2}}\,\alpha(2j+2) \\ & + \mathrm{c}_{\mathrm{pco2,3}}\,\frac{\alpha(2j+2)}{T_{\mathrm{L}}(2j+2)} + \mathrm{c}_{\mathrm{pco2,4}}\,\alpha(2j+2)^2 \\ & + \mathrm{c}_{\mathrm{pco2,5}}\,\frac{\alpha(2j+2)^2}{T_{\mathrm{L}}(2j+2)} + \mathrm{c}_{\mathrm{pco2,6}}\,\alpha(2j+2)^3 \\ & + \mathrm{c}_{\mathrm{pco2,7}}\,\frac{\alpha(2j+2)^3}{T_{\mathrm{L}}(2j+2)} + \mathrm{c}_{\mathrm{pco2,8}}\,\alpha(2j+2)^4 \quad ,\end{aligned} \tag{3.25}$$

with p^{*}_{CO2} in Pa, T_{L} in K, and α in mol CO_2 / mol alk (cf. Annex A.2). The coefficients $\mathrm{c}_{\mathrm{pco2}}$ of Eq. (3.25) for the selected solvents are given in Table A.1 in Annex A.3.1.

In case of CO_2 absorption from flue gas with reasonable fast solvents, the desorber can be represented by equilibrium stages (q.v. Section 3.3). The departure from equilibrium in the absorber, thus the difference between the actual CO_2 partial pressure in the gas phase p_{CO2} and the equilibrium partial pressure p^{*}_{CO2}, can be accounted for by the Murphree efficiency η_{m}:

$$p_{\mathrm{CO2}}(j) = p_{\mathrm{CO2}}(j+1) + (\eta_{\mathrm{m}}(j) \cdot [p^{*}_{\mathrm{CO2}}(j) - p_{\mathrm{CO2}}(j+1)]) \quad . \tag{3.26}$$

3.2.2 Enthalpy balance equations

An enthalpy balance is set up for each stage taking into consideration the heat of vaporisation of gaseous H_2O ($\Delta h_{\mathrm{vap,H2O}}$), the heat of absorption of CO_2 ($\Delta h_{\mathrm{abs,CO2}}$), the sensible heat of the liquid ($C_{\mathrm{p,L}}$), and the sensible heat of the species in the gas phase H_2O, CO_2, and N_2 ($C_{\mathrm{p,H2O}}, C_{\mathrm{p,CO2}}, C_{\mathrm{p,N2}}$). Additionally, a heat stream $\dot{Q}$ can be rejected from or added to the stage. As the vaporisation of solvent is neglected, the heat of vaporisation of the solvent is not taken into consideration in the energy balance:

$$\begin{aligned}
\dot{n}_{\mathrm{G}}(j+1)\ \Big[& y_{\mathrm{H2O}}(j+1)\left(\Delta h_{\mathrm{vap,H2O}}(j+1)\right. \\
& \left. + C_{\mathrm{p,H2O}}(j+1)\,(T_{\mathrm{G}}(j+1) - T_{\mathrm{ref}})\right) \\
& + y_{\mathrm{CO2}}(j+1)\ \left(\Delta h_{\mathrm{abs,CO2}}(j+1)\right. \\
& \left. + y_{\mathrm{N2}}\, C_{\mathrm{p,N2}}(j+1)\,(T_{\mathrm{G}}(j+1) - T_{\mathrm{ref}})\right) \\
& + y_{\mathrm{N2}}(j+1)\, C_{\mathrm{p,N2}}(j+1)\,(T_{\mathrm{G}}(j+1) - T_{\mathrm{ref}})\Big] \\
& + \dot{n}_{\mathrm{L}}(2j+1)\, C_{\mathrm{p,L}}(2j+1)\,(T_{\mathrm{L}}(2j+1) - T_{\mathrm{ref}}) + \dot{Q}(j) \\
= \dot{n}_{\mathrm{G}}(j)\ \Big[& y_{\mathrm{H2O}}(j)\ \left(\Delta h_{\mathrm{vap,H2O}}(j)\right. \\
& \left. + C_{\mathrm{p,H2O}}(j)\,(T_{\mathrm{G}}(j) - T_{\mathrm{ref}})\right) \\
& + y_{\mathrm{CO2}}(j)\ \left(\Delta h_{\mathrm{abs,CO2}}(j) + C_{\mathrm{p,CO2}}(j)\,(T_{\mathrm{G}}(j) - T_{\mathrm{ref}})\right) \\
& + y_{\mathrm{N2}}(j)\, C_{\mathrm{p,N2}}(j)\,(T_{\mathrm{G}}(j) - T_{\mathrm{ref}})\Big] \\
& + \dot{n}_{\mathrm{L}}(2j+2)\, C_{\mathrm{p,L}}(2j+2)\,(T_{\mathrm{L}}(2j+2) - T_{\mathrm{ref}})\ \ ,
\end{aligned} \tag{3.27}$$

with

$$T_{\mathrm{ref}} = 298.15\ \mathrm{K}\ \ . \tag{3.28}$$

By definition the leaving gas and liquid streams of each stage are in thermal equilibrium:

$$T_{\mathrm{G}}(j) = T_{\mathrm{L}}(2j+2)\ \ . \tag{3.29}$$

The heat of absorption of CO_2 in this work is determined via the CO_2 solubility correlation and the Gibbs-Helmholtz relationship as discussed in Section 3.1.2:

$$\begin{aligned}
\Delta h_{\mathrm{abs,CO2}}(j) = -\mathrm{R}\,\big(& \mathrm{c}_{\mathrm{pco2,1}} + \mathrm{c}_{\mathrm{pco2,3}}\,\alpha(2j+2) \\
& + \mathrm{c}_{\mathrm{pco2,5}}\,\alpha(2j+2)^2 + \mathrm{c}_{\mathrm{pco2,7}}\,\alpha(2j+2)^3\big)\ \ ,
\end{aligned} \tag{3.30}$$

with $\Delta h_{\text{abs,CO2}}$ in J / mol CO_2 and α in mol CO_2 / mol alk (cf. Annex A.2). The heat of vaporisation of water as a function of temperature is determined via an equation from the Physical Property Data Service with coefficients from the Dortmund Data Bank [145]:

$$\Delta h_{\text{vap,H2O}}(j) = \text{R}\, T_{\text{c}} \Big(5.6297\, \tau(j)^{\frac{1}{3}} + 13.962\, \tau(j)^{\frac{2}{3}} - 11.673\, \tau(j) + 2.1784\, \tau(j)^2 - 0.31666\, \tau(j)^6 \Big) , \tag{3.31}$$

with $\Delta h_{\text{vap, H2O}}$ in J / mol H_2O, where $T_{\text{c}} = 647.3$ K is the critical temperature of water, and

$$\tau(j) = 1 - \frac{T_{\text{G}}(j)}{T_{\text{c}}} \qquad \forall\ T_{\text{G}}(j) = \{273.0\,..\,647.0\ \text{K}\}\ . \tag{3.32}$$

The mixing of side streams to the liquid streams is accounted for by

$$\dot{n}_{\text{L}}(2j)\, C_{\text{p,L}}(2j)\, (T_{\text{L}}(2j) - T_{\text{ref}}) + \dot{n}_{\text{S}}(2j)\, C_{\text{p,S}}(2j)\, (T_{\text{S}}(j) - T_{\text{ref}}) = \dot{n}_{\text{L}}(2j+1)\, C_{\text{p,L}}(2j+1)\, (T_{\text{L}}(2j+1) - T_{\text{ref}})\,. \tag{3.33}$$

The molar specific heat capacities of liquid and side streams $C^{\text{m}}_{\text{p,L/S}}$ depend on solvent type and concentration, temperature, and CO_2 loading. They can be calculated via the mass-specific heat capacity $C_{\text{p,L/S}}$ of CO_2-loaded solutions which was discussed in Section 3.1.3:

$$C^{\text{m}}_{\text{p,L}}(k) = M_{\text{sol,L}}(k)\, C_{\text{p,L}}(k)\,, \tag{3.34}$$

$$C^{\text{m}}_{\text{p,S}}(j) = M_{\text{sol,S}}(j)\, C_{\text{p,S}}(j)\,, \tag{3.35}$$

with

$$M_{\text{sol,L}}(k) = \frac{\dot{n}_{\text{CO2,L}}(k)\, M_{\text{CO2}} + \dot{n}_{\text{H2O,L}}(k)\, M_{\text{H2O}} + \dot{n}_{\text{alk,L}}(k)\, M_{\text{alk}}}{\dot{n}_{\text{L}}(k)}\ , \tag{3.36}$$

$$M_{\text{sol,S}}(j) = \frac{\dot{n}_{\text{CO2,S}}(j)\, M_{\text{CO2}} + \dot{n}_{\text{H2O,S}}(j)\, M_{\text{H2O}} + \dot{n}_{\text{alk,S}}(j)\, M_{\text{alk}}}{\dot{n}_{\text{S}}(j)}\ , \tag{3.37}$$

where M_{sol}, M_{CO2}, M_{H2O}, and M_{alk} are the molar weights of the total solution, CO_2, H_2O, and alkali fraction, respectively.

The heat capacities of the species in the gas phase (CO_2, H_2O, N_2) are determined via the DIPPR equation 107 by ALY AND LEE, where the coefficients c_{Cp} as shown in Table 3.3 are taken from the Aspen Properties data base [146, 147]:

$$\begin{aligned} C_{\mathrm{p},i}^{\mathrm{m}}(j)/(\mathrm{J}/(\mathrm{mol\,K})) \\ = c_{\mathrm{Cp},i,0} + c_{\mathrm{Cp},i,1}\left(\frac{\frac{c_{\mathrm{Cp},i,2}}{T_{\mathrm{G}}(j)/\mathrm{K}}}{\sinh\left(\frac{c_{\mathrm{Cp},i,2}}{T_{\mathrm{G}}(j)/\mathrm{K}}\right)}\right)^2 \\ + c_{\mathrm{Cp},i,3}\left(\frac{\frac{c_{\mathrm{Cp},i,4}}{T_{\mathrm{G}}(j)/\mathrm{K}}}{\cosh\left(\frac{c_{\mathrm{Cp},i,4}}{T_{\mathrm{G}}(j)/\mathrm{K}}\right)}\right)^2, \end{aligned} \tag{3.38}$$

with $i = \{\mathrm{CO2},\mathrm{H2O},\mathrm{N2}\}$.

Table 3.3: Coefficients and validity range to determine the molar heat capacity of ideal gas components CO_2, H_2O, and N_2

i	CO2	H2O	N2
$c_{\mathrm{Cp},i,0}$	29.37	33.363	29.105
$c_{\mathrm{Cp},i,1}$	34.54	26.79	8.6149
$c_{\mathrm{Cp},i,2}$	1428	2610.5	1701.6
$c_{\mathrm{Cp},i,3}$	26.4	8.896	0.1034
$c_{\mathrm{Cp},i,4}$	588	1169	909.79
T_{min} / K	50	100	50
T_{max} / K	5000	22731	1500

3.3 Model validation

The equation system outlined above is capable of representing any countercurrent flow column, provided that the empirical correlations are valid within the range of parameters for which the model is applied. Before the semi-empirical column model is used for an energetic evaluation of chemical solvents for post-combustion CO_2 capture processes, it is validated by comparing the model results to measurement data from a pilot plant.

CO_2 capture units for coal-fired steam power plants do not yet exist at industrial scale. Today only around a dozen pilot plants separate CO_2 from coal-derived flue gas with a capacity of up to 10 tonnes per hour. Demonstration plants of larger scale are at the planning stage. Consequently, the availability of public measurement data from CO_2 capture units which are adequate for a model validation is limited. Published data often lack the required degree of detail to provide for the necessary input to the model.

Detailed results of test campaigns of a CO_2 capture pilot plant which is located at the Esbjerg power station in Denmark have recently been published [148, 149]. The pilot plant with a capacity of 1 tonne CO_2 per hour was installed as part of the EU project CASTOR (CO_2 from Capture to Storage) [150]. The pilot plant has been revamped by the follow-up project CESAR (CO_2 Enhanced Separation and Recovery) under which it is presently being operated [151].

In the following, the semi-empirical column model developed in this work is validated by comparing results to experimental data from nine test runs in two test campaigns where an aqueous 7 m (30 wt.-%) monoethanolamine (MEA) solution was used. In the first campaign, the flow rate of the lean solution to the absorber was optimised with respect to a minimal reboiler heat duty; in the second campaign the pressure of the desorber was varied between atmospheric pressure and 2.2 bar.

The model validation is done by separately considering the absorber and the desorber. This is necessary as the performance determining mechanisms in absorber and desorber column fundamentally differ from each other. In general, the driving force for the mass transfer of a species from the gas phase into the liquid phase (absorber) or vice versa (desorber) is the difference in actual partial pressure in the gas phase ($p_{\mathrm{CO2,g}}$) and equilibrium partial pressure with respect to the (bulk) liquid phase ($p^{*}_{\mathrm{CO2,l}}$) of that species. The resulting mole flux (N_{CO2}) is determined by multiplying the driving force with the overall mass transfer coefficient K_{g}.The flux equation can also be written using the liquid film mass transfer coefficient[5] k'_{g} [60]. In this case, the partial

[5] Note that the index "g" denotes the definition of the liquid film mass transfer coefficient k'_{g} in gas film units.

pressure at the gas-liquid interface ($p_{CO2,int}$) is used in the definition of the driving force:

$$N_{CO2} = K_g \left(p_{CO2,g} - p^*_{CO2,l}\right) = k'_g \left(p_{CO2,int} - p^*_{CO2,l}\right) \ . \qquad (3.39)$$

Table 3.4 shows the experimentally measured values for k'_g at an equilibrium CO_2 partial pressure of 5 kPa and 40 °C for five of the six selected solvents. There are no equivalent measurements for 5 m AMP / 2.5 m PZ, but experiments with 4 m AMP / 6 m PZ suggest that the mass transfer coefficient for the AMP/PZ composition selected in this work is in the order of magnitude of the other five selected solvents [152].

Table 3.4: Liquid film mass transfer coefficient at equilibrium CO_2 partial pressure of 5 kPa and 40 °C [153]

solvent	k'_g (10^{-7} mol) / (m^2 Pa s)
7 m MEA	3.1
8 m PZ	5.3
4.8 m AMP	1.7
5 m K^+ / 2.5 m PZ	4.0
7 m MDEA / 2 m PZ	5.2

In phase equilibrium the actual CO_2 partial pressure at the gas-liquid interface is equal to the equilibrium CO_2 partial pressure; therefore, the driving force and consequently the mass transfer becomes zero. Equilibrium is never reached in the columns of any real process. Yet, the approach to such conditions is referred to as an *equilibrium pinch* denoting the reduction of driving force and mass transfer of a certain species to a minimum.

In an absorber column of a CO_2 capture process an equilibrium pinch is usually not present and the driving force is well distributed through the entire packing height [154]. The main delimiting factor for an absorber is instead the reduced concentration of free solvent under rich conditions (i.e., towards the bottom of the absorber), which reduces the reaction rates and ultimately the liquid film mass transfer coefficient k'_g. Such condition is called a *rate pinch*; in the case of an absorber this means that a significant part of the packing contributes very little to the absorption and to the desired increase in CO_2 loading of the liquid phase [154]. The occurrence of a rate pinch is enhanced

by low temperatures, which reduce both the reaction rate and the diffusion of educts and products through the phases.

Regeneration of the solution in the desorber of a CCU is commonly performed under pressure and thus at elevated temperatures. Provided that a fast solvent with a high mass transfer coefficient is used, the temperatures in the desorber are usually sufficient to provide for high diffusion and reaction rates. In this case the performance of the column is determined by the vapour-liquid-equilibrium of the CO_2-H_2O-solvent system. Consequently, the heat which must be provided in the reboiler depends mainly on the required stripping steam to overcome an equilibrium pinch in the desorber column (cf. Section 5.1.2).

The difference in the performance determining mechanisms of absorber and desorber (rate pinch vs. equilibrium pinch) requires two different methodologies for the validation of the semi-empirical column model. Table 3.5 shows the main input parameters of the pilot plant that were varied during the nine runs of the two test campaigns. The data from run 6 through 9 is only used in combination with the desorber, as the operating conditions for the absorber in these four runs were practically constant.

Table 3.5: Main input parameters of pilot plant runs for model validation [148, 149]

run	solution flow m^3/s	desorber pressure kPa	run used for absorber	run used for desorber
1	23.0	181	x	x
2	19.0	181	x	x
3	16.7	181	x	x
4	14.8	181	x	x
5	12.5	181	x	x
6	15.0	216		x
7	15.5	181		x
8	17.0	143		x
9	19.0	112		x

3.3.1 Absorber

Table 3.6 shows a list of input parameters which are fixed for the five test runs used with the absorber model. The input parameters are set to the published measurement values as shown in Table A.4 in Annex A.4.

Table 3.6: Input parameters of absorber for model validation

component / stream	parameter
absorber column	CO_2 concentration profile, column pressure (bottom), pressure drop over column height
washing section	outlet gas temperature
lean solution at absorber inlet (top)	temperature, composition (CO_2 loading, MEA molality), flow
flue gas at absorber inlet (bottom)	temperature, composition, flow

As the temperature and concentration profile over the absorber column height is rate-determined, phase equilibrium between the gas and liquid outlet streams of the individual stages can no longer be assumed. The Murphree efficiencies are therefore different from unity (cf. Eq. (3.26)). In multicomponent reactive absorption systems the Murphree efficiencies can vary between negative and positive infinity and strongly depend on the considered solvent, the conditions in the column such as gas and liquid load, and the temperature and concentration profile over the column height [155, 156, 157]. Therefore, in the context of the validation of the semi-empirical column model the equation system is solved by fixing the CO_2 concentration profile and leaving the Murphree efficiencies as variables. The latter can be determined for each stage via Eq. (3.26) using the calculated equilibrium CO_2 partial pressure (model result) and the actual CO_2 partial pressure (experiment).

As the ratio of actual CO_2 partial pressure and equilibrium CO_2 partial pressure is no longer fixed, the choice of the number of theoretical stages in the context of model validation represents the level of discretisation rather than a criterion for the absorption efficiency of the column. The number of chosen stages must provide for an adequate consideration of the change in variables, in particular for concentration and temperature profiles over the column height. For the model validation the absorber is represented by 21 stages, where temperature equilibrium of gas and liquid stream leaving each stage is still assumed.

The McCabe-Thiele diagram of the absorber with a solution flow rate of 14.8 m^3/s (run 4) shows a rate pinch at the rich end (bottom) of the absorber (cf. Figure 3.4). Despite a large driving force (distance of equilibrium and bal-

ance line), equilibrium is not reached and the lower stages contribute little to the overall absorption.

Figure 3.5 shows the temperature profile over the absorber column height. The calculated temperature profile agrees well with the measurement data, indicating a good representation of the calorimetric coherences by the model. Note that each stage does not necessarily represent the same packing height. In chemical absorption processes the height equivalent to a theoretical stage (HETS), which represents the required packing height to achieve the absorption efficiency of one equilibrium stage, depends strongly on the solvent and on operational parameters (temperature, pressure, gas and liquid load). Therefore, equilibrium stage models are not capable of accurately describing the composition and temperature profiles over the height of a rate-determined packed column and are inadequate for design purposes. For such tasks more detailed rate-based models are needed.

It is notable from Figure 3.5 that the model results would fit the measurement data if the temperature profile was distorted towards the top of the column. This could suggest that the stages at the top of the absorber represent lower packing heights equivalent to increasing HETS values from the top to the bottom stage. The calculated Murphree efficiencies, which decrease from the top to the bottom as shown in Figure 3.6, underline this hypothesis.

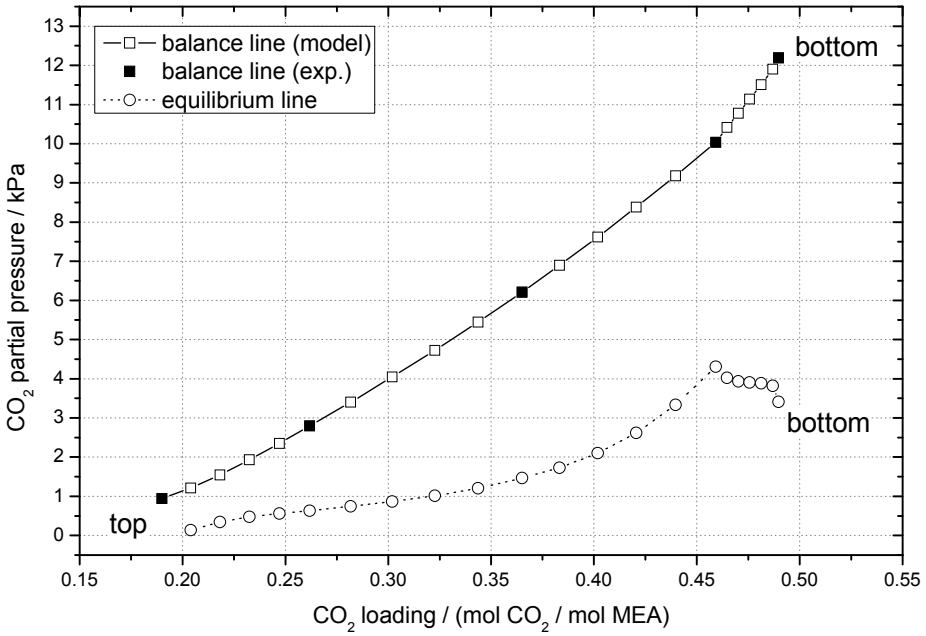

Figure 3.4: McCabe-Thiele diagram of absorber for run 4

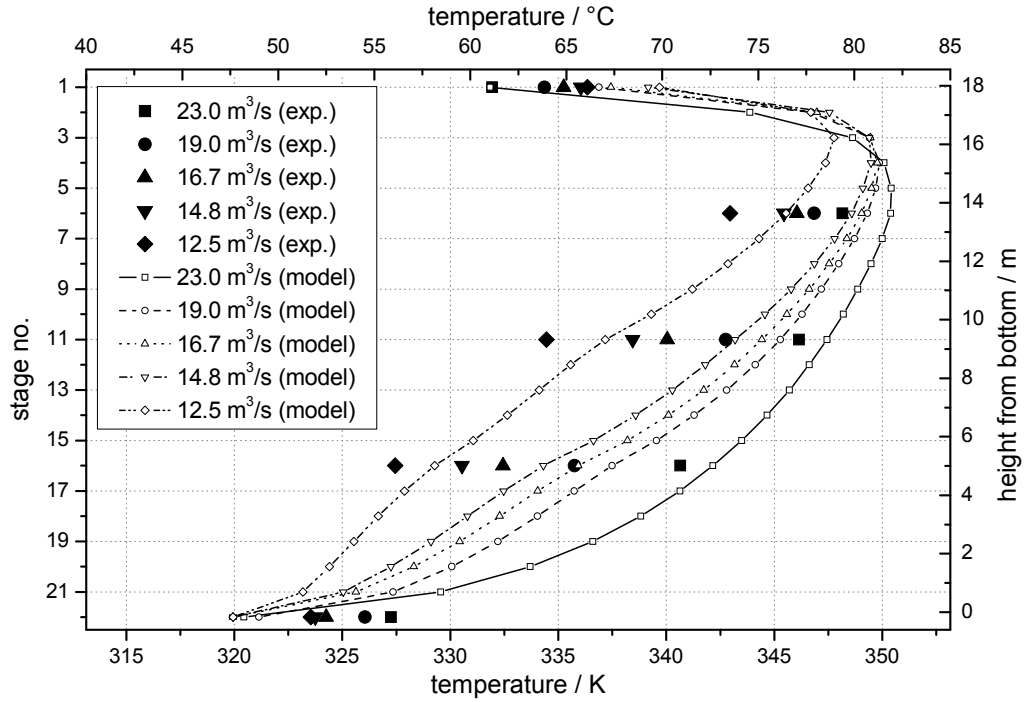

Figure 3.5: Experimental and model temperature profiles of absorber for different solution flow rates

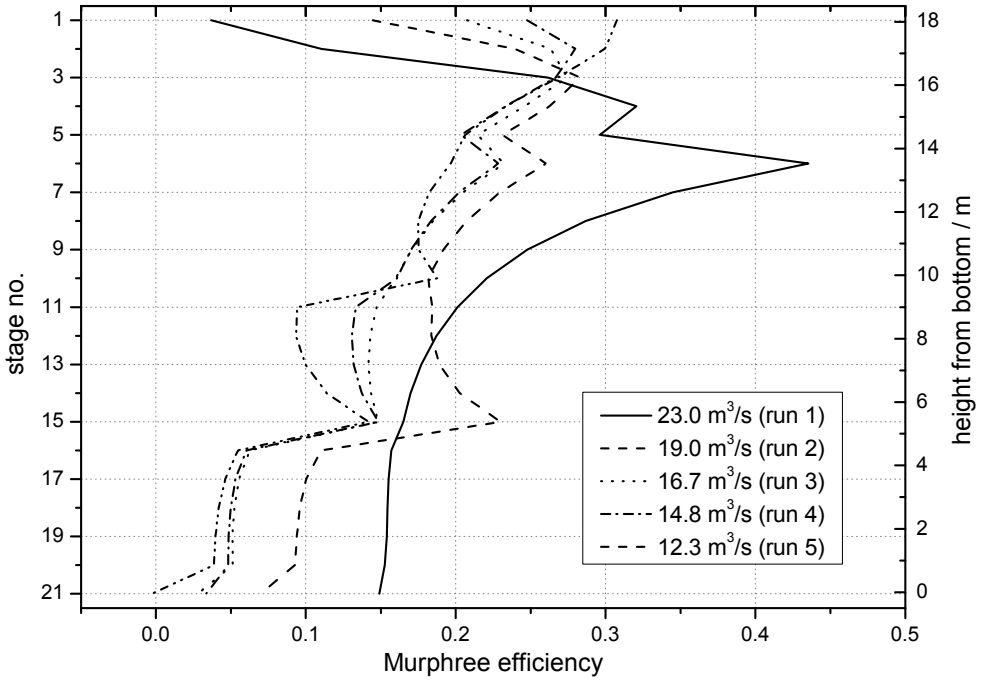

Figure 3.6: Calculated Murphree efficiencies for CO_2 in absorber for different solution flow rates

3.3.2 Desorber

Table 3.7 shows a list of input parameters that are fixed for the nine runs used with the desorber model. The input parameters are set to the published measurement values as shown in Table A.4 in Annex A.4. Typical values are assumed for those parameters for which no measurement data are available.

Table 3.7: Input parameters of desorber for model validation

component / stream	parameter	value
desorber column	column pressure	measured value
	pressure drop	50 mbar
overhead condenser	temperature	35 °C
rich solution	temperature	*
(desorber top)	CO_2 loading	measured value
	flow	measured value
lean solution	CO_2 loading	measured value
(desorber bottom)		

* A logarithmic mean temperature difference in the RLHX of 7.5 K is assumed, which corresponds to the typical value of the pilot plant before it was revamped [158].

As explained above, equilibrium is usually reached in the desorber of a CO_2 capture process, provided that a fast solvent is used in combination with regeneration under pressure and elevated temperatures. The choice of the number of equilibrium stages for the representation of the desorber is therefore a trade-off between two aspects: On the one hand, a minimal number of stages is necessary to ensure that equilibrium is reached in the desorber model; on the other hand, the number of stages should be as low as possible to provide for a reasonable computational effort. The number of equilibrium stages should therefore be as low as possible but as high as necessary to satisfy these requirements.

The minimum heat requirement for the regeneration of the solution in the desorber is obtained when equilibrium is reached in the desorber [22]. In the pilot plant test campaigns, the minimal reboiler heat duty is observed for a solution flow rate of 14.8 m^3/s (run 4). Figure 3.7 shows the McCabe-Thiele diagrams of the desorber for run 4 simulated with 5, 20, and 40 equilibrium stages. For 5 equilibrium stages the McCabe-Thiele diagram shows no pinch (a in Figure 3.7). For 20 stages, an equilibrium pinch is observed while the

CO_2 loading of the liquid phase still increases continuously from top to bottom of the column (b in Figure 3.7). For a larger number of stages an increasing fraction of the packing in the upper part of the desorber is operated under pinched conditions (c in Figure 3.7) – the computational effort increases significantly while the higher number of stages has practically no effect on the calculated reboiler heat duty.

It is concluded that 20 equilibrium stages are a good choice to adequately represent the desorber column of the pilot plant. As the mass transfer rate of the solvents selected in this work are of the same magnitude (cf. Table 3.4), it is assumed that the number of stages is a reasonable choice for the energetic evaluation of all six solvents.

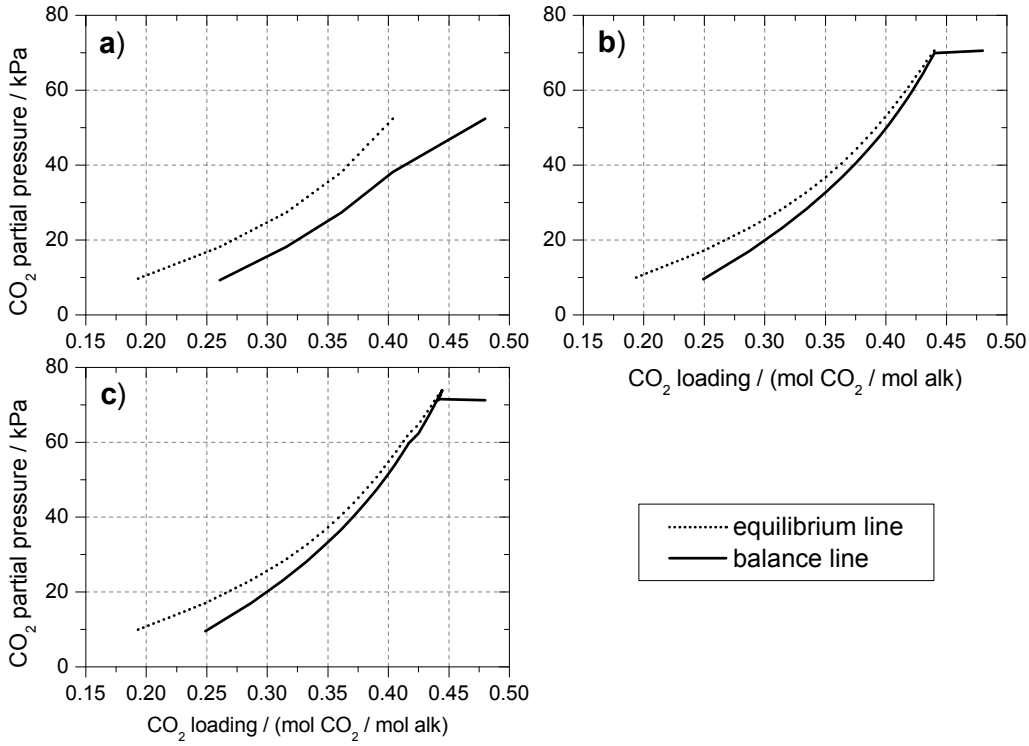

Figure 3.7: McCabe-Thiele diagrams of desorber in pilot plant run 4
a) 5 stages; b) 20 stages; c) 40 stages

The most important result of the semi-empirical column model in case of the representation of a desorber column is the reboiler heat duty. Table 3.8 shows the model results for this quantity in comparison to the measured value from the pilot plant. It is notable that the maximal relative deviation is lower than 8 %.

Table 3.8: Experimental and model results for reboiler heat duty of pilot plant

run no.	reboiler heat duty (GJ_{th} / t CO_2)		rel. deviation
	experiment	model	
1	3.897	4.035	3.54 %
2	3.722	3.740	0.48 %
3	3.725	3.725	0.01 %
4	3.626	3.742	3.21 %
5	3.745	3.815	1.87 %
6	3.738	3.647	2.44 %
7	3.692	3.967	7.45 %
8	4.006	4.144	3.46 %
9	4.185	4.468	6.76 %

Figure 3.8 and Figure 3.9 show the calculated and measured temperature profile over the desorber column height for varying solution flow rate (run 1 to 5) and desorber pressure (run 6 to 9). The upper most points of the lines representing the model results (stage no. 0) show the gas temperature downstream of the washing section for which no measurement data is available. The lower most points represent the reboiler temperature.

The temperature profile as determined by the model agrees well with the measurements. The very low values for the temperature measurement at the top of the column could be due to the cold water reflux from the above washing section. In the model a perfect heat exchange is assumed (temperature equilibrium of outlet gas (top) and outlet water reflux (bottom) in the washing section). In the real column it seems that the heat transfer from the gas onto the cold water reflux is not terminated until half way down the column, shifting the cold temperatures to the packing below the washing section. Additionally, the temperature measurement sensors are exposed to a mixture of gas and liquid phase while the model provides the theoretical values for the pure gas phase.

Concluding from the comparison of the measured and predicted values for reboiler heat duty and temperature profile, the desorber column of the pilot plant is well represented by the semi-empirical column model with 20 equilibrium stages.

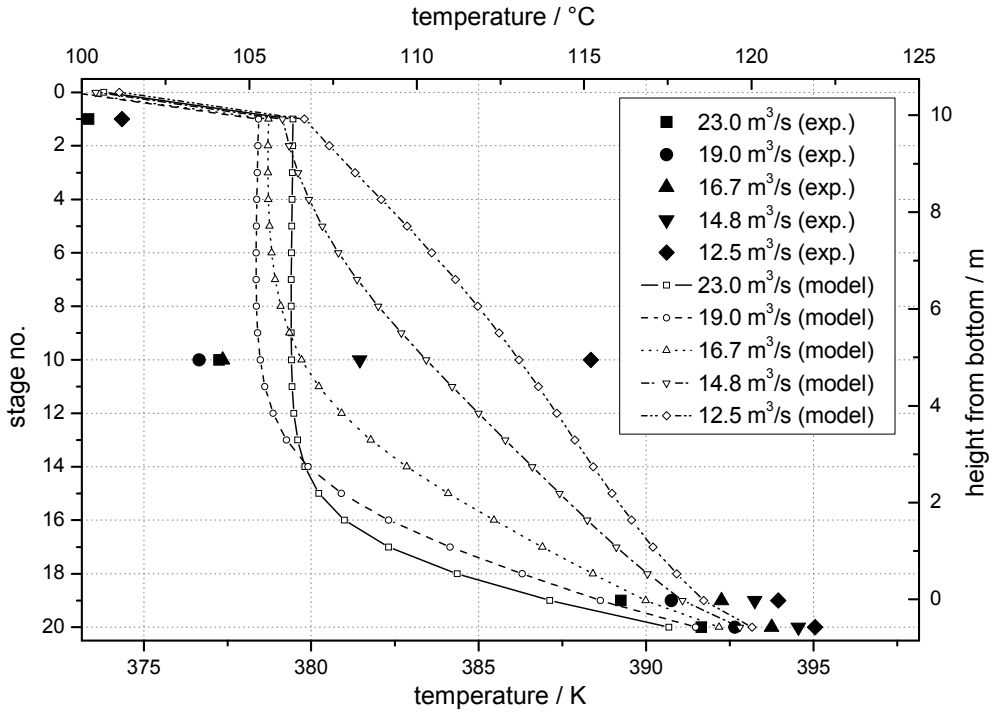

Figure 3.8: Experimental and model temperature profile of desorber column for different solution flow rates

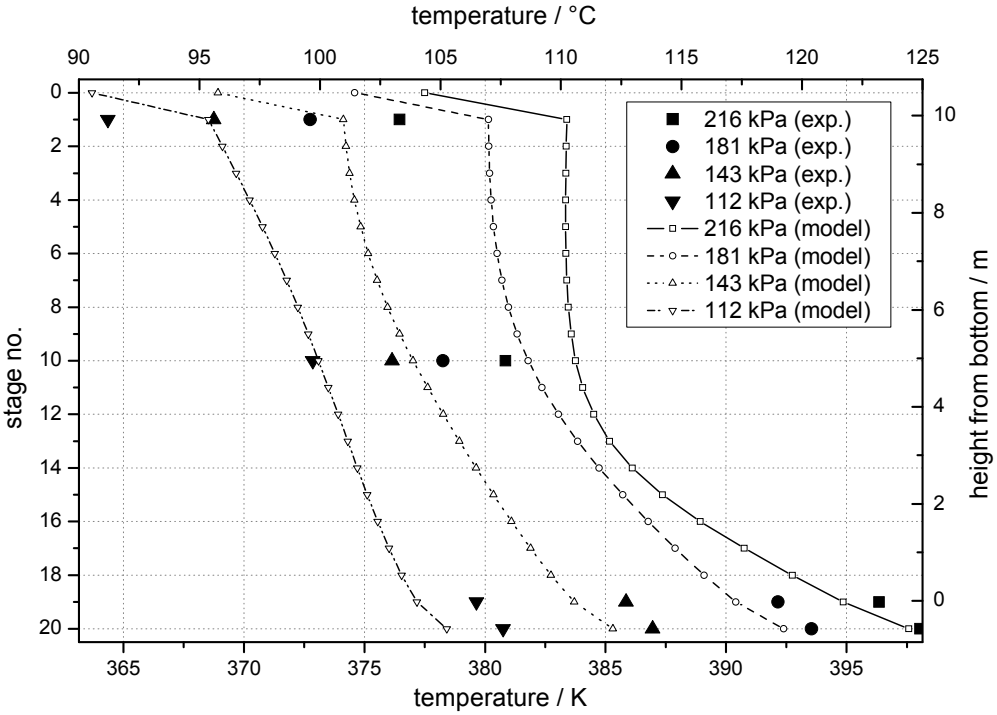

Figure 3.9: Experimental and model temperature profile of desorber column for different desorber pressures

4 MODEL DEVELOPMENT

To evaluate the impact of post-combustion CO_2 capture with the selected chemical solvents, the overall process consisting of a CO_2 capture unit, a CO_2 compressor and a hard-coal-fired steam power plant is represented by a detailed model in the simulation tool EBSILON®*Professional* [34]. This tool was originally developed to represent thermal power plants by providing a multitude of component models such as boilers, turbines, pumps, fans, and heat exchangers.

4.1 CO_2 capture unit

The flow sheet of an absorption-desorption type CO_2 capture unit (CCU) as shown in Figure 2.2 is set up in EBSILON®*Professional* (cf. Figure 4.1). Most components of the CCU can be represented by the standard models provided by the simulation tool. For the representation of the absorber and desorber column, the semi-empirical column model as outlined in Chapter 3 is implemented.

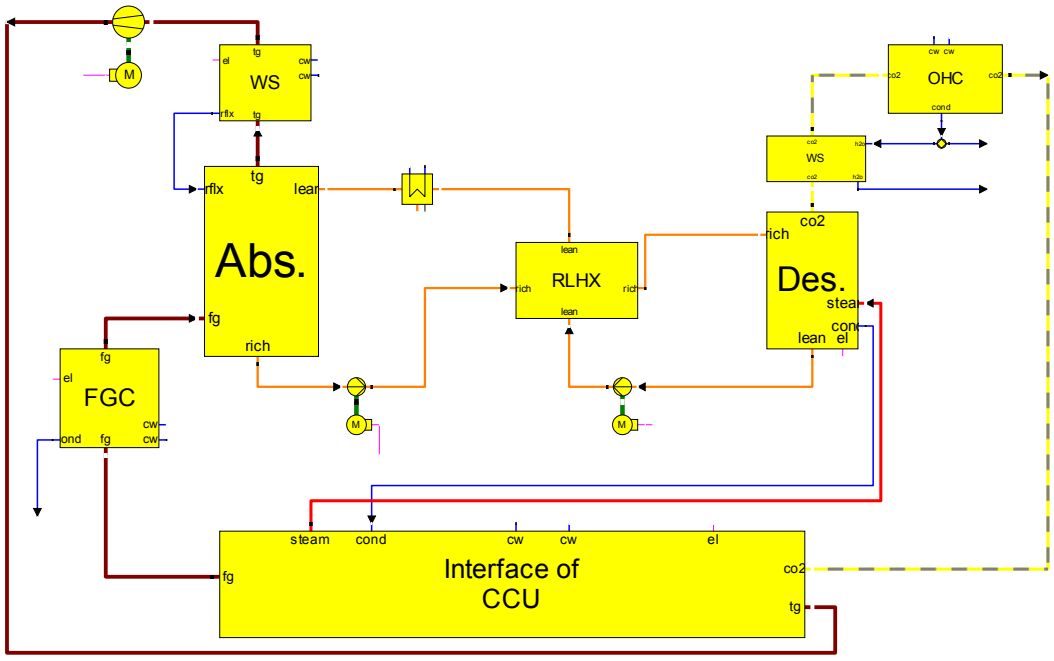

Figure 4.1: CO_2 capture unit in EBSILON®*Professional* consisting of standard component models and semi-empirical column model for absorber and desorber

Table 4.1 shows the boundary conditions of the CCU, which are the same for all selected solvents. In the course of the energetic evaluation (cf. Chapter 5), the solution flow rate and the reboiler temperature are optimised for each solvent to obtain a minimal net efficiency penalty of the overall process; additionally, the impact of an increased logarithmic mean temperature difference (LMTD) in the rich-lean heat exchanger (RLHX) is evaluated.

Table 4.1: Boundary conditions of CO_2 capture unit

LMTD[6] in RLHX	5 K
CO_2 capture rate	90 %
reboiler temperature approach	10 K
absorber solution inlet temperature	40 °C
absorber flue gas inlet temperature	40 °C
flue gas cooler pressure drop	10 mbar
absorber geodetic height	40 m
desorber geodetic height	25 m
absorber pressure drop	50 mbar
desorber pressure drop	30 mbar
pump[7] efficiency	80 %
fan isentropic efficiency	75 %
fan mechanical efficiency	95 %

Rectification processes for the separation of close-boiling multi-component mixtures show a reflux of the condensate from the overhead condenser (OHC) to the top of the rectification column. The multi-component mixture is introduced in the middle of the column, where the upper part of the column (rectifying section) realises the required purity of the head product, while the

[6] Logarithmic Mean Temperature Difference (LMTD) $= \left[\frac{(T_{\text{hot,in}} - T_{\text{cold,out}})}{(T_{\text{hot,out}} - T_{\text{cold,in}})}\right] \Big/ \ln\left[\frac{(T_{\text{hot,in}} - T_{\text{cold,out}})}{(T_{\text{hot,out}} - T_{\text{cold,in}})}\right]$

[7] including solution pumps as well as circulation pumps in the washing section and the flue gas cooler

lower part of the column (stripper section) is needed to achieve the desired purity of the bottom product.

In case of absorption-desorption CO_2 capture processes with chemical solvents, the desired CO_2 purity at the desorber top is usually sufficiently high. Only the remaining part of the water vapour, evaporated solvent, and small amounts of nitrogen, oxygen, and argon dilute the CO_2-rich stream. If the solvent shows a large vapour pressure, an additional washing section (WS) can be installed downstream of the desorber in which the solvent slip is reduced by contacting the CO_2-rich stream with cold water. The major part of the water vapour is removed in the OHC. As the purity of the CO_2-rich stream is already high, there is no need for a reflux to the desorber column. A reflux of condensate back to the desorber column is rather disadvantageous as the condensate causes a decrease in desorber temperature and leads to an increase in heat demand in the reboiler. In this work it is therefore assumed that the OHC condensate is used as make-up water, which is added to the lean solution before entering the absorber (not shown in Figure 2.2 and Figure 4.1).

RAO AND RUBIN suggested that an economically optimal CO_2 capture rate lies in the range of 80–90 % [159]. This is a consequence of the large investment costs associated with the CCU. The overall specific investment costs (e.g., in € per kW_{el}) are roughly doubled compared to the power plant without CO_2 capture. A PCC retrofit is therefore only implemented if the capture of CO_2 is either economically advantageous (compared to the payment of CO_2 tax or the purchase of emission certificates) or regulated by law. Therefore, this work focuses on the realisation of a CO_2 capture rate of 90 %. The optimal CO_2 capture rate depends on a variety of factors, among them the investment costs of the CCU, the operational costs (above all for solvent make-up), the energy penalty associated to the operation of the CCU, electricity prices, and – if applicable – CO_2 tax or the price of CO_2 emission certificates. A detailed economic analysis in combination with rate-based models, taking into account the implication of the design of CCU process components in energetic and economic terms, is required to determine if a reduction in the CO_2 capture rate could reduce the overall CO_2 capture costs.

The temperature approach in the reboiler between the boiling solution and the condensing steam that provides for the reboiler heat duty is subject of economic optimisation. The larger the temperature approach, the smaller the

heat exchanger area and thus the lower the investment cost. A larger temperature approach, however, requires the supply of heat at a higher temperature and thus leads to larger losses in the power plant (cf. Section 5.3.2). In this work a reboiler temperature approach of 10 K is assumed. Note that the choice of this parameter has a considerable impact on the power loss associated to the steam extraction for regeneration of the solution: The sensitivity of the overall net efficiency penalty is in the order of 0.7 %-pts. per 10 K of change in reboiler temperature approach [160].

The temperature of the treated flue gas at the absorber outlet is controlled to achieve a neutral water balance of the CCU. Hence, the same amount of water enters the absorber as is discharged from the process via the CO_2-rich stream to the compressor and via the treated flue gas at the absorber top. Note that significant amounts of water can condense in the flue gas cooler. Since the condensate is contaminated by fly ash, gypsum, and – in case of the application of an SO_2 polisher unit – NaOH, it cannot be used as make-up water in the CCU and instead has to be recycled to the FGD or must be processed otherwise.

The pressure increase over the fan is set to 90 mbar to overcome the pressure drop in the flue gas cooler and the absorber column. The dependency of the pressure drop on process parameters such as the solution flow rate is neglected.

The necessary outlet pressure of the two solution pumps is determined by considering the geodetic height of the corresponding column plus a minimal pressure that needs to be supplied to avoid vaporisation of water and/or solvent on the hot side of the RLHX and in the solution riser pipes. The required outlet pressure downstream of the solution pumps is determined via

$$p_{\mathrm{outlet}} = p^{\mathrm{s}}_{\mathrm{H2O}}\left(T_{\mathrm{RLHX,hot}}\right) + 0.0981\,\frac{\mathrm{bar}}{\mathrm{m}}\,h_{\mathrm{abs/des}} \quad , \tag{4.1}$$

where $h_{\mathrm{abs/des}}$ is the geodetic height of the absorber or desorber column.

The difference in the performance determining mechanisms for absorber and desorber (cf. Section 3.3) yields the necessity of developing two individual methodologies for an adequate representation of these components in the CCU model, which are outlined in the following.

4.1.1 Absorber

The aim of an optimal absorber design is to increase the amount of CO_2 that is absorbed by the solution and to achieve a CO_2 loading of the rich solution that is as high as possible. The higher this quantity, the lower is the required solution circulation rate and consequently the lower the reboiler heat duty (q.v. Section 5.2.2). As explained in Section 3.3, absorber columns commonly do not suffer from an equilibrium pinch, thus from a lack in driving force. The rate of absorption is rather limited by a rate pinch, which is due to the low temperature and the low concentration of free alkali species. The rich loading is therefore determined by the temperature profile (impact on equilibrium loading) and the column design (impact on mass transfer rate and on possible approach to equilibrium). To predict the performance of an absorber, a rate-based model or the prediction of accurate Murphree efficiencies is thus necessary.

FREGUIA proposed an equilibrium stage model in which the Murphree efficiencies are determined in each iteration of the process simulation [161]. As stated in Section 3.3.1, Murphree efficiencies in multi-component reactive absorption systems depend strongly on the considered solvent, the operational process parameters (e.g., solution flow rate), and the temperature and concentration profile over the column height. Just as in rate-based models, the estimation of efficiencies involves the consideration of effective wetted packing area and mass transfer coefficients. As both parameters are a function of the temperature and concentration profile as well as of process parameters such as the solution flow rate, the determination of the efficiencies requires an iterative algorithm. Mass transfer coefficients are either determined by correlations, which are valid within a limited range of parameters, or are calculated by considering properties such as solvent viscosity, physical CO_2 solubility, and diffusivity of reactants and products. The latter option is basically equivalent to the development of a rate-based model. However, the complexity and the required basis of measurement data associated to the development of a rate-based model contradict the aim of this work to perform a fair energetic comparison of solvents with limited available data.

Both reasons – the occurrence of a rate-pinch and difficulties in accurately predicting the Murphree efficiencies – lead to the conclusion that an equilibrium stage model is not capable of representing the absorber of a CO_2 capture process. Therefore, a simplified approach for the representation of the ab-

sorber, which yet allows for a fair energetic comparison of chemical solvents, is chosen in this work.

The flue gas of the hard-coal-fired power plant considered in this work has a CO_2 concentration downstream of the FGD of 13.9 vol.-% (wet). Part of the water content in the gas is condensed in the flue gas cooler. The flue gas enters the absorber with a temperature of 40 °C and a CO_2 partial pressure of approximately 15 kPa. If equilibrium was reached at the absorber inlet then, depending on the solvent, a certain CO_2 loading of the rich solution corresponding to an equilibrium CO_2 partial pressure of 15 kPa could be achieved. However, a minimal driving force for CO_2 absorption is required (cf. Section 3.3). With a CO_2 partial pressure of 15 kPa in the flue gas, an equilibrium CO_2 partial pressure of 5 kPa allows for a partial pressure ratio of 3. This provides for a reasonable driving force which is achievable with economically feasible packing heights in the absorber [60].

Although the flue gas enters the absorber at a temperature of 40 °C, the corresponding loadings of the rich solution are calculated at 50 °C to account for the temperature increase related to the exothermic reactions in the absorber. Note that the magnitude of the temperature increase depends on the column design and the mass flows of liquid and gas phase as well as on the heat of absorption and the heat capacity of the solution. The outlet temperature of the rich solution is therefore not predictable by the semi-empirical column model. A constant outlet temperature of 50 °C is assumed for all solvents, which is a reasonable average value observed in pilot plants operated with different solvents [144, 149]. The CO_2 loading of the rich solution at an assumed equilibrium CO_2 partial pressure of 5 kPa and 50 °C for the six selected solvents is calculated via Eq. (3.5) and shown in Table 4.2.

The described approach for the representation of the absorber column assumes that the column is well designed for the individual solvent. This implies for some (slower) solvents that certain measures with regard to the column design (higher packing, intercooling) must be applied, which might entail additional financial investment. Nevertheless, as all solvents selected in this work show similar mass transfer coefficients (cf. Table 3.4), it can be assumed that the additional effort regarding the equipment is within a range that does not impede the economic feasibility of the CO_2 capture process.

Table 4.2: CO_2 loadings for selected solvents at 50 °C

solvent	max. CO_2 loading at $p^*_{CO2} = p_{fg} = 15$ kPa mol CO_2 / mol alk	CO_2 loading at $p^*_{CO2} = 5$ kPa mol CO_2 / mol alk	approach to max. CO_2 loading %
MEA	0.5500	0.5093	92.6
PZ	0.4181	0.3762	90.0
AMP	0.6221	0.4587	73.7
K/PZ	0.5820	0.5515	94.8
MDEA/PZ	0.2859	0.1987	69.5
AMP/PZ	0.6936	0.6195	89.3

To provide for a balanced number of equations and unknowns in the equation system representing the semi-empirical column model, some additional equations and boundary conditions for the absorber column are necessary. If the CO_2 loading and the temperature of the rich solution at the absorber bottom are fixed, then the temperature of the treated flue gas stream at the absorber outlet (top) can be determined via an energy balance. The semi-empirical column model is therefore used with one theoretical stage (corresponding to stage 0 in Figure 3.2). The pressure, temperature, flow, and composition of the inlet gas stream to the stage (G(1) in Figure 3.2) are defined by the stream coming from the flue gas cooler. The CO_2 loading in combination with the specified mole flow of the lean solution (L(0) in Figure 3.2) is calculated to provide for the desired CO_2 capture rate of 90 % (cf. Eq. (5.5) in Section 5.2.2).

For the one stage representing the absorber, phase equilibrium of the gas and the liquid stream leaving the stage (L(2) and G(0) in Figure 3.2) is no longer assumed. Eq. (3.29) is therefore neglected and the Murphree efficiency and the temperature of the outlet gas stream are specified as variables:

$$ns = 1 \quad , \tag{4.2}$$

$$\eta_{\mathrm{m}}(0) = \text{var.} \quad , \tag{4.3}$$

$$T_{\mathrm{g}}(0) = \text{var.} \quad . \tag{4.4}$$

Instead, the temperature and the equilibrium CO_2 partial pressure of the liquid stream at the absorber outlet are set to fixed values:

$$T(2) = 323.15\ \text{K} \quad , \tag{4.5}$$

$$p^*_{\text{CO2}}(0) = 5\ \text{kPa} \quad . \tag{4.6}$$

The side stream from the washing section is considered as pure water:

$$\dot{n}_{\text{S}}(0) = \dot{n}_{\text{H2O,S}}(0) = \dot{n}_{\text{WS,reflux}} \quad , \tag{4.7}$$

$$\dot{n}_{\text{CO2,S}}(0) = \dot{n}_{\text{alk,S}}(0) = 0 \quad . \tag{4.8}$$

The pressure at the absorber bottom is equal to the pressure of the stream coming from the flue gas cooler. A pressure drop of $\Delta p_{\text{abs}} = 50$ mbar is considered over the column height:

$$p_{\text{tot}}(0) = p_{\text{tot}}(1) - \Delta p_{\text{abs}} \quad . \tag{4.9}$$

Heat losses are neglected in the absorber column:

$$\dot{Q}(0) = 0 \ . \tag{4.10}$$

4.1.2 Desorber

It was shown in Section 3.3.2 that the semi-empirical column model with 20 equilibrium stages is capable of accurately representing the desorber of the CCU with regard to the calculation of the required heat input to the reboiler. Note that this approach requires the consideration of solvents which show similar mass transfer characteristics as MEA. Equilibrium models are of limited value for design purposes [162]. In this work, however, the focus lies on the energetic evaluation of chemical solvents; therefore, the accurate prediction of temperature and concentration profiles or the required height of packing are of no particular interest.

A balanced number of equations and unknowns for the representation of the desorber also require some additional equations and boundary conditions. The pressure, temperature, flow and composition of the rich solution at the desorber top (L(0) in Figure 3.2) are a result of the absorber model. Furthermore, the state of the rich solution, thus temperature and pressure, is changed by the lean solution pump and the RLHX. The latter two components are modelled with the standard components provided by EBSILON®*Professional*.

The number of stages is set to 20 where all stages are considered to be in phase equilibrium:

$$ns = 20 \quad , \tag{4.11}$$

$$\eta_{\mathrm{m}}(j) = 1 \quad . \tag{4.12}$$

No gas stream is entering the desorber column and no side streams are considered:

$$\dot{n}_{\mathrm{G}}(ns) = 0 \quad , \tag{4.13}$$

$$\dot{n}_{\mathrm{S}}(j) = 0 \quad . \tag{4.14}$$

The reboiler temperature is specified:

$$T(2ns) = T_{\mathrm{reb}} \quad . \tag{4.15}$$

A pressure drop of $\Delta p_{\mathrm{des}} = 30$ mbar is considered over the column height:

$$p_{\mathrm{tot}}(j) = p_{\mathrm{tot}}(ns) - \Delta p_{des} \, \frac{ns - j}{ns} \quad . \tag{4.16}$$

Except for the last stage, which represents the reboiler ($j = (ns - 1)$), heat streams to or from the stages (heat losses) are neglected over the entire column height:

$$\dot{Q}(j) = 0 \quad (j \neq ns - 1) \quad . \tag{4.17}$$

4.2 CO_2 compressor

To transport the separated CO_2 to an adequate storage site, a pipeline pressure of 110 bar is assumed to be sufficient. In this work an integrally-geared (radial) compressor with six stages is considered. The auxiliary power duty and cooling duty of the CO_2 compressor as shown in Figure 4.2 are calculated via two empirical correlations given by LIEBENTHAL *et al.* [163]:

$$P_{\mathrm{comp,el}}/\mathrm{MW_{el}} = \varepsilon \cdot \dot{m}_{\mathrm{CO2}} \cdot \left(0.3948 \cdot p_{\mathrm{comp,inlet}}^{-0.3893} + 0.0301\right) \quad , \tag{4.18}$$

$$\dot{Q}_{\mathrm{comp,cool}}/\mathrm{MW_{th}} = \varepsilon \cdot \dot{m}_{\mathrm{CO2}} \cdot \left(0.5736 \cdot p_{\mathrm{comp,inlet}}^{-0.2698} + 0.0901\right) \quad . \tag{4.19}$$

The correlations for the heat and power demand of the CO_2 compressor consider gas cooling to 40 °C after the second, fourth, and sixth stage. A pressure drop for the intercoolers and the aftercooler of 50 mbar is assumed. After each intercooler a water knock-off is considered to dispose the condensing water. Additionally, an adsorptive drying stage is necessary to account for the

assumed strict requirements of contained water within the CO_2 for pipeline transport. An additional pressure drop of 100 mbar of the adsorption beds is assumed. The increase in heat or power demand for the discontinuous regeneration of the adsorption beds is neglected.

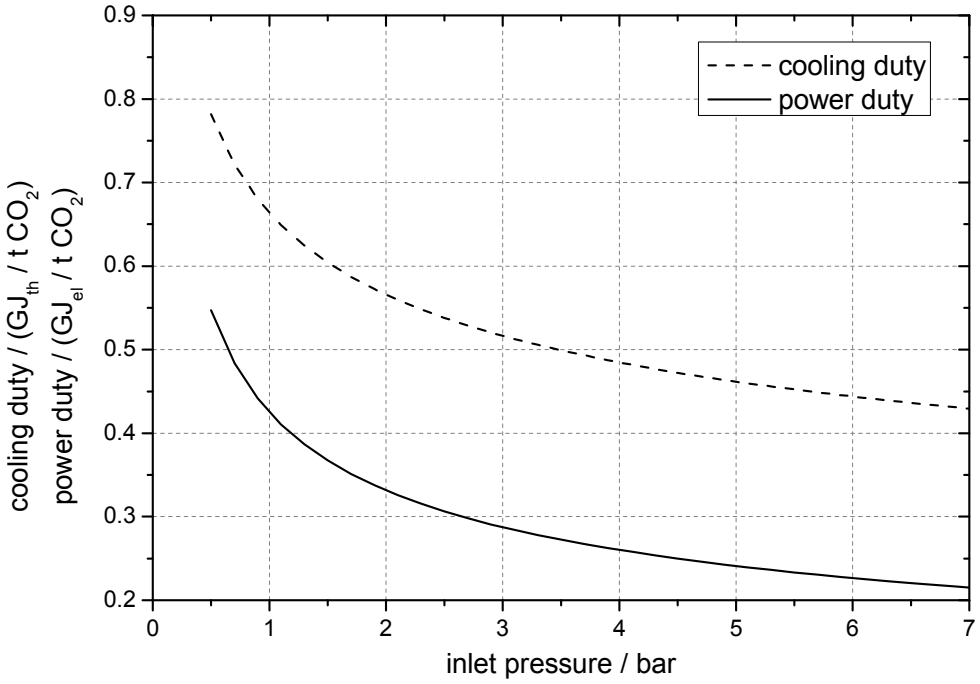

Figure 4.2: Specific auxiliary power duty and cooling duty of six-stage CO_2 compressor with 110 bar outlet pressure [163]

4.3 Power plant

The impact of a CO_2 capture unit is evaluated by the example of a hard-coal-fired steam power plant with a gross power output of 1137 MW_{el}. A simplified flow sheet of the reference power plant (without CO_2 capture) is shown in Figure 4.3.

A bituminous coal with a lower heating value (LHV) of 25.0 MJ_{th} / kg and specific CO_2 emissions of 343.6 kg CO_2 / MWh_{th} is considered. The key parameters of the power plant at design conditions (full-load without CO_2 capture) are given in Table 4.3. The semi-empirical column model does not consider interactions of oxygen and flue gas impurities with the solvent. O_2, Ar, SO_x, and NO_x are therefore treated as inert gas components and their fractions are added to the N_2 fraction. At the inlet of the flue gas cooler in the CCU model

the flue gas consequently consists of 11.2 vol.-% H_2O, 13.9 vol.-% CO_2, and 74.9 % N_2.

The model of the power plant was developed with information from an energy utility. It was validated in particular in terms of steam temperatures, steam pressures, net power output, and net efficiency.

Table 4.3: Key parameters of reference power plant at full-load without CO_2 capture

heat input	2306 MW_{th}
gross power output	1137 MW_{el}
net power output	1051 MW_{el}
gross efficiency (LHV)	49.3 %
net efficiency (LHV)	45.6 %
live steam mass flow	826.5 kg/s
live steam pressure	285 bar
live steam temperature	600 °C
reheat pressure	59 bar
reheat temperature	620 °C
boiler feed water temperature	306.9 °C
condenser pressure	49/39 mbar
IP/LP crossover pressure	3.9 bar
feed water tank pressure	11.2 bar
cooling water temperature	19 °C
cooling water temperature gain	11 K
flue gas temperature*	48.5 °C
flue gas pressure*	1.019 bar
flue gas mass flow*	1054 kg/s
flue gas volume flow*	942.3 m^3/s
flue gas composition*	
CO_2	13.9 vol.-%
H_2O	11.2 vol.-%
N_2	70.7 vol.-%
O_2	3.3 vol.-%
Ar, SO_x, NO_x	0.9 vol.-%

* downstream of FGD

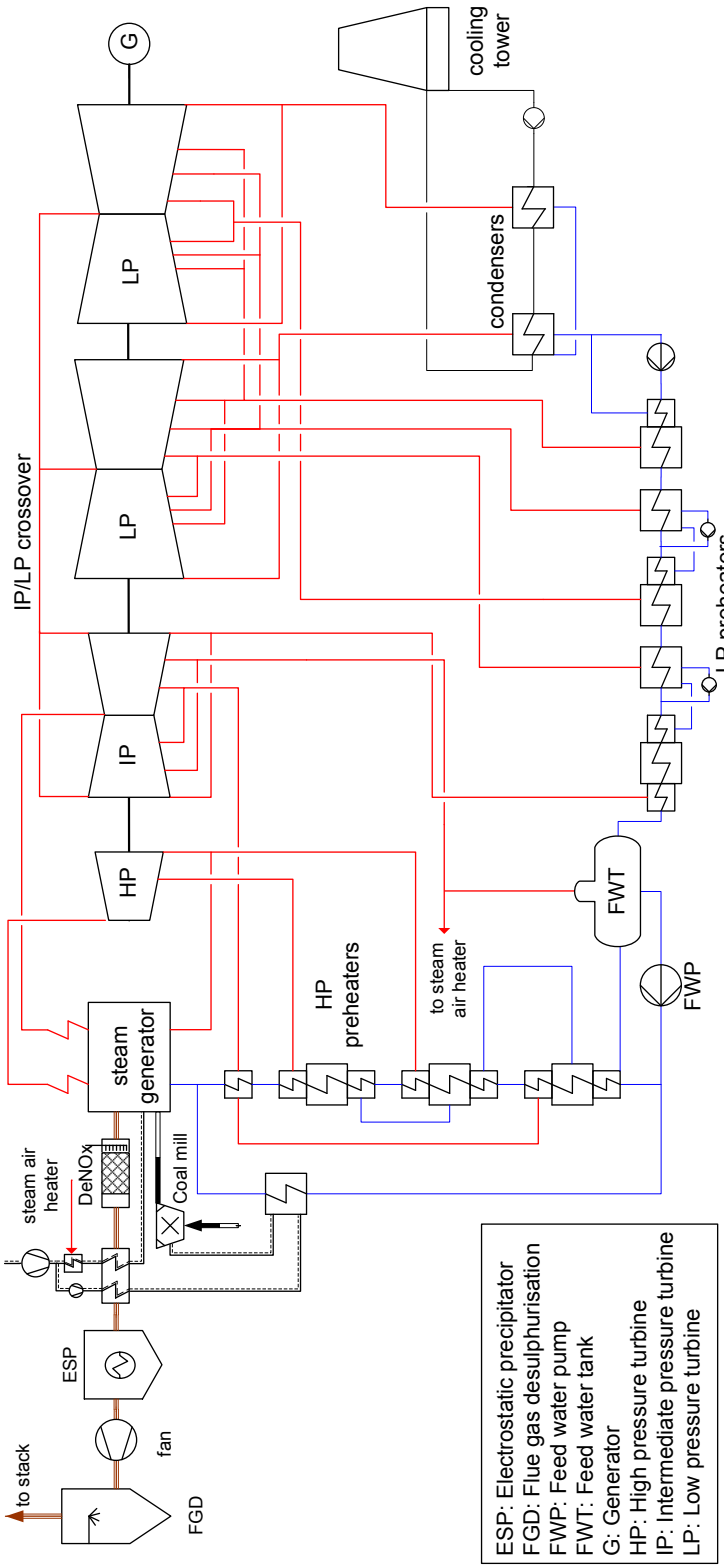

Figure 4.3: Simplified flow sheet of reference hard-coal-fired steam power plant

If the power plant is retrofitted with a CO_2 capture unit and a CO_2 compressor, certain components in the water-steam-cycle are no longer operated in their design point. The off-design behaviour of these components is considered by using two-dimensional characteristics. For the characteristics of the steam turbines, which are the main influencing components with respect to the net power output of a steam power plant, the following assumptions are made:

- The isentropic efficiencies of each steam turbine stage group are kept constant for all groups independent of the turbine steam load (HP: 91 %; IP: 92 %; LP: 95 %). The dependency of isentropic efficiencies on the pressure ratio is neglected.
- The last few stages of the LP turbine operate under wet steam conditions. The influence of moisture on the efficiency of the steam turbine is considered using a Baumann correction factor of 0.9 [164].
- In the LP turbine a loss of kinetic energy and an increase in enthalpy associated to steam exhausting from the last stage are taken into consideration [165]. These exhaust losses are considered as a function of the exhaust loss area and the exhaust volume flow.

The cooling water mass flow to the turbine condenser of the power plant is controlled to keep a cooling water temperature gain of 11 K. For cooling duties in the two turbine condensers below 80 % – such as under operation with steam extraction for CO_2 capture (cf. Section 4.5.3) – a minimal cooling water mass flow of 80 % is kept. This strategy results from an energetic optimisation of the cold end in which a possible part-load operation of the power plant is taking into consideration. On the one hand, a reduced cooling water flow results in a lower auxiliary power for the cooling water pumps. On the other hand, a decrease in cooling water flow leads to an increase in cooling water temperature gain. Consequently the turbine condenser pressure increases with a negative effect on the efficiency of the water-steam-cycle.

The integration of the CCU and the CO_2 compressor is evaluated assuming full-load operation of the power plant. Furthermore, steady state conditions are assumed and no discontinuous processes such as soot blowing or reclaiming of degraded solvent are considered.

4.4 Implementation in EBSILON®*Professional*

All components in the CCU flow sheet as shown in Figure 4.1 except the absorber and desorber column are modelled using the standard component library of EBSILON®*Professional*. The absorber and desorber column are represented by implementing the semi-empirical column model via an external direct link library (DLL).

Within EBSILON®*Professional* the CO_2-loaded aqueous solution is treated as a user-type fluid which is characterised by its composition, density, and heat capacity. The simulation tool requires the mass-specific heat capacity of the solution as a function of temperature:

$$C_{\mathrm{p,L}} = \mathrm{A}_0 + \mathrm{A}_1 t + \mathrm{A}_2 t^2 + \mathrm{A}_3 t^3 \quad , \tag{4.20}$$

with

$$t = T - 273.15 \quad . \tag{4.21}$$

Since the heat capacity of the solution depends on the CO_2 loading (cf. Eq. (3.9)), the coefficients of $C_{\mathrm{p,L}}$ of CO_2-rich and CO_2-lean streams in the simulation tool are calculated in each iteration via

$$\mathrm{A}_0 = \mathrm{c}_{\mathrm{Cp,0}} + \mathrm{c}_{\mathrm{Cp,3}}\,\alpha + \mathrm{c}_{\mathrm{Cp,4}}\,\alpha^2 + \mathrm{c}_{\mathrm{Cp,5}}\,\bar{m}_{\mathrm{alk}} + \mathrm{c}_{\mathrm{Cp,6}}\,\bar{m}_{\mathrm{alk}}^2 + \mathrm{c}_{\mathrm{Cp,9}}\,\alpha\,\bar{m}_{\mathrm{alk}} \quad , \tag{4.22}$$

$$\mathrm{A}_1 = \mathrm{c}_{\mathrm{Cp,1}} + \mathrm{c}_{\mathrm{Cp,7}}\,\alpha + \mathrm{c}_{\mathrm{Cp,8}}\,\bar{m}_{\mathrm{alk}} + \mathrm{c}_{\mathrm{Cp,10}}\,\alpha\,\bar{m}_{\mathrm{alk}} \quad , \tag{4.23}$$

$$\mathrm{A}_2 = \mathrm{c}_{\mathrm{Cp,2}} \quad , \tag{4.24}$$

$$\mathrm{A}_3 = 0 \quad . \tag{4.25}$$

The semi-empirical column model is represented by a system of non-linear equations (q.v. Section 3.2) which must be solved by an appropriate solver that is in compliance with the following requirements:

- compatibility to EBSILON®*Professional*, hence implementable in C++;
- fast and robust algorithms.

Trilinos is identified as a suitable library to solve the non-linear equation system as it fulfils the above prerequisites [166, 167].

The interaction of EBSILON®*Professional* with the external DLL is illustrated in Figure 4.4. The kernel sets-up mass, enthalpy, and pressure balance equations for all components in the flow sheet which are connected via the

graphical user interface (GUI) by material or enthalpy streams. The EBISLON®*Professional* kernel solves the linearised equation system iteratively with an adequate numerical algorithm.

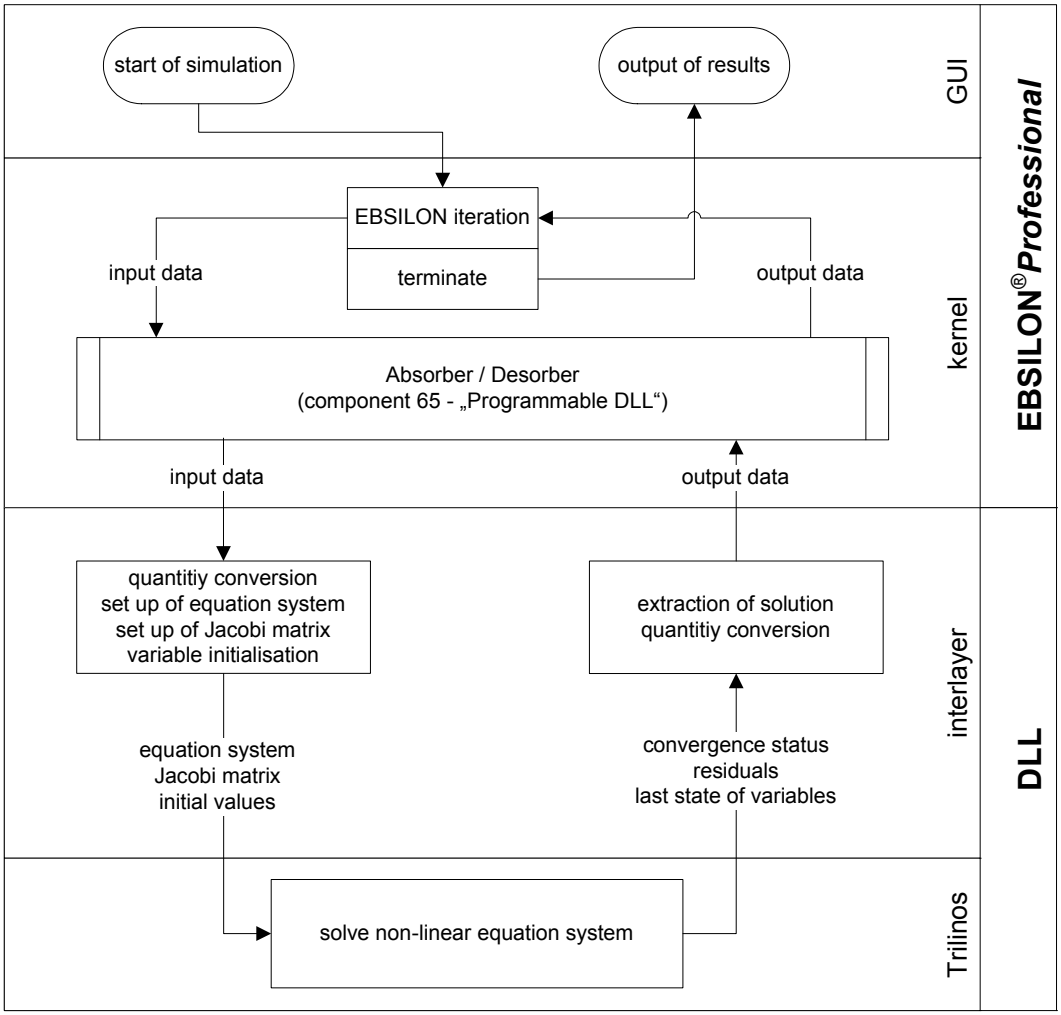

Figure 4.4: Coupling of EBSILON®*Professional* with external DLL and Trilinos non-linear equation solver

Within each iteration the kernel invokes two instances of the external DLL, which include the implementations of the semi-empirical column model as outlined in Chapter 3 with the specific additional equations for absorber and desorber as explained in Sections 4.1.1 and 4.1.2. The external DLL is invoked

via the EBSILON®*Professional* component 65 (ProgDLL[8]), which receives the information of the streams that are connected to it (flue gas, rich and lean solution, water reflux from WS) as well as any additional user-defined data (number of stages, reboiler temperature, pressure loss, etc.). Figure 4.5 illustrates the connection of flue gas, treated flue gas, reflux water, rich and lean solution, and CO_2 stream to the ProgDLL components. A stream that transfers the calculated reboiler heat duty to a heat load component in EBSILON®*Professional* is connected to the ProgDLL component that is representing the desorber.

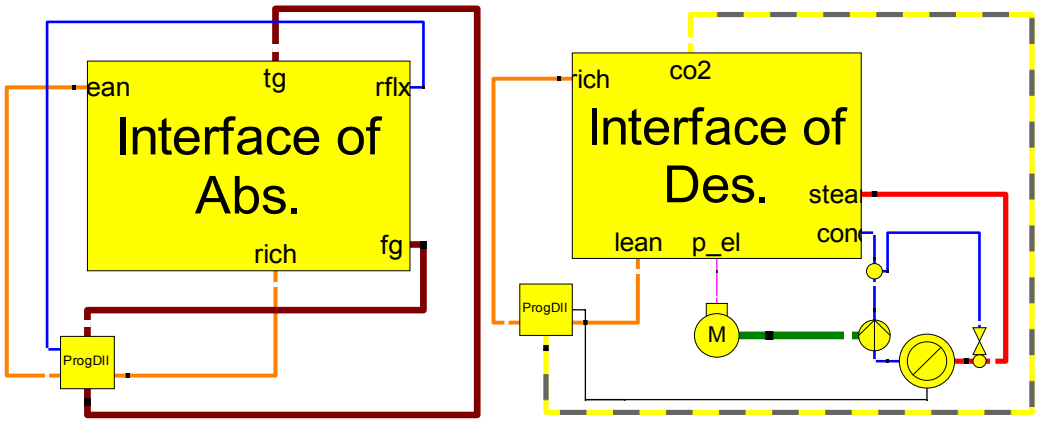

Figure 4.5: Interface of absorber and desorber column in EBSILON®*Professional* showing connection of input and output streams to ProgDLL (component 65)

EBSILON®*Professional* calculates stream information in kg/s, bar and °C; therefore, units need to be converted and molar quantities need to be calculated by an interlayer in the DLL. The interlayer also sets up the non-linear equation system in the form

$$0 = \boldsymbol{F}(\boldsymbol{x}) \ , \tag{4.26}$$

where $\boldsymbol{x}$ is the vector of variables and $\boldsymbol{F}$ is the system of non-linear equations as defined in Section 3.2 which are rearranged in accordance to Eq. (4.26). Adequate starting values for all of the variables need to be defined by the interlayer to enable the solution of the non-linear equation system.

[8] Programmable Direct Link Library

To improve the solving algorithm, the interlayer sets up the Jacobi matrix of the equation system

$$\boldsymbol{J}(\boldsymbol{x}) = \begin{bmatrix} \frac{\partial F_1(\boldsymbol{x})}{\partial x_1} & \cdots & \frac{\partial F_1(\boldsymbol{x})}{\partial x_m} \\ \vdots & \ddots & \vdots \\ \frac{\partial F_m(\boldsymbol{x})}{\partial x_1} & \cdots & \frac{\partial F_m(\boldsymbol{x})}{\partial x_m} \end{bmatrix}, \tag{4.27}$$

which consist of the first partial derivative of each of the equations in $\boldsymbol{F}$ with respect to each of the variables in $\boldsymbol{x}$, where m is number of equations. The Jacobi matrix represents the optimal linear approximation of the equation system at $\boldsymbol{x}$. It is used to determine the next approximation of $\boldsymbol{x}$ to solve the equation system[9].

The interlayer in the DLL invokes a Trilinos solver object and passes the vector of initialised variables, the equation system, and the Jacobi matrix to it. The EBSILON®*Professional* kernel is interrupted and halted as long as the solver is active and does not continue before the solver returns the convergence status, the residual vector, and the variable vector that – in case the algorithm has converged – contains the solution of the equation system.

Trilinos allows choosing from different solver algorithms. The NOX non-linear solver package that uses a direct solver combined with a trust region approach to achieve global convergence was chosen as it achieves the best results in terms of convergence and performance [168].

The interlayer extracts the required quantities from the solution vector, calculates the needed stream information in adequate units, and passes them back to the EBSILON®*Professional* kernel. The procedure is repeated until the changes in mass, enthalpy, and pressure balances fall below a certain tolerance[10]. Finally, the simulation is terminated and the results are displayed in the GUI.

---

[9] For a comprehensive discussion of numerical methods for the solution of non-linear equation systems refer, for example, to [179].

[10] The simulation in EBSILON®*Professional* is regarded as convergent if the residual errors in the enthalpy, pressure, and mass balance matrices each fall below 10^{-7}.

4.5 Overall process

When integrating a process for the capture and compression of CO_2 into a power plant, the power output is reduced due to three reasons:

1. The heat needed for the regeneration of the solution in the desorber is usually provided by using steam from the water-steam cycle of the power plant. This leads to a reduction of the steam mass flow in the turbines and thus to a decrease of the gross power output compared to the reference plant without CO_2 capture.
2. Pumps and fans in the capture process and in particular the CO_2 compressor need mechanical power which typically is supplied by electrical motors that reduce the net power output of the plant.
3. The cooling water demand of the overall process increases since the CCU and the CO_2 compressor have to reject large amounts of low temperature heat. The corresponding additional auxiliary power demand of the cooling water pumps reduces the net power output of the power plant.

The CCU can therefore be characterised by the magnitude of the three interface quantities heat, electricity, and cooling. In the overall process model, the auxiliary power demand of the CCU as well as of the CO_2 compressor are satisfied by reducing the net power output of the power plant, contributing with up to 10 % and 20–40 % to the overall power loss, respectively. The supply of heat and cooling duty demand is discussed in more detail in the following, since it has a more complex implication on the power plant than the provision of auxiliary power.

4.5.1 Supply of reboiler heat duty

There is a number of potential options to provide the heat for the regeneration of the solution at the necessary temperature level:

1. The further cooling of the flue gas downstream of the air preheater (115 °C) is not appropriate since, depending on the chosen reboiler temperature, the temperature level might not be sufficient and since the sensible heat only provides for roughly 1/10 of the heat required by the CCU.

2. The use of an auxiliary boiler or an auxiliary gas turbine with a heat recovery steam generator (HRSG) was suggested by ROMEO *et al.* but it was shown that these options lead to large efficiency penalties [29]. Additionally, the partial substitution of coal by natural gas prevents a direct comparison as natural-gas-fired power plants inherently show lower specific CO_2 emissions and thus lower net efficiency penalties than coal-fired power plants when considered for the integration of a CCU.
3. Live steam or hot reheat steam provides for sufficient heat quantities; however, the available heat quality is significantly above the level required by the CCU.
4. The latent heat of condensing low-pressure steam from the water-steam-cycle of the power plant provides heat at sufficient amounts and adequate parameters.

Roughly one fourth of the fuel heat input is needed in the desorber to separate 90 % of the CO_2, corresponding to approximately 50 % of the steam at the LP turbine inlet. Independent of the solvent type, the use of steam for regeneration of the solution therefore always has a significant impact on the power output and efficiency of a coal-fired steam power plant equipped with a CCU.

If live steam or reheat steam is considered for use in the capture process, the installation of an additional turbine is strongly recommended to reduce the overall energy penalty. However, such turbine is not only related to additional investment costs but also shows a lower isentropic efficiency than the HP and IP turbines of the power plant since it is much smaller in size. Furthermore, the thermodynamic cycle efficiency is significantly lowered if a non-reheat process is realised for the extracted steam. Additionally, it should be pointed out that whenever steam extraction involving live steam or cold reheat steam is considered, the significant changes of mass flows in the heating surfaces of superheater and/or reheater must be taken into account.

In conclusion, the choice of the optimal source for steam supply is not only affected by efficiency considerations but also by operability issues. The best extraction point to provide for the large steam quantities at the required pressure level with regard to a minimal energy penalty, low investment costs, high flexibility, and good part-load capability is the crossover pipe connecting

the IP and LP steam turbines. Figure 4.6 shows how the heat demand of the chemical absorption process can be supplied by extracting steam from the IP/LP crossover of the steam power process.

The required steam quality is determined by the temperature of the reboiler in the CCU. The heat must be available at a temperature that corresponds to the temperature of the reboiler plus a reasonable temperature approach (in this work: 10 K). Additionally, a pressure loss in the branch pipe from the power plant to the CCU is taken into consideration and assumed to be 10 % of the pressure in the IP/LP crossover. For example, a temperature of 120 °C in the reboiler with a temperature approach of 10 K leads to a required steam quality of 2.7 bar (130 °C) at the reboiler. Taking into consideration the pressure loss in the branch pipe, a steam quality of 3.0 bar is required in the IP/LP crossover. To avoid hot spots in the reboiler which could lead to thermal degradation of the solvent or increased fouling in the reboiler, the steam for solvent regeneration has to be saturated. This is realised by recycling and injecting part of the reboiler condensate into the superheated steam.

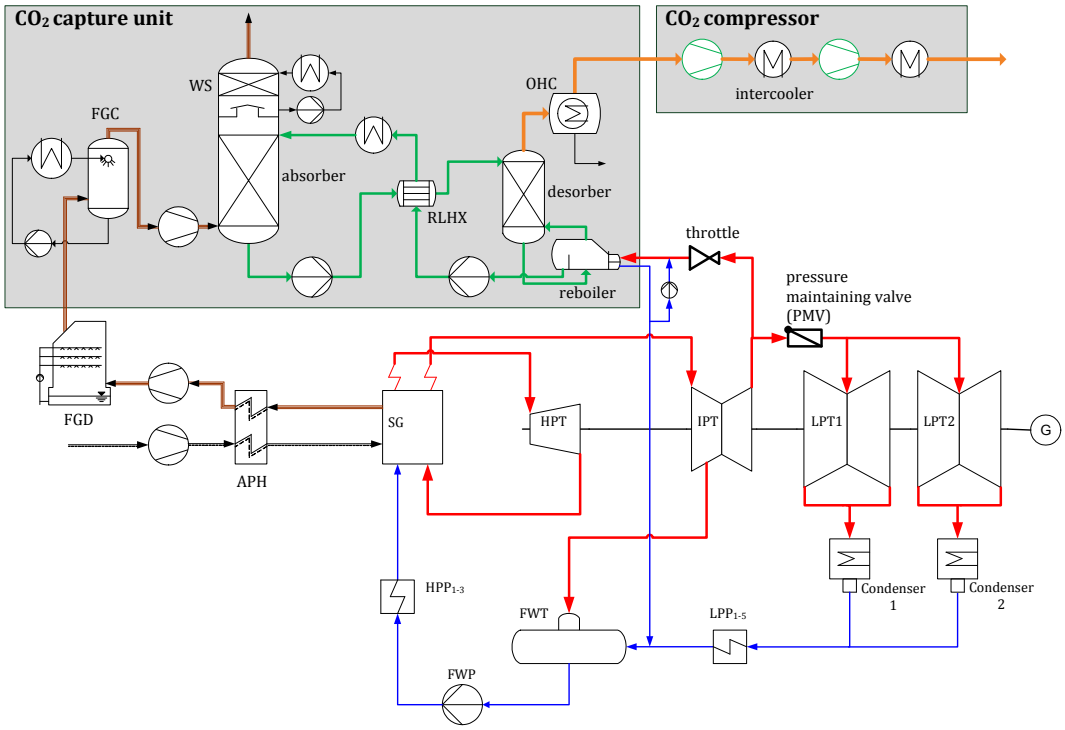

Figure 4.6: Integration of CO_2 capture unit in steam power process

4.5.2 Integration

Two integration options must be differentiated:

1. The integration of a CCU and a CO_2 compressor in an existing power plant (retrofit);
2. The integration of a CCU and a CO_2 compressor in a new power plant (greenfield).

4.5.2.1 Retrofit integration

The integration of a CO_2 capture process in an existing power plant requires additional measures to ensure the supply of steam for solvent regeneration at the right quality and quantity. The considered hard-coal-fired power plant at full-load without CO_2 capture has an IP/LP crossover pressure of 3.9 bar. When extracting steam for the CCU, the crossover pressure decreases according to Stodola's ellipse law [169]. Without any measures taken, the IP/LP crossover pressure drops from its design value of 3.9 to 1.87 bar when extracting 50 % of the steam mass flow (corresponding to a specific reboiler heat duty of approximately 3.2 GJ_{th} / t CO_2 at 90 % CO_2 capture). In this work, depending on the solvent and chosen process parameters the required steam quality varies between 1.6 and 6.9 bar (cf. Section 5.5.2).

To provide the CCU with the required steam quantity and quality, two additional components are applied (cf. Figure 4.6):

1. A throttle is located in the steam branch to the reboiler of the CCU. With this component, excessive pressure can be reduced to provide the steam at a pressure that ensures condensation at the correct temperature.
2. A pressure maintaining valve (PMV) is retrofitted to the steam pipe leading to the LP turbine inlet. With this component the pressure can be held at a certain value as required by the CCU. Depending on the amount of steam that is extracted, thus depending on the pressure drop due to Stodola's ellipse law, the maintaining of the pressure causes a pressure drop over the PMV and an additional energy penalty due to the lower LP turbine inlet pressure.

The use of a back-pressure turbine when using IP/LP steam is also possible. This option could be advantageous for steam power plants with a high crossover design pressure [31]. However, also for such power plants, in part-load

operation the IP/LP crossover pipe pressure can drop to values below the minimal required pressure. Therefore, a bypass of the back-pressure reboiler turbine in part-load operation is necessary. Such back-pressure turbine could be used in combination with an additional generator to increase the power output or alternatively to drive the CO_2 compressor by replacing the electrical motor. Besides the additional investment costs, this measure introduces an additional degree of integration between the water-steam-cycle of the power plant and the CO_2 compressor and therefore impairs operability and flexibility of the overall process. The potential to reduce the energy penalty by using a turbine-driven CO_2 compressor has to be evaluated carefully, as the partial conversion efficiency of the additional turbine must exceed the efficiency that is achieved by the fully optimised power plant turbine in connection to the generator and the motor which drives the CO_2 compressor.

In this work, in case of retrofit integration the reboiler condensate is always forwarded to the feed water tank in the water-steam-cycle, independent of the reboiler and condensate temperature. It is assumed that this is the only location at which the large flow of condensate can practically be returned to the feed water.

In the case of lower quality steam extraction ($T_{reb} < 129$ °C) the pressure level in the IP/LP crossover drops below the nominal pressure of 3.9 bar. The volume flow in the last stage of the IP turbine increases since the live steam mass flow remains constant. It shows that reboiler temperatures below 114 °C and steam extractions above 434 MW_{th} ($\cong$ 2.19 GJ_{th} / t CO_2 at 90 % CO_2 capture) lead to an increase in volume flow by 40 % or more at the IP turbine outlet in comparison to design conditions. Due to the increased steam flow, bending stresses in the last turbine stage of the IP turbine become higher compared to the design case and can lead to the destruction of the blades. A retrofit of the IP turbine might become necessary to provide for a safe operation with steam extraction for the CCU. The last stages of the IP turbine might have to be equipped with reinforced blade profiles to sustain the higher bending stresses. The losses associated to an IP turbine retrofit are likely to be within normal design variations [31]. In this work changes in turbine efficiency due to increased volume flows and modified steam flow patterns are therefore neglected.

The first stage blades of the LP turbine also experience a change in volume flow. However, the reduction in the volume flow at the LP inlet due to steam

extraction is damped by the associated pressure decrease. In total, the steam volume flow at the LP inlet is only marginally smaller than under design conditions.

Due to the large steam extraction when considering a CCU retrofit integration, there is also a considerable change in LP exhaust steam. The magnitude of the change in steam flow at the LP outlet is directly linked to the cooling system and is discussed in Section 4.5.3 below.

4.5.2.2 Greenfield integration

In a greenfield power plant, the water-steam-cycle can be adapted to optimise the integration of a CCU. As mentioned above, in this work it is assumed that a power plant equipped with a CCU would be operated at full-load and at the designed CO_2 capture rate of 90 % whenever possible. Therefore, in the greenfield integration analysis in this work the IP/LP crossover pressure is adapted so that the steam at the reboiler at full-load has the correct pressure as required by the CCU. This eliminates the losses induced by the throttle or the PMV that occur in the retrofit integration case. Note that a perfect match of IP/LP steam pressure and reboiler temperature is only valid for one operational point. As soon as the power plant load or the process parameters of the CCU are changed, the throttle or the PMV must be activated leading to an additional energy penalty.

For an optimal efficiency at full-load and operation with CO_2 capture, the reboiler condensate is returned at that point into the preheater train where the feed water shows a similar temperature. Other advanced integration configurations such as waste heat integration[11] are not considered in this work.

The outlined adaptations of the water-steam-cycle regarding the heat requirement of the CCU, allow for the highest possible efficiency of the overall process operated at full-load and with CO_2 capture. Nevertheless, part-load operation (with CO_2 capture) might become necessary if the power plant is operated in a connected grid under market conditions. Since in this case the pressure in the IP/LP crossover decreases, additional measures such as the

[11] For a detailed discussion of the potential of waste heat integration in greenfield steam power plants refer to [170].

installation of a PMV still need to be provided to ensure the supply of the CCU with steam at the right quality also during part-load operation.

There are conditions in which an operation without CO_2 capture can be economically advantageous or necessary, for example during periods of high electricity prices or in case of a trip in the CCU or the CO_2 compressor. Considering the non-capture operation of a steam power plant with integrated CCU, the steam which is usually used for the regeneration of the solution can instead be used in the LP turbine. If a water-steam-cycle configuration as outlined above is chosen, the IP/LP crossover pressure increases when additional steam is introduced, following Stodola's ellipse law. The increase in pressure (IP outlet and LP inlet) as well as in mass flow (LP inlet) has a significant effect on the flow regimes as well as on mechanical forces in the turbines. If the turbine design is not adapted to stand these high loads during non-capture operation, the amount of live steam needs to be reduced or part of the additional steam from the capture unit has to be forwarded to the turbine condenser to preserve the design parameters of the turbine.

If the power plant is not to be optimised for operation at full-load and a high CO_2 capture rate as done in this work, thus if part-load and non-capture operation of the power plant are taken into consideration, a variety of options arises to maximise the overall net efficiency for the load spectrum of the power plant in the context of its envisaged operation schedule:

1. A controlled steam extraction could be installed, designing the LP turbine for operation under non-capture operation and maximal steam flow. This option is similar to the installation of a PMV in the retrofit integration case, allowing a constant throttling of the steam to the LP turbine during the operation with CO_2 capture and corresponding steam extraction.
2. An additional peak load / standby turbine could be provided in which the additional steam during non-capture operation can be used for electricity generation. Such measure is afflicted with additional investment costs in combination with possibly large idle times of this component, which compromises the economic viability of this option.
3. The IP/LP pressure at full-load could be designed to be above the pressure required by the CCU. This option is again similar to an operation of a retrofitted steam power plant with low steam pressure re-

quirements in the CCU, in which case excessive pressure needs to be throttled in an additional component (throttle) in the steam pipe to the CCU. A higher IP/LP design pressure increases the overall net efficiency during part-load operation by reducing the losses evoked by the throttle or the PMV [170].

Although these options reduce the negative impacts of part-load or non-capture operation, all three are afflicted with disadvantages in terms of overall net efficiency at full-load and with steam extraction for CO_2 capture if compared to a water-steam-cycle configuration that is specifically optimised for this operation. As the greenfield integration analysis in this work aims at identifying the maximal net efficiency potential of CO_2 capture operation in a steam power plant at full-load, the outlined three alternatives are not taken into further consideration.

4.5.3 Cooling system

When retrofitting a post combustion CCU to a steam power plant, the overall amount of heat that has to be discharged via the cooling water system is increased by approximately 30–40 % in comparison to the power plant without CO_2 capture. Besides the increase in auxiliary power for additional cooling water pumps, there arise practical problems how the additional cooling demand can be provided. There are three options to deal with this circumstance when a CCU retrofit to the power plant is considered:

1. An additional cooling system completely independent of the existing system is installed to supply CCU and CO_2 compressor. Due to the control strategy of the main cooling water system (q.v. Section 4.3), a cooling water mass flow to the turbine condensers of 80 % is retained. As only about 50 % of the LP steam are condensed in the turbine condenser, the cooling water temperature gain and consequently the condenser pressures decrease with a positive effect on the efficiency of the water-steam-cycle.
2. The existing cooling system is impinged with an overload of 30–40 %. This would lead to an increase in temperature gain of the cooling water. The related increase in turbine condenser pressures reduces the efficiency of the water-steam-cycle.

3. An additional cooling system coupled to the existing one is installed, which provides for the 30–40 % increase in cooling duty. In this case, the cooling water temperature gain remains at 11 K and the turbine condenser pressures as well as the water-steam-cycle efficiency are unaffected.

In this work, in case of CCU retrofit integration the first option is chosen since it guarantees a flexible and autonomous operation of both cooling systems. The decrease in turbine condenser pressures and the associated increase in net efficiency and net power output are taken into consideration by the model. Note that this option also delimits the negative effects of steam extraction on the last LP turbine stages in terms of changing flow regimes: On the one hand, the steam extraction leads to a decreasing exhaust volume flow of the LP-turbines; on the other hand, this effect is counteracted by decreasing turbine condenser pressures which lead to increasing exhaust steam volume flows.

For a greenfield power plant with CO_2 capture, only about 40 % of the overall cooling duty is resulting from the condensation of steam in the turbine condensers of the power plant, since only about half of the steam mass flow remains for expansion in the LP turbine. The remaining 60 % are due to the cooling requirements of the CCU and the CO_2 compressor. In the course of the greenfield integration analysis in this work, the turbine condenser pressures are kept constant at 49 and 39 mbar. As a cooling water temperature gain of 11 K is specified, the cooling water mass flow to the turbine condensers and the auxiliary power duty of the cooling water pumps are reduced.

5 ENERGETIC EVALUATION OF SELECTED SOLVENTS

In this chapter the overall process model that was outlined in Chapter 4 is used to evaluate the impact of integrating a post-combustion CO_2 capture unit (CCU) that is operated with one of the six selected solvents on the performance of the reference steam power plant. To provide for a transparent energetic evaluation, quantities of comparison are defined (Section 5.1). To facilitate the discussion of the specific results of the energetic evaluation, certain characteristic solvent properties (Section 5.2), the general impact of the CCU and the chosen process parameters on the overall process (Section 5.3), and inherent limitations of the applied methodology (Section 5.4) are presented. Finally, the results of the energetic evaluation for retrofit (Section 5.5 and 5.6) as well as for greenfield integration (Section 5.7) are discussed.

The evaluation of the six selected solvents allows drawing some general conclusions that are valid independent of the specifics of the considered steam power plant. These **Key facts** are repeated and highlighted in the text and are summarised in Annex A.1.

5.1 Basis of comparison

As explained in Section 4.5, the integration of a CCU and a CO_2 compressor in a power plant leads to a decrease in net power output and net efficiency. The magnitude of this energy penalty does not only depend on the solvent but also on the chosen process parameters of the CCU. In the course of the energetic evaluation in this work, the optimal process parameters for each of the selected solvents are determined with regard to a minimal net efficiency penalty.

The emphasis of many studies that evaluate PCC processes is often the minimisation of the reboiler heat duty in the CCU. In this work it is shown that, depending on the underlying boundary conditions, the optimal process parameters for the operation of the CO_2 capture island do not necessarily coincide with the optimal process parameters in terms of an energy efficient operation of the overall process including CO_2 compressor and power plant. This work therefore focuses on the minimisation of the overall power loss

and net efficiency penalty in comparison to the reference power plant without CO_2 capture.

5.1.1 Net efficiency penalty and total power loss

The overall loss in net power output of the power plant ΔP_{net} due to the integration of a PCC process can be expressed as a sum of four terms:

$$\Delta P_{\mathrm{net}} = \Delta P_{\mathrm{CCU,steam}} + \Delta P_{\mathrm{CCU,el}} + \Delta P_{\mathrm{comp,el}} + \Delta P_{\mathrm{cw}} \quad , \tag{5.1}$$

where $\Delta P_{\mathrm{CCU,steam}}$ is the power decrease due to steam extraction for the regeneration of the solution in the reboiler[12], $\Delta P_{\mathrm{CCU,el}}$ is the additional auxiliary power for pumps and fans of the CO_2 capture unit, $\Delta P_{\mathrm{comp,el}}$ is the additional auxiliary power of the CO_2 compressor, and ΔP_{cw} is the auxiliary power of the cooling water pumps to provide for the cooling duty of CCU and CO_2 compressor. Steam extraction leads to a reduction in gross power produced by the generator while the latter three terms in the above equation reduce the net power output of the plant.

A reduction in net power output is equivalent to a decrease in net efficiency, since the heat input to the power plant is held constant independently of the considered solvent, CCU process parameters, and integration variant ($\dot{Q}_{\mathrm{input}} = 2306\ \mathrm{MW_{th}} = \mathrm{const.}$). The comparison of the selected solvents in the following sections is done on the basis of the net efficiency penalty $\Delta\eta_{\mathrm{net}}$, thus the difference in net efficiency of the reference power plant η_{ref} and the power plant with CO_2 capture η_{CCS}:

$$\Delta\eta_{\mathrm{net}} = \eta_{\mathrm{ref}} - \eta_{\mathrm{CCS}} = \frac{\Delta P_{\mathrm{net}}}{\dot{Q}_{\mathrm{input}}} \quad . \tag{5.2}$$

5.1.2 Reboiler heat duty

The power decrease due to steam extraction $\Delta P_{\mathrm{CCU,steam}}$ to provide for the reboiler heat duty represents the largest fraction of the overall power loss. The

[12] Steam extraction and condensation in the reboiler leads to a reduction in auxiliary power for cooling water pumps that supply the turbine condensers (q.v. Section 4.5.3). The effect is accounted for by the overall process model in the calculation of ΔP_{net} via $\Delta P_{\mathrm{CCU,steam}}$.

reboiler heat duty is therefore an important quantity which needs to be considered carefully, although the optimisation of the overall process aims at a minimal total power loss and a minimal net efficiency penalty.

The overall mass-specific heat duty q_{reb} (e.g., in $\mathrm{GJ_{th}\,/\,t\,CO_2}$), which is supplied in the reboiler of the desorber column to regenerate the solution, can be expressed as the sum of three terms:

$$q_{\mathrm{reb}} = q_{\mathrm{sens}} + q_{\mathrm{vap,H2O}} + q_{\mathrm{abs,CO2}} \quad , \tag{5.3}$$

where $q_{\mathrm{abs,CO2}}$ is the heat required to strip the CO_2 from the solution, $q_{\mathrm{vap,H2O}}$ is the heat of vaporisation required to generate the water vapour (stripping steam) in the desorber, and q_{sens} is the sensible heat to increase the temperature of the solution at the desorber inlet to the conditions in the reboiler (boiling point).

The reboiler heat duty can be estimated by

$$q_{\mathrm{reb}} \approx \overbrace{\frac{C_{\mathrm{p,L}}\,(T_{\mathrm{reb}} - T_{\mathrm{feed}})}{\Delta\alpha}\frac{M_{\mathrm{sol}}}{M_{\mathrm{CO2}}}\frac{1}{x_{\mathrm{alk}}}}^{q_{\mathrm{sens}}} + \overbrace{\Delta h_{\mathrm{vap,H2O}}\left[\frac{p_{\mathrm{H2O}}}{p_{\mathrm{CO2}}}\right]_{\mathrm{des,top}}\frac{1}{M_{\mathrm{CO2}}}}^{q_{\mathrm{vap,H2O}}} + \overbrace{\frac{\Delta h_{\mathrm{abs,CO2}}}{M_{\mathrm{CO2}}}}^{q_{\mathrm{abs,CO2}}} \quad , \tag{5.4}$$

where T_{feed} is the temperature of the rich solution at the desorber inlet, $\Delta\alpha$ is the difference in CO_2 loading between absorber outlet (rich) and inlet (lean), x_{alk} is the molar fraction of the alkali component in the solution (q.v. Annex A.2), and $p_{\mathrm{H2O}}/p_{\mathrm{CO2}}$ is the partial pressure ratio of water and CO_2 at the desorber top.

Note that the reboiler heat duty is entirely supplied by the stripping steam generated in the reboiler which consists mainly of H_2O and CO_2. Part of that steam condenses on its way up the column where the emerging latent heat provides for sensible heat as well as the heat of absorption/desorption. $q_{\mathrm{vap,H2O}}$ solely denotes that part of the stripping steam which provides for the driving force, i.e. partial pressure difference, that transfers the physically dissolved molecular CO_2 from the liquid into the gas phase and which remains uncondensed at the desorber top. The largest part of the remaining water vapour is condensed in the OHC downstream of the desorber, so that $q_{\mathrm{vap,H2O}}$ is ultimately dissipated to the cooling system.

Also note that the three terms of Eq. (5.3) and (5.4) are not mutually exclusive but depend on each other as well as on the operational parameters of the CCU. A common misguiding conclusion of the analysis of Eq. (5.3) is the statement that solvents with a low heat of absorption $\Delta h_{\mathrm{abs,CO2}}$ must also provide for a low total reboiler heat duty [171]. This is not the case, as this conclusion blends out that $q_{\mathrm{vap,H2O}}$ is in fact a function of $q_{\mathrm{abs,CO2}}$ (q.v. Section 5.3.1). It shows that high heat of absorption solvents profit from an increase in reboiler temperature in terms of a lower reboiler heat duty since the amount of required stripping steam is reduced ($q_{\mathrm{vap,H2O}} \downarrow$).

5.2 Solvent characterisation

In the course of an energetic evaluation of chemical solvents for post-combustion CO_2 capture, certain restrictions and inherent properties associated to each of the individual solvents have to be considered. Such characterisation also facilitates the interpretation of the results of the energetic evaluation for the selected solvents in Sections 5.5, 5.6, and 5.7.

5.2.1 Temperature limits

As is shown in Section 5.3 below, the reboiler temperature at which the solution is regenerated has a large impact on the performance of the overall process through a variety of mechanisms. Yet, the variation of this process parameter is limited as the amount of thermal degradation increases with the reboiler temperature. The degradation tendency also increases with a decrease in CO_2 concentration. Therefore, the majority of thermal degradation occurs in the reboiler, where the temperature is highest and the CO_2 concentration is lowest [51].

The thermal degradation pathway of MEA is the best studied: Below 200 °C thermal degradation occurs by reaction with CO_2 in a process termed carbamate polymerisation. The degradation mechanisms of other amines are less studied, but all seem to follow a carbamate polymerisation pathway as MEA [64].

In a trade-off between the increase in operational expenditures (solvent loss) and a decrease in energy costs (heat duty reduction), for MEA the optimal reboiler temperature lies in the range between 120 and 125 °C [172]. DAVIS suggests that a higher solution flow rate[13] coupled to a higher desorber pressures can be economically beneficial, as the thermal degradation rate is reduced, while reducing energy costs for CO_2 compression at the same time [64]. A complete economic evaluation of the capture process in combination with each of the six selected solvents is out of the scope of this work. Therefore, a simplified approach to determine a reasonable upper temperature limit is taken.

For PZ an operational temperature limit of 150 °C is applied, as thermal degradation (compared to 7 m MEA at 120 °C) is negligible up to this temperature [24]. Under rich conditions ($\alpha = 0.4$ mol CO_2 / mol alk) the degradation rate constant (% loss per week) of 8 m PZ at 150 °C is approximately five times as low as of 7 m MEA at 120 °C. However, the temperature for PZ solutions is not increased beyond 150 °C due to the five to six times higher price of PZ compared to MEA [72].

DAVIS showed that AMP solutions have a lower degradation tendency than 7 m MEA at comparable conditions. This is due to the added methyl groups to the primary and secondary carbons on the MEA molecule, providing the steric hindrance. Adding two methyl groups to the primary carbon of MEA, as in AMP, reduces the degradation rate by a factor of four [64]. Assuming a similar price level as MEA, the reboiler temperature for AMP solutions can therefore be increased to approximately 135 °C.

There is no information on the interaction of potassium and piperazine species in the context of thermal degradation of a K/PZ solvent blend. For the determination of a reasonable upper temperature limit for K/PZ solutions it is therefore assumed that potassium, as it is not involved in the formation of carbamate, has no impact on the thermal degradation tendency of PZ. In analogy to PZ the upper temperature limit for the K/PZ solvent is therefore set to 150 °C.

[13] A higher solution flow rate is equivalent to a higher CO_2 loading of the lean solution (cf. Section 5.2.2), leading to a lower degree of thermal degradation.

For MDEA/PZ no detailed information on the thermal degradation pathway is yet available. From preliminary degradation studies, however, CLOSMANN considers the practical upper temperature limit for reboiler operation to be no more than 120 °C [173].

ZHOU concluded that ethanolamines promote the thermal degradation of cyclic amines [174]. For this reason, an AMP/PZ blend is less stable than AMP in aqueous solution without any activator. PZ in a 4 m AMP / 6 m PZ solution at approximately 120 °C shows a similar degradation rate as PZ at 150 °C. As no other information on the selected 5 m AMP / 2.5 m PZ solvent are available, 120 °C is chosen as the upper temperature limit for this solvent.

Table 5.1 summarises the upper temperature limits for the selected solvents which are taken into consideration in the following energetic evaluation.

Table 5.1: Assumed upper temperature limits for selected solvents

solvent	max. reboiler temperature
MEA	120 °C
PZ	150 °C
AMP	135 °C
K/PZ	150 °C
MDEA/PZ	120 °C
AMP/PZ	120 °C

A lower limit for the reboiler temperature is also considered. The desorber pressure is coupled to the reboiler temperature in combination with the desired CO_2 loading of the lean solution. It is presumed that the operating pressure of the desorber must always be above atmospheric conditions (1.01325 bar) as the regeneration under vacuum would require a different column design to account for the reversed forces on the column shell. Additionally, excessively low temperatures impede the overall mass transfer and contradict the assumption of an equilibrium pinch in the desorber column (q.v. Section 3.3.2). The lower limit for the reboiler temperature is therefore set to 100 °C.

5.2.2 CO_2 capacity

The amount of solution which needs to be circulated in the process between absorber and desorber depends on the solvent concentration x_{alk} in the aqueous solution, the desired CO_2 capture rate ε (i.e., the fraction of CO_2 that is absorbed from the flue gas), and the difference in CO_2 loading between the rich and lean solution $\Delta\alpha$. The required solution circulation (mass) flow rate can be calculated via

$$\dot{m}_{\mathrm{sol}} = \frac{M_{\mathrm{sol}}\, \dot{m}_{\mathrm{fg}}\, w_{\mathrm{CO2,fg}}\, \varepsilon}{M_{\mathrm{CO2}}\, x_{\mathrm{alk}}\, \Delta\alpha} \quad , \tag{5.5}$$

where $\dot{m}_{\mathrm{fg}}$ is the mass flow of flue gas at the absorber inlet, $w_{\mathrm{CO2,fg}}$ is the corresponding mass fraction of CO_2, and where

$$\Delta\alpha = \alpha_{\mathrm{rich}} - \alpha_{\mathrm{lean}} \quad . \tag{5.6}$$

The ratio of solution and flue gas flow rate in the absorber is referred to as

$$\frac{L}{G} = \frac{\dot{m}_{\mathrm{sol}}}{\dot{m}_{\mathrm{fg}}} \quad . \tag{5.7}$$

The loading difference $\Delta\alpha$ determines the required solution flow rate and L/G and relates to the sensible heat requirement q_{sens} via Eq. (5.4). Since the absorbed CO_2 has a negligible partial heat capacity, the CO_2 capacity κ is defined on a mole CO_2 per kg of water and kg alkali fraction basis [60]:

$$\kappa = \Delta\alpha\, x_{\mathrm{alk}}\, \frac{1}{M_{\mathrm{sol}}} \frac{1}{w_{\mathrm{H2O}} + w_{\mathrm{alk}}} \quad , \tag{5.8}$$

where w_{H2O} and w_{alk} are the mass fractions of water and alkali fraction in solution, respectively.

The CO_2 capacity is a function of the difference in CO_2 loading of the rich and the lean solution $\Delta\alpha$. The lean loading depends on the temperature and pressure in the reboiler of the desorber column, which are process parameters that can be varied within certain limits. The rich loading is determined by the temperature profile and the column design of the absorber. It can be estimated by assuming a minimal required driving force for CO_2 absorption at the rich end of the absorber (q.v. Section 4.1.1). With a CO_2 partial pressure of approximately 15 kPa in the flue gas, an equilibrium CO_2 partial pressure of 5 kPa allows for a reasonable driving force that is achievable with an economically feasible height of the absorber [60]. The determined rich CO_2 load-

ings for the six selected solvents at an equilibrium CO_2 partial pressure of 5 kPa and 50 °C are presented in Table 4.2 in Section 4.1.1.

A large difference in rich and lean loading and therefore a high CO_2 capacity allows the reduction of the solution flow rate to achieve a certain CO_2 capture rate (cf. Eq. (5.5)). Therefore, less solution needs to be heated up to the reboiler temperature which ultimately reduces the heat duty to be supplied in the reboiler (cf. Eq. (5.4)). Note that the CO_2 capacity is not a single value associated to a certain solvent. It is rather a process parameter which can be adjusted in the CCU. Figure 5.1 shows the calculated CO_2 capacities of the selected solvents for varying CO_2 loadings of the lean solution at 40 °C and an assumed rich loading at an equilibrium CO_2 partial pressure of 5 kPa and 50 °C.

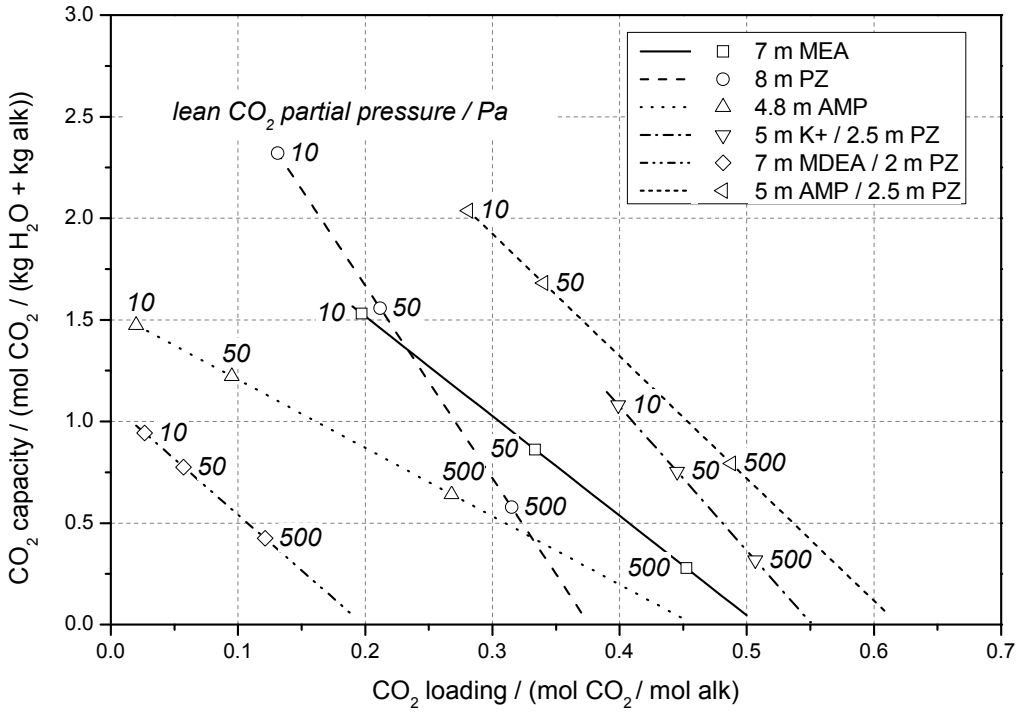

Figure 5.1: CO_2 capacity of selected solvents for varying CO_2 loadings at 40 °C and rich loading at equilibrium CO_2 partial pressure of 5 kPa and 50 °C.

5.2.3 CO_2 capacity increase by overstripping

Three distinct CO_2 loadings and corresponding equilibrium CO_2 partial pressures are highlighted for each solvent in Figure 5.1. These values correspond to different degrees of regeneration of the solution in the desorber:

- **Saturation** Under the assumption of 90 % CO_2 capture, the CO_2 partial pressure in the treated flue gas at the lean (top) end of the absorber is approximately 1.5 kPa. Assuming an evenly distributed driving force over the absorber height and following the assumption for the estimation of the rich loading (cf. Section 4.1.1), the equilibrium CO_2 partial pressure of the lean solution at the absorber inlet must not exceed 500 Pa to maintain a partial pressure ratio of 3 (cf. Figure 5.2). This operating condition is referred to as saturation and poses the upper limit for the loading of the lean solution, meaning that the solution in the desorber must be regenerated to this loading level or below.
- **Overstripping** Under certain conditions it can be beneficial to increase the CO_2 capacity by lowering the lean loading below the value that corresponds to saturation conditions. Regeneration to a related equilibrium CO_2 partial pressure of the lean solution of below 500 Pa at 40 °C is referred to as "overstripping".

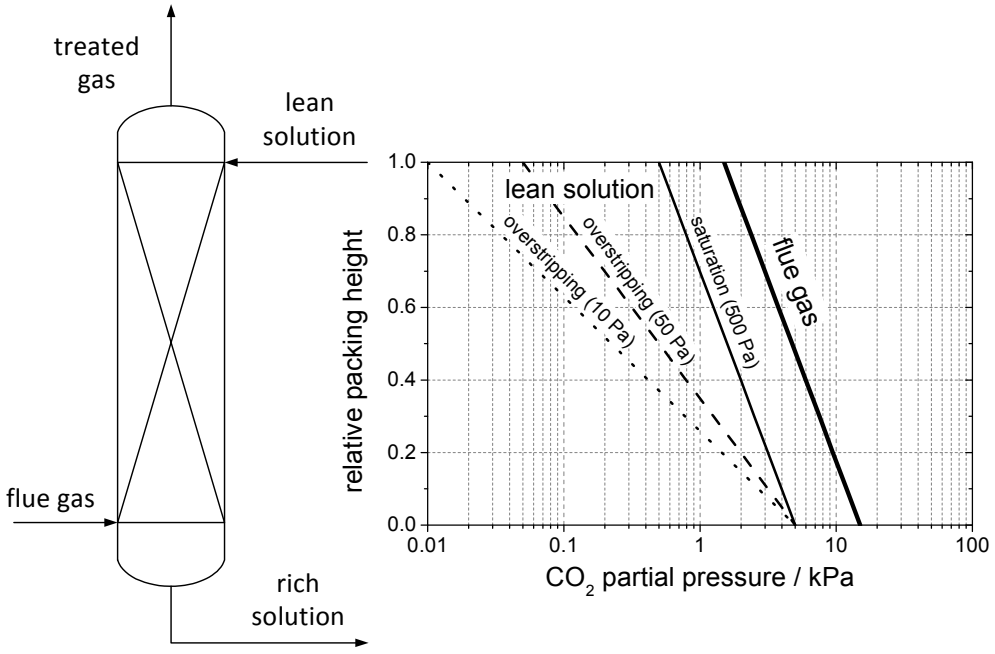

Figure 5.2: Assumed CO_2 partial pressure characteristics in absorber column for different CO_2 partial pressures of lean solution at 40 °C

A reduced CO_2 loading and respective equilibrium CO_2 partial pressure of the lean solution leads to a larger CO_2 capacity and decreases the solution flow rate that is required to achieve a specified CO_2 capture rate. Table 5.2 shows the calculated L/G in the absorber for three defined levels of regeneration.

Table 5.2: *L/G* under saturation and overstripping conditions

	saturation	overstripping	
$p^*_{CO2,lean}$	500 Pa	50 Pa	10 Pa
MEA	17.30	5.45	2.99
PZ	8.57	3.06	1.99
AMP	7.11	3.64	2.98
K/PZ	16.00	6.64	4.56
MDEA/PZ	10.63	5.73	4.68
AMP/PZ	6.24	2.84	2.31

Note that saturation conditions define an actual (upper) limit for the regeneration of the solution to ensure an equally distributed driving force in the absorber as explained above. Overstripping is merely an expression that facilitates the interpretation and explanation of the results of the energetic evaluation.

The increase in driving force for CO_2 absorption in the upper (lean) part of the absorber under overstripping conditions does not necessarily lead to an improvement in the CO_2 loading at the bottom (rich) end. The CO_2 loading of the rich solution is mainly restricted by a limited mass transfer rate at the rich end (rate pinch, q.v. Section 3.3). The reason for a restricted uptake of CO_2 is not a small driving force but rather the low concentration of free amine at the rich end which reduces the mass transfer coefficient and which ultimately impedes the flux of CO_2 from the gas into the liquid phase (q.v. Eq. (3.39)). Therefore, an increase in driving force under overstripping conditions at the lean end of the absorber column does not necessarily lead to an enhancement of the CO_2 loading of the rich solution. In this work the rich loading for each of the selected solvents is estimated by the procedure as explained in Section 4.1.1 and is kept constant independent of the change of any other parameter.

Table 5.3 shows the estimated capacity increase under overstripping conditions in comparison to the minimal degree of regeneration of the solution under saturation conditions. The minimal or inherent CO_2 capacity of the solvent under saturation conditions is an adequate quantity to assess the contribution of sensible heat to the reboiler heat duty. The possible increase in CO_2 capacity identifies the potential for sensible heat reduction by overstripping. The combination of these two properties provides an indication if overstripping can be an appropriate measure to reduce the reboiler heat duty. A low inherent CO_2 capacity in combination with a large capacity increase under overstripping conditions leads to the largest potential for sensible heat reduction. Following these criteria, MEA, PZ, and K/PZ show the largest potential of capacity increase by overstripping.

Table 5.3: Inherent CO_2 capacity and CO_2 capacity increase by overstripping compared to saturation conditions

	saturation	overstripping			
$p^*_{CO2,lean}$	500 Pa	50 Pa		10 Pa	
	κ^*	$\Delta\kappa$		$\Delta\kappa$	
	mol CO_2 / (kg H_2O + kg alk)				
MEA	0.278	+0.584	+210 %	+1.252	+450 %
PZ	0.579	+0.979	+169 %	+1.742	+301 %
AMP	0.641	+0.581	+91 %	+0.834	+130 %
K/PZ	0.317	+0.435	+137 %	+0.764	+241 %
MDEA/PZ	0.424	+0.351	+83 %	+0.519	+122 %
AMP/PZ	0.793	+0.889	+112 %	+1.245	+157 %

* inherent CO_2 capacity

Both MEA and K/PZ show a large potential of reboiler heat reduction by overstripping. The CO_2 capacity of MEA is increased almost fivefold when going from saturation to maximal overstripping conditions. 8 m PZ exhibits about a 70 % greater CO_2 capacity than 7 m MEA over the entire loading and partial pressure range due to the two functional amino groups of PZ (cf. Figure 5.1). MDEA/PZ has a medium CO_2 capacity but the lowest potential for capacity increase. AMP and AMP/PZ have the highest inherent capacity and

show a low increase in CO_2 capacity when regenerated to lower CO_2 loadings; these solvents are therefore probably not eligible to be able to profit from overstripping.

A reduction of the equilibrium CO_2 partial pressure of the lean solution requires an increased amount of stripping steam to realise a more thorough regeneration. Therefore, the potential of reducing the sensible heat requirement by overstripping must be compared to the required increase in water vapour. Additionally, the impact of the reduction in reboiler heat duty by overstripping depends on other process parameters, such as the reboiler temperature and the temperature difference in the RLHX. Therefore, a detailed analysis using an overall process model is required for a concluding assessment of the potential of overstripping for a specific solvent and its corresponding process parameters. This is done in the context of solution flow rate optimisation in Sections 5.5, 5.6, and 5.7 below, where all impacting factors are taking into consideration.

5.3 General impact of CCU on overall process

In the following some general implications of steam extraction and chosen reboiler temperature on the overall process – independent of the applied solvent – are discussed to facilitate the discussion of the specific results for the selected solvents in Sections 5.5, 5.6, and 5.7.

The steam extraction to provide for the reboiler heat duty as well as the supply of auxiliary power of CCU, CO_2 compressor, and additional cooling water pumps lead to a decrease in net efficiency of the power plant. The required steam extraction is the largest contributor to the net efficiency penalty (50–70 %). Not only the amount (quantity, reboiler heat duty) of extracted steam but also the required pressure (quality) of the necessary steam determines the equivalent loss in net power output. The required quality of the steam is specified by the reboiler temperature which in turn influences the operating pressure of the desorber and therefore indirectly impacts the required auxiliary power for CO_2 compression.

5.3.1 Reboiler temperature and steam quantity

The reboiler temperature influences the overall reboiler heat duty and thus the amount of required steam extraction, as it determines that part of the

stripping steam that is generated in the reboiler and which remains uncondensed at the desorber top ($q_{\mathrm{vap,H2O}}$, cf. Section 5.1.2). This coherence can be explained by considering the partial pressures of water and CO_2 at a certain temperature.

If assuming a constant total pressure and an ideal gas phase, the Gibbs-Helmholtz equation (Eq. (3.7)) can be written in the following form:

$$\frac{d(p^*_{\mathrm{CO2}})}{p^*_{\mathrm{CO2}}} = -\frac{\Delta h_{\mathrm{abs,CO2}}}{\mathrm{R}} \frac{d(T)}{T^2} \quad , \tag{5.9}$$

relating the equilibrium CO_2 partial pressure p^*_{CO2} and the heat of absorption $\Delta h_{\mathrm{abs,CO2}}$ of the individual solvent.

A similar relationship exists between the vapour pressure $p^{\mathrm{s}}_{\mathrm{H2O}}$ and the heat of vaporisation of water $\Delta h_{\mathrm{vap,H2O}}$ expressed by the Clausius-Clapeyron equation:

$$\frac{d(p^{\mathrm{s}}_{\mathrm{H2O}})}{p^{\mathrm{s}}_{\mathrm{H2O}}} = -\frac{\Delta h_{\mathrm{vap,H2O}}}{\mathrm{R}} \frac{d(T)}{T^2} \quad . \tag{5.10}$$

Assuming that the heat of vaporisation of water and the heat of absorption of CO_2 are constant over a considered (small) range of temperatures, one can integrate and combine Eqs. (5.9) and (5.10) yielding:

$$\frac{p^{\mathrm{s}}_{\mathrm{H2O}}}{p^*_{\mathrm{CO2}}} = \frac{p^{\mathrm{s}}_{\mathrm{H2O,ref}}}{p^*_{\mathrm{CO2,ref}}} \exp\left(\left[\frac{T - T_{\mathrm{ref}}}{\mathrm{R}\, T\, T_{\mathrm{ref}}}\right] \left[\left|\Delta h_{\mathrm{vap,H2O}}\right| - \left|\Delta h_{\mathrm{abs,CO2}}\right|\right]\right) . \tag{5.11}$$

If it is assumed that the CO_2-rich gas stream at the desorber top is in equilibrium with the rich solution at the inlet, the H_2O-CO_2 partial pressure ratio in that gas stream is directly proportional to the ratio of water vapour pressure and equilibrium CO_2 partial pressure as given by Eq. (5.11).

It is notable from Eq. (5.11) that solvents with a high heat of absorption ($\Delta h_{\mathrm{abs,CO2}} > \Delta h_{\mathrm{vap,H2O}} \approx 40$ kJ / mol) benefit from regeneration at elevated temperatures, while those with low heat of absorption (< 40 kJ / mol) profit from regeneration at low pressure and low temperature (vacuum desorption). It shows that for high heat of absorption solvents an increase in temperature results in a decrease of the ratio of water vapour and CO_2 at the de-

sorber top. Therefore, a higher reboiler temperature for these kind of solvents results in a decrease of $q_{\mathrm{vap,H2O}}$ and ultimately in a reduction of the reboiler heat duty (cf. Eq. (5.4))[14].

Key fact 1: The higher the heat of absorption, the higher the decrease in reboiler heat duty for an increasing reboiler temperature.

5.3.2 Reboiler temperature and steam quality

The required steam quality is determined by the reboiler temperature, the reboiler temperature approach (in this work: 10 K), and the pressure loss in the steam pipe from the extraction point to the reboiler (in this work: 10 % of the IP/LP crossover pressure). Figure 5.3 shows the effect of steam extraction on the reference power plant for different reboiler heat duties and varying reboiler temperature. The diagram is divided into two distinct areas by the bold black line, which represents an operation with open valves. In this case, neither the throttle in the steam branch to the reboiler of the CCU nor the pressure maintaining valve (PMV) in the steam pipe leading to the LP turbine inlet are active (cf. Figure 4.6). Hence, the pressure in the IP/LP crossover drops due to the steam extraction and perfectly matches the steam pressure as required by the CCU:

A. Throttle: Below the open valve operation line, the pressure in the IP/LP crossover is larger than the pressure required by the CCU. The excessive pressure must be throttled to the required value. The net efficiency penalty for a given steam extraction decreases slightly as the reboiler temperature is raised to higher values since the required steam pressure approaches the crossover pressure.

B. PMV: Above the open valve operation line, without any additional measure the pressure in the IP/LP crossover would drop below the

[14] For a more detailed discussion of this subject refer to [171].

necessary value. Therefore, the PMV needs to be activated. In this case, the power loss for a certain amount of steam extraction increases to higher reboiler temperatures. This is caused by a combination of effects[15], where the pressure drop over the PMV has the main impact. To provide for a constant pressure upstream of the PMV, a decrease in pressure downstream of this component is inevitable (isenthalpic throttling). The PMV therefore reduces the available pressure and exergy level of the steam at the LP turbine inlet: the higher the reboiler temperature, the higher the pressure drop in the PMV and the higher therefore the power losses for a given amount of steam extraction.

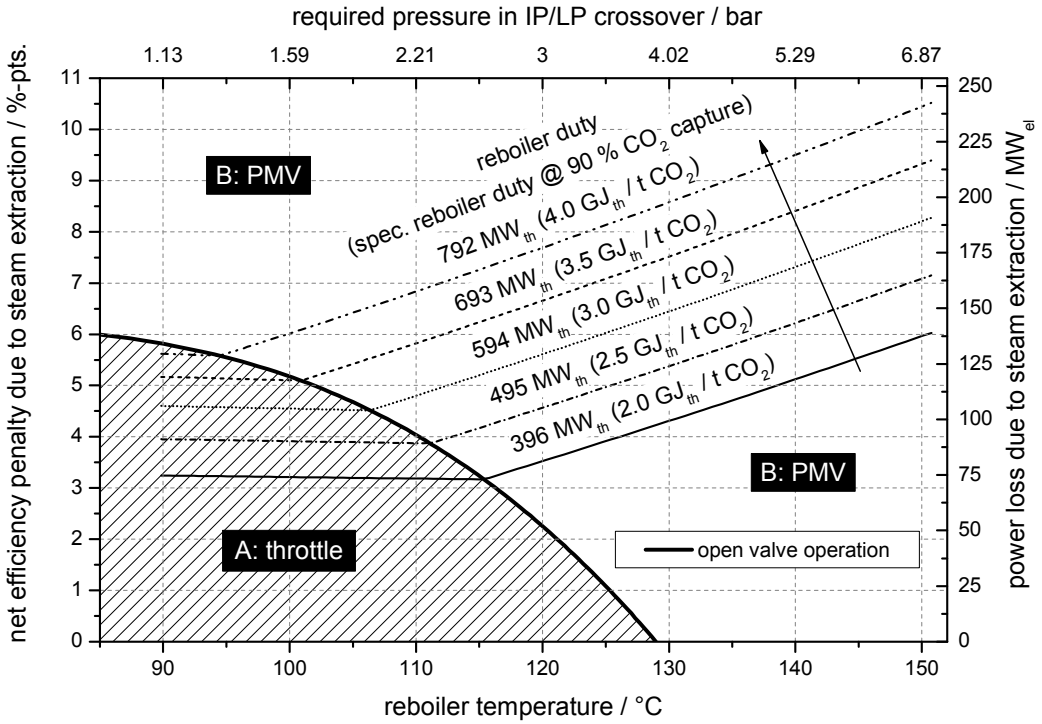

Figure 5.3: Net efficiency penalty and power loss due to steam extraction in case of retrofit integration in reference power plant for different reboiler heat duties and varying reboiler temperature

[15] For a detailed explanation of the impact of steam extraction on the water-steam-cycle refer to [163].

It is also notable from Figure 5.3 that a higher reboiler heat duty requires a lower reboiler temperature to reach open valve conditions and to achieve a minimal specific power loss for a given steam extraction.

Key fact 2: The higher the reboiler heat duty in case of retrofit integration, the lower the optimal reboiler temperature to reach open valve operation for which the net efficiency penalty due to steam extraction becomes minimal.

5.3.3 Reboiler temperature, lean loading, and CO_2 compression

The reboiler temperature not only affects the required steam quantity and quality but also has an impact on the pressure of the CO_2-rich stream downstream of the OHC which is fed to the CO_2 compressor. The reboiler temperature therefore indirectly influences the auxiliary power required for CO_2 compression to, in this work, 110 bar (cf. Eq. (4.18)).

To estimate the influence of the reboiler temperature on the auxiliary power of the CO_2 compressor, the total pressure at the lean end (bottom) of the desorber column is considered. Note that when neglecting pressure losses of desorber column, washing section, and OHC, the desorber pressure p_{des} is equal to the inlet pressure of the CO_2 compressor $p_{\mathrm{comp,inlet}}$[16]:

$$p_{\mathrm{comp,inlet}} = p_{\mathrm{des}} = p_{\mathrm{CO2}}(T_{\mathrm{reb}}, \alpha_{\mathrm{lean}}) + p_{\mathrm{H2O}} \ , \tag{5.12}$$

with

$$p_{\mathrm{H2O}} = x_{\mathrm{H2O}} \cdot p^{\mathrm{s}}_{\mathrm{H2O}}(T_{\mathrm{reb}}) \ . \tag{5.13}$$

Eqs. (5.12) and (5.13) correspond to Eqs. (3.20) and (3.23) of the semi-empirical column model.

[16] In the energetic evaluation as outlined in Sections 5.5, 5.6, and 5.7, which makes use of the overall process model, all additional pressure losses are taking into consideration.

For a constant CO_2 loading of the lean solution α_{lean}, an increase in reboiler temperature leads to an increase in both p_{CO2}, due to the characteristics of CO_2 solubility, and p_{H2O}, due to the elevated water vapour pressure $p^{\text{s}}_{\text{H2O}}$. Ultimately, an elevated reboiler temperature therefore implies an increase in desorber pressure p_{des} (cf. Eq. (5.12)). As the inlet pressure to the CO_2 compressor increases respectively, less power is needed for the compression of the CO_2 to the fixed outlet pressure of 110 bar if the reboiler temperature is increased.

If instead the reboiler temperature is to be kept constant for a changing CO_2 loading, the desorber pressure needs to be adapted simultaneously. This effect plays an important role in the optimisation of the solution flow rate (cf. Section 5.5.1). It shows that a reduction of the CO_2 loading, thus a decrease of the corresponding CO_2 partial pressure of the lean solution, impairs the compression. To provide for a constant reboiler temperature, the total pressure needs to be decreased when decreasing the lean CO_2 partial pressure (cf. Eq. (5.12)). The lean CO_2 partial pressure at the bottom of the desorber, thus at reboiler temperature, can be calculated via the equilibrium CO_2 partial pressure at 40 °C (313.15 K) and by integrating the Gibbs-Helmholtz equation (Eq. (3.7)), yielding [171]:

$$p_{\text{CO2}}(T_{\text{reb}}) = p^{*}_{\text{CO2,lean}}(313.15\ \text{K}) \exp\left(\frac{\Delta h_{\text{abs,CO2}}}{\text{R}}\left[\frac{1}{313.15} - \frac{1}{T_{\text{reb}}}\right]\right) . \qquad (5.14)$$

An examination of Eqs. (5.12) to (5.14) allows for three conclusions: i) For a given reboiler temperature, solutions with a lower solvent concentration and consequently with a higher mole fraction of water (x_{H2O}) can be regenerated at a higher desorber pressure and therefore show a lower power demand for CO_2 compression than higher concentrated solvents. ii) Solvents with a higher heat of absorption imply a more significant increase in auxiliary power for CO_2 compression when reducing the CO_2 loading and the corresponding CO_2 partial pressure of the lean solution (overstripping). iii) Solvents with a higher heat of absorption suffer from a larger increase in auxiliary power when the reboiler temperature is reduced.

Key fact 3: The lower the solvent concentration in aqueous solution, the lower the auxiliary power for CO_2 compression.

Key fact 4: The higher the heat of absorption of the solvent, the more significant the increase in auxiliary power for CO_2 compression when reducing the CO_2 loading of the lean solution.

Key fact 5: The higher the heat of absorption of the solvent, the more significant the increase in auxiliary power for CO_2 compression when lowering the reboiler temperature.

Key fact 5 implies that for high heat of absorption solvents an increase in reboiler temperature is not only beneficial in terms of a lower reboiler heat duty (cf. Key fact 1), but also in terms of a lower power demand for CO_2 compression. This coherence is referred to as thermal compression. It underlines the need for a holistic approach in the search for new solvents instead of a misguided focus on low heat of absorption.

For an estimation of the power demand for CO_2 compression, which is outlined in the following paragraphs, the heat of absorption is estimated with $\Delta h_{\mathrm{abs,CO2}} = 70\,\mathrm{kJ} \,/\, \mathrm{mol\ CO_2}$, which is approximately the average value of the solvents selected for energetic evaluation in this work (cf. Annex A.3.2). The mole fraction of water in the lean solution is estimated with $x_{\mathrm{H2O}} = 0.85$ and the water vapour pressure is calculated via Eq. (3.24). The total pressure is then substituted into Eq. (4.18) to estimate the auxiliary power demand of the CO_2 compressor.

Figure 5.4 illustrates the result of the estimation. It is notable that the auxiliary power demand of the CO_2 compressor increases with lower reboiler temperatures and lower lean CO_2 partial pressures. The latter corresponds to an operation with a lower solution flow rate, since a leaner solution can absorb more CO_2 and since less solution is therefore needed to achieve a certain CO_2 capture rate (q.v. Section 5.2.2). For the considered CO_2 compressor outlined in Section 4.2 and under the described assumptions, regeneration of the lean solution to an equivalent CO_2 partial pressure of 10 Pa (overstripping) at 40 °C at a reboiler temperature of 120 °C requires 20 % more auxiliary power (equivalent to an additional net efficiency penalty of 0.51 %-pts.) than regeneration to 500 Pa.

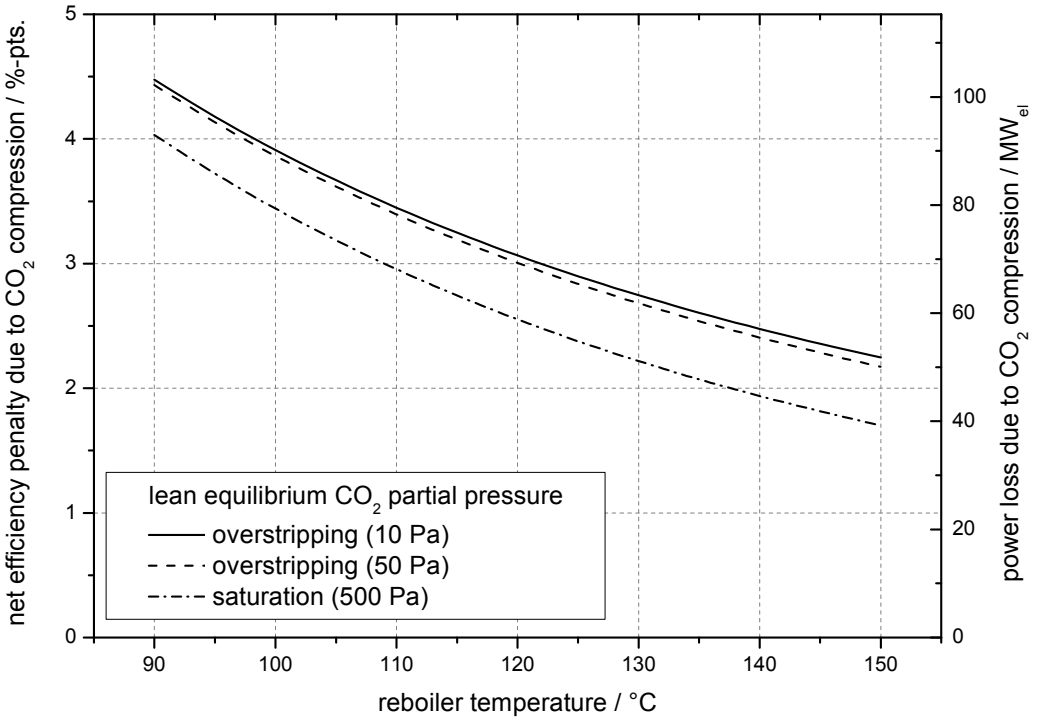

Figure 5.4: Estimated net efficiency penalty and power loss in reference power plant due to CO_2 compression for different equilibrium CO_2 partial pressures of lean solution and varying reboiler temperature

5.3.4 Summary

It can be concluded that the variation in reboiler temperature influences the overall process efficiency in both positive and negative direction. For high heat of absorption solvents, the ratio of the equilibrium partial pressures of CO_2 and water vapour is proportional to the temperature. Hence, when increasing the reboiler temperature, less stripping steam needs to be generated and less water is evaporated. Therefore, the total reboiler heat duty decreases (cf. Section 5.3.1). Furthermore, with an increase in reboiler temperature the steam for regeneration of the solution has to be extracted at higher pressure and thus at a higher exergy level, resulting in larger specific power losses in the power plant (cf. Section 5.3.2). Finally, the required energy for CO_2 compression is reduced since the CO_2 enters the compressor at a higher pressure (cf. Section 5.3.3). The impact of the described effects on the overall power loss are different in direction and – depending on the solvent – can vary significantly in magnitude. This conclusion entails the necessity of an

overall process evaluation in which the interaction of all three sub processes (CO_2 capture unit, CO_2 compressor, power plant) is taken into consideration.

Figure A.11 in Annex A.5 shows a nomogram to be used for graphical evaluation of an arbitrary CCU in terms of its corresponding power loss due to steam extraction and CO_2 compression to 110 bar in case of a retrofit integration in the reference power plant. The nomogram combines the results of the overall process evaluation for the reference power plant and the CO_2 compressor as defined in Sections 4.3 and 4.2, respectively, and presents them in graphical form. The nomogram, however, does not consider the impact of auxiliary power for the CCU and additional cooling water pumps which in sum lead to an additional net efficiency penalty of approximately 1–1.5 %-pts. Figure A.12 and Figure A.13 in Annex A.5 show similar nomograms for the evaluation of CCU retrofit integration in a power plant with increased IP/LP crossover design pressure and for the evaluation of a greenfield power plant with integrated CCU (q.v. Sections 5.6 and 5.7).

5.4 Limitations of semi-empirical column model

The semi-empirical column model includes assumptions and simplifications which must be considered when using the model for an overall process optimisation:

1. **Fast solvents**: The proposed methodology for the representation of the desorber in the CCU is only valid for solvents that show quasi-instantaneous reaction kinetics and high mass transfer rates. The heats of absorption of the solvents selected in this work are comparably high and of similar scale (cf. Figure A.7 in Annex A.3.2) which indicates a similar magnitude of the reaction kinetics. The similarity of mass transfer rates of these solvents is also suggested by their liquid phase mass transfer coefficients (cf. Table 3.4).
2. **Column pressure drop**: An increase in solution flow rate might lead to a larger pressure drop in both absorber and desorber column if the column design (diameter) is not adapted to the change in operational conditions. This would increase the auxiliary power of the fan (absorber) and CO_2 compressor (desorber) and would shift the optimal solution flow rate with respect to a minimal overall power loss to lower values.

3. **Constant rich loading**: As explained in Section 4.1.1, a simplified approach must be taken for the representation of the absorber column in the energetic evaluation. The assumed constant equilibrium CO_2 partial pressure leads to a constant CO_2 loading of the rich solution at the absorber outlet. In real absorber columns an increase in solution flow rate on the one hand causes a reduction in the magnitude of the temperature bulge over the column height due to the higher overall heat capacity[17]. On the other hand a higher solution flow rate causes the location of the temperature peak to shift downwards. The temperature and consequently the loading of the rich solution at the absorber outlet is therefore actually a weak function of the solution flow rate in combination with the design of the absorber. These quantities can be determined with higher accuracy only by applying a detailed rate-based column model.
4. **Upper limit of CO_2 loading**: The variation in CO_2 loading is limited by two issues: i) To provide for an adequate driving force and a sufficient absorption rate in the absorber, saturation conditions represent the upper limit for the lean loading and the related solution flow rate (cf. Section 5.2.3). ii) As the temperature of the rich solution at the absorber outlet is set to 50 °C, an energy balance over the absorber requires the temperature of the treated flue gas at the absorber top to decrease with an increasing solution flow rate. The reason is the higher overall heat capacity of the solution. In the course of solution flow rate optimisation in this work, the temperature of the treated flue gas must therefore not decrease to values below 30 °C.
5. **Lower limit of CO_2 loading**: The representation of CO_2 solubility via correlations poses a lower limit on the CO_2 loading and the corresponding solution flow rate. In particular AMP and MDEA/PZ suffer from scarce measurement data in the region of low CO_2 loadings. The correlations in that region are therefore assigned with large uncertainties. In the semi-empirical column model, the CO_2 loading must there-

[17] product of mass flow and specific heat capacity

fore not fall below that limit to provide for comparability of the results.

The outlined limitations of the semi-empirical column model have to be taken into consideration when interpreting the results of the energetic evaluations that are presented in the following sections.

5.5 Retrofit integration

In Section 5.3 it was shown that the choice of process parameters such as the reboiler temperature affects the quantity and quality of steam extraction as well as the auxiliary power demand of the CO_2 compressor. In fact, as shown in the following sections, the magnitude of the described effects is strongly related to the properties of the applied solvent. Therefore, an overall process evaluation is necessary in which the interaction of the power plant, the CO_2 compressor, and the CCU with a specific solvent is considered.

In the following sections the retrofit integration of an absorption-desorption-type CCU in the reference power plant using the six selected solvents is considered. It is evaluated how the three key process parameters solution flow rate (Section 5.5.1), reboiler temperature (Section 5.5.2), and temperature difference in the RLHX (Section 5.5.3) influence the performance of the overall process in terms of net output and net efficiency of the power plant.

5.5.1 Solution flow rate

As explained in Section 5.2.2, the required solution flow rate which is necessary to obtain a certain CO_2 capture rate (in this work: $\varepsilon = 90\ \% = \text{const.}$) is determined by the CO_2 capacity and the solvent concentration in aqueous solution (cf. Eq. (5.5)). The higher the level of regeneration of the solution in the desorber column is chosen, thus the lower the CO_2 loading of the lean solution, the less solution is needed to absorb a certain amount of CO_2 from the flue gas. As the reboiler heat duty and the auxiliary power of the solution pumps vary with the choice of solution flow rate, this quantity must be optimised with respect to a minimal net efficiency penalty of the overall process.

5.5.1.1 Impact on reboiler heat duty

Figure 5.5 shows by the example of 7 m MEA and a reboiler temperature of 100 °C that a minimal specific reboiler heat duty is achieved at a certain ratio

of solution mass flow and flue gas mass flow in the absorber (L/G). Figure 5.5 also shows that the total pressure in the desorber needs to be increased to higher lean loadings and higher L/G to maintain a constant reboiler temperature (q.v. Section 5.3.3).

The occurrence of a minimal reboiler heat duty for a certain solution flow rate is due to the opposing change in two of the three contributions to the reboiler heat duty. Figure 5.6 shows that when the amount of circulated solution is reduced, less energy is needed to heat the solution from the temperature at the desorber inlet to the reboiler temperature (q_{sens} ↓). A lower solution flow rate, however, requires a lower CO_2-loading of the lean solution and correspondingly a higher CO_2 capacity to achieve a specified CO_2 capture rate (q.v. Section 5.2.2). To achieve a lower lean loading, more stripping steam is needed and more water vapour remains at the desorber top ($q_{\mathrm{vap,H2O}}$ ↑)[18].

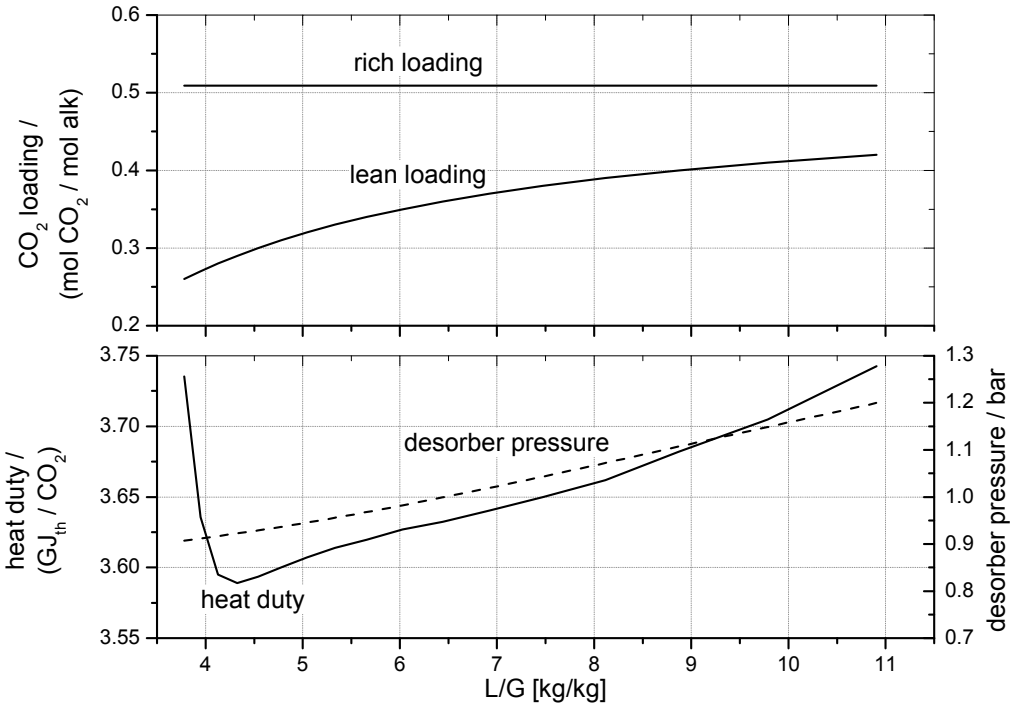

Figure 5.5: CO_2 loading, desorber pressure, and reboiler heat duty for varying L/G (7 m MEA, T_{reb} = 100 °C)

[18] For a more detailed discussion of this subject refer, for example, to [154].

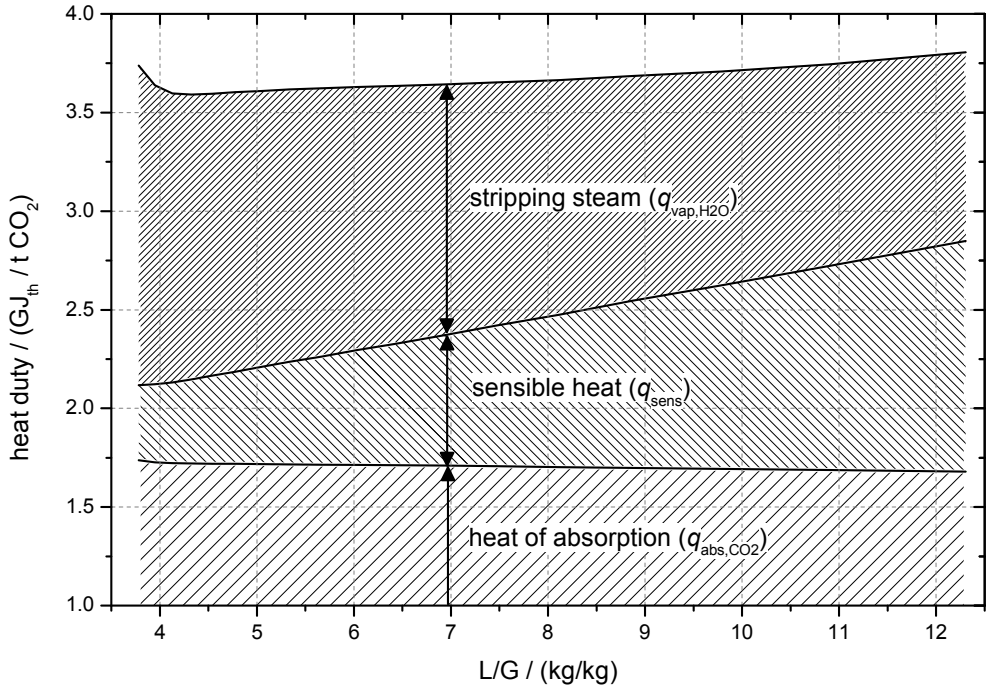

Figure 5.6: Cumulative contributions to reboiler heat duty for varying *L/G* (7 m MEA, T_{reb} = 100 °C)

5.5.1.2 Impact on net efficiency penalty

The reboiler heat duty and the corresponding steam extraction from the power plant is the largest contributor to the overall decrease in power output. The second largest contributor is the required auxiliary power to drive the CO_2 compressor. This quantity is mainly determined by the inlet pressure which, if pressure losses in desorber washing section and OHC were neglected, would be equal to the operating pressure of the desorber. As the desorber pressure increases to higher *L/G* (cf. Figure 5.5), the auxiliary power of the CO_2 compressor consequently decreases.

Figure 5.7 shows that the decrease in auxiliary power for CO_2 compression to larger solution flow rates is outweighed by the increase in reboiler heat duty, thus by the increase in power loss due to steam extraction. The auxiliary power of the CCU is required to drive water circulation pumps (in FGC and WS), reboiler condensate pump, solution pumps, and ID-fan downstream of the absorber. The latter two consumers make up approximately 90 % of the total auxiliary power demand of the CCU. The power demand of the solution pumps in the CCU also increases to higher solution flow rates and contributes

to a larger overall power loss at higher *L/G*. The auxiliary power demand of the ID-fan in the CCU remains constant for an increasing *L/G* as the pressure drop in the absorption column is assumed to be independent of the solution flow rate.

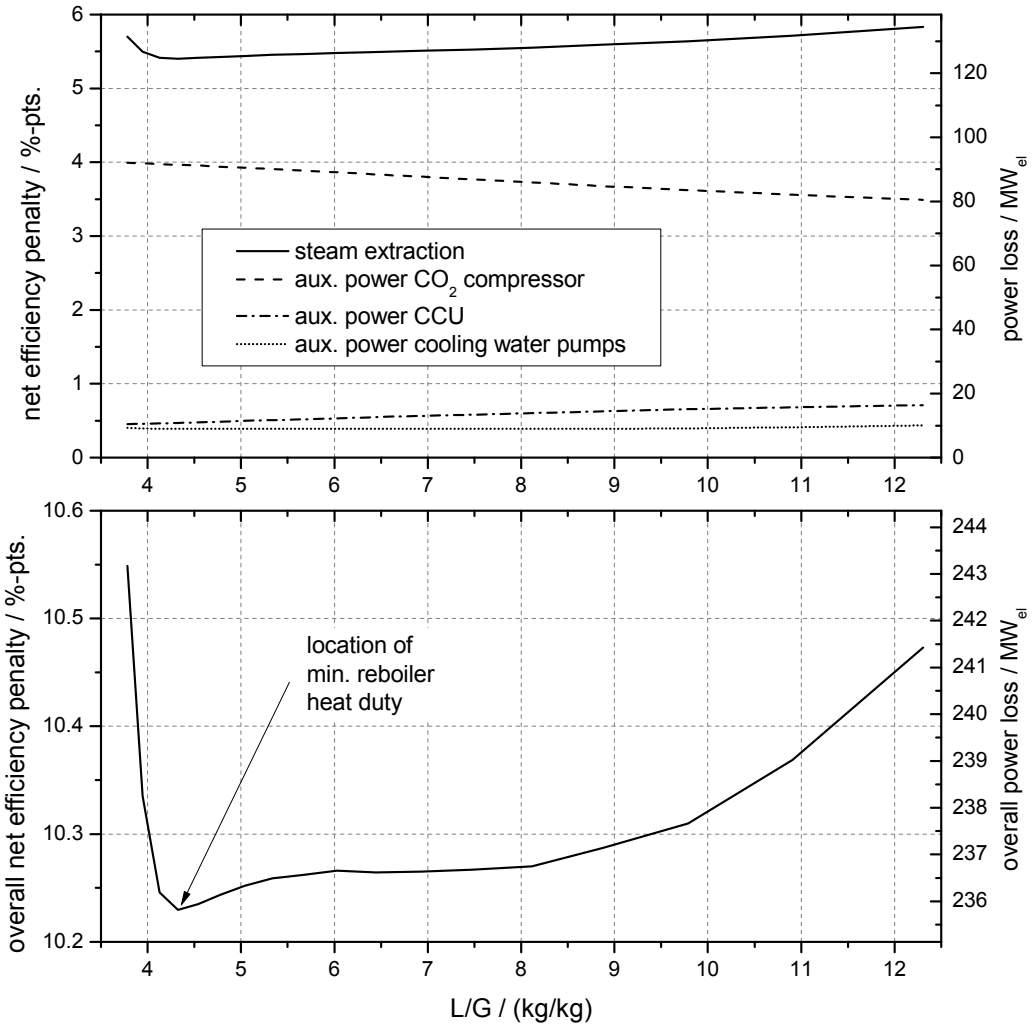

Figure 5.7: Partial (top) and overall (bottom) net efficiency penalty in case of retrofit integration in reference power plant for varying *L/G* (7 m MEA, T_{reb} = 100 °C)

It is notable that for 7 m MEA at a reboiler temperature of 100 °C the increase in steam extraction with the solution flow rate dominates the change in overall power loss. In this case, the optimal solution flow with respect to a minimal net efficiency penalty therefore corresponds to the location of the lowest reboiler heat duty at an *L/G* of approximately 4.3 kg/kg.

It was shown that the *L/G* is a critical parameter which needs to be optimised with respect to each solvent and each set of process parameters. In the following, the solution flow rate is optimised whenever the solvent or other process parameters such as the reboiler temperature and the temperature difference in RLHX are changed.

5.5.2 Reboiler temperature

In a desorber column with an attached reboiler, the three quantities desorber pressure, reboiler temperature, and CO_2 loading of the lean solution at the reboiler outlet are closely related. There is a variety of possibilities to control these quantities, depending on the reboiler type and the chosen process control strategy [175]. In the semi-empirical column model proposed in this work, the reboiler temperature as well as the CO_2 loading of the lean solution at the reboiler outlet are specified. In the model the desorber pressure is therefore a function of the reboiler temperature and the desired lean loading (cf. Eqs. (5.12) and (5.13)).

5.5.2.1 Impact on reboiler heat duty

Figure 5.8 illustrates the results of the *L/G* optimisation for MEA at reboiler temperatures of 100 and 120 °C. As explained in Section 5.3.1, the increase in reboiler temperature for high heat of absorption solvents such as MEA causes a smaller ratio of H_2O and CO_2 partial pressure at the rich end (top) of the desorber and consequently leads to a reduction of required stripping steam. Note that the absolute amount of sensible heat is similar at both reboiler temperatures. However, due to the decreasing reboiler heat duty, the relative contribution of the sensible heat to the total reboiler heat duty increases at higher reboiler temperatures.

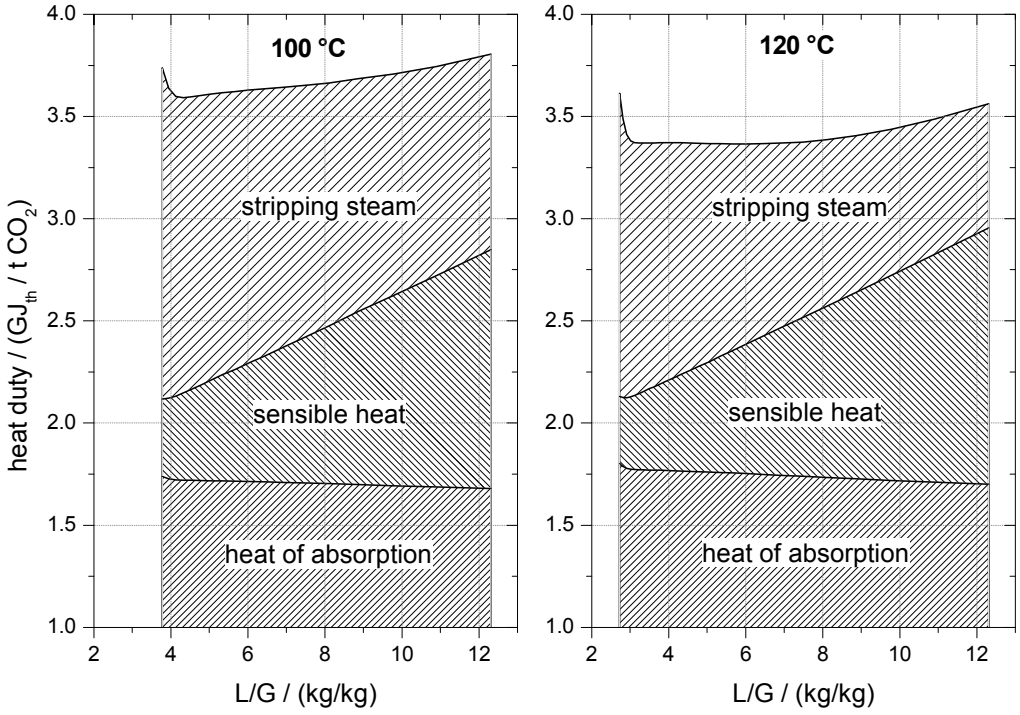

Figure 5.8: Cumulative contributions to reboiler heat duty for 7 m MEA at reboiler temperature of 100 °C (left) and 120 °C (right) and varying *L/G*

Figure 5.9 shows the effect of the variation in solution flow rate and reboiler temperature on the reboiler heat duty for all selected solvents. The L/G that corresponds to saturation conditions (regeneration of lean solution to an equilibrium CO_2 partial pressure of 500 Pa) is marked with an "s" (q.v. Table 5.2). MEA and K/PZ have such low inherent CO_2 capacity that saturation conditions occur at very high L/G which are outside the range of the diagrams (q.v. Section 5.2.3).

The reboiler heat duty is determined by i) the CO_2 solubility, ii) the heat capacity, and iii) the heat of absorption of the considered solvent. In combination with the chosen process parameters these three quantities ultimately determine the three contributions to the reboiler heat duty: i) required amount of stripping steam ($q_{\mathrm{vap,H2O}}$), ii) sensible heat (q_{sens}), and iii) heat of absorption ($q_{\mathrm{abs,CO2}}$).

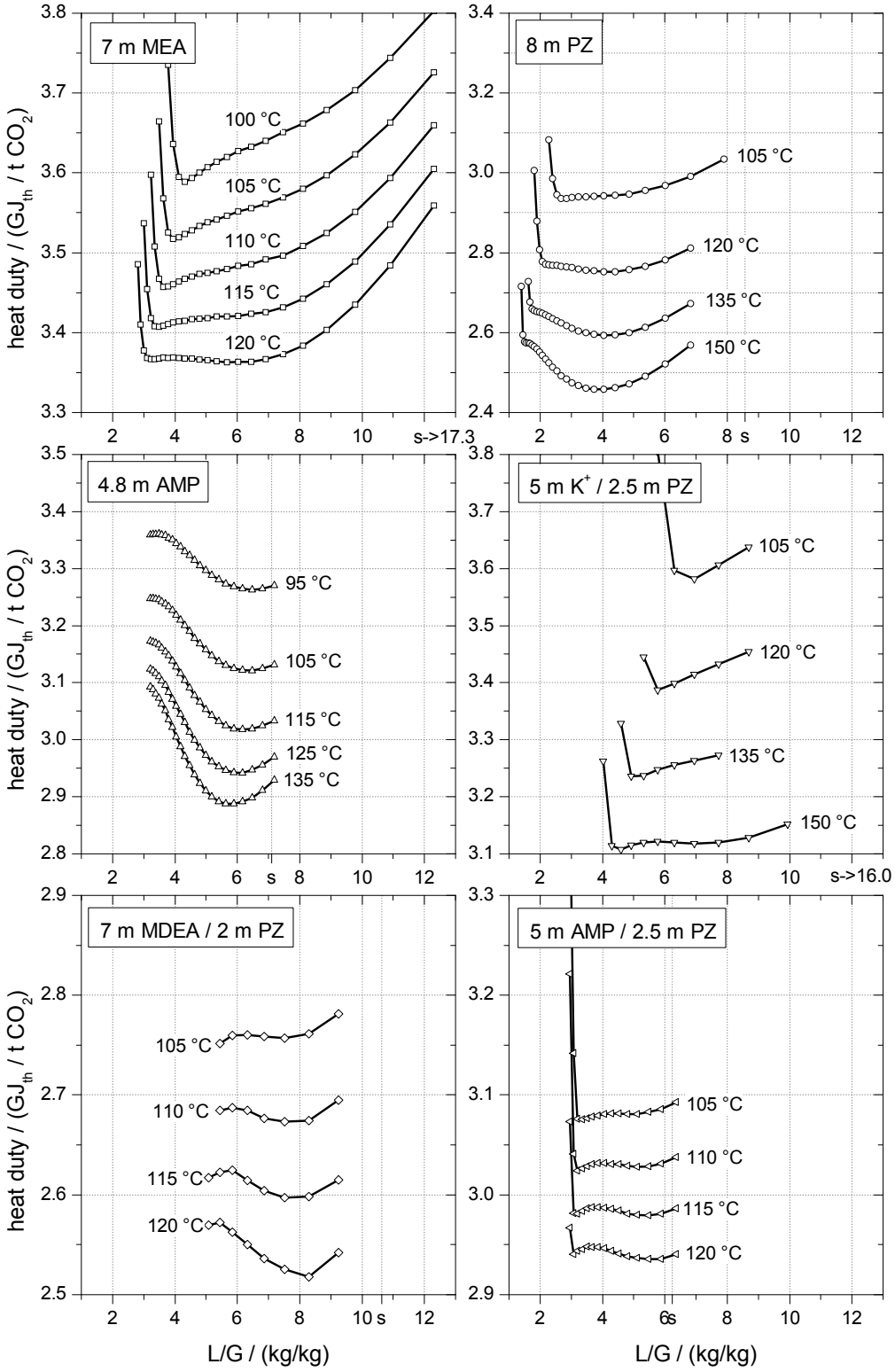

Figure 5.9: Reboiler heat duty for different reboiler temperatures and varying *L/G* with LMTD in RLHX of 5 K

As explained in Section 5.3.1 an increase in reboiler temperature leads to a reduction in reboiler heat duty for such solvents that have a high heat of absorption of CO_2 ($\Delta h_{abs,CO2} > \Delta h_{vap,H2O} \approx 40$ kJ / mol). Since the solvents selected for evaluation in this work fall into this category, all solvents profit from an increase in reboiler temperature. The lowest reboiler heat duty of 2.46 GJ_{th} / t CO_2 is achieved by PZ at the corresponding maximal[19] reboiler temperature for this solvent of 150 °C.

As discussed in Section 5.2.3, MEA and K/PZ show the lowest inherent CO_2 capacity of the six selected solvents. The *L/G* under saturation conditions are consequently very large (17.3 and 16 kg/kg, respectively; q.v. Table 5.2) and the contribution of sensible heat requirement to the reboiler heat duty for these solvents is high. As a result, overstripping for these two solvents leads to a large increase in CO_2 capacity and therefore to a significant decrease in reboiler heat duty (q.v. Table 5.3).

Key fact 6: Solvents with low inherent CO_2 capacity benefit particularly from overstripping in terms of a reduced reboiler heat duty.

The optimal solution flow rate for PZ is also found under overstripping conditions. However, due to its higher inherent CO_2 capacity the contribution of sensible heat to the reboiler heat duty is small. Consequently, the potential of overstripping for PZ is smaller than for MEA and K/PZ.

Compared to the other five selected solvents, MDEA/PZ has a medium inherent CO_2 capacity and thus shows a minimal reboiler heat duty at slightly overstripped conditions. Note that MDEA/PZ is the only of the evaluated solvents for which the heat capacity decreases to lower CO_2 loadings. Therefore, the decrease in reboiler heat duty to lower *L/G* for this solvent is damped and the potential for overstripping is further reduced.

[19] An increase in reboiler temperature is limited due to limitations imposed by thermal degradation issues (cf. Section 5.2.1).

AMP and AMP/PZ have the lowest potential for reboiler heat reduction by capacity increase through overstripping and therefore show a minimum in reboiler heat duty close to saturation conditions.

The effect of an increasing relative contribution of sensible heat to the total reboiler heat duty at higher reboiler temperatures as explained above for MEA, is observed for all six solvents. As a consequence, the decrease in reboiler heat duty to lower *L/G* is more significant at higher reboiler temperatures. This in turn shifts the optimal solution flow rate at higher reboiler temperatures to lower values.

Key fact 7: The higher the chosen reboiler temperature, the lower the optimal *L/G* with respect to a minimal reboiler heat duty.

5.5.2.2 Impact on net efficiency penalty

An optimal solution flow rate in terms of a minimal reboiler heat duty does not necessarily coincide with the occurrence of a minimal net efficiency penalty. Figure 5.10 illustrates this fact using again the example of 7 m MEA at reboiler temperatures of 100 and 120 °C. The diagram shows the power loss due to steam extraction and the sum of the auxiliary power demand for circulation pumps, ID-fan, cooling water pumps, solution pumps, and CO_2 compressor. The change in auxiliary power is mainly associated to the decrease of auxiliary power for CO_2 compression to larger *L/G*, counteracted by an increase in the power demand for the solution pumps (q.v. Section 5.5.1). Also note that the absolute auxiliary power for CO_2 compression at a reboiler temperature of 100 °C is 30–40 % higher than at 120 °C (q.v. Section 5.3.3).

Since for a reboiler temperature of 120 °C the reboiler heat duty and the corresponding power loss due to steam extraction remain almost constant between an *L/G* of 3 and 8 kg/kg (cf. Figure 5.8, right), the overall process profits from an increase in *L/G*, as the auxiliary power for CO_2 compression decreases. The decrease in auxiliary power for the CO_2 compressor prevails over the increase in power demand of the solution pumps in the CCU. Therefore, the minimal net efficiency penalty for 7 m MEA at a reboiler temperature

of 120 °C occurs under moderate overstripping conditions at an *L/G* of approximately 8.1 kg/kg.

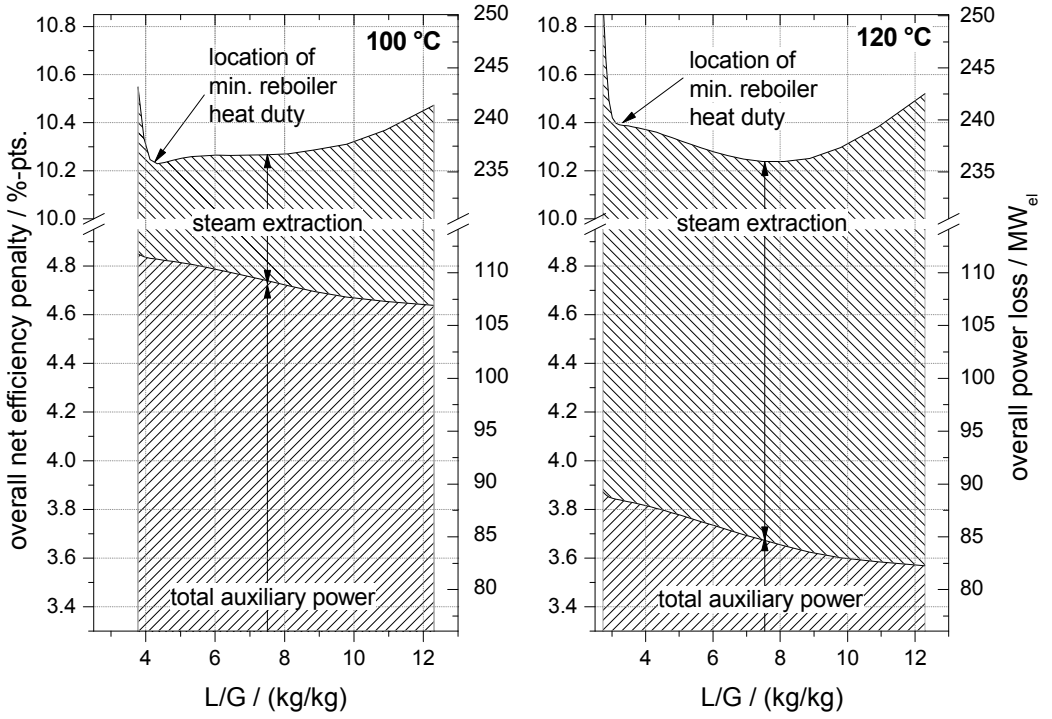

Figure 5.10: Cumulative contributions to overall net efficiency penalty and power loss in case of retrofit integration in reference power plant for 7 m MEA at reboiler temperatures of 100 °C (left) and 120 °C (right) and varying *L/G*

It is also notable from Figure 5.10 that the power loss due to steam extraction at a reboiler temperature of 120 °C is 15–22 % higher than at 100 °C, although the reboiler heat duty for 7 m MEA decreases to higher reboiler temperatures (cf. Figure 5.8). Figure 5.11 a) shows the overall net efficiency penalty of a CCU with 7 m MEA under significant overstripping conditions at an *L/G* of 4.3 kg/kg for different reboiler temperatures. Although the reboiler heat duty decreases to higher reboiler temperatures (c), the contribution of the steam extraction to the overall power loss increases (b). This is a result of the required steam quality which is coupled to the reboiler temperature (q.v. Sections 5.3.1 and 5.3.2).

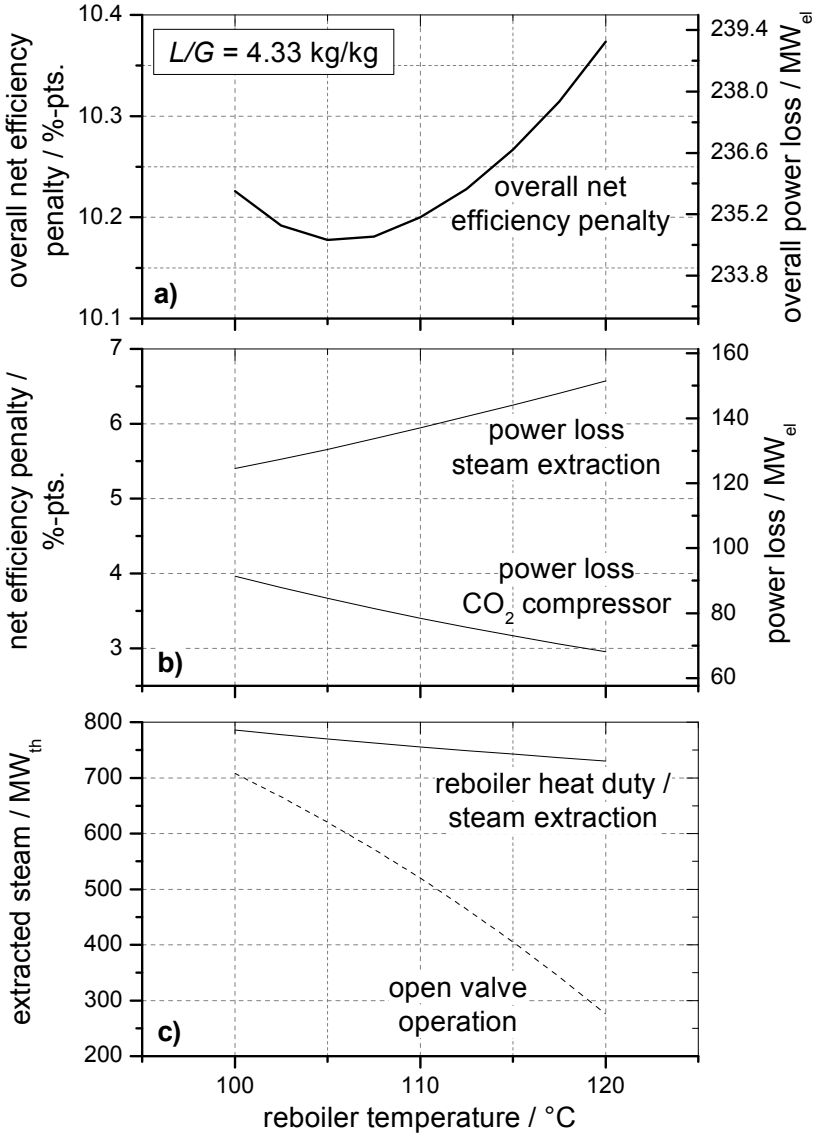

Figure 5.11: a) Overall net efficiency penalty, b) contributions of steam extraction and CO_2 compression to net efficiency penalty, and c) amount of extracted steam in case of retrofit integration in reference power plant for varying reboiler temperature (7 m MEA, L/G = 4.3 kg/kg)

The specific power loss due to steam extraction becomes minimal, if the steam pressure as required by the CCU matches the pressure that attunes in the IP/LP crossover. Such conditions are referred to as open valve operation (q.v. Section 5.3.2). Figure 5.11 c) indicates that for 7 m MEA under over-stripping conditions the amount of extracted steam is always higher than re-

quired to achieve open valve conditions. The higher the reboiler temperature, the higher the losses due to steam conditioning in the pressure maintaining valve (PMV). At a reboiler temperature of 100 °C, steam extraction of 786 MW_{th} (3.59 GJ_{th} / t CO_2) is needed by the CCU. Open valve operation at a reboiler temperature of 100 °C would occur at a steam extraction of 708 MW_{th}. At a reboiler temperature of 120 °C the reboiler heat duty is lower than at 100 °C, but considerably higher than required for open valve conditions (730 vs. 276 MW_{th}). Therefore, although the operation of the CCU at a reboiler temperature of 120 °C is achieved with a 6.1 % lower reboiler heat duty, the associated power loss due to steam extraction is 21.6 % higher than at 100 °C. The specific losses (e.g., in MW_{el} per extracted MW_{th} of heat) are therefore 29.5 % higher at a reboiler temperature of 120 °C than at 100 °C.

In summary, Figure 5.11 shows for 7 m MEA in the region of maximal overstripping at an L/G of 4.3 kg/kg that the overall net efficiency penalty decreases when the reboiler temperature is increased from 100 to 105 °C; at 105 °C the overall net efficiency penalty reaches a minimum and then increases again if the reboiler temperature is increased further. Therefore, for this solution flow rate the required steam shows the optimal combination of quantity and quality at a temperature of 105 °C.

Figure 5.12 illustrates the results of the overall process optimisation for all six selected solvents. The optimal combination of solution flow rate and reboiler temperature with respect to the lowest net efficiency penalty is marked by a solid symbol and a bold label which shows the optimal reboiler temperature. 7 m MEA, for example, reaches a minimal overall net efficiency penalty of 10.15 %-pts. at a reboiler temperature of 109 °C at an L/G of 8.1 kg/kg.

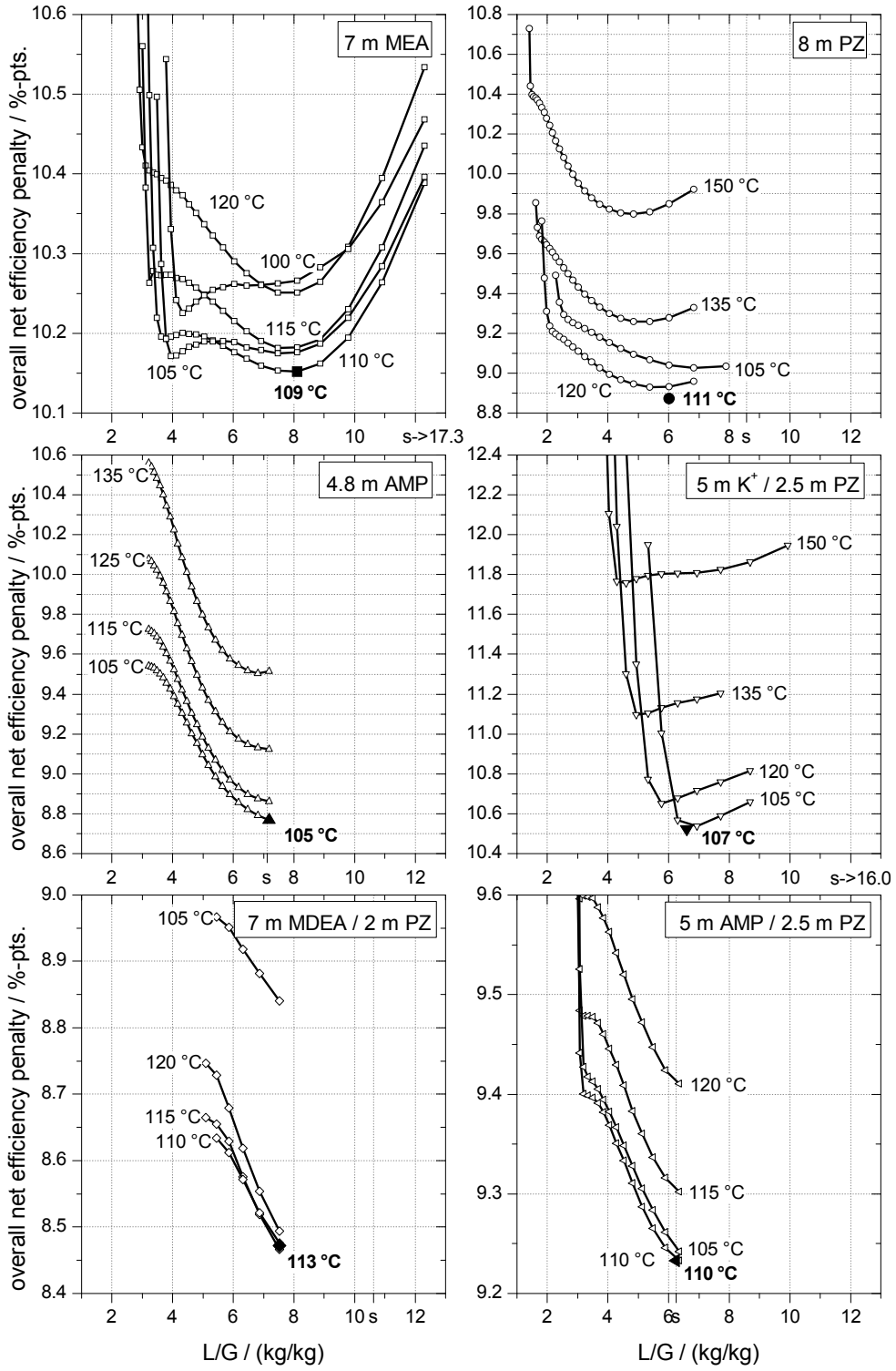

Figure 5.12: Overall net efficiency penalty in case of retrofit integration in reference power plant for different reboiler temperatures and varying *L/G* with LMTD in RLHX of 5 K

For the six selected solvents, considerable overstripping pays off only for K/PZ and in case of reboiler temperatures of 105 °C or below also for MEA. The optimal *L/G* for these two solvents is found clearly under overstripped conditions, where the corresponding solution flow rate is approximately half of the value under saturation conditions.

The contribution of steam extraction to the overall power loss for PZ is lower than for MEA and K/PZ. Therefore, PZ profits considerably from the decrease in auxiliary power of the CO_2 compressor at higher solution flow rates. The optimal *L/G* for PZ is thus found close to saturation conditions.

The solution flow rate for MDEA/PZ is limited, as the temperature of the treated flue gas decreases with an increasing *L/G* (cf. Section 5.4). To keep the temperature of the treated flue gas above 30 °C the *L/G* is not increased to values above 7.5 kg/kg. It can be expected that an increase of the solution flow rate further decreases the overall net efficiency penalty for MDEA/PZ and that, due to the medium inherent CO_2 capacity of this solvent, an optimum is found close to saturation conditions.

AMP and AMP/PZ are limited by the maximal solution flow rate under saturation conditions. For these two solvents the lowest net efficiency penalty is obtained at the highest *L/G* that still ensures a reasonable driving force for mass transfer over the entire column height in the absorber (q.v. Section 5.2.3 and Section 5.4).

For all solvents, the net efficiency penalty approaches a minimal value when decreasing the reboiler temperature, starting from the upper temperature limit. However, below a certain temperature, the penalty increases again. This is a result of the characteristics of the impact of steam quality on the total power loss (q.v. Section 5.3.2). Table 5.4 summarises the optimal process parameters of the CCU with regard to a minimal net efficiency penalty. The optimal reboiler temperature for all solvents lies in the range between 105 and 115 °C, which corresponds to an operation close to open valve conditions with minimal additional losses caused by the throttle and the PMV.

Additionally, when decreasing the reboiler temperature for a certain *L/G*, the operating pressure in the desorber must be decreased as well to maintain the specified CO_2 loading of the lean solution and the desired CO_2 capture rate. This results in a decreased inlet pressure and with it in an increased auxiliary power for the CO_2 compressor (q.v. Section 5.3.3). Therefore, the reduction of

reboiler temperature below open valve conditions suffers from a higher reboiler heat duty, from increased specific power losses due to steam extraction, and from a higher auxiliary power for CO_2 compression. This effect is most obvious for MDEA/PZ, for which the net efficiency penalty increases by more than 0.3 %-pts when going from a reboiler temperature of 114 °C to 105 °C.

Although PZ at a reboiler temperature of 150 °C shows the lowest specific reboiler heat duty of 2.45 GJ_{th} / t CO_2 (cf. Figure 5.9), MDEA/PZ achieves the lowest net efficiency penalty in case of retrofit integration in the reference power plant. This solvent reaches a similar low reboiler heat duty of 2.63 GJ_{th} / t CO_2 at a lower reboiler temperature of 113 °C with a resulting net efficiency penalty of 8.47 %-pts. PZ suffers from the large losses provoked by the PMV if operated at higher reboiler temperatures and reaches a minimal net efficiency penalty of 8.87 %-pts. at a reboiler temperature of 111 °C.

Table 5.4: Optimal process parameters in case of retrofit integration in reference power plant

solvent	L/G kg/kg	T_{reb} °C	p_{des} bar	q_{reb} GJ_{th} / t CO_2	$\Delta\eta_{net}$ %-pts.
MEA	8.1	109	1.57	3.52	10.15
PZ	6.0	111	1.58	2.89	8.87
AMP	7.6	105	1.92	3.14	8.77
K/PZ	6.6	107	1.08	3.55	10.52
MDEA/PZ	7.5	113	1.69	2.63	8.47
AMP/PZ	6.2	110	1.30	3.09	9.23

5.5.3 RLHX temperature difference

The logarithmic mean temperature difference (LMTD) between hot lean and cold rich solution in the rich-lean heat exchanger (RLHX) impacts the reboiler heat duty since it determines the sensible heat requirement to bring the solution from the temperature at the desorber inlet to the reboiler temperature (cf. Eq. (5.4)). A higher LMTD is equivalent to a lower temperature of the solution at the desorber inlet. As the temperature difference of the RLHX influences the percentage that the sensible heat contributes to the reboiler heat duty, it therefore also determines the location of the optimal solution flow

rate with respect to both a minimal reboiler heat duty as well as a minimal net efficiency penalty.

5.5.3.1 Impact on reboiler heat duty

The discussion of the impact of solution flow rate and reboiler temperature in the preceding sections considered an LMTD in the RLHX of the CO_2 capture process of 5 K. Figure 5.13 illustrates the reboiler heat duty for all six selected solvents in case of a doubled LMTD of 10 K. In Section 5.5.2 it was shown that with an LMTD in the RLHX of 5 K overstripping pays only off for K/PZ and, in case of reboiler temperatures of 105 °C or below, also for MEA. It shows that under the new boundary conditions all of the selected solvents, but in particular those with a low inherent CO_2 capacity (MEA and K/PZ), profit from overstripping, thus from an operation of the CCU with a low solution flow rate, in terms of a lower reboiler heat duty. This is a result of the enhanced contribution of sensible heat to the reboiler heat duty.

A high LMTD leads to a sharp minimum in the reboiler heat duty while a lower value flattens out the reboiler heat duty when plotted against L/G (cf. Figure 5.13 and Figure 5.9). As the sensible heat can be recovered less effectively with a high LMTD, the optimal L/G is found under overstripping conditions rather than under saturation conditions.

> **Key fact 8: The higher the temperature difference in the RLHX, the lower the optimal L/G with respect to a minimal reboiler heat duty.**

Although the reboiler heat duty increases with a higher LMTD, the impact of this parameter on the investment costs must be taken into consideration in a techno-economic optimisation of process design parameters. A higher LMTD is equivalent to a smaller RLHX. Additionally, if the process can be operated under overstripping conditions, the lower solution flow rate leads to a decrease in investment costs for columns, solutions pumps, and motors.

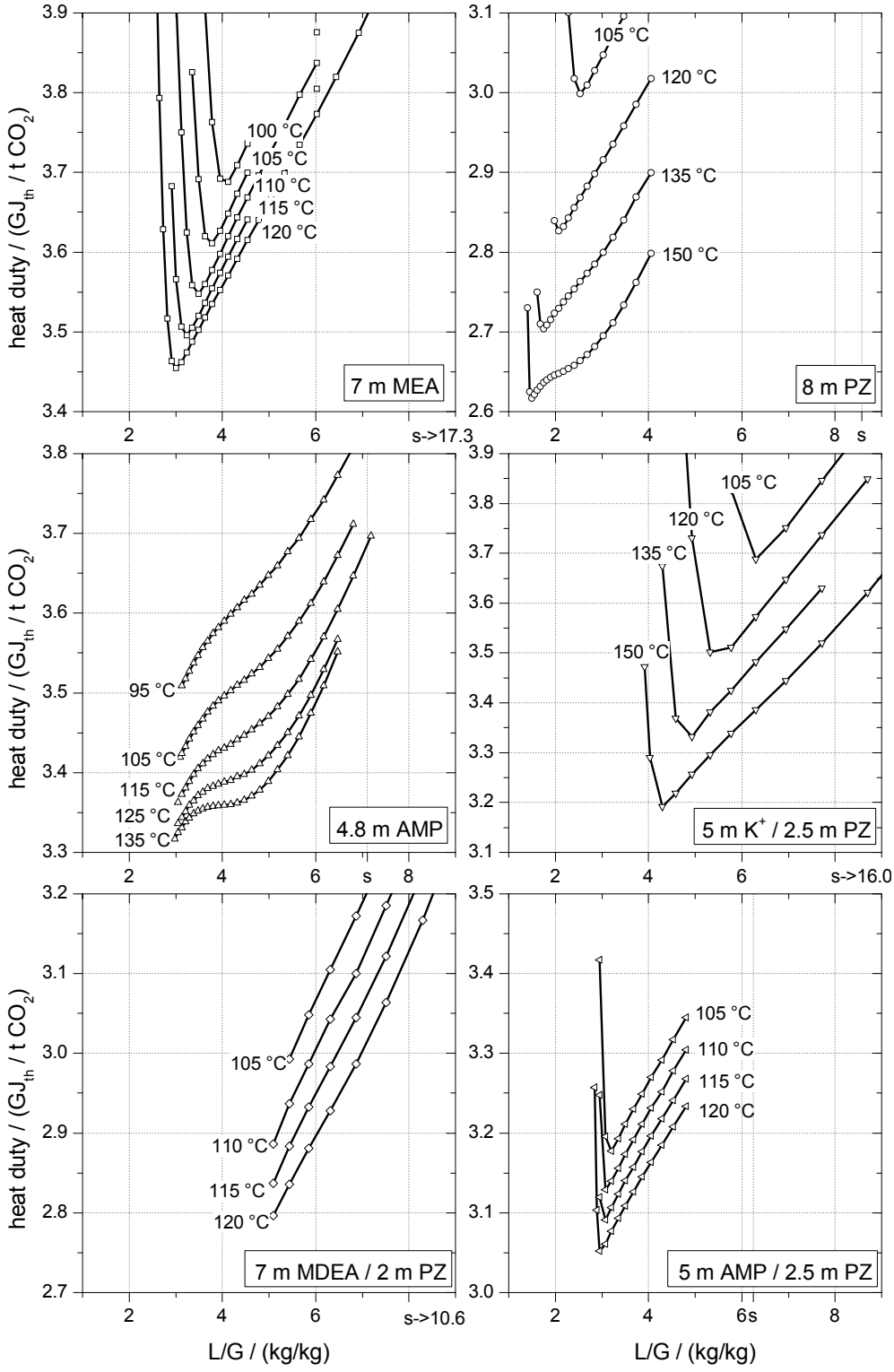

Figure 5.13: Reboiler heat duty for different reboiler temperatures and varying *L/G* with LMTD in RLHX of 10 K

5.5.3.2 Impact on net efficiency penalty

Figure 5.14 illustrates the results of the overall process evaluation for all six selected solvents with an increased LMTD in the RLHX of 10 K. Table 5.5 summarises the optimal process parameters with respect to a minimal net efficiency penalty under the new boundary conditions.

Table 5.5: Optimal process parameters in case of retrofit integration with increased LMTD in RLHX of 10 K

solvent	L/G kg/kg	T_{reb} °C	p_{des} bar	q_{reb} GJ_{th} / t CO_2	$\Delta\eta_{net}$ %-pts.
MEA	3.6	107	1.17	3.58	10.36
PZ	2.4	109	1.09	2.95	9.23
AMP	5.4	102	1.32	3.60	9.89
K/PZ	6.2	107	1.07	3.66	10.75
MDEA/PZ	5.1	110	1.25	2.89	9.09
AMP/PZ	3.2	105	1.00	3.18	9.59

A comparison of the optimal reboiler temperatures shown in Table 5.5 to the open valve operation line in Figure 5.3 shows that a minimal net efficiency penalty is still achieved close to open valve conditions, where the attuning pressure in the IP/LP crossover pipe matches the steam pressure required by the CCU. Since the reboiler heat duty increases with a larger LMTD, the corresponding reboiler temperature for open valve operation decreases accordingly. Therefore, the optimal reboiler temperatures for an increased LMTD of 10 K are slightly lower than for an LMTD of 5 K.

Key fact 9: The higher the LMTD in the RLHX, the lower the optimal reboiler temperature for which the net efficiency penalty due to steam extraction becomes minimal.

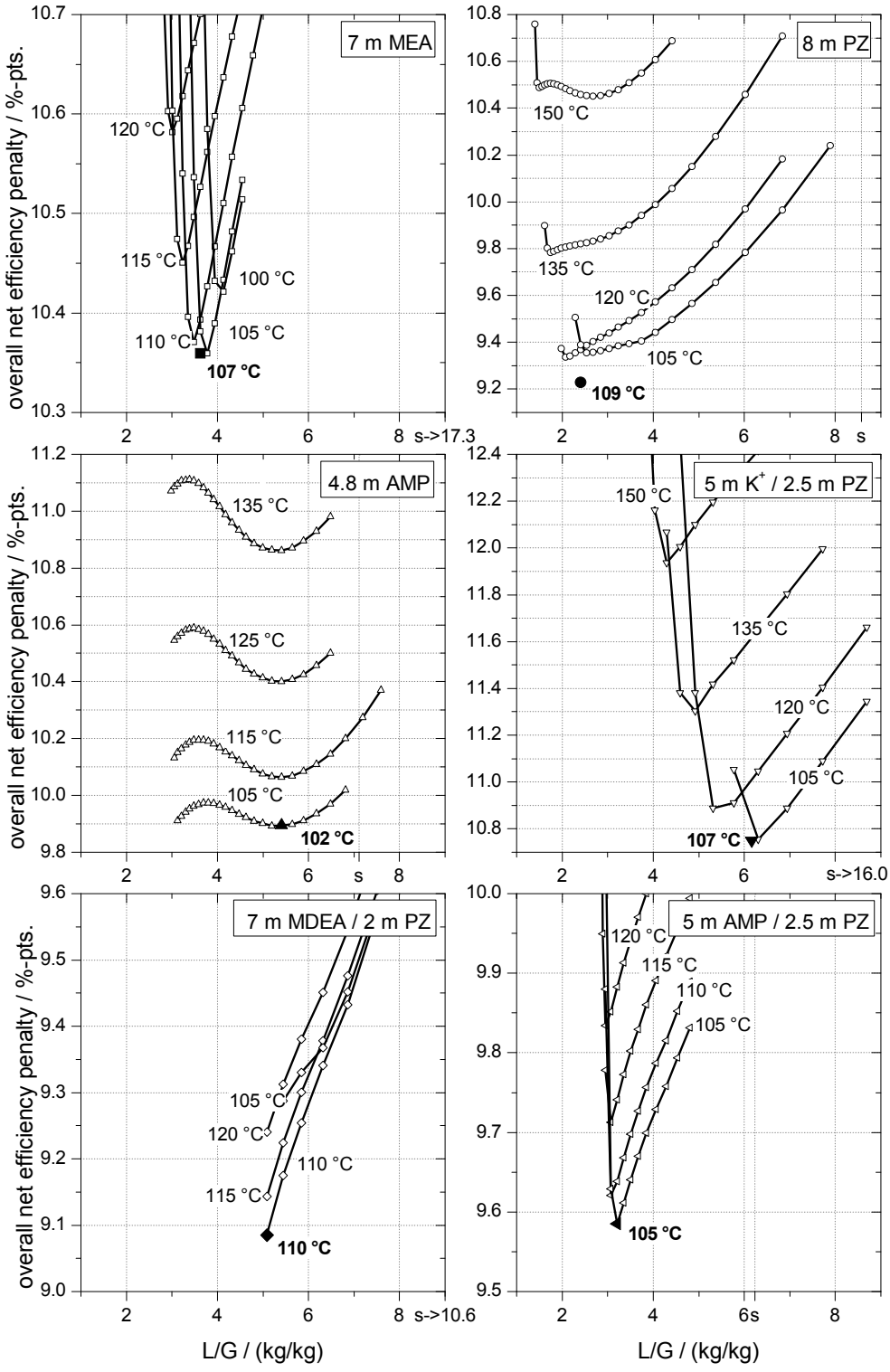

Figure 5.14: Overall net efficiency penalty in case of retrofit integration in reference power plant for different reboiler temperatures and varying *L/G* with LMTD in RLHX of 10 K

The characteristics of the net efficiency penalty with a high LMTD of 10 K in the RLHX differ significantly from the characteristics in case of a low LMTD of 5 K (cf. Figure 5.14 and Figure 5.12). The solution flow rate, for which a minimal net efficiency penalty in case of an LMTD of 5 K is found, strongly depends on the inherent CO_2 capacity of the solvent and its potential to profit from overstripping (q.v. Sections 5.2.3 and 5.5.2.2). A high LMTD of 10 K doubles the contribution of sensible heat to the overall reboiler heat duty and thus doubles the potential of overstripping. The different characteristics of the net efficiency penalty as a function of solution flow rate for a varying LMTD is in particular notable for MDEA/PZ. While the net efficiency penalty for this solvent in case of a low LMTD in the RLHX of 5 K decreases to higher *L/G* (cf. Figure 5.12), it sharply increases to higher solution flow rates for a high LMTD of 10 K (cf. Figure 5.14). This is caused by the characteristics of the reboiler heat duty for this solvent as a function of the solution flow rate. The reboiler heat duty remains nearly unchanged at a low LMTD of 5 K (cf. Figure 5.9), whereas for a high LMTD of 10 K with the corresponding increased relative contribution of sensible heat, a significant decrease of the reboiler heat duty for MDEA/PZ to lower *L/G* is notable (cf. Figure 5.13). Ultimately, the decrease in required steam extraction for a high LMTD of 10 K is reflected by the characteristic of the net efficiency penalties. Under the new boundary conditions with an increased LMTD in the RLHX, the optimal solution flow rate for all of the selected solvents except for AMP is found under clearly overstripped conditions.

In contrast to the other five solvents, the optimal *L/G* for AMP in case of a high LMTD of 10 K is found close to saturation conditions although the decrease in reboiler heat duty for this solvent (cf. Figure 5.13) suggests that overstripping could be profitable for AMP as well. This is in particular remarkable, since in Section 5.2.3 AMP/PZ was assessed similar to AMP with respect to the potential benefits of overstripping. For AMP/PZ, however, both reboiler heat duty and net efficiency penalty reach a minimum under clearly overstripped conditions. The difference in the behaviour of AMP in comparison to AMP/PZ is found in the larger relative increase in auxiliary power for CO_2 compression to lower solution flow rates. With AMP at a reboiler temperature of 115 °C the desorber pressure decreases from 2.92 to 1.66 bar when going from moderate overstripping ($p^*_{CO2,lean} = 50$ Pa) to saturation conditions, while for AMP/PZ the pressure is reduced from 1.74 to 1.36 bar.

Due to the lower solvent concentration and lower inherent CO_2 capacity, aqueous 4.8 m AMP solutions have a comparably large mole fraction of water ($x_{H2O} \approx 90$ %). At a given reboiler temperature, the desorber can therefore be operated under higher pressure than when operated with a higher concentrated 5 m AMP / 2.5 m PZ solution ($x_{H2O} \approx 79$ %, cf. Section 5.3.3 and Key fact 3). The corresponding increase in auxiliary power for CO_2 compression is 23.6 % (58.4 → 72.1 MW_{el}) for AMP and only 10.0 % (70.9 → 78.0 MW_{el}) for AMP/PZ. The larger increase in auxiliary power demand for CO_2 compression is a result of the lower heat of absorption of AMP compared to AMP/PZ (cf. Section 5.3.3 and Key fact 5). Therefore, although both solvents have approximately the same potential for overstripping, the increase in auxiliary power for the CO_2 compressor prevents overstripping to be beneficial for AMP.

Figure 5.13 and Figure 5.14 suggest that a minimal reboiler heat duty and a minimal net efficiency penalty could be found for AMP and for MDEA/PZ at even lower solution flow rates than shown in the diagrams. These minima cannot be determined due to the limitations of the applied semi-empirical column model (q.v. Section 5.4): The measurement data for AMP and MDEA/PZ in the region of low CO_2 loadings are scarce (cf. Figure A.3 and Figure A.5 in Annex A.3.1). Therefore, the derived correlations for the representation of CO_2 solubility of these two solvents in this loading region are afflicted with considerable uncertainty. As the equilibrium CO_2 partial pressure decreases more rapidly to lower loadings than the correlation predicts, the model misses the sharp increase in stripping steam requirement and the raise of $q_{H2O,vap}$ in the low loading region – an effect that is observed for all of the remaining four solvents. For AMP and MDEA/PZ the model instead gives a linear increase of stripping steam demand to lower L/G which is outweighed by the steady decrease of the dominant sensible heat requirement. The optimal process parameters in Table 5.5 for the AMP and MDEA/PZ solvents are therefore the minimal L/G and the corresponding lean loading for which the CO_2 solubility correlations are still valid.

5.6 Retrofit integration with increased crossover design pressure

The discussion of the impact of solution flow rate and reboiler temperature in the preceding sections considered the retrofit integration of a CO_2 capture process in a hard-coal-fired steam power plant with an IP/LP crossover pressure of 3.9 bar in the design point (i.e., full-load without CO_2 capture). It was concluded that a retrofit causes the lowest negative impact on the overall process if the CCU is operated at or close to open valve conditions. Such conditions are obtained if the required pressure (quality) of the steam that is extracted for the regeneration of the solution matches the pressure in the IP/LP crossover pipe. The latter attunes as a function of the amount (quantity) of extracted steam. Note that a match could be achieved by varying the reboiler temperature in the CCU if the reboiler heat duty was unaffected by a change in this process parameter. However, as the reboiler temperature affects both the required pressure in the IP/LP crossover as well as the reboiler heat duty a match of required and attuned crossover pressure might not be achievable (q.v. Figure 5.3).

If the IP/LP crossover design pressure, that is the pressure at full-load without steam extraction for CO_2 capture, is increased, the pressure that attunes with steam extraction is also higher. Therefore, to evaluate the impact of a change in this critical design parameter, in the following a power plant is considered that resembles the reference power plant but which has an increased IP/LP crossover design pressure of 5.5 bar. The key parameters of the power plant are shown in Table 5.6. Live steam and reheat parameters as well as condenser pressure and feed water temperature at the boiler inlet at full-load without CO_2 capture are the same as of the reference power plant (q.v. Table 4.3). Since the heat input and the configuration of the flue-gas-side of the power plant remain unmodified, the flue gas parameters (pressure, temperature, flow, composition) also remain unchanged. As a result, the reboiler heat duties that were determined in Section 5.5.2 to achieve a CO_2 capture rate of 90 % in case of a retrofit integration in the reference power plant are unaffected (q.v. Figure 5.9).

Table 5.6: Key parameters of the power plant model with increased IP/LP crossover design pressure at full-load without steam extraction for CO_2 capture

heat input (LHV)	2306 MW_{th}
gross power output	1138 MW_{el}
net power output	1052 MW_{el}
gross efficiency (LHV)	49.4 %
net efficiency (LHV)	45.7 %
IP/LP crossover pressure	5.5 bar
feed water tank pressure	12.8 bar

The IP/LP crossover pressure influences the pressure of the last steam bleed in the IP turbine which is used to supply the LPP 5 (q.v. Figure 4.3). To provide for a fair comparison with the results of the retrofit integration in the reference power plant with lower crossover design pressure, all steam bleed pressures of the water-steam-cycle must therefore be optimised with regard to a maximal net efficiency[20]. Thereby the choice of steam bleed pressure is a trade-off between energetic (maximal amount) and exergetic (maximal temperature increase) utilisation of the enthalpy in the steam. Note that the net efficiency of the power plant with increased crossover design pressure is slightly higher than that of the reference power plant. This is a result of the increased electricity generation in the LP turbine stage groups, which are assumed to have a higher isentropic efficiency than the IP turbine stage groups (95 % vs. 92 %, cf. Section 4.3).

Note that the problem of increased steam volume flow at the IP turbine outlet is worsened in case of a power plant with increased crossover design pressure (cf. Section 4.5.2.1): The relative steam volume flow increases to 140 % at reboiler temperatures below 126 °C and steam extractions above 439 MW_{th} ($\cong$ 2.22 GJ_{th} / t CO_2 at 90 % CO_2 capture).

Figure 5.15 shows the results of the overall process optimisation in case of retrofit integration in the power plant with increased crossover design pres-

[20] This is an n-dimensional optimisation problem, where n is the number of steam bleed points to be optimised, using a nested one-dimensional iterative solution method.

sure of 5.5 bar[21]. Table 5.7 summarises the optimal process parameters in this case with regard to a minimal net efficiency penalty.

Table 5.7: Optimal process parameters in case of retrofit integration in power plant with increased crossover design pressure of 5.5 bar with LMTD in RLHX of 5 K

solvent	L/G kg/kg	T_{reb} °C	p_{des} bar	q_{reb} GJ_{th} / t CO_2	$\Delta\eta_{net}$ %-pts.
MEA	7.8	113	1.83	3.46	9.87
PZ	5.4	125	2.67	2.71	8.39
AMP	7.2	118	3.39	3.01	8.57
K/PZ	6.3	113	1.32	3.47	10.27
MDEA/PZ	7.5	120	2.21	2.53	8.28
AMP/PZ	6.4	120	2.09	2.94	9.03

All of the conclusions that were drawn in Section 5.5 from the analysis of a CCU retrofit in the reference power plant are also valid for a retrofit of a steam power plant with increased crossover design pressure. The characteristics of net efficiency penalty as a function of reboiler temperature and solution flow rate are therefore similar. Yet, when comparing the optimal process parameters in Table 5.4 and Table 5.7 it shows that the optimal reboiler temperatures increase with the design pressure of the IP/LP crossover. This is due to a shift in the corresponding open valve operating line to higher reboiler temperatures. Figure 5.16 shows the open valve operating line for both power plants as well as the determined optimal process parameters for each of the six selected solvents. Note that the reboiler temperature for MDEA/PZ is limited to 120 °C due to thermal degradation issues (q.v. Section 5.2.1). Without this limitation, the lowest net efficiency penalty would be achieved at a reboiler temperature of 123 °C and a corresponding reboiler heat duty of 2.49 GJ_{th} / t CO_2 (indicated by the grey, hollow diamond in Figure 5.16).

[21] The net efficiency penalties in case of retrofit integration in a power plant with increased crossover design pressure of 5.5 bar for different reboiler temperatures and with an LMTD in the RLHX of 10 K are found in Figure A.14 in Annex A.6

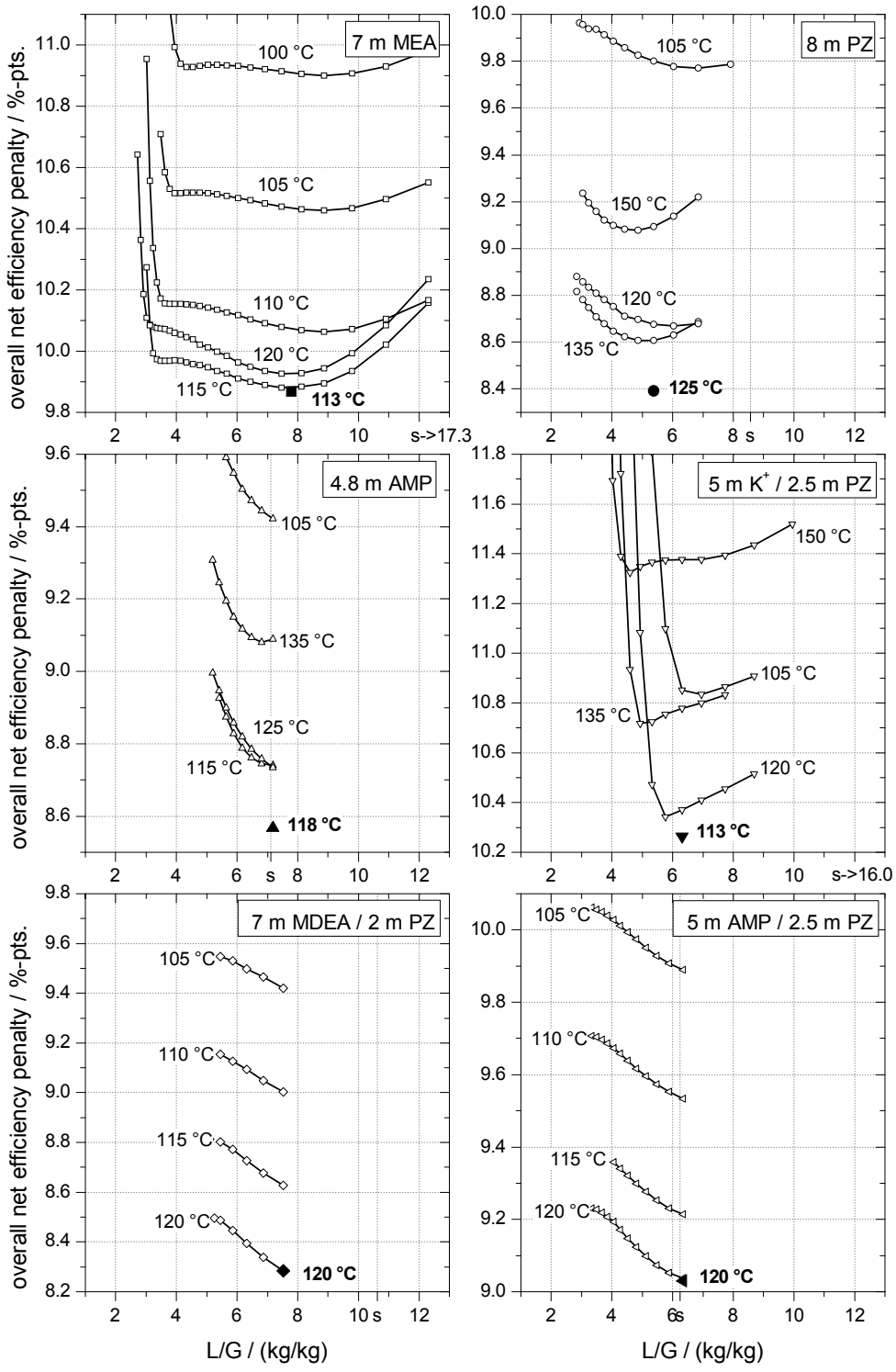

Figure 5.15: Overall net efficiency penalty in case of retrofit integration in power plant with increased crossover design pressure of 5.5 bar for different reboiler temperatures and varying *L/G* with LMTD in RLHX of 5 K

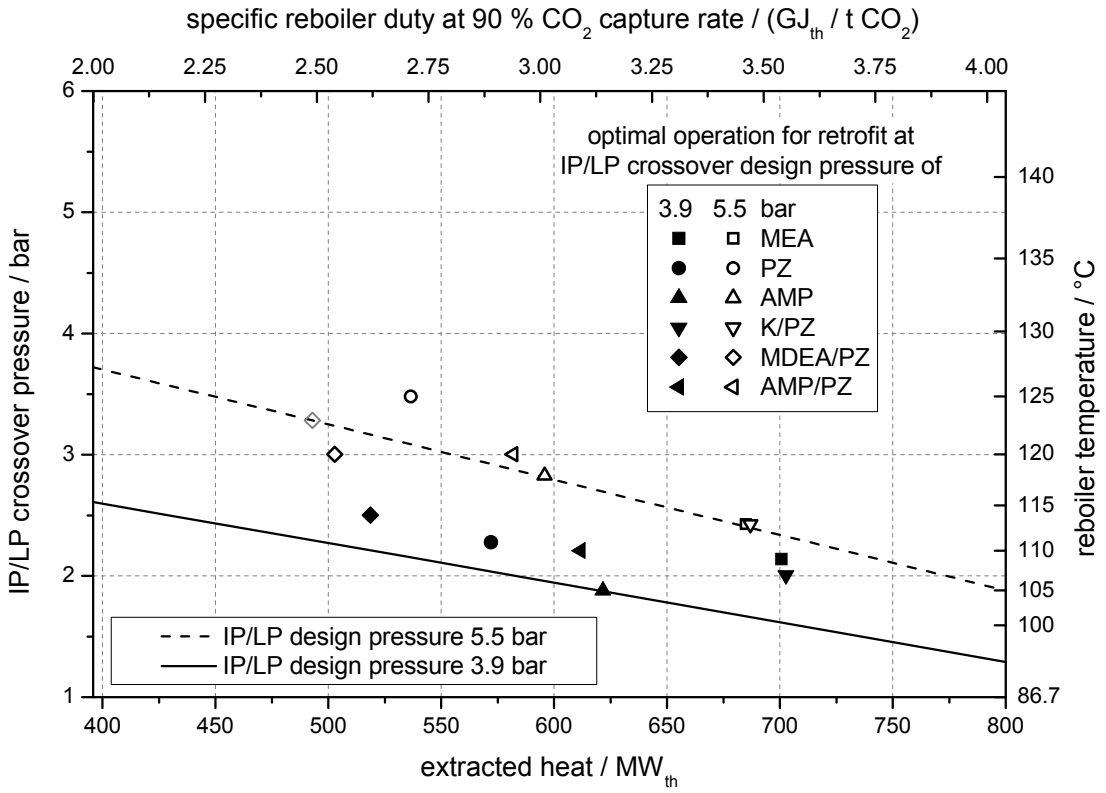

Figure 5.16: Open valve operation lines and optimal process parameters of selected solvents with regard to minimal net efficiency penalty

As an increase in reboiler temperature reduces the required power demand for CO_2 compression, an operation slightly above the open valve operation line can be beneficial with regard to a minimal net efficiency penalty for some solvents. In combination with the results from Section 5.5, a general conclusion can be drawn: In case of a CCU retrofit of a steam power plant, the operation close to or – for solvents with lower heat of absorption such as AMP – at open valve conditions is beneficial for the performance of the overall process (cf. Section 5.3.3 and Key fact 5).

Key fact 10: When considering a CCU retrofit of a steam power plant, an operation at or slightly above open valve conditions is preferable with respect to a minimal overall net efficiency penalty.

The above results have far reaching consequence with regard to solvent selection for CCU retrofit applications. Solvents such as 8 m PZ that feature a significantly lower reboiler heat duty than all of the competitors, but which require steam extraction at an elevated pressure, might not be attractive in case of a CCU retrofit in an existing power plant.

Following the above observations, an obvious conclusion would be to sacrifice the steam conditioning measures altogether and to design the retrofitted water-steam-cycle with neither a throttle nor a PMV to reduce PCC retrofit investment costs. In that case, the CCU would need to be operated at a reboiler temperature that matches the steam pressure which arises in the IP/LP crossover. However, the reduction in live steam mass flow during part-load operation of the power plant leads to a drop in crossover pressure [176]. The attuning steam pressure during part-load operation with steam extraction for CO_2 capture might therefore not be sufficient for a proper operation of the CCU. Thus, the installation of a PMV is advisable to ensure the proper operation of the power plant with CO_2 capture not only at full-load but also during part-load operation.

5.7 Greenfield integration

A new power plant that is specifically designed to be operated with CO_2 capture offers advantages over a steam power plant which is retrofitted with a CCU. All power plant components – in particular in the water-steam-cycle – can be designed to operate under the conditions which attune when the CCU is in operation; thereby the efficiency penalty associated to the application of PCC can be reduced. In contrast to a CCU retrofit of an existing power plant, greenfield integration allows the consideration of additional optimisation measures which implicate significant changes in the power plant design and layout. This includes, for example, the return of the reboiler condensate to a location in the preheating train where the feed water shows a similar temperature (q.v. Section 4.5.2.2).

The integration of waste heat from the CCU or the CO_2 compressor in the water-steam-cycle of the power plant can reduce the net efficiency penalty associated to the operation of the CCU. The efficiency potential of waste heat integration for state-of-the-art steam power plants is approximately 0.5–1.0 %-pts. Waste heat integration is rather confined by the limited presence of ade-

quate low temperature heat sinks than by the availability of heat sources [170]. As the reduction in net efficiency penalty is practically independent of the underlying CCU configuration and the used solvent, waste heat integration is not taken into consideration in this work.

For the energetic evaluation of the selected solvents in case of greenfield integration in this work, the IP/LP crossover pressure of the power plant at full-load is matched to the steam pressure demand of the CCU. Neither a throttle nor a PMV is required in the steam path, minimising the losses associated to the steam extraction. All turbine stage groups are designed for operation at full-load and steam extraction to achieve a CO_2 capture rate of 90 %. All other components are also designed for operation under these conditions. Therefore, the highest possible efficiency is achieved for the power plant operation at full-load with steam extraction for 90 % CO_2 capture.

Note that the crossover pressure drops during part-load operation of the power plant when the live steam mass flow is decreased – just as in the case of retrofit integration (q.v. Section 5.6). Since the attuning steam pressure in the crossover during part-load operation might not be sufficient for a proper operation of the CCU, a PMV, which is entirely opened during full-load operation, still needs to be installed.

Figure 5.17 shows the power loss associated to the extraction of steam from the water-steam-cycle of the power plant in case of greenfield integration. For comparison, the diagram also shows the corresponding lines for retrofit integration in the reference power plant and retrofit integration in a power plant with increased crossover design pressure at a steam extraction of 594 MW_{th} (3.0 GJ_{th} / t CO_2).

The power loss associated to steam extraction in case of greenfield integration lies below the loss in case of retrofit integration. If open valve operation is achieved in case of retrofit integration, the power loss is approximately the same as for greenfield integration, since in this case no throttling of the crossover steam is required to provide for the steam pressure as demanded by the CCU.

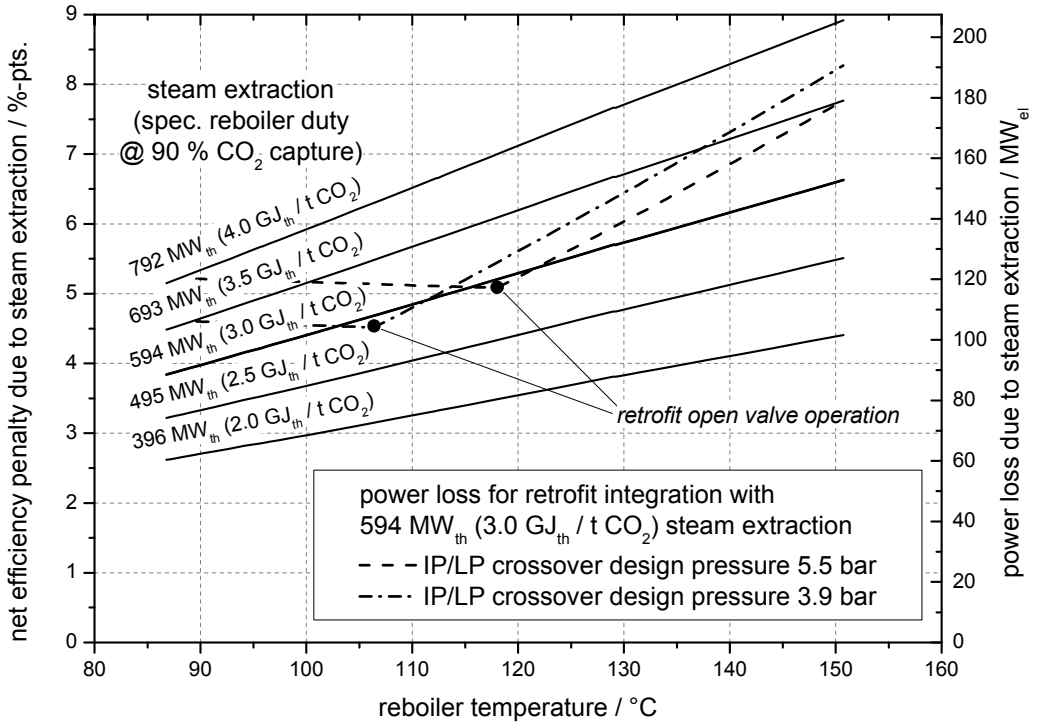

Figure 5.17: Net efficiency penalty and power loss due to steam extraction in case of greenfield integration for different reboiler heat duties and reboiler temperatures

It shows that in the greenfield integration case, a higher reboiler temperature always leads to larger specific power losses per unit of extracted steam (positive slope of the lines of constant steam extraction in Figure 5.17). An elevated reboiler temperature, however, can reduce the reboiler heat duty, i.e. the amount of required steam extraction (cf. Section 5.3.1), as well as the auxiliary power demand for CO_2 compression due to an increased desorber pressure (cf. Section 5.3.3). Therefore, also in the case of greenfield integration an increase in reboiler temperature implies a trade-off between increasing steam quality, decreasing steam quantity, and decreasing auxiliary power for CO_2 compression.

Figure 5.18 shows the results of the overall process evaluation in case of greenfield integration with all of the six selected solvents[22]. Table 5.8 summa-

[22] The net efficiency penalty in case of greenfield integration for different reboiler temperatures with an LMTD in the RLHX of 10 K are found in Figure A.15 in Annex A.6.

rises the optimal process parameters with regard to a minimal net efficiency penalty, where this quantity is determined by comparing the net efficiencies of the greenfield power plant with CO_2 capture and of the reference power plant without CO_2 capture ($\eta_{ref} = 45.6$ %).

Table 5.8: Optimal process parameters in case of greenfield integration with LMTD in RLHX of 5 K

solvent	L/G kg/kg	T_{reb} °C	p_{des} bar	q_{reb} GJ_{th} / t CO_2	$\Delta\eta_{net}$ %-pts.
MEA	8.1	120	2.51	3.38	9.57
PZ	4.9	150	6.78	2.47	8.12
AMP	7.2	118	3.39	3.01	8.42
K/PZ	5.3	130	2.24	3.28	9.97
MDEA/PZ	7.5	120	2.21	2.53	8.11
AMP/PZ	6.4	120	2.09	2.94	8.87

The results for a greenfield integration of a CCU are similar in quality to the results discussed for retrofit integration in Sections 5.5 and 5.6 above. However, for all solvents the optimal net efficiency penalty is between 0.36 and 0.75 %-pts. lower than in case of retrofit integration in the reference power plant (cf. Table 5.4).

The minimal reboiler temperatures for MEA, PZ, MDEA/PZ, and AMP/PZ are found at their respective upper temperature limit (q.v. Section 5.2.1). In contrast, a further increase of reboiler temperature beyond 118 °C and 130 °C for AMP and K/PZ, respectively, does not result in a lower net efficiency penalty. For these two solvents, the decrease in reboiler heat duty and auxiliary power for CO_2 compression to higher reboiler temperatures therefore cannot outweigh the larger specific power losses associated to the higher steam quality. For AMP, the relative contribution of the auxiliary power of the CO_2 compressor is comparably small due to the higher water fraction in the solution (q.v. Section 5.3.3 and discussion in Section 5.5.3.2). Therefore, for this solvent the negative effect of the increasing steam quality on the net efficiency is already notable at reboiler temperatures above 118 °C, while for K/PZ this is not the case until a reboiler temperature of 130 °C is reached. In fact, for AMP the three described effects counteract each other within a region of reboiler tem-

peratures between 115 and 125 °C where the determined net efficiency penalty lies in a narrow band around 8.4 %-pts.

In case of greenfield integration, PZ can profit from its potentially low reboiler heat duty at higher reboiler temperatures. In contrast to the retrofit cases, the reboiler temperature of 150 °C that is required to achieve such low reboiler heat duties no longer prevents a positive effect on the related power loss. Therefore – together with MDEA/PZ – PZ achieves the lowest net efficiency penalty of 8.1 %-pts. of all of the six selected solvents.

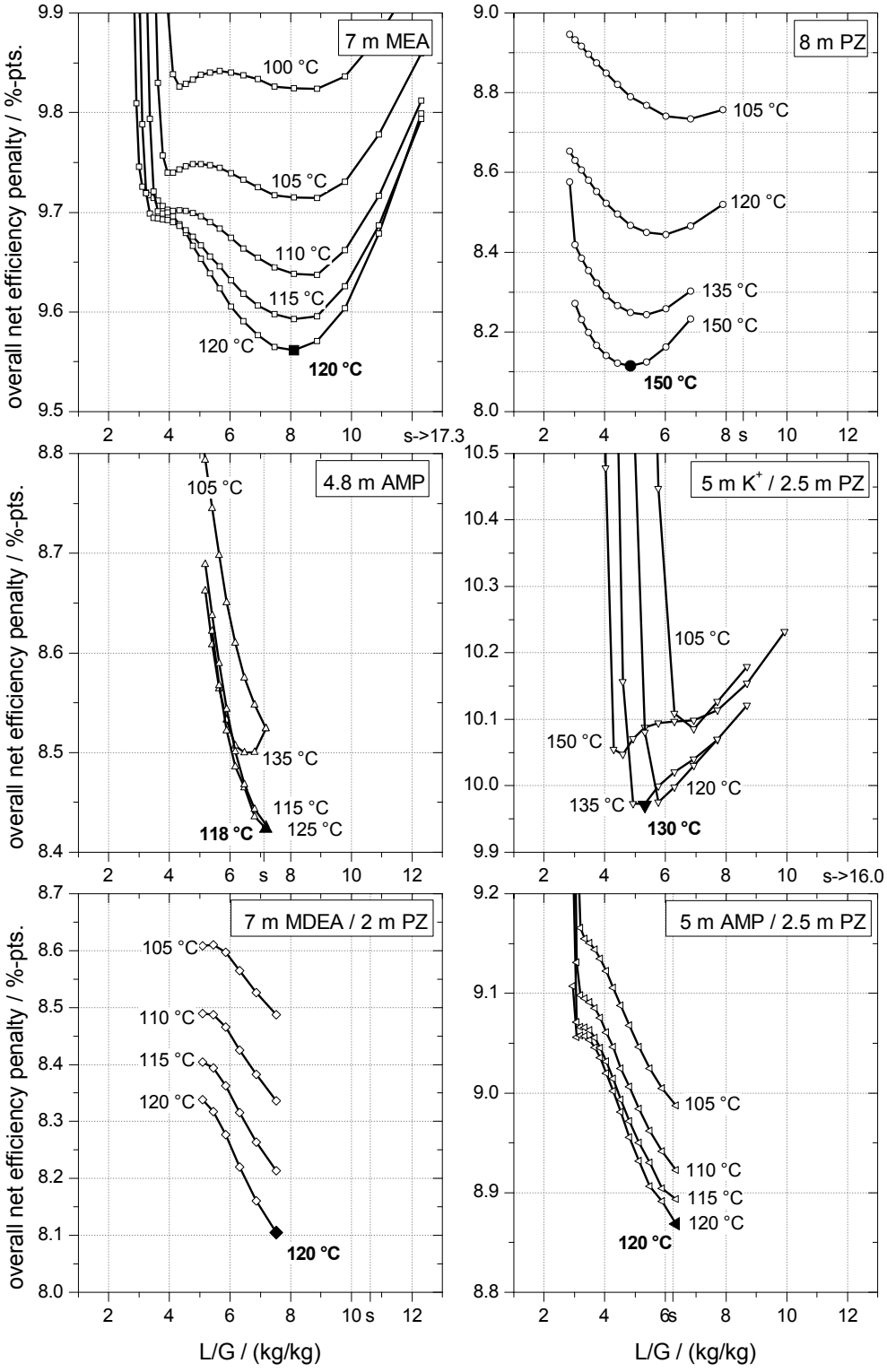

Figure 5.18: Overall net efficiency penalty in case of greenfield integration for different reboiler temperatures with LMTD in RLHX of 5 K

6 CONCLUSIONS

In this work a semi-empirical column model was developed to represent the absorber and desorber of post-combustion CO_2 capture processes with chemical solvents in coal-fired steam power plants. The properties of the solvents are represented by empirical correlations on the basis of fundamental measurement data (CO_2 solubility, heat capacity, density). The model of a CO_2 capture unit (CCU) including the column model was coupled to detailed models of a hard-coal-fired steam power plant and of a CO_2 compressor to evaluate and compare the impact of CO_2 capture on the overall power plant process using the following six solvents: 7 m MEA, 8 m PZ, 4.8 m AMP, 5 m K^+ / 2.5 m PZ, 7 m MDEA / 2 m PZ, and 5 m AMP / 2.5 m PZ. The six solvents were selected to represent certain solvent groups to allow drawing general conclusions – independent of the specific selected solvents – for the optimal integration of CO_2 capture processes by chemical absorption in coal-fired steam power plants. The major advantage of the developed overall process model and the outlined methodology is that it is generally applicable for the energetic evaluation of any solvent to be used in a post-combustion CO_2 capture process for which only limited data is available.

The integration of a CO_2 capture process in a coal-fired steam power plant leads to a reduction in net power output due to the required steam extraction for the regeneration of the solution in the desorber, due to the auxiliary power demand of the CO_2 compressor and the CCU, and due to the auxiliary power of the additional cooling water pumps. The solvent and the chosen process parameters of the CCU influence the magnitude of the reduction in power output and net efficiency of the power plant. The development of a detailed model of the overall process in one simulation tool in this work allowed the optimisation of two critical process parameters in the CCU with respect to a maximal net power output of the power plant: the solution flow rate and the reboiler temperature. Additionally, the impact of the size of the rich-lean heat exchanger (RLHX) in the CCU, indicated by the logarithmic mean temperature difference between the hot rich and cold lean stream, on the performance of the overall process was evaluated. Furthermore, the impact of the integration strategy and the power plant configuration (retrofit integration, retrofit integration with increased steam pressure, greenfield integration) were analysed.

Operation of the CCU with a low solution flow rate at a specified CO_2 capture rate requires a higher CO_2 capacity of the solution, which can be achieved by lowering the CO_2-loading of the lean solution at the outlet of the desorber column (overstripping). It was shown that for the six selected solvents in case of a low temperature difference of 5 K in the RLHX such operation is only recommendable for solvents with a low inherent CO_2 capacity such as MEA and K/PZ. For a smaller RLHX with a higher temperature difference of 10 K, the potential of overstripping with respect to a reduced net efficiency penalty is enhanced. It was shown that under these boundary conditions all solvents evaluated in this work except for AMP can benefit from a higher CO_2 capacity and overstripping operation. The increase in auxiliary power for CO_2 compression to lower solution flow rates prevents overstripping to be beneficial for AMP.

The impact of the reboiler temperature on the overall net efficiency is determined by three effects. Firstly, for the six solvents selected in this work an increase in reboiler temperature leads to a decrease in reboiler heat duty. Furthermore, an increase in reboiler temperature implies an increase in desorber pressure and therefore a decrease in auxiliary power for CO_2 compression. Finally, as the reboiler temperature determines the required pressure of the steam that is extracted from the power plant, a reboiler temperature increase implies the extraction of higher quality steam resulting in a larger specific power loss in the power plant.

Since changes in solution flow rate and in reboiler temperature have both positive and negative impacts on the net power output of the power plant, the overall net efficiency penalty becomes minimal for a certain combination of these two process parameters. It was shown for the six selected solvents and in case of retrofit integration in the reference power plant that when the reboiler temperature is increased, the net efficiency penalty first decreases due to the positive effects of decreasing reboiler heat duty and decreasing auxiliary power for CO_2 compression. It then reaches a minimum for reboiler temperatures, depending on the individual solvent, between 105 and 113 °C. If the reboiler temperature is further increased, the net efficiency penalty finally increases due to the higher specific power losses, which are related to the required steam extraction from the power plant at higher pressure.

An overall process evaluation revealed that under the boundary conditions as defined in this work MDEA/PZ is best suited for a retrofit integration in the

considered hard-coal-fired steam power plant. With this solvent a net efficiency penalty of 8.47 %-pts. compared to 10.15 %-pts. with MEA is achieved for a CO_2 capture rate of 90 % and subsequent CO_2 compression to 110 bar. PZ showed the lowest reboiler heat duty of 2.45 GJ_{th} / t CO_2 at a reboiler temperature of 150 °C (MDEA/PZ: 2.52 GJ_{th} / t CO_2 at 120 °C; MEA: 3.35 GJ_{th} / t CO_2 at 120 °C). However, steam extraction at 6.9 bar from the considered power plant is required to supply the heat to the reboiler at a temperature of 150 °C and leads to approximately 46.6 % higher specific power losses than steam extraction at 3.0 bar, which is required for a reboiler temperature of 120 °C. Therefore, PZ cannot benefit from the low reboiler heat duty at higher reboiler temperatures and shows a higher net efficiency penalty than MDEA/PZ for optimal process parameters.

The best option to provide for the reboiler heat duty for the regeneration of the solution is the extraction of steam at the crossover pipe between IP and LP turbine of the power plant. The steam extraction leads to a drop in pressure throughout the entire turbine. Steam conditioning is therefore required to provide for the necessary steam quality, which depends on the desired reboiler temperature. To provide the steam at the required pressure, a throttle in the branch pipe to the reboiler and a pressure maintaining valve (PMV) in the steam pipe upstream of the LP turbine inlet are necessary. In the course of the energetic evaluation it was shown that an operation at or close to open valve conditions, thus with neither the throttle nor the PMV being active, is most beneficial in terms of a maximal power output of the overall process.

The higher the pressure in the IP/LP crossover at the design point (full-load without CO_2 capture), the higher the pressure remains when steam is extracted for the regeneration of the solution. Therefore, if the crossover design pressure of the power plant is higher, then the corresponding reboiler temperature which allows an operation with open valves is also higher. As the reboiler heat duty decreases to higher reboiler temperatures, the net efficiency for a retrofit integration in a power plant with increased IP/LP crossover design pressure of 5.5 bar is between 0.19 and 0.49 %-pts. lower than for a retrofit integration in the reference power plant, which has a crossover pressure in the design point of 3.9 bar.

In case of a greenfield integration, thus when a CCU is integrated in a new power plant that is specifically designed for operation with CO_2 capture, the water-steam-cycle can be adapted to the requirements of the CCU. Such modi-

fication can maximise the efficiency of the individual components in the power plant process, in particular of turbines and preheaters. It was found that in particular MEA and PZ can profit from the adaptation of the water-steam-cycle. The lower reboiler heat duties which are achievable when employing higher reboiler temperatures lead to net efficiency penalties which are between 0.35 and 0.79 %-pts. lower compared to the case of retrofit integration in the reference power plant.

The methodology for energetic evaluation of chemical solvents for post-combustion CO_2 capture proposed in this work requires a consistent set of measurement data, in particular of the CO_2 solubility. Additional measurements are needed for some of the evaluated solvents in the relevant temperature and CO_2 partial pressure range. This is in particular the case for MDEA/PZ to confirm the positive results from this work with respect to the low net efficiency penalty that was determined on the basis of limited CO_2 solubility measurement data. Especially the low CO_2 loading region at low CO_2 partial pressure needs to be covered by more dense measurement series. Measurement data at low CO_2 partial pressures are also scarce and need to be updated for AMP. Finally, there is a need for a solubility measurement for AMP/PZ solvent blends with an increased concentration of PZ (e.g., 4 m AMP / 6 m PZ), to evaluate the advantage of an increased CO_2 capacity in consideration of the undesired larger risk of salt precipitation and the increased viscosity of the solution.

The determination of the heat of absorption of CO_2 via solubility and the Gibbs-Helmholtz equation as done in this work increases the uncertainty that is associated to the measurements of the CO_2 solubility. Therefore, in an energetic evaluation the use of detailed measurements of the heat of absorption for all solvents is advisable. If a broad and reliable data basis for a set of solvents for energetic evaluation and comparison was available, the proposed semi-empirical column model could be extended by a correlation that represents the heat of absorption of CO_2 as a function of temperature and CO_2 loading.

The simplified approach that was employed in this work to represent the absorber might lead to an over- or underestimation of reboiler heat duties for a particular solvent. For example, PZ and MDEA/PZ show liquid phase mass transfer coefficients under rich conditions in the absorber almost twofold of MEA. These two solvents are therefore possibly capable of achieving higher

CO_2 loadings of the rich solution than the other four solvents without any additional measures.

Due to the outlined limitations of the semi-empirical column model and uncertainties in the solvent properties, the absolute values of reboiler heat duty determined by the semi-empirical column model need to be confirmed through the development and application of validated rigorous thermodynamic models for a particular solvent and the test of promising solvents in large-scale pilot and demonstration plants.

REFERENCES

[1] THE HEADS OF STATE, HEADS OF GOVERNMENT, MINISTERS, AND OTHER HEADS OF THE DELEGATIONS PRESENT AT THE UNITED NATIONS CLIMATE CHANGE CONFERENCE 2009: *Copenhagen Accord*. http://www.denmark.dk/NR/rdonlyres/C41B62AB-4688-4ACE-BB7B-F6D2C8AAEC20/0/copenhagen_accord.pdf, December 2009

[2] PRIDDLE, R. (Ed.): *World Energy Outlook 2008*. International Energy Agency, 2008 (ISBN 978 92 64 04560-6)

[3] KATHER, A.; RAFAILIDIS, S.; HERMSDORF, C.; KLOSTERMANN, M.; MASCHMANN, A.; MIESKE, K.; OEXMANN, J.; PFAFF, I.; ROHLOFF, K.; WILKEN, J.: *Research & development needs for clean coal deployment*. IEA Clean Coal Centre, 2008 (ISBN 978-92-9029-449-3 CCC/130)

[4] HASZELDINE, R. S.: Carbon Capture and Storage: How Green Can Black Be? In: *Science* 325 (2009), pp. 1647–1652

[5] METZ, B. (Ed.); DAVIDSON, O. (Ed.); CONINCK, H. de (Ed.); LOOS, M. (Ed.); MEYER, L. (Ed.): *Carbon Dioxide Capture and Storage*. Cambridge University Press, UK : Intergovernmental Panel on Climate Change, 2005 (Special Report)

[6] IRONS, R.; SEKKAPPAN, G.; PANESAR, R.; GIBBINS, J.; LUCQUIAUD, M.: CO_2 Capture Ready Plants / IEA GHG R&D Programme. 2007 (2007/4)

[7] ROCHELLE, G. T.: Amine Scrubbing for CO_2 Capture. In: *Science* 325 (2009), pp. 1652–1654

[8] AL-BAGHLI, N. A.; PRUESS, S. A.; YESAVAGE, V. F.; SELIM, M. S.: A rate-based model for the design of gas absorbers for the removal of CO_2 and H_2S using aqueous solutions of MEA and DEA. In: *Fluid Phase Equilibria* 185 (2001), Issue no. 1-2, pp. 31-43

[9] GABRIELSEN, J.; MICHELSEN, M. L.; STENBY, E. H.; KONTOGEORGIS, G. M.: Modeling of CO_2 Absorber using an AMP solution. In: *AIChE Journal* 52 (2006), Issue no. 10, pp. 3443-3451

[10] KVAMSDAL, H. M.; JAKOBSEN, J. P.; HOFF, K. A.: Dynamic modeling and simulation of a CO_2 absorber column for post-combustion CO_2 capture. In: *Chemi-*

cal Engineering and Processing: Process Intensification 48 (2009), January, Issue no. 1, pp. 135-144

[11] LAWAL, A.; WANG, M.; STEPHENSON, P.; YEUNG, H.: Dynamic modelling of CO_2 absorption for post combustion capture in coal-fired power plants. In: *Fuel* 88 (2009), December, Issue no. 12, pp. 2455-2462

[12] PLAZA, J. M.; CHEN, E.; ROCHELLE, G. T.: Absorber intercooling in CO_2 absorption by piperazine-promoted potassium carbonate. In: *AIChE Journal* 56 (2010), Issue no. 4, pp. 905-914

[13] TOBIESEN, F. A.; SVENDSEN, H. F.; HOFF, K. A.: Desorber energy consumption amine based absorption plants. In: *International Journal of Green Energy* (2005), December, pp. 201–215

[14] OYENEKAN, B. A.; ROCHELLE, G. T.: Energy Performance of Stripper Configurations for CO_2 Capture by Aqueous Amines. In: *Industrial & Engineering Chemistry Research* 45 (2006), Issue no. 8, pp. 2457–2464

[15] OYENEKAN, B. A.; ROCHELLE, G. T.: Alternative Stripper Configurations for CO_2 Capture by Aqueous Amines. In: *A.I.Ch.E. Journal* 53 (2007), December, Issue no. 12, pp. 3144–3154

[16] ALIE, C.; BACKHAM, L.; CROISET, E.; DOUGLAS, P. L.: Simulation of CO_2 capture using MEA scrubbing: a flowsheet decomposition method. In: *Energy Conversion and Management* 46 (2005), Issue no. 3, pp. 475-487

[17] JASSIM, M. S.; ROCHELLE, G. T.: Innovative Absorber/Stripper Configurations for CO_2 Capture by Aqueous Monoethanolamine. In: *Industrial & Engineering Chemistry Research* 45 (2006), Issue no. 8, pp. 2465-2472

[18] AROONWILAS, A.; VEAWAB, A.: Cost Structure and Performance of CO_2 Capture Unit Using Split-Stream Cycle. In: *Proceedings of the 8th International Conference on Greenhouse Gas Control Technologies*, 2006

[19] ABU-ZAHRA, M..; SCHNEIDERS, L.; NIEDERER, J.; FERON, P.; VERSTEEG, G.: CO_2 capture from power plants: Part I. A parametric study of the technical performance based on monoethanolamine. In: *International Journal of Greenhouse Gas Control* 1 (2007), April, Issue no. 1, pp. 37–46

[20] AHMADI, M.; GOMES, V. G.; NGIAN, K.: Advanced modelling in performance optimization for reactive separation in industrial CO_2 removal. In: *Separation and Purification Technology* 63 (2008), pp. 107–115

[21] DARDE, V.; THOMSEN, K.; WELL, W. J. M.; STENBY, E. H.: Chilled ammonia process for CO_2 capture. In: *International Journal of Greenhouse Gas Control* 4 (2010), Issue no. 2, pp. 131-136. – The Ninth International Conference on Greenhouse Gas Control Technologies

[22] NOTZ, R.; TÖNNIES, I.; MANGALAPALLY, H. P.; HOCH, S.; HASSE, H.: A short-cut method for assessing absorbents for post-combustion carbon dioxide capture. In: *International Journal of Greenhouse Gas Control* In Press, Corrected Proof (2010)

[23] PLAZA, J. M.; VAN WAGENER, D.; ROCHELLE, G. T.: Modeling CO_2 capture with aqueous monoethanolamine. In: *International Journal of Greenhouse Gas Control* 4 (2010), pp. 161–166

[24] FREEMAN, S. A.; DUGAS, R.; VAN WAGENER, D. H.; NGUYEN, T.; ROCHELLE, G. T.: Carbon dioxide capture with concentrated, aqueous piperazine. In: *International Journal of Greenhouse Gas Control* 4 (2010), Issue no. 2, pp. 119–124

[25] GARCÍA, I.; ZORRAQUINO, J. V. M.: Energy and environmental optimization in thermoelectrical generating processes—application of a carbon dioxide capture system. In: *Energy* 27 (2002), pp. 607–623

[26] MÖLLER, B. F.; ASSADI, M.; POTTS, I.: CO_2-free power generation in combined cycles—Integration of post-combustion separation of carbon dioxide in the steam cycle. In: *Energy* 31 (2006), pp. 1520–1532

[27] PELLEGRINI, G.; STRUBE, R.; MANFRIDA, G.: Comparative study of chemical absorbents in postcombustion CO_2 capture. In: *Energy* 35 (2010), February, Issue no. 2, pp. 851–857

[28] AROONWILAS, A.; VEAWAB, A.: Integration of CO_2 capture unit using single- and blended-amines into supercritical coal-fired power plant: Implications for emission and energy management. In: *International Journal of Greenhouse Gas Control* 1 (2007), pp. 143–150

[29] ROMEO, L. M.; BOLEA, I.; ESCOSA, J. M.: Integration of power plant and amine scrubbing to reduce CO_2 capture costs. In: *Applied Thermal Engineering* 28 (2008), June, Issue no. 8-9, pp. 1039–1046

[30] ROMEO, L. M.; ESPATOLERO, S.; BOLEA, I.: Designing a supercritical steam cycle to integrate the energy requirements of CO_2 amine scrubbing. In: *International Journal of Greenhouse Gas Control* 2 (2008), pp. 563–570

[31] LUCQUIAUD, M.; GIBBINS, J.: Retrofitting CO_2 capture ready fossil plants with post-combustion capture. Part 1: requirements for supercritical pulverized coal plants using solvent-based flue gas scrubbing. In: *Proc. IMechE Part A: J. Power and Energy* 223 (2009), pp. 213–226

[32] ALSTOM: Engineering feasibility and economics of CO_2 capture on an existing coal-fired power plant / U.S. Department of Energy, National Energy Technology Laboratory. Pittsburgh, 2001 (PPL-01-CT-09). Report

[33] REDDY, S.; JOHNSON, J. D.; GILMARTIN, J.: Fluor's Econamine FG Plus^{SM} Technology for CO_2 Capture at Coal-fired Power Plants / Power Plant Air Pollutant Control "Mega" Symposium. Baltimore, august 2008

[34] EVONIK ENERGY SERVICES GMBH: *EBSILONProfessional, Version 9.00 - Release - Patch 4*. May 2010

[35] DESHMUKH, R. D.; MATHER, A. E.: A mathematical model for equilibrium solubility of hydrogen sulfide and carbon dioxide in aqueous alkanolamine solutions. In: *Chemical Engineering Science* 36 (1981), Issue no. 2, pp. 355-362

[36] POSEY, M. L.; TAPPERSON, K. G.; ROCHELLE, G. T.: A simple model for prediction of acid gas solubilities in alkanolamines. In: *Gas Separation and Purification Technology* 10 (1996), Issue no. 3, pp. 181–186

[37] GABRIELSEN, J.; MICHELSEN, M. L.; STENBY, E. H.; KONTOGEORGIS, G. M.: A Model for Estimating CO_2 Solubility in Aqueous Alkanolamines. In: *Ind. Eng. Chem. Res.* 44 (2005), April, Issue no. 9, pp. 3348-3354

[38] ARCIS, H.; RODIER, L.; COXAM, J.-Y.: Enthalpy of solution of CO_2 in aqueous solutions of 2-amino-2-methyl-1-propanol. In: *The Journal of Chemical Thermodynamics* 39 (2007), Issue no. 6, pp. 878-887

[39] CHEMBLINK: *Online Database of Chemicals from Around the World*. http://www.chemblink.com, March 2010

[40] JOU, F.-Y.; MATHER, A. E.; OTTO, F. D.: The Solubility of CO_2 in a 30 Mass Percent Monoethanolamine Solution. In: *The Canadian Journal of Chemical Engineering* 73 (1995), pp. 140–147

[41] SILVA, E. F.; SVENDSEN, H. F.: Chemistry of Solvents for CO_2 Capture, 2006

[42] KOEIJER, G. de; SOLBRAA, E.: High Pressure Gas Sweetening With Amines For Reducing CO_2 Emissions. In: *Proceedings of the 7th International Conference on Greenhouse Gas Control Technologies*. Vancouver, BC, Canada, 2004

[43] *Chapter* Alkanolamines for Hydrogen Sulfide and Carbon Dioxide Removal. In:KOHL, A.L.; NIELSEN, R. B.: *Gas Purification*. Gulf Publishing Company, 1997, 40–186

[44] CHAPEL, D.; MARIZ, C.; ERNEST, J.: Recovery of CO_2 from Flue Gases: Commercial Trends. In: *Canadian Society of Chemical Engineers annual meeting*. Saskatoon, Saskatchewan, Canada, October 1999

[45] KNUDSEN, J. N.; VILHELMSEN, P.-J.; JENSEN, J. N.: Performance Review of CASTOR Pilot Plant at Esbjerg. In: *11th Workshop of the International Network for CO_2 Capture*. Vienna, Austria, May 2008

[46] REDDY, S.: Econamine FG Plus^{SM} - Technology for Post-Combustion CO_2 Capture. In: *11th Workshop of the International Network for CO_2 Capture*. Vienna, Austria, May 2008

[47] ESBER, G. S.: *Carbon Dioxide Capture Technology for the Coal-Powered Electricity Industry: A Systematic Prioritization of Research Needs*. USA, Ohio University, Master thesis, June 2006

[48] FERAUD, A.; BILL, A.; MAROCCO, L.; HOWARD, T.: CASTOR Study on Technological Requirements for Flue Gas Clean-Up Prior to CO_2-Capture. In: *Proceedings of the 8th International Conference on Greenhouse Gas Control Technologies*. Trondheim, Norway, 2006

[49] BONIS, M. R.; BALLAGUET, J. P.; RIGAILL, C.: A Critical Look at Amines: a Practical Review of Corrosion Experience over Four Decades. In: *83rd Annual GPA Convention*, 2004

[50] BAILEY, D. W.; FERON, P. H. M.: Post-combustion Decarbonisation Processes. In: *Oil & Gas Science and Technology Revue IFP* 60 (2005), May, Issue no. 3, pp. 461–474

[51] DAVIS, J.; ROCHELLE, G. T.: Thermal degradation of monoethanolamine at stripper conditions. In: *Energy Procedia* 1 (2009), February, Issue no. 1, pp. 327-333

[52] NAINAR, M.; VEAWAB, A.: Corrosion in CO_2 capture unit using MEA-piperazine blends. In: *Energy Procedia* 1 (2009), Issue no. 1, pp. 231-235

[53] LI, M.-H.; CHANG, B.-C.: Solubilities of Carbon Dioxide in Water + Monoethanolamine + 2-Amino-2-methyl-1-propanol. In: *J. Chem. Eng. Data* 39 (1994), pp. 448–452

[54] SHEN, K.-P.; LI, M.-H.; YIH, S.-M.: Kinetics of Carbon Dioxide Reaction with Sterically Hindered 2-Piperidineethanol Aqueous Solutions. In: *Ind. Eng. Chem. Res.* 30 (1991), pp. 1811–1813

[55] MIMURA, T.; SATSUMI, S.; IIJIMA, M.; MITSUOKA, S.: Developments on energy saving technology for flue gas carbon dioxide recovery by the chemical absorption method and steam system in power plant. In: *Proceedings of the 4th International Conference on Greenhouse Gas Control Technologies*. Interlaken, Switzerland, 1999

[56] YAGI, Y.; MIMURA, T.; YONEKAWA, T.; YOSHIYAMA, R.: Development and Improvement of CO_2-Capture system. In: *Proceedings of the 8th International Conference on Greenhouse Gas Control Technologies*, 2006

[57] IWASAKI, S.; KAMIJO, T.; TAKASHINA, T.; TANAKA, H.: Large Scale Flue Gas CO_2 Recovering, CO_2 Cost and Total System for CO_2 Enhanced Oil Recovery. In: *Mitsubishi Heavy Industries Ltd. Technical Review* 41 (2004), August, Issue no. 4

[58] CULLINANE, J. T.: *Thermodynamics and Kinetics of Aqueous Piperazine with Potassium Carbonate for Carbon Dioxide Capture*. Austin, TX, USA, University of Texas, Department of Chemical Engineering, PhD Thesis, 2005

[59] HILLIARD, M.: *A Predictive Thermodynamic Model for an Aqueous Blend of Potassium Carbonate, Piperazine, and Monoethanolamine for Carbon Dioxide Capture from Flue Gas*. Austin, TX, USA, University of Texas, Department of Chemical Engineering, PhD Thesis, May 2008

[60] DUGAS, R. E.: *Carbon Dioxide Absorption, Desorption, and Diffusion in Aqueous Piperazine and Monoethanolamine*. Austin, TX, USA, University of Texas, Department of Chemical Engineering, PhD Thesis, December 2009

[61] BISHNOI, S.: *Carbon Dioxide Absorption and Solution Equilibrium Piperazine Activated Methyldiethanolamine*. Austin, TX, USA, University of Texas, Department of Chemical Engineering, PhD Thesis, December 2000

[62] SUN, W.-C.; YONG, C.-B.; LI, M.-H.: Kinetics of the absorption of carbon dioxide into mixed aqueous solutions of 2-amino-2-methyl-l-propanol and piperazine. In: *Chem. Eng. Science* 60 (2005), pp. 503–516

[63] FREEMAN, S.; HILLIARD, M.; SEXTON, A.; DUGAS, R.; ROCHELLE, G. T.: Aqueous Concentrated Piperazine - a Fast, Stable, and Effective Solvent. In: *11th Workshop of the International Network for CO_2 Capture*. Vienna, Austria, May 2008

[64] DAVIS, J. D.: *Thermal Degradation of Aqueous Amines Used for Carbon Dioxide Capture*. Austin, TX, USA, Department of Chemical Engineering. University of Texas, PhD Thesis, 2009

[65] KIM, I.; SVENDSEN, H. F.: Heat of Absorption of Carbon Dioxide (CO_2) in Monoethanolamine (MEA) and 2-(Aminoethyl)ethanolamine (AEEA) Solutions. In: *Ind. Eng. Chem. Res.* 46 (2007), pp. 5803–5809

[66] MA'MUN, S.; SVENDSEN, H. F.; HOFF, K. A.; JULIUSSEN, O.: Selection of new absorbents for carbon dioxide capture. In: *Energy Conversion and Management* 48 (2007), Issue no. 1, pp. 251-258

[67] SARLIS, J.; SHAW, D.: Cansolv Activities & Technology Focus for CO_2 Capture. In: *11th Workshop of the International Network for CO_2 Capture*. Vienna, Austria, May 2008

[68] ROCHELLE, G. T.; BISHNOI, S.; CHI, S.; DANG, H.; SANTOS, J.: Research Needs for CO_2 Capture from Flue Gas by Aqueous Absorption/Stripping / University of Texas, Department of Chemical Engineering. Austin, TX, USA, January 2001. Final Report

[69] NEWMAN, S. A.: *Acid and sour gas treating processes*. Houston, Texas, USA : Gulf Publishing Company, 1985

[70] CULLINANE, J. T.; ROCHELLE, G. T.: Carbon dioxide absorption with aqueous potassium carbonate promoted by piperazine. In: *Chemical Engineering Science* 59 (2004), pp. 3619–3630

[71] OEXMANN, J.; HENSEL, C.; KATHER, A.: Post-combustion CO_2-capture from coal-fired power plants: Preliminary evaluation of an integrated chemical absorption process with piperazine-promoted potassium carbonate. In: *International Journal of Greenhouse Gas Control* 2 (2008), Issue no. 4, pp. 539–552

[72] ALAWODE, A. O.: *Oxidative Degradation of Piperazine in the Absorption of Carbon Dioxide*. Austin, TX, USA, University of Texas, Department of Chemical Engineering, Master thesis, 2005

[73] HILLIARD, M. D.; KIM, I.; ROCHELLE, G. T.; SVENDSEN, H. F.; HOFF, K. A.: Thermodynamics of carbon dioxide in aqueous piperazine/potassium carbonate systems at stripper conditions. In: *Proceedings of the 8th International Conference on Greenhouse Gas Control Technologies*. Trondheim, Norway, 2006

[74] ROCHELLE, G. T.; SEIBERT, F.; CLOSMANN, F.; CULLINANE, T.; DAVIS, J.; GOFF, G.; HILLIARD, M.; MCLEES, J.; PLAZA, J. M.; SEXTON, A.; VAN WAGENER, D.; XU, Q.; VEAWAB, A.; NAINAR, M.: CO_2 Capture by Absorption with Potassium Carbonate / University of Texas, USA; University of Regina, Canada. Version:2007. http://www.che.utexas.edu/rochelle_group/Pubs/DOE Final Report 02NT41440.pdf. 2007

[75] KNUUTILA, H.; ANTTILA, M.; BORRESEN, E.; JULIUSSEN, O.; SVENDSEN, H. F.: CO_2 Capture with Sodium Carbonate. In: *Proceedings of the 8th International Conference on Greenhouse Gas Control Technologies*. Trondheim, Norway, 19-22 June 2006

[76] KNUUTILA, H.; SVENDSEN, H. F.; ANTTILA, M.: CO_2 capture from coal-fired power plants based on sodium carbonate slurry; a systems feasibility and sensitivity study. In: *International Journal of Greenhouse Gas Control* 3 (2009), March, Issue no. 2, pp. 143-151

[77] YEH, A. C.; BAI, H.: Comparison of ammonia and monoethanolamine solvents to reduce CO_2 greenhouse gas emissions. In: *The Science of the Total Environment* 228 (1999), pp. 121–133

[78] PENNLINE, H.; FAUTH, D.; GRAY, M.; HOFFMAN, J.; JONES, K.; LUEBKE, D.; MORSI, B.; RESNIK, K.; SIRIWARDANE, R.; YEH, J.: Recent Advances in Carbon Dioxide Capture and Separation Techniques for Power Generation Point Sources. In: *2005 AIChE Annual Meeting*. Cincinnati, OH, USA, November 2005

[79] YEH, J. T.; RESNIK, K. P.; RYGLE, K.; PENNLINE, H.: Semi-batch absorption and regeneration studies for CO_2 capture by aqueous ammonia. In: *Fuel Processing Technology* 86 (2005), pp. 1533–1546

[80] DIAO, Y.-F.; ZHENG, X.-Y.; HE, B.-S.; CHEN, C.-H.; XU, X.-C.: Experimental study on capturing CO_2 greenhouse gas by ammonia scrubbing. In: *Energy Conversion and Management* 45 (2004), pp. 2283–2296

[81] MANI, F.; PERUZZINI, M.; STOPPIONI, P.: CO_2 absorption by aqueous NH_3 solutions: speciation ammonium carbamate, bicarbonate and carbonate by a 13C NMR study. In: *Green Chemistry* (2006), August

[82] POWERSPAN: *Carbon Capture and Multi-Pollutant Control Solutions*. www.powerspan.com, March 2010

[83] BLACK, S.: Chilled ammonia process for CO_2 capture / Alstom. 2006. PT/PE Sector Communications

[84] MATHIAS, P. M.; REDDY, S.; O'CONNELL, J. P.: Quantitative Evaluation of the Aqueous-Ammonia Process for CO_2 Capture Using Fundamental Data and Thermodynamic Analysis. In: *Energy Procedia* Ed. 1. Washington DC, USA, February 2009, 1227–1234

[85] BLACK, S.: Chilled Ammonia—Update on Joint Investigations by Alstom and EPRI. In: *12th Workshop of the International Network for CO_2 Capture*. Regina, Canada, September 2009

[86] ALSTOM: *Carbon Capture & Storage (CCS)*. http://www.power.alstom.com/home/about_us/strategy/clean_power_today/carbon_capture_storage_ccs/, March 2010

[87] HOLST, J. van; VERSTEEG, G. F.; BRILMAN, D. W. F.; HOGENDOORN, J. A.: Kinetic study of CO_2 with various amino acid salts in aqueous solution. In: *Chemical Engineering Science* 64 (2009), Issue no. 1, pp. 59-68

[88] KUMAR, P. S.; HOGENDOORN, J. A.; VERSTEEG, G. F.; FERON, P. H. M.: Kinetics of the Reaction of CO_2 with aqueous potassium salt of taurine and glycine. In: *AIChE Journal* 49 (2003), Issue no. 1, pp. 203–213

[89] KUMAR, P. S.; HOGENDOORN, J. A.; FERON, P. H. M.; VERSTEEG, G. F.: Equilibrium Solubility of CO_2 in Aqueous Potassium Taurate Solutions: Part 1. Crystallization in Carbon Dioxide Loaded Aqueous Salt Solutions of Amino Acids. In: *Ind. Eng. Chem. Res.* 42 (2003), pp. 2832–2840

[90] KUMAR, P. S.; HOGENDOORN, J. A.; TIMMER, S. J.; FERON, P. H. M.; VERSTEEG, G. F.: Equilibrium Solubility of CO_2 in Aqueous Potassium Taurate Solutions: Part 2. Experimental VLE Data and Model. In: *Ind. Eng. Chem. Res.* 42 (2003), pp. 2841–2852

[91] HOLST, J. van; KERSTEN, S. R. A.; HOGENDOORN, K. J. A.: Physiochemical Properties of Several Aqueous Potassium Amino Acid Salt. In: *J. Chem. Eng. Data* 53 (2008), pp. 1286–1291

[92] KUMAR, P. S.; HOGENDOORN, J. A.; FERON, P. H. M.; VERSTEEG, G. F.: New absorption liquids for the removal of CO_2 from dilute gas streams using mem-

brane contactors. In: *Chemical Engineering Science* 57 (2002), Issue no. 9, pp. 1639-1651

[93] JOCKENHÖVEL, T.; SCHNEIDER, R.; RODE, H.: Development of an Economic Post-Combustion Carbon Capture Process. In: *Energy Procedia* Ed. 1. Washington DC, USA, February 2009, 1043–1050

[94] MAGINN, E. J.: Design and Evaluation of Ionic Liquids as Novel CO_2 Absorbents / U.S. Department of Energy. 2004 (Award Number: DE-FG26-04NT42122). Quarterly Technical Report

[95] WAPPEL, D.; GRONALD, G.; KALB, R.; DRAXLER, J.: Ionic liquids for post-combustion CO_2 absorption. In: *International Journal of Greenhouse Gas Control* 4 (2010), May, Issue no. 3, pp. 486-494

[96] ANTHONY, J. L.; MAGINN, E. J.; BRENNECKE, J. F.: Solubilities and thermodynamic properties of gases in the ionic liquid 1-n-butyl-3-methylimidazolium hexafluorophosphate. In: *Journal of Physical Chemistry B* 106 (2002), Issue no. 29, pp. 7315–7320

[97] ANTHONY, J. L.; ANDERSON, J. L.; MAGINN, E. J.; BRENNECKE, J. F.: Anion effects on gas solubility in ionic liquids. In: *Journal of Physical Chemistry B* 109 (2005), Issue no. 13, pp. 6366–6374

[98] PETERS, C. J.; RAEISSI, S.; SCHILDERMAN, A.: A Potential Ionic Liquid for CO_2-Separating Membranes: Selection and Gas Solubility Studies / GCEP. 2006. Technical Report

[99] JOU, F.-Y.; OTTO, F.D.; MATHER, A.E.: Solubility of H_2S, CO_2, and Their Mixtures in an Aqueous Solution of 2-Piperidineethanol and Sulfolane. In: *J. Chem. Eng. Data* 43 (1998), pp. 409–412

[100] CHEN, E.: *Carbon Dioxide Absorption into Piperazine Promoted Potassium Carbonate using Structured Packing*. Austin, TX, USA, University of Texas, Department of Chemical Engineering, PhD Thesis, December 2007

[101] APPL, M.; WAGNER, U.; HENRICI, H. J.; KUESSNER, K.; VOLKAMER, F.; NEUST, N. E.: Removal of CO_2 and/or H_2S and/or COS From Gases Containing These Constituents / U.S. Patent 4336233. 1982

[102] MATHONAT, C.; MAJER, V.; MATHER, A. E.; GROLIER, J.-P. E.: Use of Flow Calorimetry for Determining Enthalpies of Absorption and the Solubility of CO_2 in

Aqueous Monoethanolamine Solutions. In: *Industrial & Engineering Chemistry Research* 37 (1998), October, Issue no. 10, pp. 4136-4141

[103] CARSON, J. K.; MARSH, K. N.; MATHER, A. E.: Enthalpy of solution of carbon dioxide in (water + monoethanolamine, or diethanolamine, or N-methyldiethanolamine) and (water + monoethanolamine + N-methyldiethanolamine) at T = 298.15 K. In: *The Journal of Chemical Thermodynamics* 32 (2000), September, Issue no. 9, pp. 1285-1296

[104] KIM, I.; SVENDSEN, H. F.: Comparative study of the heats of absorption of post-combustion CO_2 absorbents. In: *International Journal of Greenhouse Gas Control* In Press, Corrected Proof (2010)

[105] ERMATCHKOV, V.; KAMPS, A. P.-S.; SPEYER, D.; MAURER, G.: Solubility of Carbon Dioxide in Aqueous Solutions of Piperazine in the Low Gas Loading Region. In: *J. Chem. Eng. Data* 51 (2006), pp. 1788–1796

[106] ROBERTS, B. E.; MATHER, A. E.: Solubility of CO_2 and H_2S in a hindered amine solution. In: *Chem. Eng. Commun.* 64 (1988), pp. 105–111

[107] TENG, T. T.; MATHER, A. E.: Solubility of CO_2 in an AMP Solution. In: *J. Chem. Eng. Data* 35 (1990), pp. 410–411

[108] TONTLWACHWUTHLKUL, P.; MEISEN, A.; LIM, C.J.: Solubility of CO_2 in 2-Amino-2-methyl-1-propanol Solutions. In: *Journal of Chemical and Engineering Data* 36 (1991), pp. 130 – 133

[109] SILKENBÄUMER, D.; RUMPF, B.; LICHTENTHALER, R. N.: Solubility of Carbon Dioxide in Aqueous Solutions of 2-Amino-2-methyl-1-propanol and N-Methyldiethanolamine and Their Mixtures in the Temperature Range from 313 to 353 K and Pressures up to 2.7 MPa. In: *Ind. Eng. Chem. Res.* 37 (1998), pp. 3133–3141

[110] PARK, S. H.; LEE, K. B.; HYUN, J. C.; KIM, S. H.: Correlation and Prediction of the Solubility of Carbon Dioxide in Aqueous Alkanolamine and Mixed Alkanolamine Solutions. In: *Ind. Eng. Chem. Res.* 41 (2002), pp. 1658–1665

[111] YANG, Z.-Y.; SORIANO, A. N.; CAPARANGA, A. R.; LI, M.-H.: Equilibrium solubility of carbon dioxide in (2-amino-2-methyl-1-propanol + piperazine + water). In: *J. Chem. Thermodynamics* 42 (2010), May, Issue no. 5, pp. 659–665

[112] XU, G.-W.; ZHANG, C.-F.; QIN, S.-J.; GAO, W.-H.; LIU, H.-B.: Gas-Liquid Equilibrium in a CO_2-MDEA-H_2O System and the Effect of Piperazine on It. In: *Ind. Eng. Chem. Res.* 37 (1998), pp. 1473–1477

[113] LIU, H.-B.; ZHANG, C.-F.; XU, G.-W.: A Study on Equilibrium Solubility for Carbon Dioxide in Methyldiethanolamine-Piperazine-Water Solution. In: *Ind. Eng. Chem. Res.* 38 (1999), pp. 4032–4036

[114] PEREZ-SALADO KAMPS, A.; XIA, J.; MAURER, G.: Solubility of CO_2 in (H_2O+ piperazine) and in (H_2O + MDEA + piperazine). In: *AIChE J.* 49 (2003), pp. 2662–2670

[115] DERKS, P. W. J.: *Carbon Dioxide Absorption in Piperazine Activated N-Methyldiethanolamine*, Univesity of Twente, PhD Thesis, 2006

[116] VAHIDI, M.; MATIN, N. S.; GOHARROKHI, M.; JENAB, M. H.; ABDI, M. A.; NAJIBI, S. H.: Correlation of CO_2 solubility in N-methyldiethanolamine + piperazine aqueous solutions using extended Debye–Hückel model. In: *J. Chem. Thermodynamics* 41 (2009), pp. 1272–1278

[117] SPEYER, D.; ERMATCHKOV, V.; MAURER, G.: Solubility of Carbon Dioxide in Aqueous Solutions of N-Methyldiethanolamine and Piperazine in the Low Gas Loading Region. In: *J. Chem. Eng. Data* 55 (2010), pp. 283–290

[118] CHEN, X.: *Personal Communication*. University of Texas at Austin, Department of Chemical Engineering, January 2010

[119] SCHÄFER, B.; MATHER, A. E.; MARSH, K. N.: Enthalpies of solution of carbon dioxide in mixed solvents. In: *Fluid Phase Equilibria* 194-197 (2002), March, pp. 929-935

[120] PAGE, M.; HUOT, J. Y.; JOLICOEUR, C.: A Comprehensive Thermodynamic Investigation of Water-Ethanolamine Mixtures at 10, 25, and 40 °C. In: *Canadian Journal of Chemistry* 71 (1993), Issue no. 7, pp. 1064–1072

[121] CHENG, S.; MEISEN, A.; CHAKMA, A.: Predict amine solution properties accurately. In: *Hydrocarbon Processing* (1996), February, pp. 81–84

[122] CHIU, L.-F.; LI, M.-H.: Heat Capacity of Alkanolamine Aqueous Solutions. In: *J. Chem. Eng. Data* 44 (1999), pp. 1396–1401

[123] WEILAND, R. H.; DINGMAN, J. C.; CRONIN, D. B.: Heat Capacity of Aqueous Monoethanolamine, Diethanolamine, N-Methyldiethanolamine, and N-

Methyldiethanolamine-Based Blends with Carbon Dioxide. In: *J. Chem. Eng. Data* 42 (1997), pp. 1004–1006

[124] HSU, C.-H.; LI, M.-H.: Densities of aqueous blended amines. In: *J. Chem. Eng. Data* 42 (1997), MAY-JUN, Issue no. 3, pp. 502–507

[125] WEILAND, R. H.; DINGMAN, J. C.; CRONIN, D. B.; BROWNING, G. J.: Density and Viscosity of Some Partially Carbonated Aqueous Alkanolamine Solutions and Their Blends. In: *J. Chem. Eng. Data* 43 (1998), pp. 378–382

[126] AMUNDSEN, T. G.; OI, L. E.; EIMER, D. A.: Density and Viscosity of Monoethanolamine + Water + Carbon Dioxide from (25 to 80) °C. In: *J. Chem. Eng. Data* 54 (2009), pp. 3096–3100

[127] ZHANG, K.; HAWRYLAK, B.; PALEPU, R.; TREMAINE, P. R.: Thermodynamics of aqueous amines: excess molar heat capacities, volumes, and expansibilities of water + methyldiethanolamine (MDEA) and water 2-amino-2-methyl-1-p+ropanol (AMP). In: *J. Chem. Thermodynamics* 34 (2002), pp. 679–710

[128] ROCHELLE, G. T.: CO_2 Capture by Aqueous Absorption - Summary of 1st Quarterly Progress Reports 2009 / University of Texas, Department of Chemical Engineering. 2009

[129] DERKS, P. W.; HOGENDOORN, K. J.; VERSTEEG, G. F.: Solubility of N_2O in and Density, Viscosity, and Surface Tension of Aqueous Piperazine Solutions. In: *J. Chem. Eng. Data* 50 (2005), pp. 1947–1950

[130] ROCHELLE, G. T.: CO_2 Capture by Aqueous Absorption - Summary of 2nd Quarterly Progress Reports 2008 / University of Texas, Department of Chemical Engineering. 2008

[131] ROCHELLE, G. T.: CO_2 Capture by Aqueous Absorption - Summary of 3rd Quarterly Progress Reports 2008 / University of Texas, Department of Chemical Engineering. 2008

[132] CHEN, Y.-R.; LI, M.-H.: Heat Capacity of Aqueous Mixtures of Monoethanolamine with 2-Amino-2-methyl-l-propanol. In: *J. Chem. Eng. Data* 46 (2001), Issue no. 4, pp. 102–106

[133] XU, S.; OTTO, F. D.; MATHER, A. E.: Physical Properties of Aqueous AMP Solutions. In: *Journal of Chemical and Engineering Data* 36 (1991), pp. 71 – 75

[134] CHAN, C.; MAHAM, Y.; MATHER, A. E.; MATHONAT, C.: Densities and volumetric properties of the aqueous solutions of 2-amino-2-methyl-1-propanol, n-

butyldiethanolamine and n-propylethanolamine at temperatures from 298.15 to 353.15 K. In: *Fluid Phase Equilibria* 198 (2002), pp. 239–250

[135] GABRIELSEN, J.: *CO_2 Capture from Coal Fired Power Plants*. Department of Chemical Engineering Lyngby, Denmark, Technical University of Denmark, PhD Thesis, 2007

[136] CHEN, Y.-R.; CAPARANGA, A. R.; SORIANO, A. N.; LI, M.-H.: Liquid heat capacity of the solvent system (piperazine + n-methyldiethanolamine + water). In: *J. Chem. Thermodynamics* 42 (2010), pp. 54–59

[137] FRAILIE, P.: *University of Texas, Department of Chemical Engineering*. Personal Communication, February 2010

[138] PAUL, S.; MANDAL, B.: Density and Viscosity of Aqueous Solutions of (N-Methyldiethanolamine + Piperazine) and (2-Amino-2-methyl-1-propanol + Piperazine) from (288 to 333) K. In: *J. Chem. Eng. Data* 51 (2006), pp. 1808–1810

[139] CHEN, Y.-R.; CAPARANGA, A. R.; SORIANO, A. N.; LI, M.-H.: Liquid heat capacity of the solvent system (piperazine + 2-amino-2-methyl-lpropanol + water). In: *J. Chem. Thermodynamics* 42 (2010), Issue no. 4, pp. 518–523

[140] SAMANTA, A.; BANDYOPADHYAY, S. S.: Density and Viscosity of Aqueous Solutions of Piperazine and (2-Amino-2-methyl-1-propanol + Piperazine) from 298 to 333 K. In: *J. Chem. Eng. Data* 51 (2006), pp. 467–470

[141] OEXMANN, J.; KATHER, A.: Post-combustion CO_2 capture in coal-fired power plants: comparison of integrated chemical absorption processes with piperazine promoted potassium carbonate and MEA. In: *Energy Procedia* Ed. 1. Washington DC, USA, February 2009, 799–806

[142] OYENEKAN, B. A.; ROCHELLE, G. T.: Rate modeling of CO_2 stripping from potassium carbonate promoted by piperazine. In: *International Journal of Greenhouse Gas Control* 3 (2009), March, Issue no. 2, pp. 121-132

[143] CORNELL COMPUTATIONAL SYNTHESIS LABORATORY: *Eureqa 0.81*. http://ccsl.mae.cornell.edu/eureqa, June 2010

[144] OYENEKAN, B. A.: *Modeling of Strippers for CO_2 Capture by Aqueous Amines*, University of Texas, Department of Chemical Engineering, PhD Thesis, May 2007

[145] DDBST - Dortmund Data Bank Software and Separation Technology GmbH: *Online Property Calculation*. http://www.ddbst.com/en/online/Online_Calc.php, March 2010

[146] Aly, F. A.; Lee, L. L.: Self-consistent equations for calculating the ideal gas heat capacity, enthalpy, and entropy. In: *Fluid Phase Equilibria* 6 (1981), Issue no. 3-4, pp. 169-179

[147] Aspen Technology, Inc.: *Aspen Properties V7.1*. 2010

[148] Knudsen, J. N.; Vilhelmsen, P.-J.; Jensen, J. N.; Biede, O.: CASTOR deliverable D2.5.4 Appendix A: Experimental report - 1000 hours MEA campaign at the CASTOR pilot plant at Esbjerg power plant / DONG Energy Power Vattenfall Nordic. 2007

[149] Abu Zahra, M.: *Carbon Dioxide Capture from Flue Gas - Development and Evaluation of Existing and Novel Process Concepts*, Technische Universiteit Delft, PhD Thesis, 2009

[150] *CASTOR - CO_2 from Capture to Storage - Integrated Project partially funded by the European Commission under the 6th Framework Programme*. www.co2castor.com,

[151] *CESAR - CO_2 Enhanced Separation and Recovery - Collaborative Project partially funded by the European Commission under the 7th Framework Programme*. www.co2cesar.eu/,

[152] Chen, X.: Screening Amines with Wetted Wall Column: Equilibrium and Rate measurements. In: *Research Review Meeting of the Luminant Carbon Management Program*, 2010

[153] Rochelle, G. T.: Amine Selection to Minimize Energy for CO_2 Capture. In: *Research Review Meeting of the Luminant Carbon Management Program*, 2010

[154] Freguia, S.; Rochelle, G. T.: Modeling of CO_2 Capture by Aqueous Monoethanolamine. In: *AIChE Journal* 49 (2003), Issue no. 7, pp. 1676–1686

[155] Pelkonen, S.: *Multicomponent Mass Transfer in Packed Distillation Columns*. Dortmund, Germany, Universität Dortmund, PhD Thesis, 1997

[156] Kenig, E. Y.; Schneider, R.; Górak, A.: Reactive absorption: Optimal process design via optimal modelling. In: *Chemical Engineering Science* 56 (2001), January, Issue no. 2, pp. 343-350

[157] ASPRION, N.: Nonequilibrium Rate-Based Simulation of Reactive Systems: Simulation Model, Heat Transfer, and Influence of Film Discretization. In: *Ind. Eng. Chem. Res.* 45 (2006), pp. 2054–2069

[158] KNUDSEN, J. N.: Evaluation of Process Improvements in Pilot Scale Activities Under the EU CESAR Project. In: *12th Workshop of the International Network for CO_2 Capture*. Regina, Canada, September 2009

[159] RAO, A. B.; RUBIN, E. S.: Identifiying Cost-Effective CO_2 Control Levels for Amines-Based CO_2 Capture Systems. In: *Ind. Eng. Chem. Res.* 45 (2006), pp. 2421–2429

[160] KATHER, A.; OEXMANN, J.; LIEBENTHAL, U.; LINNENBERG, S.: Using Overall Process Simulation to Minimize the Energy Penalty of Post-Combustion CO_2 Capture Processes in Steam Power Plants. In: *35th International Technical Conference on Clean Coal & Fuel Systems*. Clearwater, FL, USA, 2010

[161] FREGUIA, S.: *Modeling of CO_2 Removal from Flue Gases with Monoethanolamine*. Austin, TX, USA, University of Texas, Department of Chemical Engineering, Master thesis, May 2002

[162] HIGLER, A.; TAYLOR, R.; KRISHNA, R.: Modeling of a reactive separation process using a nonequilibrium stage model. In: *Computers & Chemical Engineering* 22 (1998), March, Issue no. Supplement 1, pp. S111-S118

[163] LIEBENTHAL, U.; LINNENBERG, S.; OEXMANN, J.; KATHER, A.: Derivation of correlations to evaluate the impact of retrofitted post-combustion CO_2 capture processes on steam power plant performance. In: *International Journal of Greenhouse Gas Control* submitted for publication (2010)

[164] TRAUPEL, W.: *Thermische Turbomaschinen: Zweiter Band. Geänderte Betriebsbedingungen, Regelung, Mechanische Probleme, Temperaturprobleme*. Springer, Berlin, Germany, 2000 (ISBN 978-354-0673774)

[165] DRBAL, L. F.; BOSTON, P.; WESTRA, K. L.: *Power Plant Engineering*. Springer, Netherlands, 1995 (ISBN 0-412-06401-4)

[166] SANDIA NATIONAL LABORATORIES: *Trilinos Release 10.2.1*. http://trilinos.sandia.gov/download/trilinos-10.2.html, July 2010

[167] HEROUX, M. A.; BARTLETT, R. A.; HOWLE, V. E.; HOEKSTRA, R. J.; HU, J. J.; KOLDA, T. G.; LEHOUCQ, R. B.; LONG, K. R.; PAWLOWSKI, R. P.; PHIPPS, E. T.; SALINGER, A. G.; THORNQUIST, H. K.; TUMINARO, R. S.; WILLENBRING, J. M.; WILLIAMS, A.;

STANLEY, K. S.: An overview of the Trilinos project. In: *ACM Trans. Math. Softw.* 31 (2005), Issue no. 3, pp. 397–423

[168] HASENBEIN, C.: *Implementierung eines semi-empirischen Modells für die direkte Abbildung der Post-Combustion CO_2-Abtrennung in einem Gesamt-kraftwerksprozess*, TU Hamburg-Harburg, Institut für Energietechnik, Master thesis, February 2010

[169] STODOLA, A.; LOEWENSTEIN, L. C.: *Steam and Gas Turbines*. McGraw-Hill, New York, USA, 1927

[170] PFAFF, I.; OEXMANN, J.; KATHER, A.: Optimised integration of post-combustion CO_2 capture process in greenfield power plants. In: *Energy* 35 (2010), October, Issue no. 10, pp. 4030-4041

[171] OEXMANN, J.; KATHER, A.: Minimising the Regeneration Heat Duty of Post-Combustion CO_2-Capture Processes by Wet Chemical Absorption: The Misguided Focus on Low Heat of Absorption Solvents. In: *International Journal of Greenhouse Gas Control* 4 (2010), January, Issue no. 1, pp. 36–43

[172] STEWART, E. J.; LANNING, R. A.: Reduce amine plant solvent losses: Part 1. In: *Hydrocarbon Processing* (1994), pp. 67–81

[173] CLOSMANN, F.: *Personal Communication*. University of Texas at Austin, Department of Chemical Engineering, June 2010

[174] ZHOU, S.: Thermal degradation screen and update of EDA evaluation. In: *Research Review Meeting of the Luminant Carbon Management Program*. Austin, TX, USA, 2010

[175] KISTER, H. Z.: *Distillation Design*. New York, USA : McGraw-Hill, 1992

[176] LINNENBERG, S.; KATHER, A.: Evaluation of an Integrated Post-Combustion CO_2 Capture Process for Varying Loads in a Coal-Fired Power Plant using Monoethanolamine. In: *4th International Conference on Clean Coal Technologies*. Dresden, Germany, May 2009

[177] BAEHR, H. D.; KABELAC, S.: *Thermodynamik - Grundlagen und technische Anwendungen*. 14. Springer-Verlag, Berlin Heidelberg, Germany, 2009 (ISBN 978-3-642-00555-8)

[178] ALONSO, M.; RODRÍGUEZ, N.; GONZÁLEZ, B.; GRASA, G.; MURILLO, R.; ABANADES, J. C.: Carbon dioxide capture from combustion flue gases with a calcium oxide

chemical loop. Experimental results and process development. In: *International Journal of Greenhouse Gas Control* 4 (2010), Issue no. 2, pp. 167-173

[179] DENNIS, J.; SCHNABEL, R. B.: *Numerical methods for unconstrained optimization and nonlinear equations*. Society for Industrial and Applied Mathematics, 1996

A ANNEX

A.1 Summary of key facts

Key fact 1: The higher the heat of absorption, the higher the decrease in reboiler heat duty for an increasing reboiler temperature. (Page 98)

Key fact 2: The higher the reboiler heat duty in case of retrofit integration, the lower the optimal reboiler temperature to reach open valve operation for which the net efficiency penalty due to steam extraction becomes minimal. (Page 100)

Key fact 3: The lower the solvent concentration in aqueous solution, the lower the auxiliary power for CO_2 compression. (Page 101)

Key fact 4: The higher the heat of absorption of the solvent, the more significant the increase in auxiliary power for CO_2 compression when reducing the CO_2 loading of the lean solution. (Page 102)

Key fact 5: The higher the heat of absorption of the solvent, the more significant the increase in auxiliary power for CO_2 compression when lowering the reboiler temperature. (Page 102)

Key fact 6: Solvents with low inherent CO_2 capacity benefit particularly from overstripping in terms of a reduced reboiler heat duty. (Page 113)

Key fact 7: The higher the chosen reboiler temperature, the lower the optimal L/G with respect to a minimal reboiler heat duty. (Page 114)

Key fact 8: The higher the temperature difference in the RLHX, the lower the optimal L/G with respect to a minimal reboiler heat duty. (Page 121)

Key fact 9: The higher the LMTD in the RLHX, the lower the optimal reboiler temperature for which the net efficiency penalty due to steam extraction becomes minimal. (Page 123)

Key fact 10: When considering a CCU retrofit of a steam power plant, an operation at or slightly above open valve conditions is preferable with respect to a minimal overall net efficiency penalty. (Page 131)

A.2 CO_2 loading definition

The CO_2 loading generally denotes the amount of CO_2 that is absorbed in molecular or dissociated form by the solution. The definition of the loading, however, varies from author to author. In this work CO_2 loading is defined as the ratio of CO_2 mole fraction and the mole fraction of the alkali component in solution:

$$\alpha = \frac{x_{\mathrm{CO2}}}{x_{\mathrm{alk}}} \quad .$$

For all solvents considered in this work except for PZ, the alkali mole fraction is equal to the mole fraction of the pure solvent. PZ has two amino groups and is therefore capable of bonding two molecules of CO_2 per mole of amine. This is taking into account in the definition of the alkali mole fraction:

$$x_{\mathrm{alk}} = \frac{x_{\mathrm{MEA}} + 2\,x_{\mathrm{PZ}} + x_{\mathrm{AMP}} + x_{\mathrm{K+}} + x_{\mathrm{MDEA}}}{x_{\mathrm{H2O}} + x_{\mathrm{CO2}} + x_{\mathrm{MEA}} + 2\,x_{\mathrm{PZ}} + x_{\mathrm{AMP}} + x_{\mathrm{K+}} + x_{\mathrm{MDEA}}} \quad .$$

A.3 Solvent properties

A.3.1 CO_2 solubility

Table A.1: Coefficients to determine CO_2 solubility via Eq. (3.5)

solvent	MEA	PZ	AMP
source	[40, 59, 60]	[105, 59, 60]	[53, 110]
$\bar{m}_{\mathrm{alk}}$	7 m	4 m	4.8 m
M_{alk}	61.08 g/mol	86.14 g/mol	89.14 g/mol
range			
t	25–120 °C	40–120 °C	40–100 °C
α	0.03-0.58	0.03-0.48	0.05-1.0
$c_{\mathrm{pco2},0}$	22.53	29.13	29.28
$c_{\mathrm{pco2},1}$	-7904	-9288	-8610
$c_{\mathrm{pco2},2}$	105.0	94.31	41.03
$c_{\mathrm{pco2},3}$	-16810	-21530	-4457
$c_{\mathrm{pco2},4}$	-286.4	-434.9	-80.68
$c_{\mathrm{pco2},5}$	26480	121200	9094
$c_{\mathrm{pco2},6}$	381.70	610.4	52.32
$c_{\mathrm{pco2},7}$	8295	-143600	763.2
$c_{\mathrm{pco2},8}$	-257.4	-132.6	-18.88
n^*	87	154	47
$\sigma^\dagger$	16.7 %	15.3 %	11.9 %

* shown in Figure A.1 to Figure A.3

$^\dagger \sigma = \frac{1}{n}\sum_i^n \left(\left|p^*_{\mathrm{CO2,exp}} - p^*_{\mathrm{CO2,calc}}\right| / p^*_{\mathrm{CO2,exp}}\right)$

Table A.1: Coefficients to determine CO_2 solubility via Eq. (3.5), continued

solvent	**K/PZ**	**MDEA/PZ**	**AMP/PZ**
source	[59]	[117] ([116])	[111]
$\overline{m}_{\mathrm{alk}}$	10 m	11 m	10 m
M_{alk}	41.08 g/mol	91.49 g/mol	66.10 g/mol
range			
t	40–120 °C	40–120 °C	40–120 °C
α	0.3–0.65	0.03–0.25	0.1–0.9
$c_{\mathrm{pco2},0}$	-167.7	35.88	-9.956
$c_{\mathrm{pco2},1}$	62880	-11070	-3146
$c_{\mathrm{pco2},2}$	1180	-28.04	177.7
$c_{\mathrm{pco2},3}$	-463700	31760	-9482
$c_{\mathrm{pco2},4}$	-2163	-12.20	-322.7
$c_{\mathrm{pco2},5}$	966800	-83870	-1323
$c_{\mathrm{pco2},6}$	940.0	298.9	310.6
$c_{\mathrm{pco2},7}$	-641300	80480	8040
$c_{\mathrm{pco2},8}$	490.3	-406.2	-122.5
n^*	28	37	24
$\sigma^\dagger$	16.6 %	16.1 %	15.8 %

* shown in Figure A.4 to Figure A.6

† $\sigma = \frac{1}{n}\sum_i^n \left(\left|p^*_{\mathrm{CO2,exp}} - p^*_{\mathrm{CO2,calc}}\right| / p^*_{\mathrm{CO2,exp}}\right)$

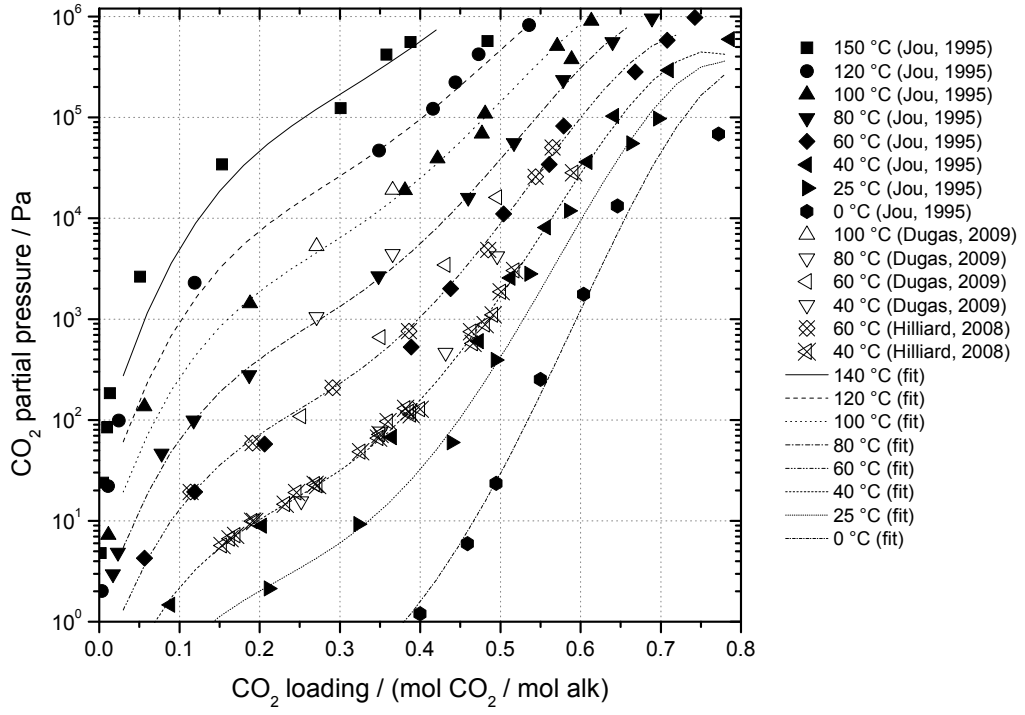

Figure A.1: CO_2 solubility of 7 m MEA solutions [40, 59, 60]

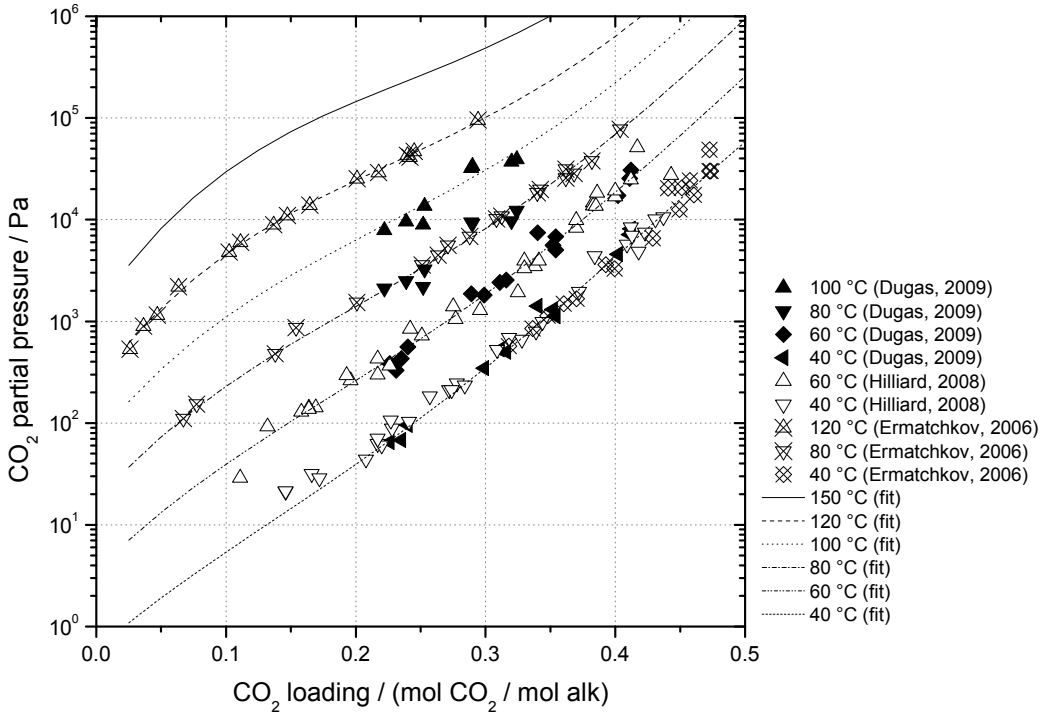

Figure A.2: CO_2 solubility of 8 m PZ solutions [105, 59, 60]

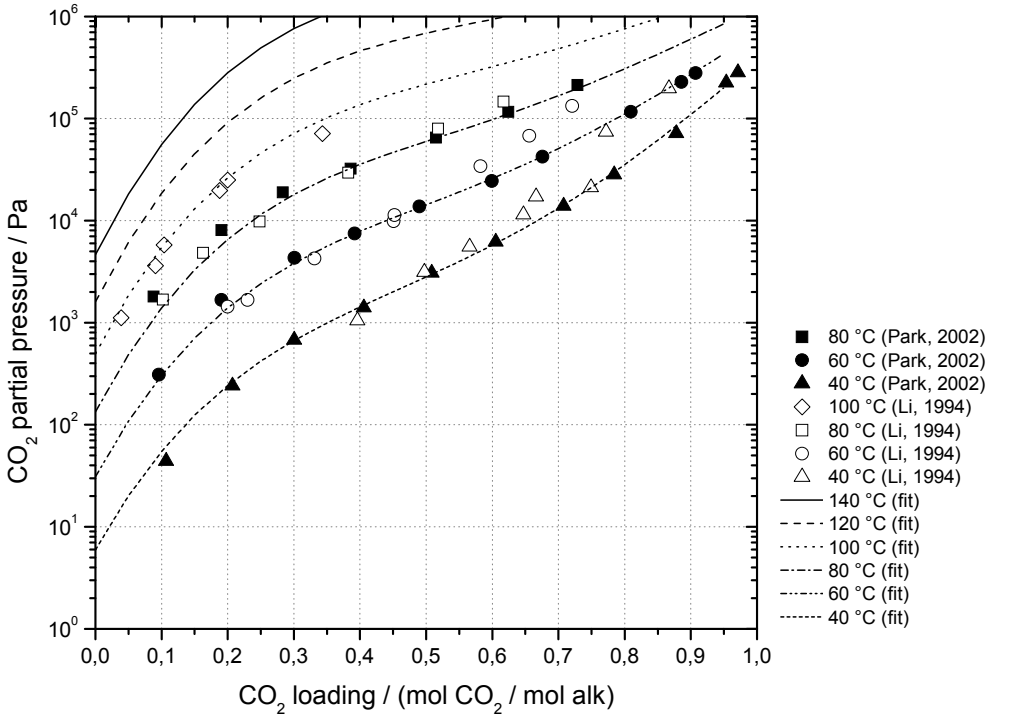

Figure A.3: CO_2 solubility of 4.8 m AMP solutions [53, 110]

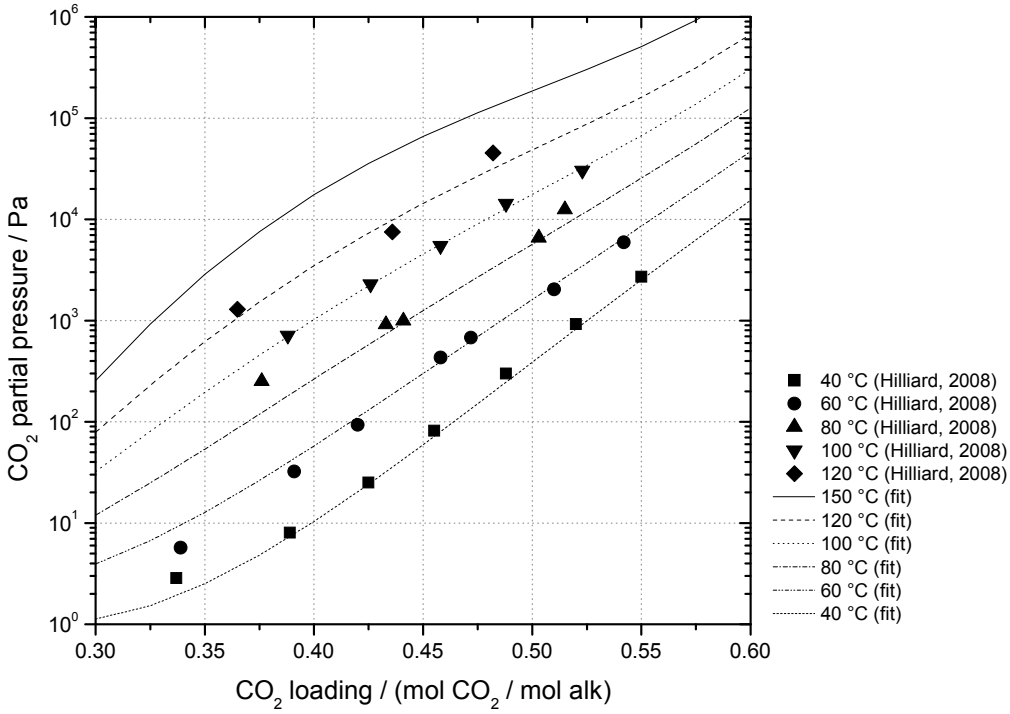

Figure A.4: CO_2 solubility of 5 m K^+ / 2.5 m PZ solutions [59]

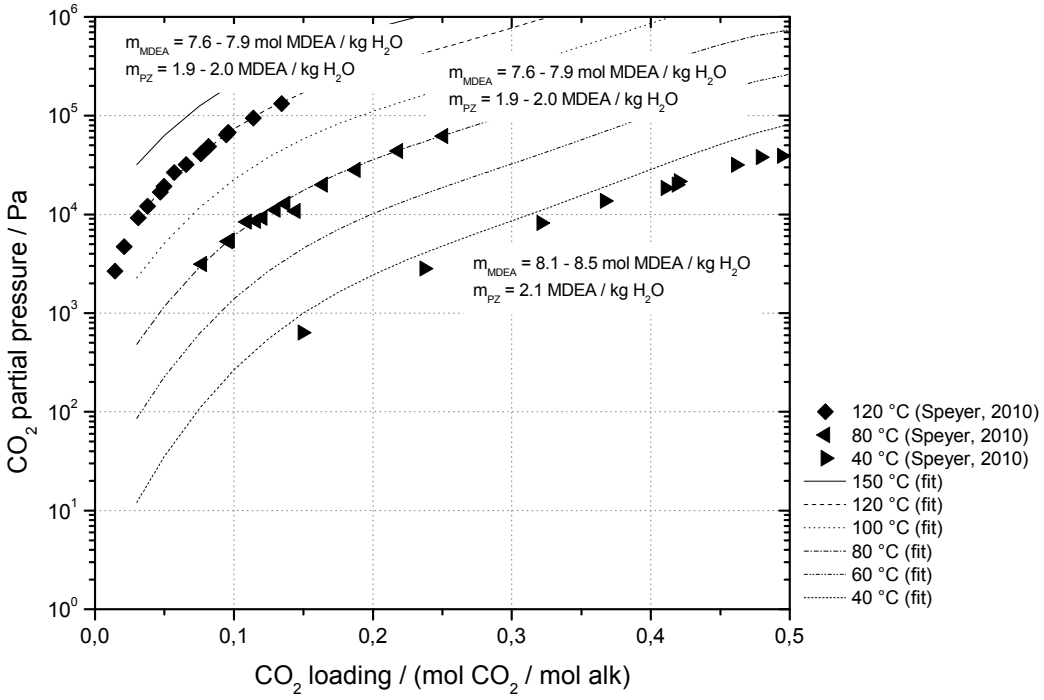

Figure A.5: CO_2 solubility of 7 m MDEA / 2 m PZ solutions [117]

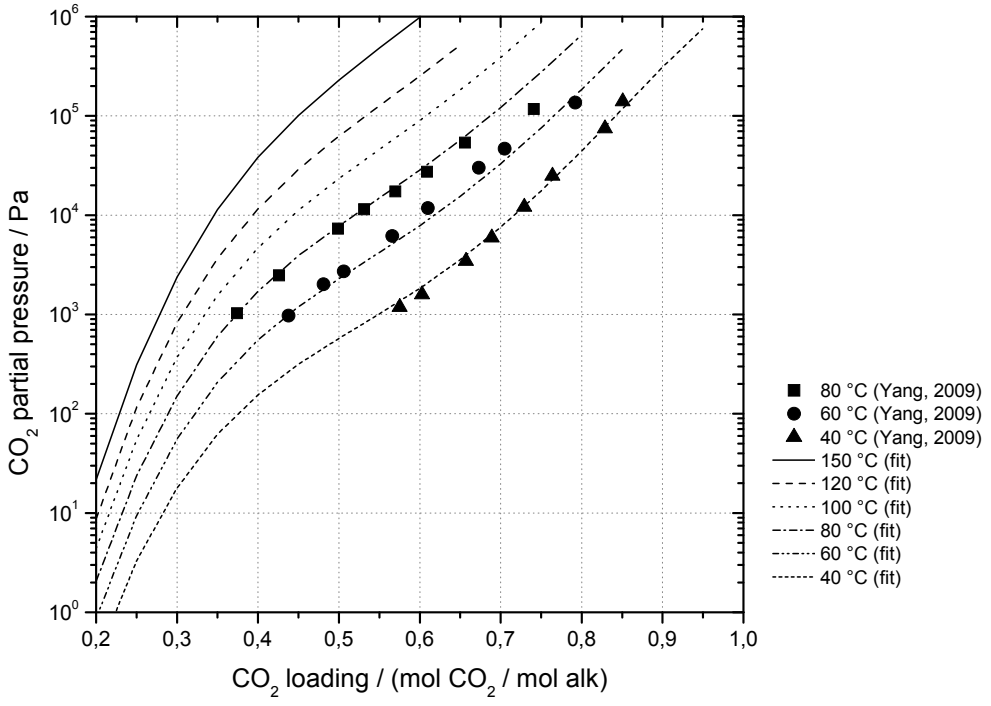

Figure A.6: CO_2 solubility of 5 m AMP / 2.5 m PZ solutions [111]

A.3.2 Heat of absorption

Figure A.7 shows the heat of absorption over the CO_2 loading for the six selected solvents calculated via Eq. (3.8).

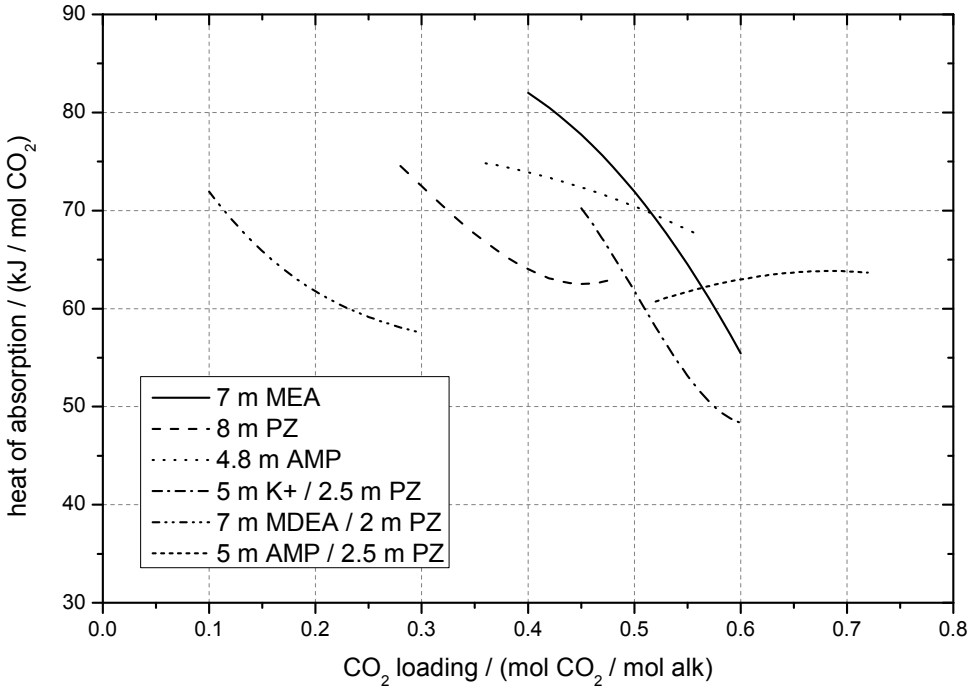

Figure A.7: Heat of absorption for selected solvents in the region of the corresponding rich CO_2 loading calculated from CO_2 solubility correlation

A.3.3 Heat capacity

Table A.2: Coefficients to determine specific heat capacity via Eq. (3.9)

solvent	MEA	PZ	AMP
source	[123, 59]	[59, 128]	[132]*
$\overline{m}_{\mathrm{alk}}$	1.8–10.9 m	1.8-6 (3.6-12) m	4.8 m
t	40–120 °C	40–120 °C	30–80 °C
α	0–0.583	0–0.40	0.0
$c_{\mathrm{Cp},0}$	4.294E+03	3.788E+03	4.267E+03
$c_{\mathrm{Cp},1}$	-1.859E+00	1.733E-01	-1.859E+00
$c_{\mathrm{Cp},2}$	2.575E-02	3.207E-03	2.575E-02
$c_{\mathrm{Cp},3}$	-7.819E+02	-1.809E+03	-7.819E+02
$c_{\mathrm{Cp},4}$	6.536E+02	6.333E+02	6.536E+02
$c_{\mathrm{Cp},5}$	-1.124E+02	-9.776E+00	-1.124E+02
$c_{\mathrm{Cp},6}$	4.746E+00	-1.289E+00	4.746E+00
$c_{\mathrm{Cp},7}$	8.181E-01	9.475E+00	8.181E-01
$c_{\mathrm{Cp},8}$	8.267E-02	2.061E-01	8.267E-02
$c_{\mathrm{Cp},9}$	-5.364E+01	2.372E+01	-5.364E+01
$c_{\mathrm{Cp},10}$	-1.909E-01	-3.353E-01	-1.909E-01
n	160	136	-
$\sigma^{\dagger}$	0.74 %	0.44 %	-

* correlation

† $\sigma = \frac{1}{n}\sum_i^n \left(\left| C_{\mathrm{p,exp}} - C_{\mathrm{p,calc}} \right| / C_{\mathrm{p,exp}} \right)$

Table A.2: Coefficients to determine specific heat capacity via Eq. (3.9), continued

	K/PZ	**MDEA/PZ**	***MEA/PZ***	**AMP/PZ**
source	[59]	[137]	*[59]*	[139]*
$\overline{m}_{alk}$	10 (5/2.5) m	11 (7/2) m	*9.5–11 m*	10 (5/2.5) m
t	40–120 °C	40–120 °C	*40–120 °C*	30–80 °C
α	0.39–0.55	0.1–0.25	*0–0.43*	0.0
$c_{Cp,0}$	2.963E+03	3.037E+03	*5.129E+03*	5.090E+03
$c_{Cp,1}$	3.212E+00	3.599E+00	*1.015E+01*	1.015E+01
$c_{Cp,2}$	-8.794E-03	3.369E-03	*-1.731E-02*	-1.731E-02
$c_{Cp,3}$	-1.877E+02	2.080E+03	*-1.343E+03*	-1.343E+03
$c_{Cp,4}$	0	0	*4.528E+02*	4.528E+02
$c_{Cp,5}$	0	0	*-1.686E+02*	-1.686E+02
$c_{Cp,6}$	0	0	*0*	0
$c_{Cp,7}$	8.309E-01	6.398E+00	*-4.154E+00*	-4.154E+00
$c_{Cp,8}$	0	0	*-4.095E-01*	-4.095E-01
$c_{Cp,9}$	0	0	*1.434E+01*	1.434E+01
$c_{Cp,10}$	0	0	*4.991E-01*	4.991E-01
n	34	34	*136*	-
σ†	0.02 %	0.21 %	*0.43 %*	-

* correlation

† $\sigma = \frac{1}{n}\sum_i^n \left(\left|C_{p,exp} - C_{p,calc}\right| / C_{p,exp}\right)$

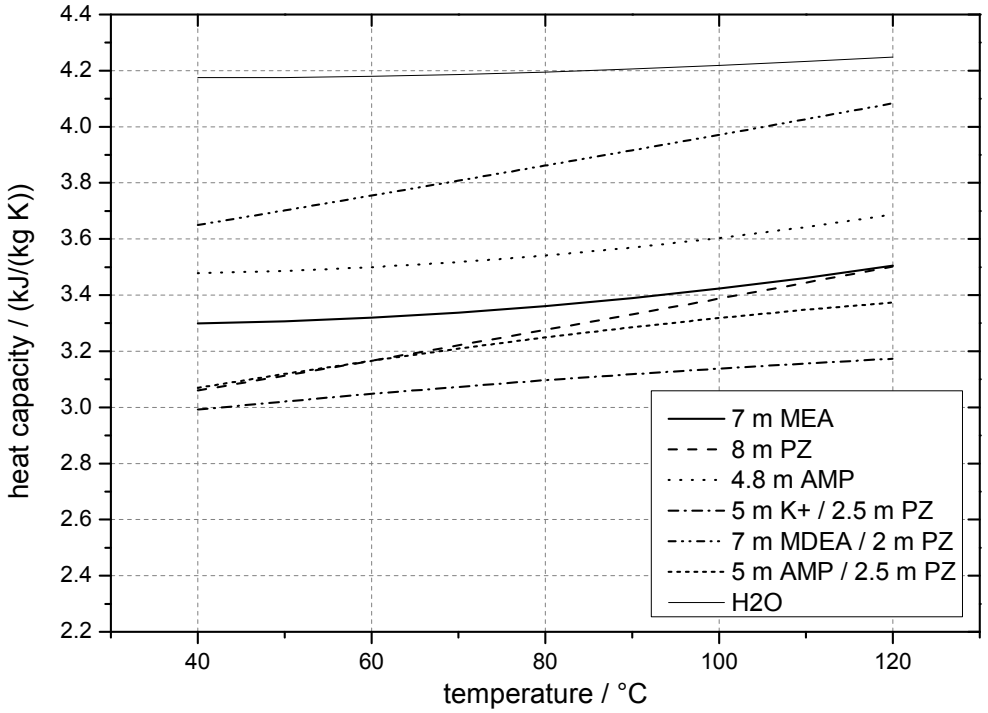

Figure A.8: Calculated heat capacity for varying temperature at equilibrium CO_2 partial pressure of 5 kPa

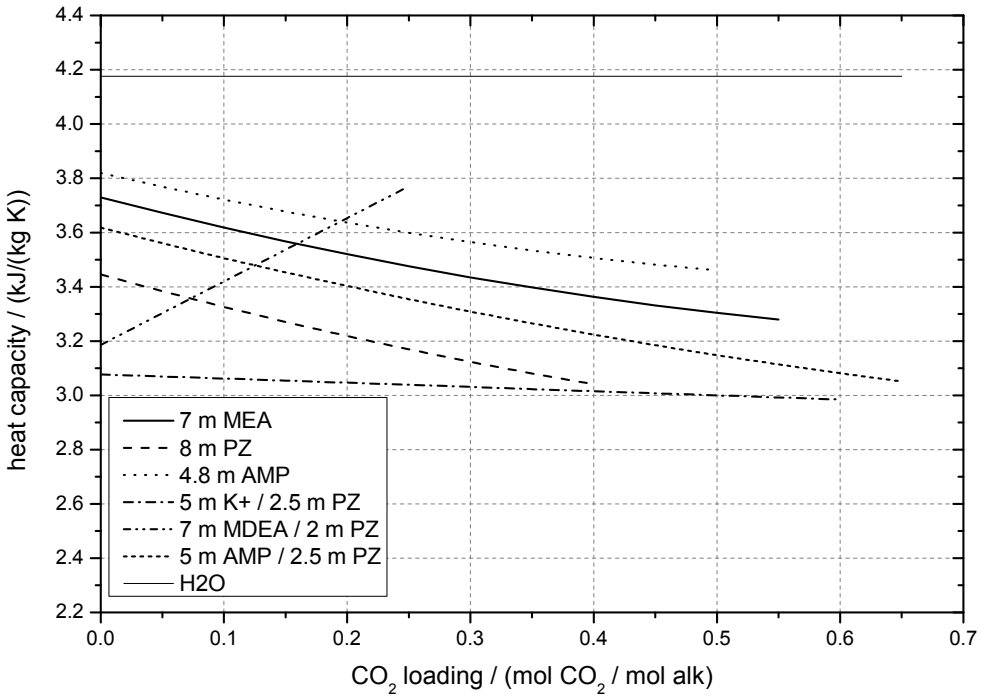

Figure A.9: Calculated heat capacity for varying CO_2 loading at 40 °C

A.3.4 Density

Table A.3: Coefficients to determine density via Eq. (3.11)

solvent	MEA	PZ	AMP
source	[125, 126]	[128]	[135]
$\overline{m}_{\mathrm{alk}}$	1.8–10.9 m	1-10 (2-20) m	4.5 m
t	25–80 °C	20–60 °C	20 °C
α	0-0.5	0-0.53	0-0.3
$c_{\mathrm{dens},0}$	1.005E+03	1.002E+03	9.790E+02
$c_{\mathrm{dens},1}$	-5.993E-01	-4.905E-01	-5.993E-01
$c_{\mathrm{dens},2}$	0	0	0
$c_{\mathrm{dens},3}$	2.492E+01	6.904E+01	2.492E+01
$c_{\mathrm{dens},4}$	1.135E+02	3.983E+01	1.135E+02
$c_{\mathrm{dens},5}$	6.172E+00	2.255E+01	6.172E+00
$c_{\mathrm{dens},6}$	-3.570E-01	-1.726E+00	-3.570E-01
$c_{\mathrm{dens},7}$	1.917E+01	3.962E+01	1.917E+01
n	127	145	4
$\sigma^{\dagger}$	0.30 %	0.39 %	0.11 %

$^{\dagger}\sigma = \frac{1}{n}\sum_i^n \left(\left|\rho_{\mathrm{p,exp}} - \rho_{\mathrm{p,calc}}\right| / \rho_{\mathrm{p,exp}}\right)$

Table A.3: Coefficients to determine density via Eq. (3.11), continued

solvent	**K^+/ PZ**	**MDEA / PZ**	**AMP / PZ**
data source	[58]*	[137]*	[138]
range			
$\bar{m}_{alk}$	10 (5/2.5) m	11 (7/2) m	5.3-6.9 m
t	20–120 °C	20–120 °C	15-60 °C
α	0-0.5	0-0.3	0.0
$c$dens,0	1.118E+03	1.057E+03	9.890E+02
$c_{dens,1}$	-4.420E-01	-6.847E-01	-3.001E-01
$c_{dens,2}$	0	0	-3.718E-03
$c_{dens,3}$	1.205E+01	2.705E+02	2.492E+01
$c_{dens,4}$	-7.144E-02	-4.313E+01	1.135E+02
$c_{dens,5}$	0	0	6.172E+00
$c_{dens,6}$	0	0	-3.570E-01
$c_{dens,7}$	0	0	1.917E+01
n	-	-	40
$\sigma^\dagger$	-	-	0.87 %

* correlation

$^\dagger \sigma = \frac{1}{n}\sum_i^n \left(\left| \rho_{p,exp} - \rho_{p,calc} \right| / \rho_{p,exp} \right)$

A.4 Model validation data

Table A.4: Selected measurement data of pilot plant test runs [148, 149]

run		1	2	3	4	5	6	7	8	9
flue gas flow	m^3/h, wet	4920	5010	4940	4930	4990	4917	4971	4935	4874
lean solution flow	m^3/h	23	19	16.7	14.8	12.5	15	15.5	17	19
flue gas CO_2 concentration	vol.-%, dry	13.2	13.4	13.1	13.5	13.1				
flue gas CO_2 concentration	vol.-%, wet	11.9	11.9	11.8	12.1	11.8				
absorber pressure drop	mbar	73.2	68.4	63	60.1	58.1				
flue gas inlet temperature	°C	47.3	48	46.8	46.8	47.2				
flue gas outlet temperature	°C	47.8	49.1	48.6	48.8	49.2				
lean solution loading	mol CO_2/mol MEA	0.28	0.25	0.22	0.19	0.17	0.21	0.21	0.23	0.24
rich solution loading	mol CO_2/mol MEA	0.46	0.48	0.48	0.48	0.48	0.48	0.46	0.46	0.46
desorber pressure	kPa	181	181	181	181	181	216	181	143	112
reboiler temperature	°C	119	120	121	121	122	125	120	114	108
reboiler heat duty	$GJ_{th}/t\,CO_2$	3.9	3.72	3.73	3.63	3.75	3.74	3.69	4.01	4.19

Table A.4: Selected measurement data of pilot plant test runs [148,149], continued

run		1	2	3	4	5	6	7	8	9
absorber temperature profile										
1st (top)	°C	58.8	61.2	62.1	62.9	63.2				
2nd	°C	75	73.7	72.9	72.3	69.8				
3rd	°C	73	69.6	66.9	65.3	61.3				
4th	°C	67.5	62.6	59.3	57.4	54.3				
5th (bottom)	°C	54.1	52.9	51.1	50.6	50.4				
absorber CO_2 concentration profile										
1st (top)	vol.-% (dry)	1.5	1.59	1.4	1.32	1.55				
2nd	vol.-% (dry)	3.1	4.29	4.43	4.54	5.99				
3rd	vol.-% (dry)	6.3	7.9	8.3	8.82	10.7				
4th	vol.-% (dry)	9.5	11.7	12	12.4	12.7				
5th (bottom)	vol.-% (dry)	13.2	13.5	13.3	13.6	13.3				
desorber temperature profile										
1st (top)	°C	100	99.6	99.6	99.9	101	103	99.6	95.6	91.3
2nd	°C	104	104	104	108	115	108	105	103	99.7
3rd (bottom)	°C	116	118	119	120	121	123	119	113	107

A.5 Nomograms for graphical CO_2 capture process evaluation

Figure A.11, Figure A.12, and Figure A.13 provide nomograms for the evaluation of a CO_2 capture process in one of three cases. The desorber (regeneration) pressure, the reboiler temperature, and the specific reboiler heat duty need to be provided to determine the overall net efficiency penalty. Note that the total power loss and the net efficiency penalty do not account for the increase in auxiliary power demand to drive any additional fans and pumps, including the additional power demand of the cooling water pumps.

Figure A.10 shows an example for the use of the nomograms. Consider a CO_2 capture process with a specific reboiler heat duty of 3.5 GJ_{th} / t CO_2, a reboiler temperature of 120 °C, and a desorber pressure of 1.75 bar. The line connecting the power loss due to the CO_2 compressor and the power loss due to steam extraction from the power plant on the y-axis of the right diagram intersects the third axis in between the two diagrams and gives a total power loss of approximately 225 MW_{el} corresponding to an overall net efficiency penalty of 9.7 %-pts. These values neither include the auxiliary power required for any additional pumps and fans in the capture process nor auxiliary power of additional cooling water pumps which together account for roughly an additional net efficiency penalty of 1 to 1.5 %-pts.

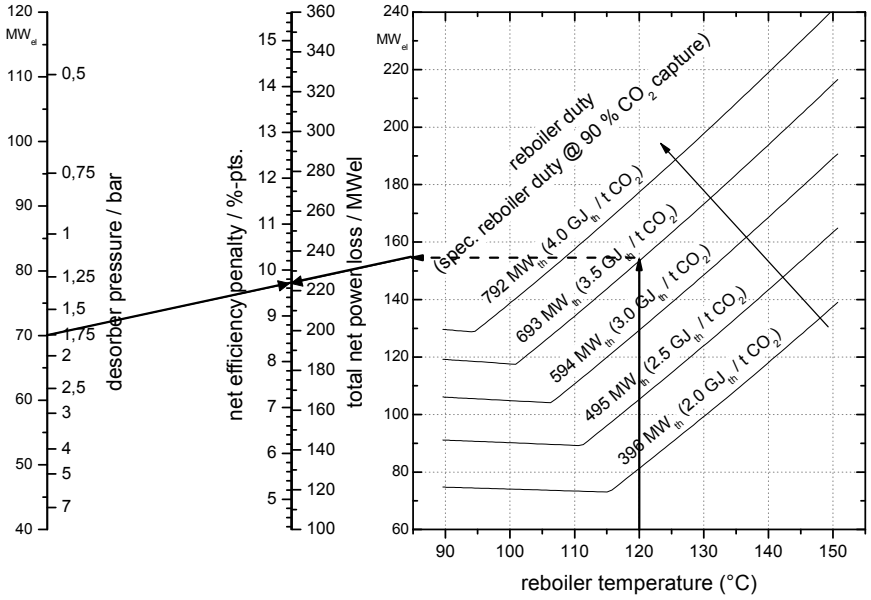

Figure A.10: Example for graphical CO_2 capture process evaluation

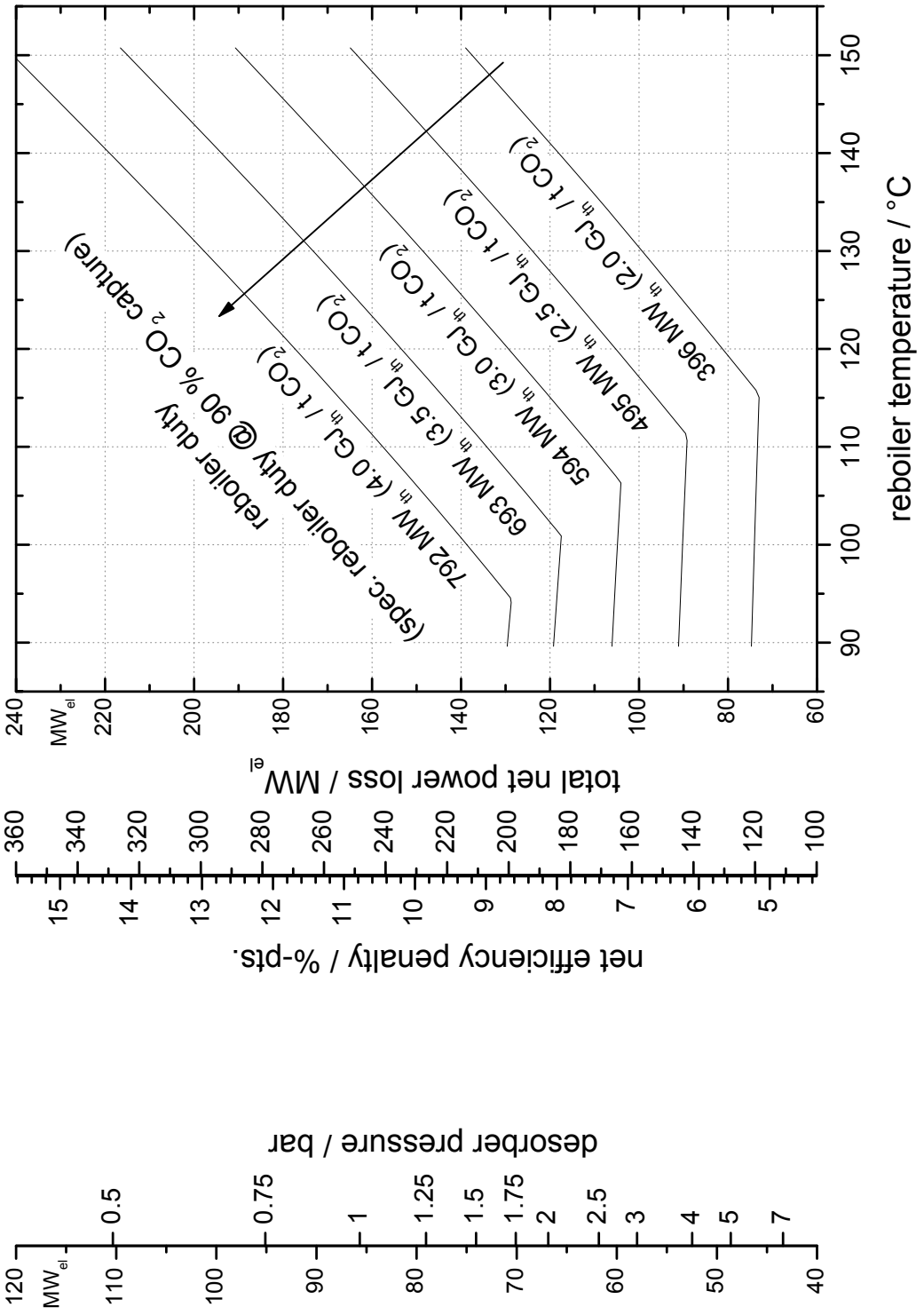

Auxiliary power required for pumps and fans in the capture process and for additional cooling water pumps are NOT considered in the nomogram (+ 1–1.5 %-pts.).

Figure A.11: Nomogram for graphical evaluation of retrofit integration in reference power plant with crossover design pressure of 3.9 bar

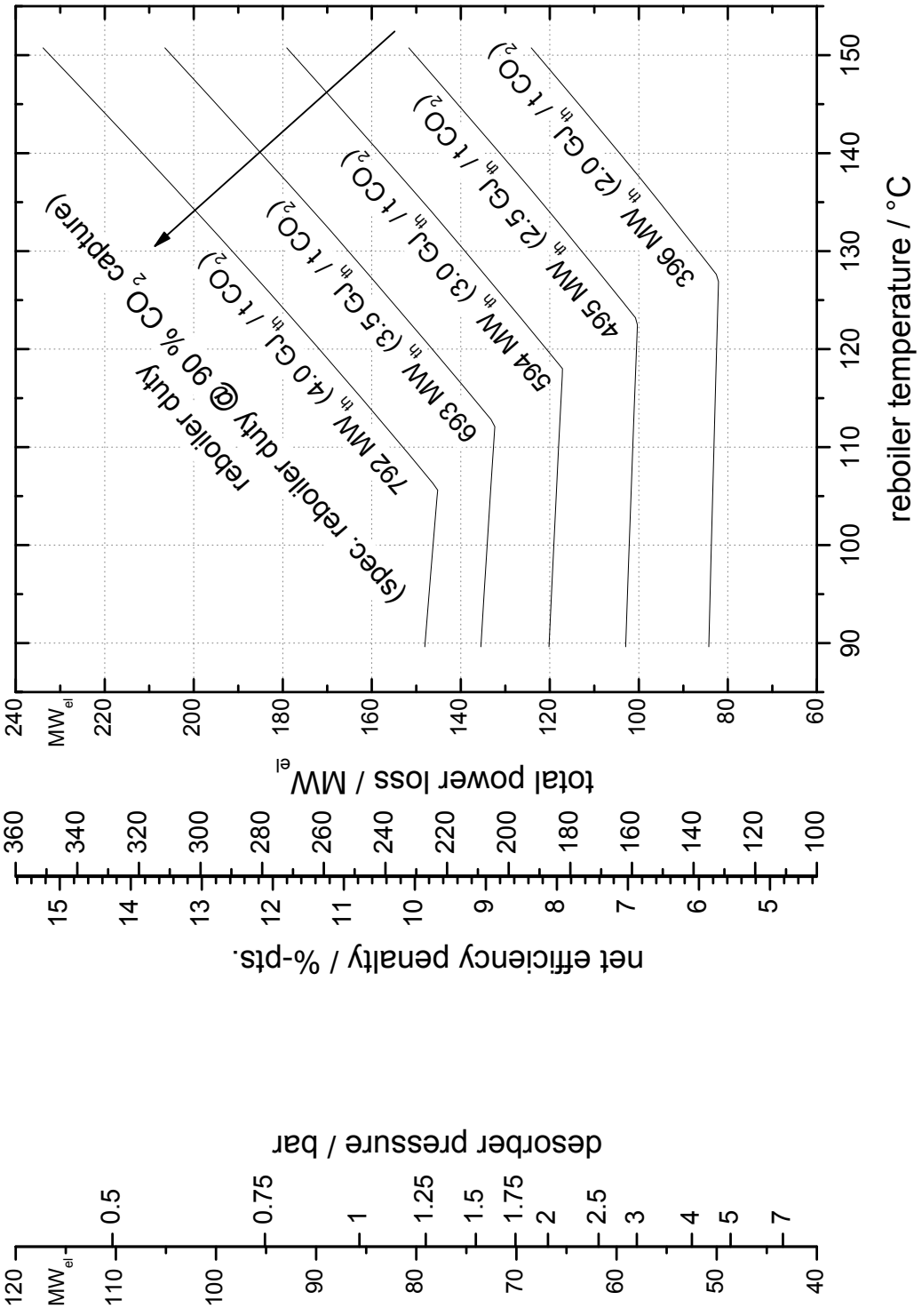

Auxiliary power required for pumps and fans in the capture process and for additional cooling water pumps are NOT considered in the nomogram (+ 1–1.5 %-pts.).

Figure A.12: Nomogram for graphical evaluation of retrofit integration in power plant with increased crossover design pressure of 5.5 bar

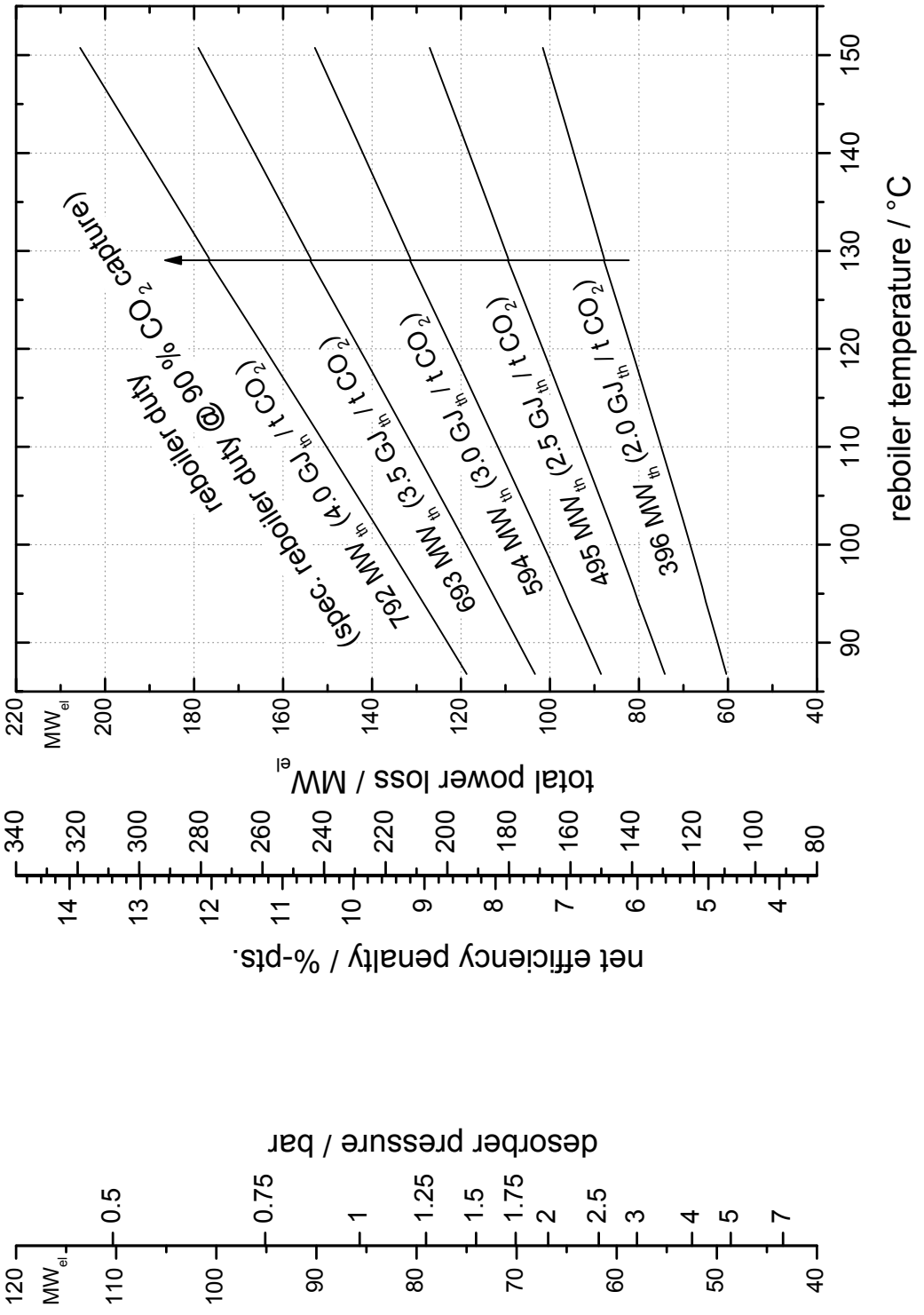

Auxiliary power required for pumps and fans in the capture process and for additional cooling water pumps are NOT considered in the nomogram (+ 1–1.5 %-pts.).

Figure A.13: Nomogram for graphical evaluation of greenfield integration in power plant designed for operation with CO_2 capture with variable crossover design pressure

A.6 Additional diagrams

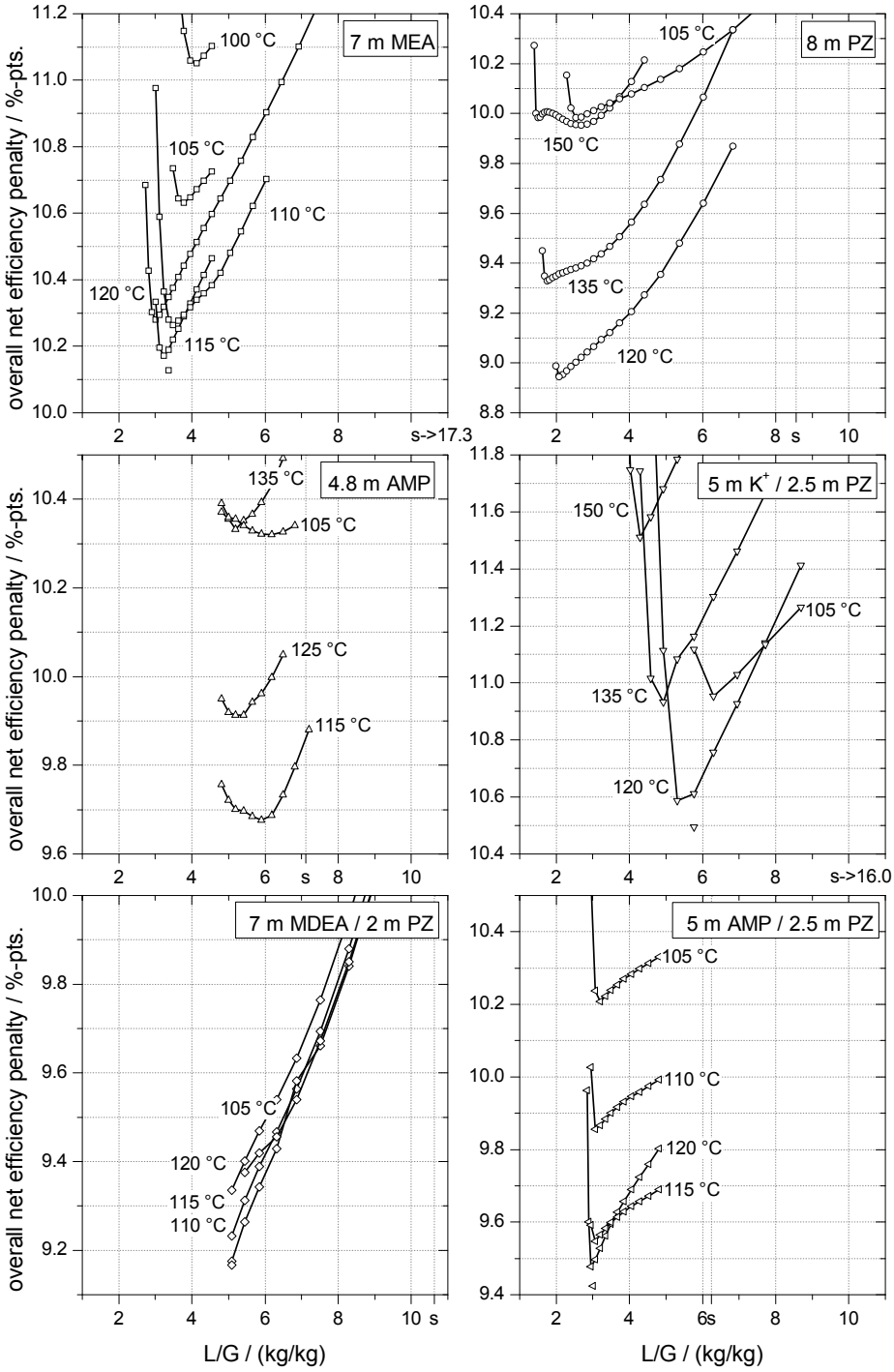

Figure A.14: Overall net efficiency penalty in case of retrofit integration in power plant with increased crossover design pressure of 5.5 bar for different reboiler temperatures and varying L/G with LMTD in RLHX of 10 K

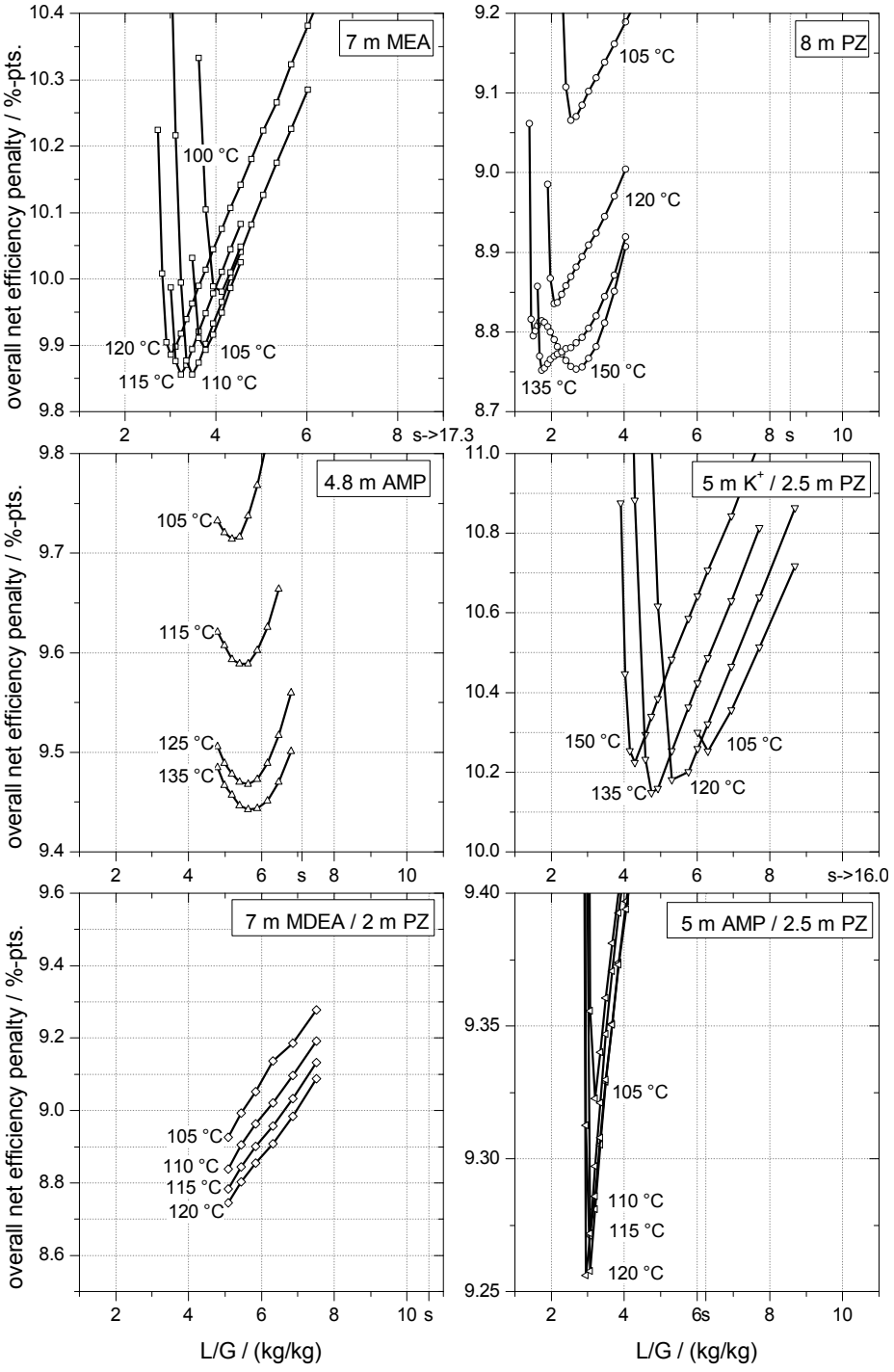

Figure A.15: Overall net efficiency penalty in case of greenfield integration for different reboiler temperatures and varying *L/G* with LMTD in RLHX of 10 K